IV International Conference

CONDENSED MATTER & LOW TEMPERATURE PHYSICS 2024

3rd — 7th June 2024 | Online

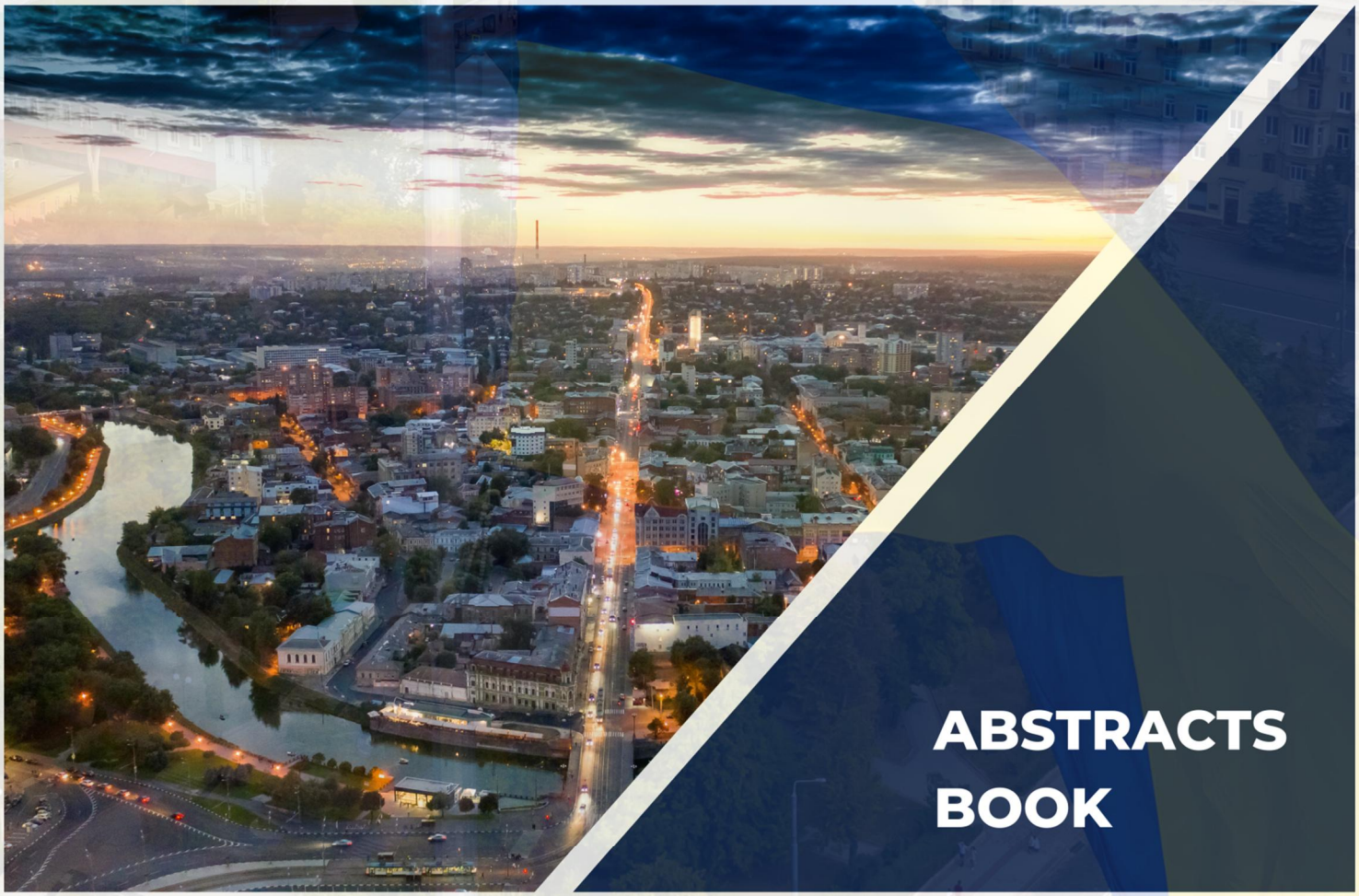

ABSTRACTS BOOK

B. Verkin Institute for Low Temperature Physics and Engineering of NAS of Ukraine

IV International Conference
“CONDENSED MATTER & LOW-TEMPERATURE PHYSICS”

June 3 – 7, 2024

Conference Program

&

Book of Abstracts

Kharkiv 2024

Program Committee

Chair: Prof. Yurii Naidyuk, Corr. Member NASU, ILTPE NASU (Kharkiv, Ukraine)
Vice-chair: Prof. Alexander Dolbin, ILTPE NASU (Kharkiv, Ukraine)

Dr. Mykola Glushchuk, ILTPE NASU (Kharkiv, Ukraine)
Dr. Volodymyr P. Gnezdilov, ILTPE NASU (Kharkiv, Ukraine)
Dr. Alexander Yu. Glamazda, ILTPE NASU (Kharkiv, Ukraine)
Prof. Viktor Chabanenko, DonFTI NASU (Kyiv, Ukraine)
Dr. Alexey Fedorchenko, ILTPE NASU (Kharkiv, Ukraine)
Dr. Oleksandr Kalinenko, ILTPE NASU (Kharkiv, Ukraine)
Prof. Gennadii Kamarchuk, ILTPE NASU (Kharkiv, Ukraine)
Prof. Yuriy Kolesnichenko, ILTPE NASU (Kharkiv, Ukraine)
Prof. Pavel Pal-Val, ILTPE NASU (Kharkiv, Ukraine)
Prof. Leonid Pastur, Full Member NASU, ILTPE NASU (Kharkiv, Ukraine)
Prof. Elena Savchenko, ILTPE NASU (Kharkiv, Ukraine)
Dr. Sergiy Shevchenko, ILTPE NASU (Kharkiv, Ukraine)
Dr. Victor Slavin, ILTPE NASU (Kharkiv, Ukraine)
Dr. Svyatoslav Sokolov, ILTPE NASU (Kharkiv, Ukraine)
Prof. Andrzej Szewczyk, IF PAN (Warsaw, Poland)
Prof. Yevgen Syrkin, ILTPE NASU (Kharkiv, Ukraine)
Dr. Andrii Terekhov, ILTPE NASU (Kharkiv, Ukraine)

Organizing Committee

Chair: PhD St. Diana Hurova
Vice-chair: Dr. Maksym Barabashko
Vice-chair: Dr. Vusal Geidarov
Secretary: Dr. Yuliya Savina

Organizing Committee members:
Dr. Razet Basnukaeva
PhD St. Anna Herus
Dr. Valentin Koverya
Dr. Oleksii Konotop
Dr. Yevhen Petrenko
Dr. Sergii Poperezhai

CONFERENCE PROGRAM

Time is specified for the Time Zone UTC/GMT+3, Eastern European Time

MONDAY, 3rd of JUNE

9:50-10:00 **Opening Remarks**
Director of the B. Verkin ILTPE of NAS of Ukraine
Corresponding Member of NAS of Ukraine
Prof. Yurii Naidyuk
and
Chair of Organizing Committee Diana Hurova

PLENARY LECTURES OF INVITED SPEAKERS

Chair *Valentin Koverya*

10:00-10:30 **Desorption of excited atoms via bi-exciton creation from solid Ne surfaces by electron impact** **34**
Issei Kawada[1], Takayuki Tachibana[1,2] and Takato Hirayama[1,2]
[1] *Department of Physics, Rikkyo University, Tokyo, Japan*
[2] *Research Center for Measurements in Advanced Science, Rikkyo University, Tokyo, Japan*

10:30-11:00 **Quantum Scaling for the Metal-Insulator Transition in a Two-Dimensional Electron System** **36**
V. Kagalovsky[1], S.V. Kravchenko[2], D. Nemirovsky[1]
[1] *Shamoon College of Engineering, Beer-Sheva, Israel*
[2] *Physics Department, Northeastern University, Boston, Massachusetts, USA*

ELECTRONIC PROPERTIES OF CONDUCTING AND SUPERCONDUCTING SYSTEMS

Chair *Valentin Koverya*

11:00-11:15 **Topological features and transport properties of Sr_2FeMoO_6 double perovskite** **55**
S. M. Konoplyuk, M. M. Krupa, Yu. B. Skyrta
Institute of magnetism of NAS of Ukraine and MES of Ukraine, Kyiv, Ukraine

11:15-11:30 **Effect of dysprosium trioxide on the structural and electrical properties of Tl-1223 HTS** **56**
I. R. Metskhvarishvili[1,2], G. N. Dgebuadze[1], D. L. Surmanidze[1,3], T. E. Lobzhanidze[3], B. G. Bendeliani[1], V. M. Gabunia[1,4], M. R. Metskhvarishvili[5], D. A. Jishiashvili[1,6]
[1] *Ilia Vekua Sukhumi Institute of Physics and Technology, Laboratory of Cryogenic Technique and Technologies, Tbilisi, Georgia*
[2] *Georgian Technical University, Faculty of Informatics and Control Systems, Department of Microprocessor and Measurement Systems, Tbilisi, Georgia*
[3] *Ivane Javakhishvili Tbilisi State University, Faculty of Exact and Natural Sciences, Department of Chemistry, Tbilisi, Georgia*
[4] *Petre Melikishvili Institute of Physical and Organic Chemistry of the Iv. Javakhishvili Tbilisi State University, Tbilisi, Georgia*
[5] *"Talga" Institute of Georgian Technical University, Tbilisi, Georgia*
[6] *V. Chavchanidze Institute of Cybernetics of the Georgian Technical University, Tbilisi, Georgia*

11:30-11:45 **New states of Fermi superliquid with conformational degrees of freedom** **57**
M. Yu. Kovalevsky[1], A. A. Rozhkov[2]
[1] NSC "Kharkiv Institute of Physics and Technology", Kharkiv,Ukraine
[2] National Technical University Kharkiv Polytechnical Institute, Kharkiv,Ukraine

11:45-12:00 **Influence of strong electron irradiation on fluctuation conductivity and pseudogap in $YBa_2Cu_3O_{7-\delta}$ single crystals** **58**
A. L. Solovjov[1,2], M. V. Shytov[1], E. V. Petrenko[1], L. V. Bludova[1], R. V. Vovk[3], K. Rogacki[2]
[1] B. Verkin Institute for Low Temperature Physics and Engineering, Kharkiv, Ukraine
[2] Institute for Low Temperatures and Structure Research, Wroclaw, Poland
[3] Department of Physics, V. N. Karazin Kharkiv National University, Kharkiv, Ukraine

12:00-12:15 **A detailed investigation of anomalies on the temperature dependences of the electrical resistance of $Bi_{88.08}Mn_{11.92}$ in fields up to 90 kOe** **59**
V. M. Yarovyi[1], K. Rogacki[2], A. V. Terekhov[1], E. Lähderanta[3], A. L. Solovjov[1,2]
[1] B. Verkin Institute for Low Temperature Physics and Engineering, Kharkiv, Ukraine
[2] Institute for Low Temperatures and Structure Research, Wroclaw, Poland
[3] Lappeenranta University of Technology, School of Engineering Science, Lappeenranta, Finland

12:15-13:00 **BREAK**

PLENARY LECTURES OF INVITED SPEAKERS

Chair *Yuliya Savina*

13:00-13:30 **Quantum transport and optics theory and simulations with applications to noninvasive medical diagnostics and novel photonic functionalities** **42**
M.F. Pereira[1,2], Humaira Zafar[1] and A. Apostolakis[2]
[1] Department of Physics, Khalifa University of Science and Technology, UAE
[2] Institute of Physics, Czech Academy of Sciences, Czech Republic

13:30-14:00 **Analysis, design, and applications of polygon mirror-based laser scanners** **33**
V.-F. Duma[1-3] and M.-A. Duma[4]
[1] 3OM Optomechatronics Group, Faculty of Engineering, Aurel Vlaicu University of Arad, Arad, Romania
[2] Faculty of Electronics, Telecommunications, and Information Technology, Polytechnic University of Timisoara, Timisoara, Romania
[3] National University of Science and Technology POLITEHNICA Bucharest, Center of Research and Development for Mechatronics, Bucharest, Romania
[4] School of Science and Engineering, University of Groningen, The Netherlands

OPTICS, PHOTONICS AND OPTICAL SPECTROSCOPY

Chair *Yuliya Savina*

14:00-14:15 **Luminescent and scintillation properties of $CsPbCl_3$ perovskite crystal** **103**
V. Kolomiets, V. Kapustianyk
I. Franko National University of Lviv, Physics Department, Lviv, Ukraine

14:15-14:30 **Peculiarities of J-Aggregate Formation in Liquid Crystal Matrices: Enhancing Stability and Optoelectronic Characteristics** **104**
I. Yu. Ropakova[1], O. M. Samoilov[1], I. I. Grankina[1], S. L. Yefimova[1], O. V. Sorokin[1], N. A. Kasian[1], S. S. Hrankina[1,2], L. N. Lisetski[1]
[1] Institute for Scintillation Materials of NAS of Ukraine Kharkiv, Kharkiv 61072, Ukraine
[2] Kharkiv National Medical University, Kharkiv, Ukraine

14:30-14:45 **Engineering optical metasurfaces for far- and near-field applications** **105**
A. A. Hrinchenko[1], O. Yu. Demianyk[1], S. Yu. Polevoy[2], A. I. Ovcharenko[1], V. R. Tuz[1], K. E. Nemchenko[1], O. Y. Yermakov[1]
[1] V. N. Karazin Kharkiv National University, Kharkiv, Ukraine
[2] O. Ya. Usikov Institute for Radiophysics and Electronics NAS of Ukraine, Kharkiv, Ukraine

14:45-15:00 **Polaritons in the magnetic-«epsilon-near-zero» multilayers, with noncollinear orientation of magnetizations** **106**
A. F. Bukhanko
Donetsk Institute for Physics and Engineering Named after O.O. Galkin, Kyiv, Ukraine

15:00-15:30 **BREAK**

PLENARY LECTURES OF INVITED SPEAKERS

Chair *Oleksii Konotop*

15:30-16:00 **Optical emission studies of C_2 formation upon electron irradiation of Ar matrices doped with CH_4** **45**
M. A. Bludov, I. V. Khyzhniy, S. A. Uyutnov, E. V. Savchenko
B. Verkin Institute for Low Temperature Physics and Engineering, Kharkiv, Ukraine

QUANTUM LIQUIDS AND QUANTUM CRYSTALS, CRYOCRYSTALS

Chair *Oleksii Konotop*

16:00-16:15 **Influence of acoustic emission on the resonance properties of a quartz tuning fork vibrating in superfluid ^{3}He - ^{4}He mixtures** **123**
V. K. Chagovets, V. E. Syvokon, S. S. Sokolov
B. Verkin Institute for Low Temperature Physics and Engineering, Kharkiv, Ukraine

16:15-16:30 **Two-step energy dissipation of oscillating tuning fork in ^{3}He-^{4}He superfluid mixtures** **124**
J. Amrit[1], N. Herashchenko[2], K. Nemchenko[2], S. Rogova[2], T. Vikhtinskaya[2]
[1] LISN, CNRS, Université Paris-Saclay, Orsay, France
[2] V. N. Karazin Kharkiv National University, Kharkiv, Ukraine

16:30-16:45 **Phase composition of large substrate-free binary Ar-Kr clusters** **125**
O. P. Konotop, O. G. Danylchenko
B. Verkin Institute for Low Temperature Physics and Engineering, Kharkiv, Ukraine

16:45-17:00 **BREAK**

17:00-18:40 POSTER SESSION (1 AND 4 SECTIONS)

ELECTRONIC PROPERTIES OF CONDUCTING AND SUPERCONDUCTING SYSTEMS

Chairs *Valentin Koverya and Oleksii Konotop*

17:00-17:15 **All participants of Stage 1 (short presentation one by one for 1,5 – 2 minutes)**

17:15-17:30 **Breakout Rooms Stage 1**

P1 **The acoustoelectric transformation in the mixed state in superconducting chalcogenides $FeSe_{1-x}S_x$ (x=0.075)** **60**
G. A. Zvyagina[1], V. D. Fil[1], I. V. Bilych[1], K. R. Zhekov[1], D. V. Fil[2,3]
[1] B. Verkin Institute for Low Temperature Physics and Engineering, Kharkiv, Ukraine
[2] Institute for Single Crystals, NAS of Ukraine, Kharkiv, Ukraine
[3] V.N. Karazin Kharkiv National University, Kharkiv, Ukraine

P2 **Combined electrical breakdown of a dielectric nanolayer between thin film electrodes** **61**
S. I. Bondarenko, A. V. Krevsun, V. P. Koverya
B. Verkin Institute for Low Temperature Physics and Engineering, Kharkiv, Ukraine

P3 **The formation of IV-characteristics of long Josephson junctions at zero-field steps** **62**
A. Grib, O. Chykina
V. N. Karazin National University, Kharkiv, Ukraine

P4 **Experimental evidences for a favor of the staged nature of temperature evolution of the HTSC's pseudogap state** **63**
N. A. Azarenkov, V. A. Frolov, E. V. Karaseva, V. I. Sokolenko, A. V. Poida
National Science Center Kharkiv Institute of Physics and Technology, Kharkiv, Ukraine

P5 **Quantum capacitance of qubit-based systems** **64**
O. Y. Kitsenko[1,2], S. N. Shevchenko[1]
[1] B. Verkin Institute for Low Temperature Physics and Engineering, Kharkiv, Ukraine
[2] V. N. Karazin Kharkiv National University, Kharkiv, Ukraine

P6 **Electron transport in one dimensional disordered lattice** **65**
M. V. Klimov
V. N. Karazin Kharkiv National University, Kharkiv, Ukraine

P7 **Pressure effect on electronic structure and magnetic properties of LaFeAsO** **66**
A. S. Panfilov, I. P. Kobzar, G. E. Grechnev, A. V. Fedorchenko
B. Verkin Institute for Low Temperature Physics and Engineering, Kharkiv, Ukraine

17:35-17:50 **All participants of Stage 2 (short presentation one by one for 1,5 – 2 minutes)**

17:50-18:05 **Breakout Rooms Stage 2**

P8 **Edge states at the boundary of hexagonal and Lieb lattices in a quantizing magnetic field** **67**
I. V. Kozlov, Yu. A. Kolesnichenko
B. Verkin Institute for Low Temperature Physics and Engineering, Kharkiv, Ukraine

P9 **Manifestation of homogeneous superconductivity in single-crystalline [100] boron-doped diamond film near Superconductor-Insulator transition** **68**
O. Onufriienko[1], P. Szabó[1], V. V. Moshchalkov[2], P. Samuely[1], G. Zhang[3,4] and T. Samuely[1]
[1] *Centre of Low Temperature Physics, Institute of Experimental Physics, Slovak Academy of Sciences and Faculty of Science, P.J. Šafárik University, Košice, Slovakia*
[2] *Department of Physics and Astronomy, KU Leuven, Heverlee, Belgium*
[3] *National Key Laboratory of Science and Technology on Advanced Composites in Special Environments, Harbin Institute of Technology, Harbin, China*
[4] *Zhengzhou Research Institute, Harbin Institute of Technology, Zhengzhou, China*

P10 **Study of the pseudogap temperature dependence in YBCO films in magnetic fields up to 8 T** **69**
E. V. Petrenko[1], L. V. Bludova[1], A. V. Terekhov[1], A. L. Solovjov[1], K. Rogacki[2]
[1] *B. Verkin Institute for Low Temperature Physics and Engineering, Kharkiv, Ukraine*
[2] *Institute for Low Temperatures and Structure Research, Wroclaw, Poland*

P11 **Experimental verification of the occurrence of rectified voltage ("diode effect") in multiply connected superconducting structures** **70**
A. G. Sivakov[1], O. G. Turutanov[2,1], A. S. Pokhila[1], A. V. Krevsun[1], A. E. Kolinko[1], and S. I. Bondarenko[1]
[1] *B.Verkin Institute for Low Temperature Physics and Engineering, Kharkiv, Ukraine*
[2] *Department of Experimental Physics, Comenius University, Bratislava, Slovakia*

P12 **Hopping Hall effect in multi-walled carbon nanotubes** **71**
R. M. Rudenko[1], O. O. Voitsihovska[1], A. A. Abakumov[2], V. M. Poroshin[1]
[1] *Institute of Physics, Kyiv, Ukraine*
[2] *L.V. Pisarzhevskii Institute of Physical Chemistry, Kyiv, Ukraine*

P13 **Controlling the efficiency of the superconducting "diode effect" using microwave radiation** **72**
A. G. Sivakov[1], O. G. Turutanov[2,1], A. S. Pokhila[1], A. E. Kolinko[1], M. Grajcar[2,3]
[1] *B. Verkin Institute for Low Temperature Physics and Engineering, Kharkiv, Ukraine*
[2] *Department of Experimental Physics, Comenius University, Bratislava, Slovakia*
[3] *Institute of Physics, Slovak Academy of Sciences, Bratislava, Slovakia*

P14 **Josephson weak link based on proximity effect in long bimetallic thin-film bridge** **73**
O. G. Turutanov[1,2], A. G. Sivakov[2], A. S. Pokhila[2], M. Grajcar[1,3]
[1] *Department of Experimental Physics, Comenius University, Bratislava, Slovakia*
[2] *B. Verkin Institute for Low Temperature Physics and Engineering, Kharkiv, Ukraine*
[3] *Institute of Physics, Slovak Academy of Sciences, Bratislava, Slovakia*

QUANTUM LIQUIDS AND QUANTUM CRYSTALS, CRYOCRYSTALS

Chairs *Valentin Koverya and Oleksii Konotop*

18:10-18:25 **All participants of Stage 3 (short presentation one by one for 1,5 – 2 minutes)**

18:25-18:40 **Breakout Rooms Stage 3**

P15 **Structural characteristics of solid nitrogen. Isotopic effect** **127**
N. A. Aksenova[1], D. E. Hurova[2], N. N. Galtsov[2]
[1] *V. N. Karazin Kharkiv National University, Kharkiv, Ukraine*
[2] *B.Verkin Institute for Low Temperature Physics and Engineering, Kharkiv, Ukraine*

P16 **Observation of new band in stimulated luminescence of solid nitrogen** **128**
M. A. Bludov, I. V. Khyzhniy, S. A. Uyutnov, E. V. Savchenko
B. Verkin Institute for Low Temperature Physics and Engineering, Kharkiv, Ukraine

P17 **The influence of a point impurity on the phonon spectrum of a chain of noble gas atoms adsorbed on a carbon nanobundle** **129**
E. V. Manzhelii, S. B. Feodosyev, E. S. Syrkin
B. Verkin Institute for Low Temperature Physics and Engineering, Kharkiv, Ukraine

P18 **Observation of dynamic- and thermo- anomalies at surface electron to surface anions transition over helium film on structured substrate** **130**
V. A. Nikolaenko, A. V. Smorodin, E. Ya. Rudavskii and S. S. Sokolov
B. Verkin Institute for Low Temperature Physics and Engineering, Kharkiv, Ukraine

P19 **Four-particle states of low-dimensional fermions with three-body interaction** **131**
V. Polkanov, V. Pastukhov
Professor Ivan Vakarchuk Department for Theoretical Physics, Ivan Franko National University of Lviv, Lviv, Ukraine

P20 **Heat capacity features of epoxy-based composites with different graphene oxide contributions at low temperatures** **132**
O. O. Romantsova[1,2], D. Szewczyk[2], A. Jeżowski[2], Yu. Horbatenko[1], O. Krivchikov[1,2], M. Vinnikov[1], S. Cherednichenko[1]
[1] B. Verkin Institute for Low Temperature Physics and Engineering, Kharkiv, Ukraine
[2] Institute of Low Temperatures and Structure Research, Wroclaw, Poland

P20a **Thermal conductivity of ABS polymer composite with 0.5 wt% of the thermally reduced graphene oxide** **126**
V. V. Sagan, A. I. Krivchikov, V. A. Konstantinov
B. Verkin Institute for Low Temperature Physics and Engineering, Kharkiv, Ukraine

TUESDAY, 4th of JUNE

PLENARY LECTURES OF INVITED SPEAKERS

Chair *Maksym Barabashko*

10:00-10:30 **Electronic and Reactive Properties of Nano- and Sub-nano Clusters** **31**
Tore Brinck
Department of Chemistry, CBH, KTH Royal Institute of Technology, Stockholm, Sweden

NANOPHYSICS AND NANOTECHNOLOGIES

Chair *Maksym Barabashko*

10:30-10:45 **Rate-equation approach for a driven two-electron four-level double-quantum dot** **135**
M. P. Liul[1,2], A. I. Ryzhov[1,2], S. N. Shevchenko[1]
[1] B.Verkin Institute for Low Temperature Physics and Engineering, Kharkiv, Ukraine
[2] Theoretical Quantum Physics Laboratory, Cluster for Pioneering Research, RIKEN, Wakoshi, Saitama, Japan

10:45-11:00 **Selective uptake and desorption of carbon dioxide in carbon honeycombs** **136**
D. G. Diachenko, N. V. Krainyukova
B. Verkin Institute for Low Temperature Physics and Engineering, Kharkiv, Ukraine

11:00-11:15 **Aluminum uptake in carbon honeycomb** **137**
M. A. Kabanenko, D. G. Diachenko, N. V. Krainyukova
B. Verkin Institute for Low Temperature Physics and Engineering, Kharkiv, Ukraine

11:15-11:30 **Low-temperature ultrasonic investigation of severe deformed high-purity titanium** **138**
V. S. Klochko, A. V. Korniiets, V. I. Sokolenko, V. I. Spitsyna, M. A. Shulgin, I. F. Kislyak, I. V. Kolodiy, O. O. Kondratov, T. M. Tikhonovska
National Scientific Center "Kharkov Institute of Physics and Technology", Kharkiv, Ukraine

11:30-11:45 **Impact of pressure on electrical properties of silver nanofilms** **153**
S. Udachan[1], S. B. Kolavekar[1], N. H. Ayachit[1], L. A. Udachan[2], S. Siddanna[2], S. S. Kolkundi[3], K. N. Kumar[4], S. Ramya[5], S. Veeresh[5]
[1] Department of Physics, School of Advanced Sciences, KLE Technological University, Hubballi-580031, India
[2] S. S. Tegnoor Degree College, Kalaburagi-585105, India
[3] Government First Grade College, Shahapur-585223, Yadgir, India
[4] Department of Physics and Center for Nanomaterials and MEMS, Nitte Meenakshi Institute of Technology, Yelahanka, Bangalore-560064, India.
[5] Shree Sangam Vidya Mandir, Kalburagi, Karnataka, India.

11:45-12:00 **Interpolation expressions for dependencies of heat transfer parameters on the boundary diffusivity factor in nanoribbons** **140**
J. Amrit[1], K. Nemchenko[2], Ye. Nemchenko, S. Rogova[2], M. Spotar[2], T. Vikhtinskaya[2]
[1] LISN, Université Paris-Saclay, CNRS, Orsay, France
[2] V. N. Karazin Kharkiv National University, Kharkiv, Ukraine

12:00-12:15 **Heat transfer in 3D samples of definite cross-section at diffusive boundary scattering** **141**
J. Amrit[1], K. Nemchenko[2], Ye. Nemchenko[2], S. Rogova[2], T. Vikhtinskaya[2]
[1] LISN, Université Paris-Saclay, CNRS, Orsay, France
[2] V. N. Karazin Kharkiv National University, Kharkiv, Ukraine

12:15-12:30 **Iterative analytical solution to the problem of heat flow in a two-dimensional conductor** **142**
J. Amrit[1], K. Nemchenko[2], M. Spotar[2], T. Vikhtinskaya[2]
[1] LISN, Université Paris-Saclay, CNRS, Orsay, France
[2] V.N.Karazin Kharkiv National University, Kharkiv, Ukraine

12:30-13:30 **BREAK**

PLENARY LECTURES OF INVITED SPEAKERS

Chair *Sergii Poperezhai*

13:30-14:00 **Challenging properties of magnetic shape memory alloys** **41**
V. A. L'vov[1,2]
[1] Institute of Magnetism NAS of Ukraine and MES of Ukraine, Kyiv, Ukraine
[2] Taras Shevchenko National University of Kyiv, Kyiv, Ukraine

14:00-14:30 **Controlling multimagnon processes in magnetic nanostructures** **48**
R. Verba[1], J. Kharlan[1,2], V. Borynskyi[1], D. Slobodianiuk[3,1], A. Etesamirad[4], I. Barsukov[4]
[1] Institute of Magnetism NAS of Ukraine and MES of Ukraine, Kyiv, Ukraine,
[2] Institute of Spintronics and Quantum Information, Adam Mickiewicz University, Poznań, Poland
[3] Institute of High Technologies, Taras Shevchenko National University of Kyiv, Kyiv, Ukraine,
[4] Physics and Astronomy, University of California, Riverside, USA

MAGNETISM AND MAGNETIC MATERIALS

Chair *Sergii Poperezhai*

14:30-14:45 **Effect of higher-order exchange interactions for skyrmion stability in monolayer MnSeTe** **77**
Megha Arya[1], Lionel Calmels[1], Rŭmi Arras[1], Soumyajyoti Haldar[2], Stefan Heinze[2], and Dongzhe Li[1]
[1] *CEMES, Universitŭ de Toulouse, CNRS, Toulouse, France*
[2] *Institute of Theoretical Physics and Astrophysics, University of Kiel, Kiel, Germany*

14:45-15:00 **Ni-Fe-based layered double hydroxides: cluster glass and low-temperature magnetic phase separation** **79**
A. V. Fedorchenko[1], E. L. Fertman[1], Yu. G. Pashkevich[2], D. E. L. Vieira[3], E. Čižmár[4], V. Tkáč[4], R. Tarasenko[4], A. Feher[4], A. N. Salak[3]
[1] *B.Verkin Institute for Low Temperature Physics and Engineering, Kharkiv, Ukraine*
[2] *O. Galkin Donetsk Institute for Physics and Engineering, Kyiv, Ukraine*
[3] *Aveiro Institute of Materials, University of Aveiro, Aveiro, Portugal*
[4] *Institute of Physics, Faculty of Science, P.J. Šafárik University in Košice, Košice, Slovakia*

15:00-15:15 **Nano-Oscillator Based on a 3D Non-Uniform Antiferromagnetic Spin Texture** **80**
V. S. Gerasimchuk[1], Yu. I. Gorobets[1,2], O. Yu. Gorobets[1], I. V. Gerasimchuk[1,2]
[1] *National Technical University of Ukraine "Igor Sikorsky Kyiv Polytechnic Institute", Kyiv, Ukraine*
[2] *Institute of Magnetism, NAS of Ukraine and MES of Ukraine, Kyiv, Ukraine*

15:15-15:30 **Multiphonon Raman scattering in $BaBiO_3$** **81**
A. Glamazda[1,4], V. Gnezdilov[1,2], P. Lemmens[2,3]
[1] *B. Verkin Institute for Low Temperature Physics and Engineering, Kharkiv, 61103, Ukraine*
[2] *Institute for Condensed Matter Physics, TU-Braunschweig, Braunschweig, Germany*
[3] *Technische Universität Braunschweig, Braunschweig, Germany*
[4] *V. N. Karazin Kharkiv National University, Kharkiv, Ukraine*

15:30-15:45 **Quasi-two-dimensional S = 1/2 antiferromagnet $Cu[C_6H_2(COO)_4][C_2H_5NH_3]_2$: evidence of field-induced Berezinskii–Kosterlitz–Thouless transition** **82**
I. Kozin[1], R. Tarasenko[1] A. Orendáčová[1], E. Čižmár[1], P. Danylchenko[1], V. Tkáč[1], and M. Orendáč[1]
[1] *Institute of Physics, Faculty of Science, P.J. Šafárik University in Košice, Košice, Slovakia*

15:45-16:00 **Locked domain structure of magnetostrictive FeTb/Fe multilayers via the Fe sublayers** **83**
Iryna Lukiienko[1,2], Vojtěch Uhlíř[1]
[1] *Central European Institute of Technology, Brno University of Technology, Brno, Czechia*
[2] *B. Verkin Institute for Low Temperature Physics and Engineering, Kharkiv, Ukraine*

16:00-16:15 **Single-layer methods for three-dimensional tensor networks** **84**
I. V. Lukin[1,2], A. G. Sotnikov[1,2]
[1] *Karazin Kharkiv National University, Kharkiv, Ukraine*
[2] *Akhiezer Institute for Theoretical Physics, NSC KIPT, Kharkiv, Ukraine*

16:15-16:30 **Spectroscopic signatures of cross-Kerr coupling in a vibrating magnetic beam** **85**
A. M. Sokolov[1], T. T. Heikkilä[2]
[1] *Institute of Physics of the National Academy of Sciences, Kyiv*
[2] *University of Jyväskylä, Jyväskylä, Finland*

16:30-16:45 **Electrical and magnetic properties of $(C_2H_5NH_3)_2CuCl_4$ magnetic multiferroic at low temperatures** **86**
O. I. Vira[1], Yu. Eliashevskyy[1], V. Kapustianyk[1], R. Tarasenko[2]
[1] *Ivan Franko National University of Lviv, Faculty of Physics, Lviv, Ukraine*
[2] *Pavol Jozef Safarik University, Institute of Physics, Faculty of Science, Kosice, Slovakia*

16:45-17:15 **BREAK**

17:15-19:30 **POSTER SESSION (2 AND 3 SECTIONS)**

MAGNETISM AND MAGNETIC MATERIALS

Chairs *Sergii Poperezhai and Yuliya Savina*

17:15-17:30 **All participants of Stage 1 (short presentation one by one for 1,5 – 2 minutes)**

17:30-17:45 **Breakout Rooms Stage 1**

P21 **Features of magnetic properties of α-$Cr_3(PO_4)_2$ crystal** **87**
O. Bludov[1], Yu. Savina[1], V. Pashchenko[1], M. Kobets[1] T. Zajarniuk[2], M.U. Gutowska[2], A. Szewczyk[2]
[1] *B.Verkin Institute for Low Temperature Physics and Engineering, Kharkiv, Ukraine*
[2] *Institute of Physics of PAS, Warsaw, Poland*

P22 **Temperature changes in magnetostatic properties of Al-doped yttrium iron garnets** **88**
V. Yu. Borynskyi[1], A. F. Kravets[1], D. L. Popadiuk[1], Yu. Yu. Shlapa[2], S. O. Solopan[2], A. G. Belous[2], A. I. Tovstolytkin[1]
[1] *Institute of Magnetism of the NAS of Ukraine and MES of Ukraine, Kyiv, Ukraine*
[2] *V.I. Vernadsky Institute of General and Inorganic Chemistry, Kyiv, Ukraine*

P23 **Lattice dynamics in the thiospinel $CuIr_2S_4$: Raman spectroscopic studies across the metal-insulator transition** **89**
A. Glamazda[1,3], V. Gnezdilov[1,2], V. Tsurkan[4,5], P. Lemmens[2,6]
[1] *B. Verkin Institute for Low Temperature Physics and Engineering, Kharkiv, Ukraine*
[2] *Institute of Condensed Matter Physics, TU Braunschweig, Braunschweig, Germany*
[3] *V. N. Karazin Kharkiv National University, Kharkiv, Ukraine*
[4] *Experimental Physics V, Center for Electronic Correlations and Magnetism, University of Augsburg, Augsburg, Germany*
[5] *Institute of Applied Physics, Moldova State University, Chisinau, Moldova*
[6] *Laboratory of Emerging Nanometrology LENA, Braunschweig, Germany*

P24 **Magnetic Properties of Low-dimensional Spin System Formed by Spin-1/2 XX Chains Coupled through Ising Spins** **90**
E. V. Ezerskaya, A. O. Kabatova, S. Ye. Kononenko
V. N. Karazin Kharkiv National University, Kharkiv, Ukraine

P25 **On the Energy Spectrum and Magnetic Properties of Quasi-One-Dimensional Branched Spin Chain** **91**
E. V. Ezerskaya, D. D. Kolesnyk
V. N. Karazin Kharkiv National University, Kharkiv, Ukraine

P26 **Low Temperature Magnetic Properties of Anisotropic Spin Ladder Systems** **92**
V. O. Cheranovskii, E. V. Ezerskaya, S. Ye. Kononenko
V. N. Karazin Kharkiv National University, Kharkiv, Ukraine

P27 **Tunnel Magnetic Contacts with Perpendicular Anisotropy of Magnetic Electrodes as Promising Elements for Recording Information** **93**
M. M. Krupa
Institute of Magnetism of the NAS of Ukraine and MES of Ukraine, Kyiv, Ukraine

17:50-18:05 **All participants of Stage 2 (short presentation one by one for 1,5 – 2 minutes)**

18:05-18:20 **Breakout Rooms Stage 2**

P28 **The possibility of existence the magnetic field induced structural phase transition in $KEr(MoO_4)_2$** **94**

N. Nesterenko[1], K. Kutko[1], B. Bernáth[2], D. Kamenskyi[3]

[1] B.Verkin Institute for Low Temperature Physics and Engineering, Kharkiv, Ukraine
[2] High Field Magnet Laboratory (HFML - EMFL) Radboud University, Nijmegen, The Netherlands
[3] Experimental Physics V, Center for Electronic Correlations and Magnetism, Institute of Physics, University of Augsburg, Augsburg, Germany

P29 **Magnetic susceptibility as a tool for studying the phenomenon of mixed valence in SmB_6** **95**

A. A. Lyogenkaya[1], A. S. Panfilov[1], V. A. Desnenko[1], G. E. Grechnev[1], and N. Yu. Shitsevalova[2]

[1] B. Verkin Institute for Low Temperature Physics and Engineering, Kharkiv, Ukraine
[2] Institute for Problems of Materials Science of the NAS of Ukraine, Kyiv, Ukraine

P30 **Position of optical axes of magnetized along tetragonal axis antiferromagnetic garnet $Ca_3Mn_2Ge_3O_{12}$** **96**

O. V. Bibik[2], O. V. Myloslavska[1], Yu. Kharchenko[1], M. Kharchenko[1]

[1] B.Verkin Institute for Low Temperature Physics and Engineering, Kharkiv, Ukraine
[2] Georgia Institute of Technology | GT · School of Aerospace Engineering Atlanta, Georgia, USA

P31 **Spectroscopic peculiarities of a trigonal $TbAl_3(BO_3)_4$ single crystal** **97**

A. V. Peschanskii[1], A. Yu. Glamazda[1,2]

[1] B. Verkin Institute for Low Temperature Physics and Engineering, Kharkiv, Ukraine
[2] V. N. Karazin Kharkiv National University, Kharkiv, Ukraine

P32 **Determination of Nd-Fe exchange interaction signs in excited states of Nd^{3+} in $NdFe_3(BO_3)_4$ crystal using optical spectroscopy** **98**

V. G. Piryatinskaya, V. S. Kurnosov, I. S. Kachur

B. Verkin Institute for Low Temperature Physics and Engineering, Kharkiv, Ukraine

P33 **Impact of the magnetic Fe^{3+} ions substitution by nonmagnetic Ga^{3+} on the properties of holmium iron borate** **99**

Yu. Savina[1], O. Bludov[1], V. Pashchenko[1], T. Zajarniuk[2], A. Lynnyk[2], M.U. Gutowska[2], A. Szewczyk[2]

[1] B. Verkin Institute for Low Temperature Physics and Engineering, Kharkiv, Ukraine
[2] Institute of Physics, Polish Academy of Sciences, Warsaw, Poland

P34 **Nickel-zinc spinel ferrites: Synthesis and magnetic characterization** **100**

V. O. Zamorskyi[1], A. F. Kravets[1], D. L. Popadiuk[1], Yu. Yu. Shlapa[2], S. O. Solopan[2], A.G. Belous[2], A. I. Tovstolytkin[1]

[1] Institute of Magnetism of the NAS of Ukraine and MES of Ukraine, Kyiv, Ukraine
[2] V.I. Vernadsky Institute of General and Inorganic Chemistry of the NAS of Ukraine, Kyiv, Ukraine

OPTICS, PHOTONICS AND OPTICAL SPECTROSCOPY

Chairs *Sergii Poperezhai and Yuliya Savina*

18:25-18:40 **All participants of Stage 3 (short presentation one by one for 1,5 – 2 minutes)**

18:40-18:55 **Breakout Rooms Stage 3**

P35 **Temperature-dependent operation of laser passive Q-switches based on polyurethane matrices** **107**
T. Bezrodna[1], V. Bezrodnyi[1], A. Negriyko[1], L. Kosyanchuk[2], O. Antonenko[2], V. Nesprava[1]
[1] *Institute of Physics NAS of Ukraine, Kyiv, Ukraine*
[2] *Institute of Macromolecular Chemistry NAS of Ukraine, Kyiv, Ukraine*

P36 **First-principles investigation of optical features for gyrotropic α-$Hg_3S_2Cl_2$ polymorph** **108**
O. V. Bokotey[1], T. V. Vu[2], O. O. Bokotey[1], A. G. Slivka[1]
[1] *Faculty of Physics, Uzhhorod National University, Ukraine*
[2] *Laboratory for Computational Physics, Institute for Computational Science and Artificial Intelligence, Van Lang University, Ho Chi Minh City, Vietnam*

P37 **Spectral characteristics of three-particle ionic molecular system of the exotic Carbon atom in one-dimensional space** **109**
A. I. Haysak[1], M. I. Haysak[2]
[1] *Uzhhorod National University, Uzhhorod, Ukraine*
[2] *Institute of Electron Physics NASc of Ukraine, Uzhhorod, Ukraine*

P38 **Emission of monochromatic sub-THz radiation by IR-active phonons in KY(MoO4)2** **110**
D. Kamenskyi[1,2,3], K. Vasin[3], K. Kutko[4], V. Khrustalyov[4], S. G. Pavlov[1], H.-W. Hübers[1,2]
[1] *Institute of Optical Sensor Systems, German Aerospace Center (DLR), Berlin, Germany*
[2] *Department of Physics, Humboldt-Universität zu Berlin, Berlin, Germany*
[3] *Experimental Physics V, Center for Electronic Correlations and Magnetism, Institute of Physics, University of Augsburg, Augsburg, Germany*
[4] *B. Verkin Institute for Low Temperature Physics and Engineering, Kharkiv, Ukraine*

P39 **Enhancement of local fields in the vicinity of biconic and bipyramidal metal nanoparticles** **111**
A. V. Korotun[1,2]
[1] *National University Zaporizhzhia Politechnic, Zaporizhzhya, Ukraine*
[2] *G.V. Kurdyumov Institute for Metal Physics of the NAS of Ukraine, Kyiv, Ukraine*

P40 **Frequency splitting of surface plasmon resonance in a cylindrical shell of variable thickness** **112**
R. O. Malysh[1], A. V. Korotun[1,2], I. M. Titov[1]
[1] *National University Zaporizhzhia Politechnic, Zaporizhzhia, Ukraine*
[2] *G.V. Kurdyumov Institute for Metal Physics of the NAS of Ukraine, Kyiv, Ukraine*

P41 **Methodology for studying the properties of gas discharge plasma in mixtures of inert gases with chalcogen atoms vapours** **117**
A. General, E. Svitlichnyi
Institute of Electron Physics of NAS of Ukraine, Uzhhorod, Ukraine

19:00-19:15 **All participants of Stage 4 (short presentation one by one for 1,5 – 2 minutes)**

19:15-19:30 **Breakout Rooms Stage 4**

P42 **Radiation efficiency of an ensemble of disk-shaped plasmonic nanoparticles** **114**
N. I. Pavlyshche[1], A. V. Korotun[1,2], V. P. Kurbatsky[1]
[1] National University Zaporizhzhia Politechnic, Zaporizhzhia, Ukraine
[2] G.V. Kurdyumov Institute for Metal Physics of the NAS of Ukraine, Kyiv, Ukraine

P43 **Color centers in undoped lithium fluoride LiF** **115**
O.M. Pop, V.I. Roman, I.H. Megela, V.T. Maslyuk, I.V. Pylypchynets, E.V. Olejnikov, O.O. Papp
Institute of Electron Physics of NAS of Ukraine, Uzhhorod, Ukraine

P44 **Time limits for measurement of gravitational waves with dynamical Casimir effect in solid-state detectors** **116**
A. M. Sokolov
Institute of Physics of the National Academy of Sciences, Kyiv, Ukraine

P45 **Optical response of chains of oblate metal nanospheroids on a dielectric substrate** **113**
M. S. Maniuk[1], A. V. Korotun[1,2], V. P. Kurbatsky[1]
[1] National University Zaporizhzhia Politechnic, Zaporizhzhia, Ukraine
[2] G.V. Kurdyumov Institute for Metal Physics of the NAS of Ukraine, Kyiv, Ukraine

P46 **Experimental setup for spraying chalcogens onto a surface in a gas discharge** **118**
A. Minya[1], E. Svitlichnyi[2]
[1] Uzhgorod National University, Uzhgorod, Ukraine
[2] Institute of Electron Physics of NAS of Ukraine, Uzhhorod, Ukraine

P47 **Relevance and prospects for studying low-temperature photoluminescence of GO of various morphologies and its derivatives with impurities** **119**
V. N. Zoryansky, P. V. Zinoviev
B. Verkin Institute for Low Temperature Physics and Engineering, Kharkiv, 61103, Ukraine

WEDNESDAY, 5th of JUNE

PLENARY LECTURES OF INVITED SPEAKERS

Chair *Diana Hurova*

10:00-10:30 **Swift Ion Irradiation Related to Complex Organic Molecules in Cold Space Environments** **43**
P. Boduch, A. Domaracka, H. Rothard
Centre de Recherche sur les Ions, les Matériaux et la Photonique, Normandie Univ, ENSICAEN, UNICAEN, CEA, CNRS, CIMAP, Caen 14000, France

10:30-11:00 **Contribution of mass spectrometry to molecular biophysics of nucleic acids** **37**
M. V. Kosevich
B. Verkin Institute for Low Temperature Physics and Engineering, Kharkiv, Ukraine

BIOPHYSICS AND PHYSICS OF MACROMOLECULES

Chair *Diana Hurova*

11:00-11:15 **Characterization of graphene oxide by Raman spectroscopy and atomic force microscopy** **157**

A. Glamazda[1,2], A. Linnik[1], O. Lytvyn[3], V. Karachevtsev[1]
[1] *B.Verkin Institute for Low Temperature Physics and Engineering, Kharkiv, Ukraine*
[2] *V. N. Karazin Kharkiv National University, Kharkiv, Ukraine*
[3] *Borys Grinchenko Kyiv University, Kyiv, Ukraine*

11:15-11:30 **Biopharmaceutical studies of a novel sedative drug based on glycine and tryptophan in model membrane medium: revealing of bioavailability and synergistic properties** **163**

O. V. Vashchenko[1], R. Ye. Brodskii[2], I. O. Davydova[3], P. V. Vashchenko[1], O. I. Ivaniuk[3], O. A. Ruban[3]
[1] *Institute for Scintillation Materials of NAS of Ukraine, Kharkiv, Ukraine*
[2] *Institute for Single Crystals of NAS of Ukraine, Kharkiv, Ukraine*
[3] *National University of Pharmacy, Kharkiv, Ukraine*

11:30-11:45 **Electronic transport in composite film of reduced graphene oxide with molybdenum disulfide** **159**

N. V. Kurnosov[1], A. M. Plokhotnichenko[1], V. A. Karachevtsev[1]
B. Verkin Institute for Low Temperature Physics and Engineering, Kharkiv, Ukraine

11:45-12:00 **Metal-dielectric metasurface sensoring structure for IgG/glucose concentration determination in solutions** **160**

K. S. Kuznetsova[1], V. A. Pashynska[1, 2], Z. E. Eremenko[1,3]
[1] *Usikov Institute for Radiophysics and Electronics of the NAS of Ukraine, Kharkiv Ukraine*
[2] *B. Verkin Institute for Low Temperature Physics and Engineering, Kharkiv, Ukraine*
[3] *Leibniz Institute for Solid State and Materials Research, Dresden, Germany*

12:00-12:15 **Biologically significant intermolecular interactions of doxorubicin with phospholipids and supporting drug molecules** **161**

V. A. Pashynska[1], V. O. Karachevtsev[1], A. Gomory[2], L. Drahos[2]
[1] *B. Verkin Institute for Low Temperature Physics and Engineering, Kharkiv, Ukraine*
[2] *Institute of Organic Chemistry of the HUN-REN Research Center for Natural Sciences, Budapest, Hungary*

12:15-12:30 **Influence of structural defects in MoS_2 on interaction with biological molecules** **162**

T. Piddubnyi[1], S. Stepanian[1], L. Adamowicz[2]
[1] *B. Verkin Institute for Low Temperature Physics and Engineering, Kharkiv, Ukraine*
[2] *Department of Chemistry and Biochemistry, University of Arizona, Tucson AZ, USA*

12:30-12:45 **Mathematical modeling of the freezing zone temperature dynamics of the hydrogel for cryoablation and cryotherapy applications** **158**

O. V. Ivakhnenko[1,2], S. N. Shevchenko[1], and O. F. Todrin[3]
[1] *B.Verkin Institute for Low Temperature Physics and Engineering, Kharkiv, Ukraine*
[2] *Theoretical Quantum Physics Laboratory, Cluster for Pioneering Research, RIKEN, Wako, Saitama Japan*
[3] *Institute for Problems of Cryobiology and Cryomedicine, Kharkiv, Ukraine*

12:45-14:00 **BREAK**

PLENARY LECTURES OF INVITED SPEAKERS

Chair *Diana Hurova*

14:00-14:30 **War-derived nanohybrids composed of carbon-containing smoke nanoparticles, copper and sulphur compounds poses health hazard** **32**
G. Dovbeshko[1,2], O. Gnatyuk[1,2], V. Boiko[1,2], N. Kirsanova[1,3], O. Bezkrovnyi[1], N. Pozdnyakova[1,3], W. Strek[1], T. Borisova[1,3]
[1] Institute of Low Temperature and Structure Research, Wrocław, Poland
[2] Institute of Physics of National Academy of Sciences of Ukraine, Kyiv, Ukraine
[3] O.V. Palladin Institute of Biochemistry of NAS of Ukraine, Kyiv, Ukraine

14:30-15:00 **DNA as an exemplary polymer** **39**
Oleg Krichevsky
Physics Department, Ben-Gurion University of the Negev, Beer-Sheva, Israel

OPTICS ROUND TABLE

Chair *Maksym Barabashko*

15:00-15:30 **International opportunities for researchers: Light of your future career**
Nataliia Mysko-Krutik
Ruhr-Universität, Bochum, Germany

15:30-16:00 **Communicating Technical Expertise to Non-Technical Audiences**
Olha Kravchuk
Kharkiv National University of Radio Electronics, Kharkiv, Ukraine

16:00-16:20 **Photonics Cluster Ukraine** **50**
K. Gorokhovskyi
Public Union Photonics Cluster Ukraine, Kyiv, Ukraine

16:20-16:40 **BREAK**

16:40-19:00 **POSTER SESSION (5 AND 6 SECTIONS)**

NANOPHYSICS AND NANOTECHNOLOGIES

Chairs *Maksym Barabashko and Diana Hurova*

16:40-16:55 **All participants of Stage 1 (short presentation one by one for 1,5 – 2 minutes)**

16:55-17:10 **Breakout Rooms Stage 1**

P48 **Aluminium doped ZnO thin films** **143**
V. V. Zaika, N. K. Shvachko, I. V. Sukhenko, V. L. Karbivskyy
G. V. Kurdyumov Institute for Metal Physics of NAS of Ukraine, Kyiv, Ukraine

P49 **Modeling and calibration of the electrical features of submicron p-n and p-i-n junction structures based on Si and GaAs over a broad temperature.** **144**
J. Sh. Abdullayev, I. B. Sapaev
National Research University TIIAME, Tashkent, Uzbekistan

P50 **On the Energy Spectrum and Magnetic Properties of low-dimensional spin systems of complex topology** **145**
K. S. Dzhenzherova, O. S. Dzhenzherov, E. V. Ezerskaya, V. O. Kovalenko
V. N. Karazin Kharkiv National University, Kharkiv, Ukraine

P51 **Influence of the defects on the behavior of the heat capacity of MWCNTs with Ø9.4 nm** **146**
M. I. Bagatskii[1], V. V. Sumarokov[1], M. S. Barabashko[1], A. I. Krivchikov[1], A. Jeżowski[2], D. Szewczyk[2,3]
[1] B. Verkin Institute for Low Temperature Physics and Engineering, Kharkiv, Ukraine
[2] W. Trzebiatowski Institute for Low Temperatures and Structure Research, Wroclaw, Poland
[3] Low Temperature Laboratory, Condensed Matter Physics Department, Universidad Autónoma de Madrid, Madrid, Spain

P52 **Raman, UV-Vis, MS and IR Characterization of Molecular-Colloidal Solution of Hydrated Fullerenes C_{60} Obtained Using Vacuum-Sublimation Cryogenic Deposition Method** **147**
R. M. Basnukaeva[1], S. V. Cherednichenko[1], G. V. Andrievsky[2], N. A. Vinnikov[1], A. V. Dolbin[1], M. V. Kosevich[1], V. S. Shelkovsky[1], L. M. Buravtseva[1], G. I. Dovbeshko[3,4], O. P. Gnatyuk[3], O. Bezkrovnyi[4], M. Ptak[4], M. Chaika[4], P. O. Kuzema[5]
[1] B. Verkin Institute for Low Temperature Physics and Engineering, Kharkiv, Ukraine
[2] Institute of Physiologically Active Compounds LLC, Kharkiv, Ukraine,
[3] Institute of Physics of the National Academy of Sciences of Ukraine, Kiev, Ukraine
[4] Institute of Low Temperatures and structural Research PAS, Wroclaw, Poland
[5] Chuiko Institute of Surface Chemistry of NAS of Ukraine, Kyiv, Ukraine

P53 **Electron excitation energy transfer in mixed krypton-xenon clusters** **148**
Yu. S. Doronin, A. A. Tkachenko, V. L. Vakula, G. V. Kamarchuk, O. G. Danylchenko and O. P. Konotop
B. Verkin Institute for Low Temperature Physics and Engineering, Kharkiv, Ukraine

17:15-17:30 **All participants of Stage 2 (short presentation one by one for 1,5 – 2 minutes)**

17:30-17:45 **Breakout Rooms Stage 2**

P54 **Mechanical stability and electronic properties of heterostructures based on β-InSe/$MoSe_2$** **149**
O. I. Korolov, K. E. Glukhov, L. Yu. Kharkhalis
Institute for Physics and Chemistry of Solid State, Uzhhorod National University, Uzhhorod, Ukraine

P55 **Electronic and Sensing Properties of ZnO Nanoribbons: a DFT Analysis** **150**
M. Kovalenko, O. Bovgyra, D. Malanchuk
Ivan Franko National University of Lviv, Lviv, Ukraine

P56 **Magnetotransport properties of carbon nanotubes decorated with magnetic alloys** **151**
I. Ovsiienko[1], D. Shpylka[1], D. Zaiatc[1], T. Len[1], L. Matzui[1], I. Mirzoiev[2], E. Beliayev[2]
[1] Taras Shevchenko National University of Kyiv, Departments of Physic, Kyiv, Ukraine
[2] B. Verkin Institute for Low Temperature Physics and Engineering, Kharkiv, Ukraine

P57 **Reversible luminescent hydrogen peroxide sensors based on CeO_{2-x} and CeO_{2-x}:Eu^{3+} nanocrystals** **152**
P. Maksimchuk[1], Ye. Neuhodov[1], K. Hubenko[1], A. Onishchenko[2], S. Yefimova[1], V. Seminko[1]
[1] Institute for Scintillation Materials NAS of Ukraine, Kharkiv, Ukraine
[2] Kharkiv National University of Radio Electronics, Kharkiv, Ukraine

P58 **Modification of transmission gaps by an optical field in a molecular field-effect transistor** **139**
V.O. Leonov, E.G. Petrov, Ye.V. Shevchenko
Bogolyubov Institute for Theoretical Physics of NAS of Ukraine, Kyiv, Ukraine

BIOPHYSICS AND PHYSICS OF MACROMOLECULES

Chairs *Maksym Barabashko and Diana Hurova*

17:50-18:05 **All participants of Stage 3 (short presentation one by one for 1,5 – 2 minutes)**

18:05-18:20 **Breakout Rooms Stage 3**

P59 **Binding characteristics of systemic glucocorticoids with the SARS-CoV-2 spike glycoprotein: in-silico evaluation** **164**
N. V. Khmil[1,2], V. G. Kolesnikov[1], A. O. Boiechko-Nemovcha[2]
[1] O. Ya. Usikov Institute for Radiophysics and Electronics of NAS of Ukraine, Kharkiv, Ukraine
[2] Kharkiv National University of Radio Electronics, Kharkiv, Ukraine,

P60 **Intermolecular interactions of glutathione with molybdenum disulfide probed by laser desorption/ionization mass spectrometry** **165**
O. A. Boryak[1], V. A. Pashynska[1], M. V. Kosevich[1], P. O. Kuzema[2], V. A. Karachevtsev[1]
[1] B. Verkin Institute for Low Temperature Physics and Engineering, Kharkiv, Ukraine
[2] Chuiko Institute of Surface Chemistry of the NAS of Ukraine, Kyiv, Ukraine

P61 **Analysis of cholinomimetic pharmacological properties of a new agonist of muscarinic cholinergic receptors** **166**
T. O. Fedirko[1], O. V. Tsymbalyuk[1], I. S. Voiteshenko[1], S. A. Starosyla[2], V. G. Bdzhola[3], A. O. Prykhod'ko[3], A. Yu. Nyporko[1]
[1] Taras Shevchenko National University of Kyiv, Kyiv, Ukraine
[2] Receptor AI Inc., 20-22 Wenlock Road, London N1 7GU, United Kingdom
[3] Institute of Molecular Biology and Genetics of NAS of Ukraine, Kyiv, Ukraine

P62 **The influence of the type of charged particles on the parameters of zigzag patterns in BSA films** **167**
D. Glibitskiy[1], O. Gorobchenko[2], O. Nikolov[2], T. Dzhimieva[2], I. Zaitseva[2,3], A. Roshal[4], M. Semenov[1], G. Glibitskiy[1]
[1] O. Ya. Usikov Institute for Radiophysics and Electronics, NAS of Ukraine, Kharkiv, Ukraine;
[2] V. N. Karazin Kharkiv National University, Kharkiv, Ukraine;
[3] O. M. Beketov National University of Urban Economy in Kharkiv, Kharkiv, Ukraine;
[4] Institute for Chemistry, V. N. Karazin Kharkiv National University, Kharkiv, Ukraine

P63 **Immobilization of glucose oxidase on graphene using 1-pyrenebutanoic acid succinimide ester: molecular dynamics study** **168**
M. V. Karachevtsev, V. A. Karachevtsev
B.Verkin Institute for Low Temperature Physics and Engineering, Kharkiv, Ukraine

P64 **Fluorescence responses of silica gel films with two coumarin dyes measured on a portable endogenous acetone analyzer in the microconcentration range** **169**
Ya. P. Lazorenko, V. P. Mitsai
Institute of Magnetism NAS of Ukraine and MES of Ukraine, Kyiv, Ukraine

P65 **Study of fluorescent responses of film polymer structures with dyes and quantum dots using a model of a portable analyzer of endogenous ammonia trace concentrations** **170**
V. P. Mitsai, Ya. P. Lazorenko
Institute of Magnetism NAS of Ukraine and MES of Ukraine, Kyiv, Ukraine

18:25-18:40 **All participants of Stage 4 (short presentation one by one for 1,5 – 2 minutes)**

18:40-19:00 **Breakout Rooms Stage 4**

P66 **Binding of Pheophorbide-*a* and its Derivatives to Biopolymers of Different Composition and Secondary Structure: a Spectroscopic Study** **171**
O. A. Ryazanova[1], I. M. Voloshin[1], L. V. Dubey[2], I. Ya. Dubey[2], and V. A. Karachevtsev[1]
[1] B.Verkin Institute for Low Temperature Physics and Engineering, Kharkiv, Ukraine
[2] Institute of Molecular Biology and Genetics of NAS of Ukraine, Kyiv, Ukraine

P67 **Mass spectrometric probing of nanocomposite of methylene blue with molybdenum disulfide flakes** **172**
V. S. Shelkovsky[1], O. A. Boryak[1], M. V. Kosevich[1], P. O. Kuzema[2], V. A. Karachevtsev[1]
[1] B. Verkin Institute for Low Temperature Physics and Engineering, Kharkiv, Ukraine
[2] Chuiko Institute of Surface Chemistry of the NAS of Ukraine, Kyiv, Ukraine

P68 **The comparative characterization of DNA:TiO_2 nanoparticle and DNA:MoS_2 nanoparticle nanoassemblies colloidal solutions investigated by dynamic light scattering method** **173**
A. Yu. Svidzerska[1], V. A. Valeev[1], A. N. Lahuta[2,3], S. I. Petrushenko[2], A. Yu. Glamazda[1], V. A. Karachevtsev[1]
[1] B.Verkin Institute for Low Temperature Physics and Engineering, Kharkiv, Ukraine
[2] V.N. Karazin Kharkiv National University, Kharkiv, Ukraine
[3] Aston University, Birmingham B4 7ET, U.K.

P69 **Effect of TiO_2 nanoparticles on the thermal stability of native DNA under conditions close to physiological ones** **174**
E. L. Usenko, A. Yu. Glamazda, V. A. Valeev, V. A. Karachevtsev
B. Verkin Institute for Low Temperature Physics and Engineering, Kharkiv, Ukraine

P70 **PEGylation of cytosine nucleic acid base: experiment and modeling** **175**
V. G. Zobnina, M. V. Kosevich
B. Verkin Institute for Low Temperature Physics and Engineering, Kharkiv, Ukraine

P71 **The effect of glycocalyx on the partitioning of antimicrobial peptides into plasma membrane of erythrocytes** **176**
O. Yu. Borikov, D. A. Liadov, V. P. Berest
V.N. Karazin Kharkiv National University, 4 Svobody Sq., Kharkiv, 61022, Ukraine

THURSDAY, 6th of JUNE

PLENARY LECTURES OF INVITED SPEAKERS

Chair *Anna Herus*

10:00-10:30 **Leverage cloud technologies for enhanced research data accessibility and more effective scientific collaboration** **35**
Philipp Jaeger
Pexon Consulting GmbH, Eschborn, Germany

TECHNOLOGIES AND INSTRUMENTATION FOR PHYSICAL EXPERIMENTS

Chair *Anna Herus*

10:30-10:45 **Control of the effective value of b_L parameter in an RF SQUID by the high-frequency electromagnetic field** **235**
V. I. Shnyrkov[1,2], V. Yu. Lyakhno[1,3], O. G. Turutanov[4,3], O. O. Leha[3]
[1] *G.V. Kurdyumov Institute for Metal Physics, N.A.S. of Ukraine, Kyiv, Ukraine*
[2] *Kiev Academic University, Kiev, Ukraine*
[3] *B.Verkin Institute for Low Temperature Physics and Engineering, Kharkiv, Ukraine*
[4] *Department of Experimental Physics, Comenius University, Bratislava, Slovakia*

10:45-11:00 **System spectral analysis of infrasonic waves in the atmosphere caused by a powerful explosion of a unique volcano** **236**
L. F. Chernogor[1], O. I. Liashchuk[2], M. B. Shevelev[1], N. M. Tilichenko[1]
[1] *V.N. Karazin Kharkiv National University, Kharkiv, Ukraine*
[2] *Main Center of Special Monitoring, urban village Gorodok, Zhitomir region, Ukraine*

PLENARY LECTURES OF INVITED SPEAKERS

Chair *Yevhen Petrenko*

11:00-11:30 **Exploring the Unified Theory of Thermal Transport: Experimental Insights, Predictive Precision, and Phenomenological Implications** **47**
D. Szewczyk[1], A. I. Krivchikov[1,2], A. Jeżowski[1]
[1] *Institute for Low Temperatures and Structure Research, Wroclaw, Poland*
[2] *B. Verkin Institute for Low Temperature Physics and Engineering, Kharkiv, Ukraine*

11:30-12:00 **Functional properties of Ni-Mn-based alloys: Theory and experiment** **38**
Anna Kosogor[1,2]
[1] *Institute of Magnetism NASU and MESU, Kyiv, Ukraine*
[2] *University of Vienna, Faculty of Physics, Vienna, Austria*

12:00-12:30 **Topological semimetals in heavy fermion compounds** **51**
Silke Paschen
Institute of Solid State Physics, Vienna University of Technology, Vienna, Austria

MATERIALS SCIENCE

Chair *Yevhen Petrenko*

12:30-12:45 **First-principles study of point defects in C-doped yttrium aluminum garnet** **179**
K. V. Hermash[1], D. V. Fil[1,2]
[1] *Institute for Single Crystals of NAS of Ukraine, Kharkiv, Ukraine*
[2] *Karazin Kharkiv National University, Kharkiv, Ukraine*

12:45-13:00 **Ring and linear structures of CdTe clusters** **180**
I. V. Semkiv[1], M. Y. Rudysh[2, 3], R. S. Yavorskyi[4], N. Y. Kashuba[1], P. A. Shchepanskyi[2], A. I. Kashuba[1]
[1] *Lviv Polytechnic National University, Lviv, Ukraine*
[2] *Ivan Franko National University of Lviv, Lviv, Ukraine*
[3] *Jan Długosz University in Częstochowa, Częstochowa, Poland*
[4] *Vasyl Stefanyk Precarpathian National University, Ivano-Frankivsk, Ukraine*

13:00-14:00 **BREAK**

MATERIALS SCIENCE

Chair *Yevhen Petrenko*

14:00-14:15 **Influence of Long-Term Exposure on Mechanical Properties of Polyimide Kapton H Films** **182**
V. A. Lototskaya, L. F. Yakovenko
B. Verkin Institute for Low Temperature Physics and Engineering, Kharkiv, 61103, Ukraine

14:15-14:30 **Radiation-Induced Effects in Polyimide Kapton H Films of Different Thicknesses. Influence on Mechanical Properties** **183**
V. A. Lototskaya, L. F. Yakovenko, G. I. Saltevskiy, I. P. Zaritskiy, Yu. S. Doronin, A. A. Tkachenko
B.Verkin Institute for Low Temperature Physics and Engineering, Kharkiv, 61103, Ukraine

14:30-14:45 **Hysteresis phenomena in $Cd_2P_2S_6$ layered crystals** **184**
H. Ban, D. Gal, S. Motrja, A. Molnar
Uzhhorod National University, Department of the Physics of Semiconductors, Uzhhorod, Ukraine

14:45-15:00 **Multiple phase transitions in thin ethanol films obtained by physical deposition from the gas phase** **185**
A. Aldiyarov[1], D. Yerezhep[1,2,3], D. Yu. Sokolov[1,4], E. Korshikov[1], A. Nurmukan[1]
[1] *Al-Farabi Kazakh National University, Almaty, Kazakhstan*
[2] *Satbayev University, Almaty, Kazakhstan*
[3] *Institute of Physics and Technology, Satbayev University, IAlmaty, Kazakhstan*
[4] *Almaty Technological University, Almaty, Kazakhstan*

15:00-15:15 **Thermal conductivity of epoxy resin polymer composites with thermally reduced graphene oxide** **186**
V. V. Sagan[1], A. I. Krivchikov[1], A. Jeżowski[2]
[1] *B. Verkin Institute for Low Temperature Physics and Engineering, Kharkiv, Ukraine*
[2] *Institute of Low Temperature and Structure Research, Wroclaw, Poland*

15:15-15:30 **Peculiarities of lattice dynamics of cadmium iodide and its appearance in photoelectric effects** **187**
M. Rudka[1], M. Orendáč[2], R. Tarasenko[2], M. Karkuliovska[1], N. Tovstyuk[1], B. Seredyuk[3]
[1] *Lviv Polytechnic National University, Lviv, Ukraine,*
[2] *Institute of Physics, Faculty of Science, P.J. Šafárik University, Košice, Slovakia*
[3] *Hetman Petro Sahaidachnyi National Army Academy, Lviv, Ukraine,*

15:30-15:45 **Conditions for the formation of new structural phases in BEDT-TTF** **188**
Y. M. Trotskyi[1], E. S. Syrkin[1], V. O. Lykah[2]
[1] *B.Verkin Institute for Low Temperature Physics and Engineering, Kharkiv, Ukraine*
[2] *National Technical University "Kharkiv Polytechnic Institute", Kharkiv, Ukraine*

15:45-16:20 **BREAK**

16:20-19:05 **POSTER SESSION (7 AND 9 SECTIONS)**

TECHNOLOGIES AND INSTRUMENTATION FOR PHYSICAL EXPERIMENTS

Chairs *Yevhen Petrenko and Diana Hurova*

16:20-16:30 **All participants of Stage 1 (short presentation one by one for 1,5 – 2 minutes)**

16:30-16:45 **Breakout Rooms Stage 1**

P72 **Microcomputers' applications at robotic medical systems prototypes** **237**
V. V. Anufriiev, O. O. Kravchuk, E. P. Fedorenko
Kharkiv National University of Radio Electronics, Kharkiv, Ukraine

P73 **Development of low-temperature cell for IR Fourier-spectroscopy of hydrocarbon materials** **238**
A. Kenbay[1], D. Yerezhep[2], A. Aldiyarov[1], E. Korshikov[1]
[1] Al-Farabi KazNU, Almaty, Kazakhstan
[2] Satbayev University, Almaty, Kazakhstan

P74 ***In vitro* pilot study of temperature field dynamics with cryoimpact** **239**
G. Kovalov[1], M. Chyzh[1], V. Globa[1], G. Shustakova[2], Yu. Fomenko[2], E. Gordienko[2], D. Nikolenko[3]
[1] Institute for Problems of Cryobiology and Cryomedicine of NAS of Ukraine, Kharkiv, Ukraine
[2] B. Verkin Institute for Low Temperature Physics and Engineering, Kharkiv, Ukraine
[3] V. N. Karazin Kharkiv National University, Kharkiv, Ukraine

P75 **The advanced device for the fine purification of synthetic organic conductors for the quantum point-contact sensors development** **240**
M. Romanov[1], D. Harbuz[1], V. Gudimenko[1], O. Pospelov[2], D. Chudak[3], G. Kamarchuk[1]
[1] B. Verkin Institute for Low Temperature Physics and Engineering, Kharkiv, Ukraine
[2] National Technical University "Kharkiv Polytechnic Institute", Kharkiv, Ukraine
[3] V. Karazin Kharkiv National University, Kharkiv, Ukraine

MATERIALS SCIENCE

Chairs *Yevhen Petrenko and Diana Hurova*

16:50-17:05 **All participants of Stage 2 (short presentation one by one for 1,5 – 2 minutes)**

17:05-17:20 **Breakout Rooms Stage 2**

P76 ***In situ* video recording of crystallization of amorphous Sb_2Se_3 films** **189**
A. G. Bagmut
National Technical University "Kharkiv Polytechnic Institute", Kharkiv, Ukraine

P77 **Optical properties of Tl_3TaSe_4 chalcogenide crystals** **190**
O. V. Bokotey, O. O. Bokotey, P. P. Guranich, A. G. Slivka
Faculty of Physics, Uzhhorod National University, Uzhhorod, Ukraine

P78 **Study of Structural and Mechanical Properties of the Half Heusler Alloy C_2CaNa** **191**
M. E. Ishaje[1], K. A. Minakova[2], V. A. Sirenko[3], I. S. Bondar[3]
[1] Cross River University of Technology, Cross River State. Nigeria
[2] National Technical University Kharkiv Polytechnic Institute, Kharkiv, Ukraine
[3] B. Verkin Institute for Low Temperature Physics and Engineering, Kharkiv, Ukraine

P79 **Relationship between microhardness and yield strength of nanostructured CoCrFeNiMn high-entropy alloy at *T* = 77-290 K** **192**
L. S. Fomenko[1], H. V. Rusakova[1], S. N. Smirnov[1], E. D. Tabachnikova[1], M. A. Tikhonovsky[2], Y. Huang[3], T. Langdon[4]
[1] *B. Verkin Institute for Low Temperature Physics and Engineering, Kharkiv, Ukraine*
[2] *National Science Center "Kharkiv Institute of Physics and Technology", Kharkiv, Ukraine*
[3] *Bournemouth University, Poole, Dorset, UK*
[4] *University of Southampton, Southampton, UK*

P80 **Annealing of PMA polyimide film. X-ray data** **193**
V. Geidarov, I. Braude, Yu. Pohribna
B. Verkin Institute for Low Temperature Physics and Engineering, Kharkiv, Ukraine

P81 **The influence of internal strains induced by hydrogen on the electrical resistivity of the nanocrystalline vanadium film** **194**
A. Grib, A. Kononenko, S. Petrushenko, S. Dukarov
V. N. Karazin National University, Kharkiv, Ukraine

P82 **Strength and plasticity of SPD magnesium alloy at low temperatures** **195**
T. Hryhorova[1], P. Zabrodin[1,2], S. Shumilin[1]
[1] *B. Verkin Institute for Low Temperature Physics and Engineering, Kharkiv, Ukraine*
[2] *Czech Academy of Sciences, Institute of Theoretical and Applied Mechanics, Czech Republic*

17:25-17:40 **All participants of Stage 3 (short presentation one by one for 1,5 – 2 minutes)**

17:40-17:55 **Breakout Rooms Stage 3**

P83 **Thermal conductivity analysis of composites with superlattice structure** **196**
Yu. V. Horbatenko[1], O. O. Romantsova[1,2], A. I. Krivchikov[1], O. A. Koroluyk[1]
[1] *B.Verkin Institute for Low Temperature Physics and Engineering, Kharkiv, Ukraine*
[2] *Institute for Low Temperatures and Structure Research, Wroclaw, Poland*

P84 **Study of the process cryocapture of carbon dioxide molecules by solid water films** **197**
E. Korshikov, A. Aldiyarov, A. Nurmukan, O. Vorobyova, D. Sokolov
Al Farabi Kazakh National University, Almaty, Kazakhstan

P85 **Influence of phase disequilibrium on changes in elastic properties of superplastic eutectic alloys caused by prior plastic deformation and aging** **198**
V. F. Korshak[1], Y. O. Shapovalov[2], P. P. Pal-Val[2], L. N. Pal-Val[2]
[1] *V. N. Karazin Kharkiv National University, Kharkiv, Ukraine*
[2] *B. Verkin Institute for Low Temperature Physics and Engineering, Kharkiv, Ukraine*

P86 **Electronic Structure of Sr-doped $CsPbCl_3$ Crystal: First Principles Investigation** **199**
M. Kovalenko, O. Bovgyra, Ya. Chornodolskyy, O. Pidhornyi
Ivan Franko National University of Lviv, Lviv, Ukraine

P87 **Low-temperature micromechanical properties of epoxy resin/graphene oxide nanocomposites** **206**
H. V. Rusakova, L. S. Fomenko, S. V. Lubenets, A. V. Dolbin, N. A. Vinnikov, R. M. Basnukaeva, S. V. Cherednichenko
B. Verkin Institute for Low Temperature Physics and Engineering, Kharkiv, Ukraine

P88 **Features of thermal transport processes in van der Waals chalcogenides** **201**
V. Liubachko, Yu. Vysochanskii
Institute for Solid State Physics and Chemistry, Uzhhorod National University, Uzhhorod, Ukraine

18:00-18:15 **All participants of Stage 4 (short presentation one by one for 1,5 – 2 minutes)**

18:15-18:30 **Breakout Rooms Stage 4**

P89 **The specificity of the interaction of palladium with hydrogen** **202**
O. M. Liubymenko
Donetsk National Technical University "Donetsk National Technical University", Lutsk, Ukraine

P90 **X-ray determination of the influence of cryodeformation on the microstructure of ultrafine-grained/nanocrystalline titanium** **203**
Yu. M. Pohribna, V. A. Moskalenko
B. Verkin Institute for Low Temperature Physics and Engineering, Kharkiv, Ukraine

P91 **The electric field induced light birefrigence in $HoAl_3(BO_3)_4$** **204**
V. A. Bedarev, D. M. Merenkov, S. M. Poperezhai
B. Verkin Institute for Low Temperature Physics and Engineering, Kharkiv, Ukraine

P92 **Dilatometric properties of Rb_2SO_4 crystals in the region of low temperatures** **205**
I. A. Pryshko[1], V. Yo. Stadnyk[1], O. V. Shtuka[1], I. S. Novosad[1,2]
[1] Physics Faculty, Ivan Franko National University of Lviv, Lviv, Ukraine
[2] Department of General Physics, Lviv Politechnic National University, Lviv, Ukraine

P93 **Temperature-induced phase transformation in $(As_{1-x}Bi_x)_2S_3$ glasses** **200**
S. Hasynets[1], V. Kryshenik[1], A. V. Gomonnai[1,2], V. Lopushansky[1], V. Loya[1], I. Chychura[1], V. Rubish[3]
[1] Institute of Electron Physics of NAS of Ukraine, Uzhhorod, Ukraine
[2] Uzhhorod National University, Uzhhorod, Ukraine
[3] Uzhhorod Laboratory of Institute for Information Recording of NAS of Ukraine, Uzhhorod, Ukraine

P94 **The reverse indentation size effect in heavily deformed materials** **207**
S. V. Lubenets, L. S. Fomenko, H. V. Rusakova
B. Verkin Institute for Low Temperature Physics and Engineering, Kharkiv, Ukraine

18:35-18:50 **All participants of Stage 5 (short presentation one by one for 1,5 – 2 minutes)**

18:50-19:05 **Breakout Rooms Stage 5**

P95 **Nonlinearity effect of highly elastic deformation of an amorphous polymer** **208**
V. D. Natsik, H. V. Rusakova
B. Verkin Institute for Low Temperature Physics and Engineering, Kharkiv, Ukraine

P96 **A study of composition and annealing temperature influence on the mechanical properties of Fe-Cr-Al alloys** **209**
V. O. Kharchenko[1,2], D. O. Kharchenko[1,2], O. M. Shchokotova[1], B. O. Lysenko[1], A. V. Dvornichenko[2]
[1] Institute of Applied Physics, National Academy of Sciences of Ukraine, Sumy, Ukraine
[2] Sumy State University, Sumy, Ukraine

P97 **On the degradation of structural polymers exposed to high-energy atomic oxygen ions** **210**
V. A. Shuvalov, N. B. Gorev, G. S. Kochubei, Yu. P. Kuchugurnyi, N. I. Pismennyi, N. A. Tokmak
Institute of Technical Mechanics, Dnipro, Ukraine

P98 **Deformation behavior of hcp solid solutions Ti-Nb under tension in the temperature range 1.7 - 423 K** **211**
V. A. Moskalenko, R. V. Smolianets
B. Verkin Institute for Low Temperature Physics and Engineering, Kharkiv, Ukraine

P99 **Dislocation mechanisms of low temperature acoustic relaxation and plastic deformation of a high-entropy alloy $Al_{0.5}CoCrCuFeNi$** **212**
Yu. O. Semerenko, V. D. Natsik, E. D. Tabachnikova
B. Verkin Institute for Low Temperature Physics and Engineering, Kharkiv, Ukraine

P100 **The influence of the Gorsky effect on the hydrogen diffusion and the formation of microcracks in vanadium films** **213**
A. Grib, A. Yaroshenko
V. N. Karazin National University, Kharkiv, Ukraine

P101 **Mechanical properties of high-entropy $CoCrFeNiC_x$ alloys at 77 K and 300 K** **181**
A. V. Levenets, V. S. Okovit, M. A. Tikhonovsky, O. M. Velikodnyi
National Science Center "Kharkiv Institute of Physics and Technology" of NAS of Ukraine, Kharkiv, Ukraine

FRIDAY, 7th of JUNE

PLENARY LECTURES OF INVITED SPEAKERS

Chair *Denys Laptev*

10:00-10:30 **Fractional types of statistics: state of the art and some historical flashbacks** **44**
A. Rovenchak
Professor Ivan Vakarchuk Department for Theoretical Physics, Ivan Franko National University of Lviv, Lviv, Ukraine

THEORY OF CONDENSED MATTER PHYSICS

Chair *Denys Laptev*

10:30-10:45 **Spectral characteristics and energy gaps of 2D and 3D quantum many-body systems in thermodynamic limit** **217**
I. V. Lukin[1,2], D. I. Bondar[3], A. G. Sotnikov[1,2]
[1] *Karazin Kharkiv National University, Kharkiv, Ukraine*
[2] *Akhiezer Institute for Theoretical Physics, NSC KIPT, Kharkiv, Ukraine*
[3] *Department of Physics and Engineering Physics, Tulane University, New Orleans, LA, USA*

10:45-11:00 **Quantum control and enhancement of superconducting pairing in one-dimensional Fermi-Hubbard chains** **218**
O. V. Povitchan[1], D. I. Bondar[2], A. G. Sotnikov[1,3]
[1] *V.N. Karazin Kharkiv National University, Kharkiv, Ukraine*
[2] *Department of Physics and Engineering Physics, Tulane University, New Orleans, LA, USA*
[3] *Akhiezer Institute for Theoretical Physics, NSC KIPT, Kharkiv, Ukraine*

11:00-11:15 **Identification of Open Quantum Systems: A Novel Approach Based on Polynomial Optimization** **219**
Z. Popovych, D. Bondar
Department of Physics and Engineering Physics, Tulane University, New Orleans, LA, USA

11:15-11:30 **Effects of symmetry breaking in four component interacting Fermi gas in periodic potential** **220**
V. I. Unukovych[1], A. G. Sotnikov[2]
[1] *V.N. Karazin Kharkiv National University, Kharkiv, Ukraine*
[2] *Akhiezer Institute for Theoretical Physics, NSC KIPT, Kharkiv, Ukraine*

11:30-11:45 **Magnetic states in the XY Heisenberg model on the honeycomb lattice** **221**
I. V. Lukin[1,2], M. O. Luhanko[1], A. G. Sotnikov[1,2]
[1] *Karazin Kharkiv National University, Kharkiv, Ukraine*
[2] *Akhiezer Institute for Theoretical Physics, NSC KIPT, Ukraine*

11:45-12:00 **Residual symmetry and classification of degenerate states of equilibrium SU(4) magnets with spin s=3/2** **222**
M. Yu. Kovalevsky, A. A. Rozhkov
National Scientific Center "Kharkov Physics and Technology Institute" Kharkiv, Ukraine

12:05-12:30 **POSTER SESSION (8 SECTION)**

THEORY OF CONDENSED MATTER PHYSICS

Chairs *Denys Laptev and Diana Hurova*

12:05-12:15 **All participants of Stage 1 (short presentation one by one for 1,5 – 2 minutes)**

12:15-12:30 **Breakout Rooms Stage 1**

P102 **Many-body hamiltonian on the basis of spherical tensor operators for studying collective phenomena in quantum high-spin systems** **229**
M. Bulakhov[1], A. S. Peletminskii[1,2], and Yu. V. Slyusarenko[1,2]
[1] Akhiezer Institute for Theoretical Physics, National Science Center "Kharkiv Institute of Physics and Technology", NAS of Ukraine, Kharkiv, Ukraine
[2] V.N. Karazin Kharkiv National University, Kharkiv, Ukraine

P103 **Calculation of optical modes for chalcogenide compounds $Sn_2P_2X_6$ (X=S, Se)** **230**
V. Yu. Klevets, N. D. Savchenko, A. G. Slivka, A. I. Susla, V. Yu. Bihanych
Uzhhorod National University, Uzhhorod, Ukraine

P104 **Nonequilibrium protection effect and spatial localization of noise-induced fluctuations under gas flow scattering on partially penetrable obstacle** **231**
S. P. Lukyanets, O. V. Kliushnichenko
Institute of Physics of NAS of Ukraine, Kyiv, Ukraine

P105 **Electron-impact excitation and ionization of K atom** **232**
V. Roman
Institute of Electron Physics, National Academy of Sciences of Ukraine, Uzhhorod, Ukraine

12:30-13:30 **BREAK**

PLENARY LECTURES OF INVITED SPEAKERS

Chair *Denys Laptev*

13:30-14:00 **Engineering electronic flat bands in two dimensions** **46**
Yu. Skrypnyk
Bogolyubov Institute for Theoretical Physics of NAS of Ukraine, Kyiv, Ukraine

14:00-14:30 **Controlled rotations of a hot hole spin qubits** **49**
T. Patlatiuk[1], M. J. Carballido[1], S. Svab[1], S. Bosco[2], P. Chevalier Kwon[1], R. Eggli[1], E. Bakkers[3], J. C. Egues[1], D. Loss[1,4], D. Zumbühl[1]
[1] University of Basel, Switzerland
[2] QuTech and Kavli Institute of Nanoscience, Delft University of Technology, Netherlands
[3] Eindhoven University of Technology, Netherlands 4 Instituto de Física de São Carlos, Universidade de São Paulo, São Carlos, Brazil

THEORY OF CONDENSED MATTER PHYSICS

Chair *Denys Laptev*

14:30-14:45 **Dynamics of acoustic superradiance model in the ferromagnetism method** **223**
S. F. Lyagushyn, A. I. Sokolovsky
Oles Honchar Dnipro National University, Dnipro, Ukraine

14:45-15:00 **Application of Langevin dynamics for machine learning and optimization tasks** **224**
O. Borysenko
National Science Center "Kharkiv Institute of Physics and Technology", Kharkiv, Ukraine

15:00-15:150 **Asymmetry-induced ratchet effect in polariton graphene** **225**
O. M. Bahrova[1,2], S. V. Koniakhin[2]
[1] B.Verkin Institute for Low Temperature Physics and Engineering, Kharkiv, Ukraine
[2] Center for Theoretical Physics of Complex Systems, Institute for Basic Science, Daejeon Republic of Korea

15:15-15:30 **Investigation of the opto-electronic properties of $RbGeI_3$ cubic perovskite solar material** **226**
T. Abera
Wachemo University, Hossana, Ethiopia

15:30-15:45 **Reset dynamics of a photon detector based on a flux-biased phase qubit** **227**
O. A. Ilinskaya[1,2], A. I. Ryzhov[1,3], S. N. Shevchenko[1]
[1] B. Verkin Institute for Low Temperature Physics and Engineering, Kharkiv, Ukraine
[2] G. V. Kurdyumov Institute for Metal Physics, Kyiv Ukraine
[3] Theoretical Quantum Physics Laboratory, Cluster for Pioneering Research, RIKEN, Wakoshi, Saitama, Japan

15:45-16:00 **Quantum Signal Processing with adiabatic impulse model** **228**
D. O. Shendryk[1,2,3], O. V. Ivakhnenko[2,4] and S. N. Shevchenko[2]
[1] Ruhr University Bochum, Germany
[2] B. Verkin Institute for Low Temperature Physics and Engineering, Kharkiv, Ukraine
[3] V. N. Karazin Kharkiv National University, Kharkiv, Ukraine
[4] Theoretical Quantum Physics Laboratory, Cluster for Pioneering Research, RIKEN, Wakoshi, Saitama 351-0198, Japan

PLENARY LECTURES OF INVITED SPEAKERS

Chair *Denys Laptev*

16:00-16:30 **Transport signatures of plasmon fluctuations in electron hydrodynamics** **40**
Dmitry Zverevich and Alex Levchenko
Department of Physics, University of Wisconsin-Madison, Madison, USA

16:30-17:00 **Closing Remarks**
Deputy Director of the B. Verkin ILTPE of NAS of Ukraine
Prof. Oleksandr Dolbin
and
Chair of Organizing Committee Diana Hurova

PLENARY LECTURES OF INVITED SPEAKERS

Electronic and Reactive Properties of Nano- and Sub-nano Clusters

Tore Brinck

Department of Chemistry, CBH, KTH Royal Institute of Technology,
SE-100 44 Stockholm, Sweden
e-mail: tore@kth.se

Nanoparticles of metals and metal oxides often have physical and chemical properties that are distinctly different from crystalline materials of the same chemical composition. A classic example is the reactivity of gold; crystalline gold is chemically inert whereas nanoparticles are known to be efficient catalysts. Most commonly, the size dependence of properties has been rationalized in terms of electronic structure modulation due to quantum confinement. However, this rationale is in many instances in disagreement with empirical observations. As an example, the size effect in gold catalysis has been connected to an increasing frequency of low coordinated binding sites, i.e. corners, with diminishing particle size rather than quantum confinement. Moreover, nanostructural effects induced by local structure variations, e.g. steps or dislocations, on crystalline metal surfaces cannot be attributed to a reduction in the translational freedom of electrons.

We have recently shown that the nanostructural effect on the catalytic properties of coinage metals, i.e. Cu, Ag, Au, is a consequence of high positive surface electrostatic potential [$V_S(\mathbf{r})$] at the low-coordinated atomic sites, e.g. the corner of nanoclusters[1,2]. The magnitude of $V_S(\mathbf{r})$ at the corner sites is independent of particle size for symmetrical clusters within the range of 8-512 atoms. In non-symmetrical clusters there is a direct correlation between the $V_S(\mathbf{r})$ maxima and the binding affinity of Lewis bases at those sites. Positive $V_S(\mathbf{r})$ at low coordinated sites are also found for other metals and the magnitude of $V_S(\mathbf{r})$ can be rationalized from the atomic electron configuration by means of the s-hole concept[1-3]. In this presentation, I will discuss how the $V_S(\mathbf{r})$ of nanoclusters and crystalline surfaces can be modulated by changes to the chemical and geometric structure and how the resulting $V_S(\mathbf{r})$ affects physical and chemical properties[1-4]. The procedure for calculating $V_S(\mathbf{r})$ by means of periodic density functional theory will also be described.

In the final part of the talk, I will focus on the recent observation by Savchenko et al. of vibrational fine structure in the g-line of solid N_2 as detected by NIR cathodoluminescence spectroscopy[5]. The potential molecular species behind this observation will be discussed with reference to our earlier quantum chemical studies of sub-nano nitrogen clusters[6,7].

[1] J. H. Stenlid, T. Brinck. *J. Am. Chem. Soc.* **139**, 11012-5 (2017). http://dx.doi.org/10.1021/jacs.7b05987

[2] J. H. Stenlid, A. J. Johansson, T. Brinck. *Phys. Chem. Chem. Phys.* **20**, 2676-92 (2018). http://dx.doi.org/10.1039/C7CP06259A

[3] J. H. Stenlid, A. J. Johansson, T. Brinck. *Crystals* **7**, 222 (2017). http://dx.doi.org/10.3390/cryst7070222

[4] J. H. Stenlid, A. J. Johansson, T. Brinck. *Phys. Chem. Chem. Phys.* **21**, 17001-9 (2019). http://dx.doi.org/10.1039/C9CP03099A

[5] E. V. Savchenko, I. V. Khyzhniy, S. A. Uyutnov, M. A. Bludov. *Low Temp. Phys.* **50**, 89-96 (2024). http://dx.doi.org/10.1063/10.0023897

[6] M. Bittererova, H. Ostmark, T. Brinck. *Chem. Phys. Lett.* **347**, 220-8 (2001).

[7] T. Brinck, M. Bittererova, Ostmark, H. in *Theoretical and Computational Chemistry* (Elsevier, 2002).

War-derived nanohybrids composed of carbon-containing smoke nanoparticles, copper and sulphur compounds poses health hazard

G. Dovbeshko[1,2], O. Gnatyuk[1,2], V. Boiko[1,2], N. Kirsanova[1,3], O. Bezkrovnyi[1], N. Pozdnyakova[1,3], W. Strek[1], T. Borisova[1,3]

[1] Institute of Low Temperature and Structure Research, Polish Academy of Sciences, ul. Okólna 2, 50-422 Wrocław, Poland
[2] Institute of Physics of National Academy of Sciences of Ukraine, 46 Nauky Ave., Kyiv, 03028, Ukraine
[3] O.V. Palladin Institute of Biochemistry of the National Academy of Sciences of Ukraine, 9 Leontovicha Str., Kyiv, 01054, Ukraine
e-mail: matinelli@gmail.com

The air pollution with heavy particles is a significant health hazard. Especially now, as the impact of such pollution is increased due to the explosions and fires caused by the war in Ukraine. Because of the artillery shelling and missile attacks a large amount of smoke enters the atmosphere bearing copper, iron, sulphur, and carbon particles. And this is the main danger, because the toxic effect of such particles can be significantly increased due to the formation of complex nanohybrids in the atmosphere.

In this work, a modelling of such nanohybrids and their characterization using a number of mutually complementary methods is performed. We applied FTIR spectroscopy, optical and electron microscopy, photoluminescence spectroscopy and dynamic light scattering to investigate the structure, morphology, optical and dynamic properties of such nanohybrids. According to SEM and DLS studies, the size of nanoparticles in an aqueous suspension increases with the addition of copper ions. FTIR spectra of poplar smoke display the absorption bands originating from the wood combustion products, cellulose and lignin oxidation products. One of the most toxic components of the wood burning smoke are polycyclic aromatic hydrocarbons, aldehydes, benzopyrene, various solid particles, as well as heavy metal ions. The neurotoxic effects associated with the formation of the nanohybrids comprising metal ions and smoke nanoparticles are discussed.

References

[1]. Galyna Dovbeshko and Tatiana Borisova. War-derived air pollution nanohybrids and their membrane-active properties, Fizyka Nyzkykh Temperatur/Low Temperature Physics, 2024, Vol. 50, No. 3, pp. 205–209.

[2]. Tarasenko, A., Pozdnyakova, N., Paliienko, K. et al. A comparative study of wood sawdust and plastic smoke particulate matter with a focus on spectroscopic, fluorescent, oxidative, and neuroactive properties. Environ Sci Pollut Res 29, 38315–38330 (2022). https://doi.org/10.1007/s11356-022-18741-x

Funding/ Acknowledgement

Project “War-derived air pollution nanohybrids composed of carbon-containing smoke nanoparticles and metal compounds: FTIR/Raman spectroscopic, fluorescent and membrane-active properties, their potential neurotoxicity and its prevention”. Project PAN.BFB.S.BWZ.380.022.2023.

Analysis, design, and applications of polygon mirror-based laser scanners

V.-F. Duma[1-3] and M.-A. Duma[4]

[1] 3OM Optomechatronics Group, Faculty of Engineering, Aurel Vlaicu University of Arad, Str. Elena Dragoi no. 2, 310177 Arad, 3 Vasile Milea Ave, Arad 310131, Romania
[2] Faculty of Electronics, Telecommunications, and Information Technology, Polytechnic University of Timisoara, Bd. Vasile Parvan nr. 2, Timisoara 300223, Romania
[3] National University of Science and Technology POLITEHNICA Bucharest, Center of Research and Development for Mechatronics, Splaiul Independentei 313, Sector 6, Bucharest, Romania
[4] School of Science and Engineering, University of Groningen, W.F. Bathoornstraat, Groningen 9731 CG, The Netherlands
e-mail: duma.virgil@osamember.org

Laser scanning systems are utilized in a wide range of applications, from commercial (such as barcode scanning or laser printers) to industrial (for optical micrometers, laser manufacturing, or 3D printing) and to high-end ones (including biomedical imaging, for example for Optical Coherence Tomography (OCT) [1]). Such systems include mostly galvanometer scanners (GSs), Micro-Electro-Mechanical Systems (MEMS), polygon mirror (PM), and Risley prisms [2].

This presentation briefly reviews laser scanning systems, scanning modalities (from raster [3] to Lissajous and spiral scanning [4]), as well as some of their main applications. Further on, the main focus is on PM scanners, because of their advantages, i.e. fast and versatile scanning, the former in contrast to GSs and the latter in contrast to scanners with refractive elements. An overview of the different types of PMs is made. Our newly-developed theory of PMs is presented in detail, with its multi-parameter optical analysis [5]. Characteristic parameters and functions have been defined, deduced, and studied, with regard to all the constructive and functional parameters of such systems. The kinematics of the deflected laser beams are investigated, in comparison to the simpler case of GSs. The non-linearity of the scanning functions of PMs versus GSs is approached, as well as the variable scanning velocities they produce. The two pairs of characteristic angles, angular and linear Fields-of-View (FOV), as well as duty cycles are analyzed. We point out to how this theory allows for extending the (simpler, usually approached) case of a single ray to the more general case of finite diameter laser beams [6]. Rules-of-thumbs are extracted from the analysis for designing such systems. Also, a device with two supplemental mirrors is proposed and designed to increase the distance between a GS- or a PM-based scanning head and its objective lens (or scanned plane) in order to linearize the scanning function and thus, to reach a more constant scanning velocity, in a lower-cost solution compared to using F-theta lenses.

The optical analysis and design are complemented by a Finite Element Analysis (FEA) of PMs, in order to evaluate their capability to hold structural integrity and to be within the elastic deformation domain – for fast movements of up to 120 krpm in terms of rotational velocity. Our studies have been concluded so far with a design scheme of PM scanners that connects optical and mechanical aspects – in order to allow for an as comprehensive as possible approach of such scanners. One must point out that such a scheme can be utilized for other, different types of optomechanical scanners, with moving mirrors or refractive elements, as well.

Acknowledgement: This work was supported by the Romanian IPCEI (Important Project of Common European Interest) on microelectronics, via Continental Automotive Romania.

[1] W. Drexler, M. Liu, et al. *J. Biomed. Opt.* 19, 071412 (2014). Doi: 10.1117/1.JBO.19.7.071412
[2] G.F. Marshall, G.E. Stutz, Eds., Handbook of optical and laser scanning (CRC, London 2011).
[3] V.-F. Duma, Appl. Math. Modelling 67, 456-476 (2019). Doi: 10.1016/j.apm.2018.11.001
[4] V.-F. Duma, A-L. Dimb, Appl. Sci. 11, 8451 (2021). Doi: 10.3390/app11188451
[5] V.-F. Duma, Proc. of the Romanian Academy Series A 18, 25-33 (2017).
[6] V.-F. Duma, M.-A. Duma, Appl. Sci. 12, 5592 (2022). Doi: 10.3390/app12115592

Desorption of excited atoms via bi-exciton creation from solid Ne surfaces by electron impact

Issei Kawada[1], Takayuki Tachibana[1,2] and Takato Hirayama[1,2]

[1] Department of Physics, Rikkyo University, Tokyo 171-8501 JAPAN
[2] Research Center for Measurements in Advanced Science (RCMAS), Rikkyo University, Tokyo 171-8501, Japan.
e-mail: hirayama@rikkyo.ac.jp

Desorption induced by electronic transitions (DIET) in rare gas solids by elementary excitation has been investigated over the past 30 years [1]. Cavity ejection (CE) is one of the mechanisms that lead to excited atom desorption. In this process, an excited atom created on the surface of the solid by incident electrons or photons is repelled by surrounding atoms in the ground state and desorbs from the surface.

A bi-exciton is a pair of neighboring excitons produced by a single incident particle. The desorption of ions via bi-excitation creation from solid Ar and Ne surfaces has been previously reported in electron- [2] and photon- [3-5] stimulated ion desorption studies. These studies suggest that doubly excited molecules can desorb from the surface via the CE mechanism and autoionize in a vacuum.

Figure 1 shows the desorption yield of metastable Ne atoms in $^3P_{0,2}$ states as a function of incident electron energy. The resonant feature, peaking at around 35 eV, is clearly visible. This resonant peak has previously been observed in photon-stimulated ion desorption [5]. However, our results show a slight shift in the peak position to higher energy, which can be attributed to the lower kinetic energy of incident electrons in solid compared to vacuum, owing to the negative electron affinity of solid Ne (-1.4 eV).

The kinetic energy of desorbed metastable atoms at the resonance is measured to be 0.36 eV, while that resulting from single exciton creation is 0.18 eV [1]. This small kinetic energy can provide evidence for the desorption of a doubly excited Ne molecule (Ne* - Ne*) through the cavity ejection mechanism. A detailed discussion will be given at the conference.

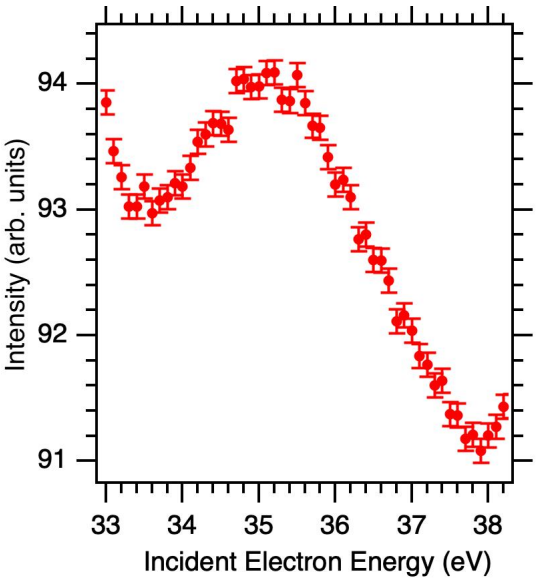

Figure 1: Dependence of the desorption yield of metastable atoms from solid Ne on the incident electron energy. The film thickness is 100 ML.

[1] T. Hirayama and I. Arakawa, J. Phys. Condens. Matter 18, S1563 (2006), https://doi.org/10.1088/0953-8984/18/30/S10 and references therein.
[2] Y. Baba et al., Phys. Rev. Lett. 66, 3269 (1991). https://doi.org/10.1103/PhysRevLett.66.3269 .
[3] T. Schwabenthan et al., Solid State Comm. 80, 773(1991). https://doi.org/10.1016/0038-1098(91)90906-C .
[4] G. Dujardin et al., Appl. Phys. A66, (1998) 527. https://doi.org/10.1007/s003390050708 .
[5] P. Wiethoff et al., Fiz. Nizk. Temp. 29, 351 (2003). https://doi.org/10.1063/1.1542447

Leverage cloud technologies for enhanced research data accessibility and more effective scientific collaboration

Philipp Jaeger

Pexon Consulting GmbH, Alfred-Herrhausen-Allee 3-5, 65760 Eschborn, Germany
e-mail: philipp.jaeger@pexon-consulting.de

In this presentation I will outline a conceptual design for managing research data using Cloud Computing technologies based on Microsoft Azure [1]. Using the Internet of Things (IoT) Hub and Azure Digital Twins alongside metadata storage on Azure Cosmos DB and analytics services such as Azure Machine Learning (AML) or Synapse Analytics [2-6], I will present an example architecture for such a setup, with only minor changes to measurement automation programs.

By storing research data on the cloud, researchers will

- Ensure easy access to all data across international collaborations
- Have the ability to restrict access to certain sensitive data
- Make their data interchangeable and compatible for analytics across several data sets
- Prepare data for publication in a collaborative way
- Annotate all their data with relevant metadata
- Automatically trace data related to certain setups or samples using Digital Twins
- Enable data recovery, e.g. after failure of local hard disks

In doing so, they implement the best practices as outlined by the Research Data Alliance (RDA) [7] and the FAIR principles for findable, accessible, interoperable and reusable data [8]. Additionally, by using the analytics capabilities Synapse and AML, many data processing steps can be automized, increasing efficiency and output of research collaborations, while also ensuring a constant data quality.

With this infrastructure in place, individual datasets can easily be published compliant with ISO 26324 and receive a DOI [9], which can be cross-referenced with journal publications. Hence, publications increase in quality regarding transparency of the research process and making it easier to reproduce the results for other researchers.

[1]Microsoft, https://azure.microsoft.com/en-us/resources/cloud-computing-dictionary/what-is-azure
[2] Microsoft, https://learn.microsoft.com/en-us/azure/iot-hub/iot-concepts-and-iot-hub
[3] Microsoft, https://learn.microsoft.com/en-us/azure/digital-twins/overview
[4] Microsoft, https://learn.microsoft.com/en-us/azure/cosmos-db/introduction
[5] Microsoft, https://learn.microsoft.com/en-us/azure/machine-learning/overview-what-is-azure-machine-learning
[6] Microsoft, https://learn.microsoft.com/en-us/azure/synapse-analytics/overview-what-is
[7] Klump, J., Wyborn, L., Downs, R., Asmi, A., Wu, M., Ryder, G., & Martin, J. (2020). Principles and best practices in data versioning for all data sets big and small. Version 1.1. Research Data Alliance. DOI: https://doi.org/10.15497/RDA00042
[8] Wilkinson, M., Dumontier, M., Aalbersberg, I. et al. The FAIR Guiding Principles for scientific data management and stewardship. Sci Data 3, 160018 (2016).
https://doi.org/10.1038/sdata.2016.18
[9] DOI Foundation, DOI Handbook, DOI https://doi.org/10.1000/182 (Links [1-6] were last accessed on March 15, 2024)

Quantum Scaling for the Metal-Insulator Transition in a Two-Dimensional Electron System

V. Kagalovsky[1], S.V. Kravchenko[2], D. Nemirovsky[1]

[1] Shamoon College of Engineering, Beer-Sheva 84105, Israel
[2] Physics Department, Northeastern University, Boston, Massachusetts 02115, USA
e-mail: victork@sce.ac.il

We suggest Gaussian approximation to describe the quantum phase transition observed experimentally in seminal studies of two-dimensional (2D) electron systems [1-3]. Our approach explains self-consistently the universal value of the critical exponent 3/2 (found after scaling measured resistivities on both sides of the transition as a function of temperature) as the result of the divergence of the correlation length when the electron density approaches the critical one. We also provide numerical evidence for the exponential temperature dependence of the metallic phase's resistivities (never suggested before) and show that it leads to correct qualitative results. Finally, we interpret the phase diagram on the density-temperature plane exhibiting the quantum phase transition and two crossover lines (see Fig. 1 below).

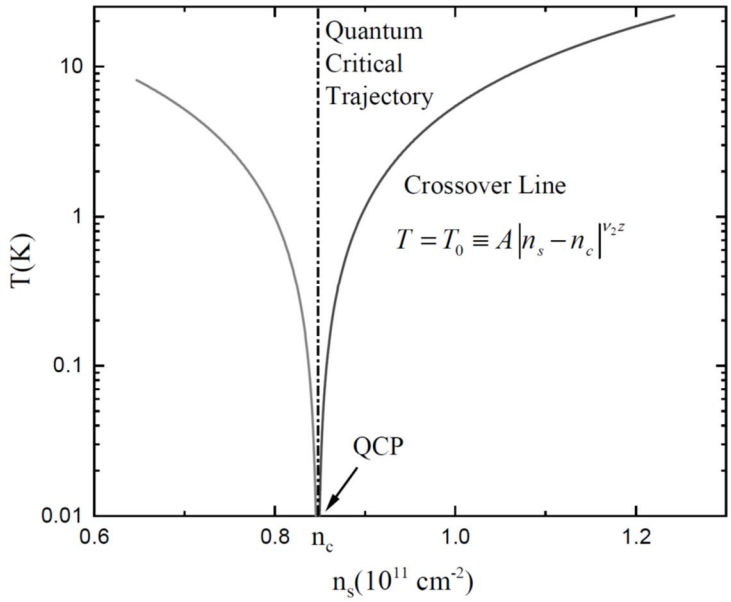

Fig. 1. Phase diagram of the system. The quantum critical point (QCP) is on the horizontal axis $T = 0$ $n_c \approx 0.85$. Quantum critical trajectory is a vertical dash-dotted line starting at QCP. Solid lines represent crossover lines ($n < n_c$ for an insulator and $n > n_c$ a metal).

[1] T. N. Zavaritskaya and E. I. Zavaritskaya, JETP Lett. 45, 609 (1987).
[2] S. V. Kravchenko, G. V. Kravchenko, J. E. Furneaux, V. M. Pudalov, and M. D'Iorio, Phys. Rev. B 50, 8039 (1994).
[3] S. V. Kravchenko, W. E. Mason, G. E. Bowker, J. E. Furneaux, V. M. Pudalov, and M. D'Iorio, Phys. Rev. B 51, 7038 (1995).

Contribution of mass spectrometry to molecular biophysics of nucleic acids

M. V. Kosevich

B. Verkin Institute for Low Temperature Physics and Engineering of the NAS of Ukraine,
47 Nauky Ave., Kharkiv, 61103, Ukraine
e-mail: mvkosevich@gmail.com

The impact of deciphering of the structure of DNA molecule by X-ray method in 1953 was not limited by demonstration of efficiency of addressing biological problems by physical methods, thus initiating the development of molecular biophysics as such. It also stimulated the race in elaboration of novel physical techniques and instrumentation for biophysical studies, which is exemplified in the present communication by a story of biological mass spectrometry. To convert mass spectrometry from a method of nuclear physics research employed in the middle of the last century for creation of nuclear weapon, to peaceful biomedical method, it was necessary to overcome two main obstacles: transfer of fragile biomolecules to the gas phase and their nondestructive "soft" ionization.

In this mainstream, the initiated by B.I. Verkin, the founder of the Institute for Low Temperature Physics and Engineering (ILTPE), investigations on physics of nucleic acids were supported by development of the relevant physical methods [1]. ILTPE scientists not only witnessed, but actively participated in the biological conversion of mass spectrometry, successively introducing field ionization, field desorption, fast atom bombardment, and secondary ion mass spectrometry. Applying these techniques fundamental data on ionization energies of DNA nitrogen bases, included into the database of the National Institute of Standards and Technology (USA), were obtained at the ILTPE. Numerical data on the energy of interactions of DNA nitrogen bases [1, 2] were used as empirical parameters in the first quantum chemical methods of computer simulation being under development at that time. Later on, a number of aspects of nucleic acids functioning were studied by mass spectrometry, including hydration, DNA components interactions with anticancer chemotherapeutic agents, protein-nucleic acids interactions.

Further efforts of international community in elaboration of electrospray ionization and matrix-assisted laser desorption/ionization methods for study of biopolymers, awarded by the Nobel Prize in 2002, permitted creation of "Nucleic acids in the gas phase" [3] branch of molecular biophysics. The up-to-date mass spectrometry is positioned not only as an analytical technique, but as a branch of science dealing with all phenomena related to molecules and ions. In this direction mass spectrometric approaches were developed aimed at elucidation of DNA damages caused by low-energy (units of eV) or high-energy (MeV) ionizing radiation. Biophysical experiments on DNA melting were reproduced in the gas phase by variation of the electrospray conditions. Sequencing of nucleic acids under mass spectrometric conditions becomes possible. Mass spectrometry contributed to the success of "The Human Genome Project". Emerging imaging mass spectrometric approaches are applied to nucleic acids as well.

Finally, recent achievements of ILTPE in nanotechnology-related mass spectrometric and computer modeling of PEGylation of nucleic acids components [4], aimed to drug delivery application, will be described.

[1] B.I. Verkin, I.K. Yanson, L.F. Sukhodub, and A.B. Teplitsky, Interactions of biomolecules: new experimental approaches and methods (Naukova Dumka, Kiev, 1985).
[2] I.K. Yanson, A.B. Teplitsky, and L.F. Sukhodub, Biopolymers 18, 1149-1170 (1979). https://doi.org/10.1002/bip.1979.360180510
[3] V. Gabelica (Ed.), Nucleic acids in the gas phase (Springer, Berlin, Heidelberg, 2014).
[4] V.G. Zobnina, V.V. Chagovets, O.A. Boryak, and M.V. Kosevich, A mass spectrometric study and computer modeling of noncovalent interactions of cytosine with polyethylene glycol oligomers. J Anal Chem 70, 1533–1541 (2015). https://doi.org/10.1134/S1061934815130110

Functional properties of Ni-Mn-based alloys: Theory and experiment

Anna Kosogor[1,2]

[1] *Institute of Magnetism NASU and MESU, Vernadsky Blvd 36-b, Kyiv 03142, Ukraine*
[2] *University of Vienna, Faculty of Physics, Boltzmanngasse 5, A-1090 Vienna, Austria*
e-mail: annakosogor@gmail.com

Exploring the properties of Ni-Mn-based alloys is of great significance owing to their extraordinary magnetic and structural characteristics, positioning them as highly prospective materials across diverse applications. These alloys exhibit notable features such as magnetocaloric and elastocaloric effects, shape memory behavior, superelasticity, and giant magnetoresistance [1]. The exceptional properties of Ni-Mn-based alloys arise from the magnetic, structural, and magnetostructural phase transitions. Comprehending the mechanisms behind these transitions and elucidating them is crucial for advancing our knowledge in this field. Thus, a phenomenological approach combining experimental data with theoretical models has arisen as a powerful tool for characterizing functional properties during these phase transitions. The Landau theory, a key theoretical framework within this approach, offers a systematic method for describing phase transitions and linked physical phenomena [2-5]. In particular, the application of this approach resulted in:

1) Prediction of giant anhysteretic deformation of martensitic alloys in post-critical regime [2]. It has been demonstrated that the presence of a critical point in the stress-temperature phase diagram leads to two distinct modes of deformation behavior: one characterized by significant hysteresis inherent in first-order phase transitions, and another exhibiting nonlinear anhysteretic deformation of crystal lattice.

2) Quantitative description of the conventional and inverse magnetocaloric effects in Ni-Mn-based Heusler alloys [3,4]. It enabled the estimation of both the conventional magnetocaloric effect near the Curie temperature and the giant inverse magnetocaloric effect resulting from the transition between ferromagnetic austenite and weakly magnetic martensite. Notably, these computations were conducted without relying on the magnetic Maxwell relationship, as its applicability to first-order phase transitions remains uncertain.

3) Elaboration of procedure of determination of magnetic part of the low-temperature specific heat of ferromagnetic (FM) solid from the results of the low-temperature measurements. It has been shown that the disregard of magnetic contribution to the specific heat of FM solid results in the noticeable underestimation of Debye temperature and overestimation of the specific heat of electron subsystem of FM solid [5].

[1] A. Planes, L. Mañosa, and M. Acet, J. Phys.: Condens. Matt. 21, 233201 (2009). DOI 10.1088/0953-8984/21/23/233201.
[2] A. Kosogor, N. J. Matsishin, and V.A. L'vov, Phase Trans. 86, 796 (2013). https://doi.org/10.1080/01411594.2012.726725.
[3] V.A. L'vov, A. Kosogor, J.M. Barandiaran, and V.A. Chernenko, J. Appl. Phys. 119, 013902 (2016). https://doi.org/10.1063/1.4939556.
[4] A. Kosogor, V.A. L'vov, P. Lázpita, C. Seguí, and E. Cesari. Metals, 9, 11 (2018). https://doi.org/10.3390/met9010011.
[5] A. Kosogor, V.A. L'vov, R.Y. Umetsu, X. Xu, and R. Kainuma, J. Magn. Magn. Mater. 541, 168549 (2022). https://doi.org/10.1016/j.jmmm.2021.168549.

DNA as an exemplary polymer

Oleg Krichevsky

Physics Department, Ben-Gurion University of the Negev, Beer-Sheva, 84105, Israel
e-mail: okrichev@bgu.ac.il

Different topics in polymer physics textbooks start with simple, beautiful, exactly solvable models. However, in order to describe actual polymer systems, different corrections have to be introduced that render these models heavy and often mathematically intractable. In my talk, I will review our work demonstrating that in several experimental situations DNA polymers follow the predictions of the simplest polymer theories.

We developed a new approach to study DNA structure and dynamics through a combination of fluorescence labeling and fluorescence correlation spectroscopy. We show that DNA behaves as an “ideal” coil in dilute solutions and a “mean-field” polymer in semi-dilute solutions.

Finally, I will describe our current measurements of bacterial DNA/chromatin structure tentatively supporting a fractal globule model of its organization.

I would also like to say a few words about my (and your) dear colleague Prof. Sergey Gredeskul, who together with his wife Victoria have been brutally murdered by Hamas terrorists in their home on Oct. 7th.

[1] E. Shafran, A. Yaniv and O. Krichevsky, Marginal nature of DNA solutions, Phys. Rev. Lett. 104, 128101 (2010 https://doi.org/10.1103/PhysRevLett.104.128101
[2] Nepal M., Yaniv A., Shafran E. and O. Krichevsky, Structure of DNA coils in dilute and semidilute solutions, Phys. Rev. Lett. 110, 058102 (2013). https://doi.org/10.1103/PhysRevLett.110.058102
[3] M. Nepal, A. Oyler-Yaniv and O. Krichevsky, Scanning fluorescence correlation spectroscopy as a versatile tool to measure static and dynamic properties of soft matter systems, Soft Matter 11, 8939-47 (2015). https://doi.org/10.1039/c5sm01582k

Transport signatures of plasmon fluctuations in electron hydrodynamics

Dmitry Zverevich and Alex Levchenko

Department of Physics, University of Wisconsin-Madison, Madison, WI 53706, USA
e-mail: levchenko@physics.wisc.edu

In two-dimensional electron systems, plasmons are gapless and long-lived collective excitations of propagating charge density oscillations. We study the fluctuation mechanism of plasmon-assisted transport in the regime of electron hydrodynamics. We consider pristine electron liquids where charge fluctuations are thermally induced by viscous stresses and intrinsic currents, while attenuation of plasmons is determined by the Maxwell mechanism of charge relaxation. It is shown that, while the contribution of plasmons to the shear viscosity and thermal conductivity of a Fermi liquid is small, plasmon resonances in the bilayer devices enhance the drag resistance and near field heat transfer. In systems without Galilean invariance, fluctuation-driven contributions to dissipative coefficients can be described only in terms of hydrodynamic quantities: intrinsic conductivity, viscosity, and plasmon dispersion relation.

[1] Low. Temp. Phys. **49**, 1515-1524 (2023) https://doi.org/10.1063/10.0022363

Challenging properties of magnetic shape memory alloys

V. A. L'vov[1,2]

[1] Institute of Magnetism NAS of Ukraine and MES of Ukraine,
36-b Akad. Vernadskogo blvd, Kyiv 03142, Ukraine
[2] Taras Shevchenko National University of Kyiv,64/13,
Volodymyrska Street Kyiv 01601, Ukraine
e-mail: victor.a.lvov@gmail.com

The properties of magnetic shape memory alloys (SMAs) are traditionally considered as the important subject for researchers working in the area of material science, while the understanding and improvement of these properties need the great efforts of physicists. Present communication is aimed to explain the essence of physical problems related to these properties.

At present, those magnetic SMAs, which attract attention of researches, are conventionally subdivided into ferromagnetic and "metamagnetic" SMAs (FMSMAs and MMSMAs, respectively).

FMSMAs undergo the first-order magnetostructural phase transition from the cubic ferromagnetic phase to the low-symmetry ferromagnetic phase possessing the twinned crystal lattice. The external magnetic field displaces the twin boundaries and induces a giant deformation ($\Delta l/l \sim 5\times10^{-2}$) of the single crystalline samples of FMSMAs [1]. This deformation masks the ordinary magnetostriction in the twinned low-temperature phase, and therefore, the measurement of the temperature dependence of magnetostriction of FMSMAs is an open problem [2]. The magnetoelastic constant of the piezopolymer/FSMA composite material was estimated recently from the value of magnetoelectric coefficient [3]. It was concluded that the magnetoelastic constant, which characterizes the whole material, increased by one order of magnitude due to the phase transition in FSMA filler; it pointed to the existence of special mechanism of magnetostriction of composite material, because the volume fraction of filler was equal to 3% only [4].

MMSMAs undergo the first-order magnetostructural phase transition from the high-temperature ferromagnetic phase to one of the low-temperature "weakly magnetic" phases [5]. First of all, it should be emphasized that the magnetic structure of the weakly magnetic phases (probably antiferromagnetic, ferrite, spin glass, e.t.c.) is not firmly established and their properties strongly depend on the chemical composition of MMSMAs. The identification of these phases is strongly needed for the improvement of practically important properties of MMSMAs, in particular, for the enhancement of inverse magnetocaloric effect, which is considered promising for applications.

The subject of present communication involves the following points:

- The procedures of estimation of magnetostriction and magnetoelastic constants characterizing the twinned FMSMAs.
- Magnetically induced piezoelectric effect in the piezopolymer/FMSMA composite materials.
- Two probable explanations of the temperature dependence of magnetization of MMSMAs.
- Two theoretical approaches to evaluation of the inverse magnetocaloric effect caused by the magnetostructural phase transitions; the agreement between theoretical and experimental results.

[1] O. Heczko, A. Sozinov, K. Ullakko, IEEE Trans. Mag. 36, 3266 (2000).
https://www.researchgate.net/publication/224068920. doi: 10.1109/20.908764.
[2] O. Heczko, Journ. Magn. Magn. Matter. 290–291, 846 (2005).
https://doi.org/10.1016/j.jmmm.2004.11.391.
[3] P. Martins, A. C. Lima, V. A. L'vov, et al. Applied Materials Today 29, 101682 (2022).
https://doi.org/10.1016/j.apmt.2022.101682
[4] V. A. L'vov, P. Martins, N. Pereira, et al., Composite Sci. Technol. 241, 110101 (2023).
https://doi.org/10.1016/j.compscitech.2023.110101.
[5] R. Y. Umetsu, X. Xu, R. Kainuma, Scripta Materialia, 116, 1 (2016).
https://doi.org/10.1016/j.scriptamat.2016.01.006.

Quantum transport and optics theory and simulations with applications to noninvasive medical diagnostics and novel photonic functionalities

M.F. Pereira[1,2], Humaira Zafar[1] and A. Apostolakis[2]

[1] Department of Physics, Khalifa University of Science and Technology, UAE
[2] Institute of Physics, Czech Academy of Sciences, Czech Republic
e-mail: mauro.pereira@ku.ac.ae

A nonequilibrium many-body approach is used to predict and control giant THz nonlinearities in superlattices at both steady state and time domains in excellent agreement with experiments [1-5]. Both analytical approximations and numerical solutions, with outlines of the corresponding methods will be presented. Superlattices are promising nanomaterials for a wide range of applications in the Sub-Terahertz and Terahertz (THz) region is their ability to generate high-order harmonic generation (HHG). Superlattice multipliers have been recently applied to the experimental detection of nitrides in the urine of cancer patients treated by chemotherapy, heralding the potential for a new non-invasive metabolomics approach for diagnostics technique that can potentially detect side effects of chemotherapy using THz spectroscopy, much before conventional diagnostics could indicate damage to the kidneys [6]. In the second part of the talk, superlattice waveguides are used to demonstrate theoretically and experimentally functionalities such as rotators and splitters in a silicon on insulator platform [7-10]. Progress in all projects highlighted above will be presented at the conference.

[1] M.F. Pereira, Nanomaterials 12, 1504 (2022).
[2] M.F. Pereira, et al, Sci. Rep. 10, 15950 (2020).
[3] M.F. Pereira et al, J. Nanophoton 11 (4), 046022 (2017).
[4] A. Apostolakis and M.F. Pereira, Nanophotonics, vol. 9, no. 12, pp. 3941-3952 (2020).
[5] A. Al-Ateqi and M.F. Pereira, Opt Quant Electron 55, 1287 (2023).
[6] V. Vaks, V. et al., Sci Rep. 12, 18117 (2022).
[7] H. Zafar, et al, IEEE Journal of Selected Topics in Quantum Electronics 29, 4400109, 1-9 (2023).
[8] H. Zafar, et al, Opt. Express 31, 21389-21398 (2023).
[9] Zafar, H. et al, Opt. Express 2022, 30, 10087-10095.
[10] Zafar, H. et al, AIP Advances 2020, 10, 125214.

Swift Ion Irradiation Related to Complex Organic Molecules in Cold Space Environments

P. Boduch, A. Domaracka, H. Rothard

Centre de Recherche sur les Ions, les Matériaux et la Photonique,
Normandie Univ, ENSICAEN, UNICAEN, CEA, CNRS, CIMAP, Caen 14000, France
e-mail: rothard@ganil.fr

“Where do we come from” is one of the important fascinating open questions of science and philosophy. How did life emerge, what is the origin of organic matter in the universe? Could life also emerge on other worlds than our Earth? Complex organic molecules have indeed been observed in space (comets, meteorites, molecular clouds). In cold space environments, the synthesis of complex organic molecules (COMs) is possible by implantation of ions trapped in the magnetospheres of giant planets into the icy surfaces of their satellites (like e.g. C or S ejected by Io's volcanism impacting Europe) [1]; following radiolysis of small molecules (H_2O, CO, CH_4, NH_3 etc.) on cold surfaces of icy bodies in the outer solar system or grains in the dense molecular clouds) [2]. Irradiation of COMs also occurs in condensed phase in radiobiology cases (cancer therapy, dosimetry and radiation protection). Thus, it is pertinent to study both formation and radio-resistance of COMs under swift charged particle irradiation of icy samples in a wide temperature range (10-300K).

We performed ion irradiation experiments related to COMs at different accelerator facilities (GANIL/Caen/France, GSI/ Darmstadt/Germany, ATOMKI/Debrecen/ Hungary). Infrared absorption spectroscopy FTIR and mass spectrometry QMS allow in situ observation of physico-chemical modifications of the icy layers. Ex-situ analysis of residues is performed by e.g. high resolution mass spectrometric methods. Within the PEPR Origins [pepr-origins.fr], a unique multi-beam irradiation device (UV photons, keV electrons and keV-GeV ions delivered by the GANIL-Grand Accélérateur National d'Ions Lourds, Caen/France) equipped with an infrared spectrometer and a cold head to prepare layers of ices made of mixtures of small molecules is under construction. Complex organic molecules formed during the irradiation of ice layers will be detected using gas phase chromatography and in-situ mass spectrometry. This new versatile MIRRPLA platform [3] will be open to the various scientific communities (astrophysics, radiobiology, environmental and materials sciences) as well as to industry via the CIMAP-GANIL user platform CIRIL [4].

[1] G. Strazzulla, M.E. Palumbo, P. Boduch, H. Rothard, *Ion Implantation and Chemical Cycles in the Galilean Satellites*, Earth, Moon, and Planets 127:2 (2023), doi: 10.1007/s11038-023-09550-4
[2] H. Rothard, A. Domaracka, P. Boduch, M. E. Palumbo, G. Strazzulla, E. F. da Silveira and E. Dartois, *Modification of ices by cosmic rays and solar wind*, J. Phys. B : At. Mol. Opt. Phys. 50, 062001 (2017), doi: 10.1088/1361-6455/50/6/062001
[3] Alicja Domaracka and Grégoire Danger, *Multiple Beam Irradiation Platform MIRRPLA: Origin and Evolution of Organic Matter in the Solar System*, Nuclear Physics News 33(4), 36–37 (2023), doi: 10.1080/10619127.2023.2265772
[4] J. Rangama, C. Grygiel, A. Mery, P. Rousseau and H. Rothard, *CIRIL: Interdisciplinary Research at GANIL*, Nucl. Phys. News. 32(1), 29-33 (2022), doi: 10.1080/10619127.2021.1990680

Fractional types of statistics: state of the art and some historical flashbacks

A. Rovenchak

Professor Ivan Vakarchuk Department for Theoretical Physics,
Ivan Franko National University of Lviv,
12, Drahomanov St., Lviv, 79005, Ukraine
e-mail: andrij.rovenchak@lnu.edu.ua

The history of quantum statistics dates back to the mid-1920s, with seminal works by Bose (1924) and Einstein (1925) for what is now known as bosons, as well as Fermi (1926) and Dirac (1926) for what is now known as fermions. As the current scientific understanding states, real particles can be classified as either fermions or bosons. Various generalizations, known as "intermediate," "fractional," "nonstandard," "interpolation," "modified," or "exotic" statistics, arise effectively, often due to consideration of interactions or the transition to two-dimensional space. In many cases, the application of such new types statistics is also linked to the simplification of mathematical formulations.

In 1940, Gentile, Jr., proposed the first generalization of the statistics, suggesting that the maximum occupation of a particular level can be a finite number larger than unity. In subsequent decades, other types of non-standard statistics were proposed by various authors, including Green's parastatistics (1953), q-oscillator by Arık and Coon (1976), and fractional exclusion statistics by Haldane (1991) and Wu (1994), just to mention a few. Approaches included deformations of commutation relations, modifications of wave-function symmetry properties, new ways of microstate counting, etc.

We will focus of a few types of statistics, including anyons and models for their effective description, approaches based on nonadditive substitutions of the Gibbs factor, as well as modifications arising, in particular, from deformations of algebras of creation and annihilation operators. Possibilities of establishing at least approximate correspondence between some types of fractional statistics will also be discussed.

Approaches utilizing fractional statistics concepts have demonstrated success in analyzing phenomena such as the fractional quantum Hall effect, high-temperature superconductivity, interactions in low-dimensional systems, cold atomic gases, nuclear matter, and even models of dark matter. Nonadditive modifications of statistics have the capacity to explain various phenomena across a broad spectrum of physical systems, including cold atoms, open quantum systems, plasma dynamics, or cosmological models, and extending beyond traditional physics domains to encompass complex networks, linguistics, financial data, and epidemiology.

Anyons arise effectively in descriptions of the fractional quantum Hall effect in two-dimensional systems. Modifications of the Gibbs factor and even more complicated changes of the functional form of the occupation numbers allow for effective descriptions of real-world systems as ideal systems of particles obeying some fractional statistics. Deformed algebras are sometimes linked to searches for nonconventional formulations of thermodynamics. Virial and cluster expansions are efficient techniques for relating parameters in various types of fractional statistics, even coming from different approaches.

To conclude, the study of quantum statistics continues to evolve, driven not only by pure mathematical and academic interest but also by its practical applications in understanding the behavior of particles in diverse physical systems.

Optical emission studies of C_2 formation upon electron irradiation of Ar matrices doped with CH_4

M. A. Bludov, I. V. Khyzhniy, S. A. Uyutnov, E. V. Savchenko

B. Verkin Institute for Low Temperature Physics and Engineering of NAS of Ukraine,
47 Nauky Ave., Kharkiv, 61103, Ukraine
e-mail: elena.savchenko@gmail.com

Radiation-induced fragmentation of carbon-containing species and formation of new ones is currently the topic of considerable interest in different fields of science (see e.g. [1-3] and references therein). Methane, as the simplest hydrocarbon molecule, attracted a lot of attention in these studies. The original approach, based on combination of the matrix isolation technique with excitation by electrons and nonstationary spectroscopy [4], permitted unravel both neutral and charge channels of relaxation. Our previous research [3, 4] were focused on the dynamics of H and CH_3 species, the recombination of which resulted in a delayed burst of desorption.

The presented study is devoted to the processes of molecular carbon formation in CH_4-doped Ar matrices irradiated with electrons. Mixture of Ar and CH_4 of chosen concentration (from 0.1 to 10%) was deposited onto a cooled to LHe temperature substrate. The irradiation was performed in dc regime with electrons of subthreshold energy. Three type experiments were carried out – (i) measurements of optical emissions in the visible and VUV range, (ii) recording the curves of nonstationary luminescence NsL at the selected wavelengths during gradual heating of samples under the electron beam and (iii) measurements of the thermally stimulated exoelectron emission TSEE from preirradiated samples. C lines and Swan bands of C_2 molecule were detected in the optical emission spectra. Due to the small penetration depth of the electron beam the main part of the matrix was excited preferentially via energy transfer processes involving free FE and self-trapped excitons STE of the Ar matrix, what can be considered as "internal photolysis". Additional channel of energy transfer is charge transfer from matrix holes to the products of CH_4 radiation-induced transformation because of the high ionization potential I of Ar (I=15.76 eV) exceeding the I of methane and its fragments. Analysis of direct formation of C atom from CH_4 via internal photolysis shows that this channel is down. The most efficiently C atoms are formed from CH_2 radical in reaction: $CH_2 + h\nu \rightarrow C+2H$ with branching ratio BR=1 via FE and BR=0.4 via STE of Ar matrix. Measurements of NsL demonstrated correlation of NsL recorded at C or C_2 line and H line with TSEE yield pointing that atoms C and H are formed simultaneously in reactions of dissociative recombination: $CH_3^+ + e^- \rightarrow C + H + H_2$ with BR=0.35 and $CH_2^+ + e^- \rightarrow C + H + H$ with BR=0.68 [5, 6]. Migration of C atoms at low temperatures to recombine with C_2 formation becomes possible due to the kinetic energy of „hot" atoms that are formed in these reactions. Thermally induced mobility was detected around 35 K.

[1] G. Strazzulla, M.E. Palumbo, P. Boduch, H. Rothard, Earth, Moon, and Planets 127:2 (2023), https://doi.org/10.1007/s11038-023-09550-4
[2] O. Kirichek, C.R. Lawson, G.L. Draper, D.M. Jenkins, D.J. Haynes and S. Lilley, Journal of Neutron Research, vol.22, 281 (2020), https://doi.org/10.3233/JNR-190132
[3] M. Bludov, I. Khyzhniy, S. Uyutnov, E. Savchenko, *Methane*, *2*(4), 372 (2023); https://doi.org/10.3390/methane2040025
[4] E. Savchenko, I. V. Khyzhniy, S. A. Uyutnov, M. A. Bludov**,** and V. E. Bondybey, J. Mol. Structure, 1221, 128803 (2020), https://doi.org/10.1016/j.molstruc.2020.128803
[5] T. Taketsugu and Y. Kobauashi, Computational and Theoretical Chemistry, 1150, 1 (2019), https://doi.org/10.1016/j.comptc.2019.01.010
[6] A. Larson, A. Le Padellec, J. Semaniak, C. Stromholm, M. Larsson, S. Rosen, R. Peverall, H. Danared, N. Djuric, G. Dunn, & S. Datz, Astrophys. J., 505, 459 (1998), DOI**:** 10.1086/306164

Engineering electronic flat bands in two dimensions

Yu. Skrypnyk

Bogolyubov Institute for Theoretical Physics of NAS of Ukraine,
14b Metrolohichna Str., Kyiv 03680, Ukraine
e-mail: yuriy.v.skrypnyk@gmail.com

The electronic band structure of several intentionally designed lattices is analyzed using the tight-binding approximation. By assumption, the tight-binding model's transfer integrals are nonzero exclusively for electron hopping between the nearest neighbors in the lattices under consideration. The spatial arrangement and the connectivity of lattice sites in each crystal lattice are deliberately engineered so that their respective band structures can feature at least one flat (in other words, dispersionless) band under a specific set of model parameters. The corresponding restrictions that must be imposed on the parameters of the tight-binding model to ensure the existence of a flat band are formulated.

A kind of one-dimensional diamond ladder with the ABC composition is studied as a toy lattice structure. The results obtained for its electronic spectrum provide insight into methods of devising novel two-dimensional lattices capable of yielding flat bands in their band structure. The conventional square lattice serves as the underlying framework for their construction. Two distinct new lattice structures are suggested. They are tentatively named "Tornado Siren" and "Clous De Paris" based on their visual appearance. The necessary conditions for the presence of a flat band or almost flat band in their spectra are determined. Special attention is paid to the case when the flat band is composed of compact localized states with a dumbbell-like configuration. In this case, all the eigenstates corresponding to the flat band do not overlap spatially. The developed method for analyzing the electronic spectrum for the existence of a flat band is also applied to the dual kagome lattice with the ABC composition.

It is found that adherence to the straightforward rules listed below is essential to achieve a flat band within a described set of lattice structures. Electron hoppings between lattice sites of the chosen bare lattice should occur only through additional intermediate sites. At least two different paths should be present for each indirect hopping between sites of the bare lattice, which implies the existence of two supplementary sublattices. Then, the electronic band structure of such lattice has a flat band when on-site potentials in these sublattices coincide. If the above conditions are met, the flat band appears in the spectrum regardless of the hopping integral values.

In addition, it is demonstrated that the band structure features an almost flat band when on-site potentials in these supplementary sublattices differ, and one hopping integral is much less than the other.

Exploring the Unified Theory of Thermal Transport: Experimental Insights, Predictive Precision, and Phenomenological Implications

D. Szewczyk[1], A. I. Krivchikov[1,2], A. Jeżowski[1]

[1] Institute for Low Temperatures and Structure Research, Polish Academy of Sciences, ul. Okólna 2, 50-422 Wroclaw, Poland
[2] B. Verkin Institute for Low Temperature Physics and Engineering of NAS of Ukraine, 47 Nauky Ave., Kharkiv, 61103, Ukraine
e-mail: d.szewczyk@intibs.pl

Appreciating thermal transport phenomena is essential from both theoretical and experimental standpoints. The 2019 introduced unified theory of thermal transport in crystals and glasses [1] centers on diffusive thermal transport, particularly evident in the temperature dependencies of thermal properties in both crystalline and disordered systems. The collaborative work of Simoncelli, Marzari, and Mauri not only offered a qualitative understanding of thermal conductivity but also facilitated the quantitative prediction of the thermal conductivity coefficient $\kappa(T)$ for any given substance. According to this theory, thermal transport occurs through two channels concurrently: a "classical" pathway, acknowledged by Peierls, and other - grounded in tunneling mechanisms and diffusion laws. Furthermore, it posits that this novel "diffusive" channel is universal, irrespective of the material's crystalline structure or amorphous composition.

The significance of determining thermal properties will be underscored, not solely for cognitive reasons, but also in light of future applications, as demonstrated by experimental instances and related phenomena. These will include thermal conductivity exhibiting amorphous characteristics [2-4], an atypical elevation of $\kappa(T)$ at high temperatures [2-7], and anomalous low-temperature heat capacity [8-12].

[1] M. Simoncelli et al. Nature Physics 15, 809 (2019)
[2] Yu.V. Horbatenko et al.Journal of Physics and Chemistry of Solids 127, 15l (2019)
[3] A.I. Krivchikov et al. Thermochimica Acta, 733, 179696 (2024)
[4] D. Szewczyk et al. Journal of Physics Communications, 8(1), 015001 (2024)
[5] M.A. Strzhemechny et al. Chemical Physics Letters 647, 55 (2016)
[6] A. Jeżowski et al. AIP Advances 9, 015121 (2019)
[7] A.I. Krivchikov et al. Materialia, 32, 101944 (2023)
[8] J. F. Gebbia et al. Physical Review Letters 119, 215506 (2017)
[9] D. Szewczyk et al. Low Temperature Physics, 49(5), 593 (2023)
[10]A. Jeżowski et al. Physical Review B 97, 201201(R) (2018)
[11]D. Szewczyk et al. Scientific Reports 11, 18640 (2021)
[12]A.I. Krivchikov et al. Journal of Physical Chemistry Letters 13, 5061 (2022)

The authors acknowledge support of Polish National Science Centre (Grant No. 2022/45/B/ST3/02326).

Controlling multimagnon processes in magnetic nanostructures

R. Verba[1], J. Kharlan[1,2], V. Borynskyi[1], D. Slobodianiuk[3,1], A. Etesamirad[4], I. Barsukov[4]

[1] Institute of Magnetism, 36-b Vernadskogo blvd., Kyiv 03142, Ukraine,
[2] Institute of Spintronics and Quantum Information, Adam Mickiewicz University, ul. Wieniawskiego 1, Poznań, 61-712, Poland
[3] Institute of High Technologies, Taras Shevchenko National University of Kyiv, 64 Volodymyrska str., Kyiv, 01601, Ukraine,
[4] Physics and Astronomy, University of California, 900 University Ave., Riverside, CA 92521, USA
e-mail: verrv@ukr.net

Variety of nonlinear processes is a prominent feature of ferromagnetic materials, which has already become a basis for many technological applications. Tailoring nonlinearity on demand is an intriguing feature, opening a way for novel functionalities of magnetic and spintronic devices in microwave electronics, signal processing, logic and beyond-Boolean applications. Although been studied for several decades, nonlinear processes in bulk samples and thin films were found to exhibit just a few ways for their control, such as a whole spectrum shift or alternation of the static magnetization direction by a bias magnetic field [1-2].

In contrast, magnetic nanostructures offer much wider possibilities to control nonlinear multimagnon scattering. The simplest method relies on the discreteness of spin-wave spectrum, which allows one to change the detuning from the resonance condition for a particular multimagnon splitting or confluence process, thus enhancing or suppressing this process [3-4]. This ability becomes particularly prominent in magnetic nanostructures with a sufficiently sparse spectrum – when intermode distance overcomes the eigenmode linewidth [3].

In this work, we report another, more involved methods for controlling nonlinear processes, specifically the most important three- and four-magnon scattering. Specific symmetry of static magnetization state and spin-wave modes results in specific selection rules for multimagnon scattering. Altering this symmetry is a key for a powerful tool for mode-selective control of multimagnon scattering, especially for three-magnon interaction. Detailed analytical and micromagnetic study of an exemplary system – a thin elliptic nanodot – uncovers the potential of the method. While in a symmetric ground state three-magnon scattering is restricted to a few specific allowed channels or could be even prohibited at all, a weak perturbation could open additional scattering channels with a considerable efficiency. Important, that different perturbations, e.g., a field tilt or field gradient, are mode-specific, affecting interaction of modes with a certain symmetry only. Four-magnon processes are harder to control as most of them do not possess specific symmetry restrictions for interacting modes. We present an alternative way, which relies on the mode hybridization in multilayer structures, which also can be efficiently altered by a perturbation field.

Our results could serve as a guide for static and dynamic control of multimagnon scattering processes in magnetic nanostructures and spintronic devices, in particular, for boosting their performance or engineering a specific nonlinear response of a device used in signal processing and non-Boolean spintronic application.

Support by the NAS of Ukraine project No. 08/01-2024(5) is gratefully acknowledged.

[1] P.E. Wigen, *Nonlinear Phenomena and Chaos in Magnetic Materials* (World Scientific, Singapore, 1994).
[2] V.S. L'vov, *Wave Turbulence under Parametric Excitation* (Springer-Verlag, New York, 1994).
[3] Y. Kobljanskyj, G. Melkov, K. Guslienko, V. Novosad, S.D. Bader, M. Kostylev, A. Slavin, Sci. Rep. 2, 478 (2012). https://doi.org/10.1038/srep00478
[4] G.A. Melkov, D.V. Slobodianiuk, V.S. Tiberkevich, G. de Loubens, O. Klein, A.N. Slavin, IEEE Magn. Lett. 4, 4000504 (2013). https://doi/org/10.1109/LMAG.2013.2278682

Controlled rotations of a hot hole spin qubits

T. Patlatiuk[1], M. J. Carballido[1], S. Svab[1], S. Bosco[2], P. Chevalier Kwon[1], R. Eggli[1], E. Bakkers[3], J. C. Egues[1], D. Loss[1,4], D. Zumbühl[1]

[1] University of Basel, Switzerland
[2] QuTech and Kavli Institute of Nanoscience, Delft University of Technology, 2628 CJ Delft, Netherlands
[3] Eindhoven University of Technology, Netherlands 4 Instituto de Física de São Carlos, Universidade de São Paulo, São Carlos, Brazil
e-mail: taras.patlatiuk@unibas.ch

We report on the first realization of conditional rotations of two exchange-coupled hole spin qubits, at the elevated temperature of 1.5 K. To this end, we tuned a double quantum dot (DQD) formed inside a Ge/Si core/shell nanowire into the regime where both hole spins can be individually addressed by two different microwave frequencies. Tuning the interdot tunnel barrier allowed us to operate the device in the regime with exchange coupling changing from 50 MHz to almost 300 MHz for different DQD detunings - a basic requirement to perform exchange-based two-qubit gates. As a proof of principle, we performed conditional rotation(s) of two spins at 1.5 K. Limited coherence resulted in qubit resonances with the linewidth larger than the exchange splitting J. Thus, in order to extract the magnitude of J we performed a two-tone spectroscopy, allowing us to transfer the spin-occupation of the DQD between the four possible spin states. Using Pauli spin blockade, the weakly coupled DQD is initialized in one of the two spin-polarized Triplet states with equal probabilities. The other two states with antiparallel spin orientations are not blocked and produce current through the DQD during the readout. We also developed a simple theoretical model that includes spin-orbit interaction and isotropic exchange which was able to capture our expenmental observations. Our experimental results lay the foundation for the next required step towards large-scale quantum computation with hole spins.

Funding Acknowledgement:
Supported by NCCR SPIN of the SNSF, SNI, EMP Nr. 824109, FET TOPSQUAD Nr. 862046 and G. H. E. Foundation

Photonics Cluster Ukraine

K. Gorokhovskyi

Public Union Photonics Cluster Ukraine
36 Akademik Vernadsky avenue, Kyiv, Ukraine
email: coordinator@photonics.org.ua

Photonics Cluster Ukraine is a Public Union, established in 2024 by initiative of Ukrainian Clusters Alliance and Kyiv Academic University to join efforts of research institutions, universities and enterprises in photonics industry to support technology transfer and innovations in the field and provide international cooperation and business services for cluster members. We have technology and business experts who provide such services as technology evaluation, matchmaking academia-industry, SME support, startup evaluation and mentorship, innovation roadmap development, grant application support and others. During the full scale war our mission is support of photonics military applications, with focus on laser weapons, optoelectronic and optoacoustic surveillance systems, optic and quantum communications, quantum programming and quantum machine learning. Photonics Cluster Ukraine works with the Ministry of Defense, Ministry of Strategic Industries and military cluster Brave1. We are partners with OptecBerlinBrandebourg, Polish Photonics Technology Platform, AlphaRLH (France). We are members of the EPIC (European Photonic Industry Consortium) and applied for membership at PhotonHub Europe. We provide support for university programs in photonics and quantum technologies and student chapters of Optica and SPIE. If you are research institution, university or manufacturer of equipment/software feel free to contact us for cooperation opportunities.

https://photonics.org.ua/

Topological semimetals in heavy fermion compounds

Silke Paschen

Institute of Solid State Physics, Vienna University of Technology (TU Wien),
Wiedner Hauptstr. 8-10, 1040 Vienna, Austria
e-mail: paschen@ifp.tuwien.ac.at

Gapless electronic topology driven by strong correlations is an emerging field of great interest, with heavy fermion compounds at its forefront. I will introduce the first such materials class, Weyl-Kondo semimetals [1-3], and report on the giant signatures of topology observed in $Ce_3Bi_4Pd_3$ [1,3] and the genuine topology control that can be achieved by magnetic field tuning [4]. I will also discuss design strategies for further correlation-driven topological phases [5], and highlight a new emergent topological phase that nucleates out of a strange metal state [6].

This work was supported by the Austrian Science Fund (FWF-I4047, I5868-FOR5249-QUAST, SFB F 86, Q-M&S), the European Union’s Horizon 2020 Research and Innovation Programme (824109, EMP), and the European Research Council (ERC Advanced Grant 101055088, CorMeTop).

[1] S. Dzsaber et al., Phys. Rev. Lett. 118, 246601 (2017).
[2] H.-H. Lai et al., PNAS 115/1, 93 (2018).
[3] S. Dzsaber et al., PNAS 118, e2013386118 (2021).
[4] S. Dzsaber et al., Nat. Commun. 13, 5729 (2022).
[5] L. Chen et al., Nat. Phys. 18, 1341 (2022).
[6] D. M. Kirschbaum et al., arXiv2404.15924 (2024).

ELECTRONIC PROPERTIES OF CONDUCTING AND SUPERCONDUCTING SYSTEMS

Topological features and transport properties of Sr_2FeMoO_6 double perovskite

S. M. Konoplyuk, M. M. Krupa, Yu. B. Skyrta

Institute of magnetism of NAS of Ukraine and MES of Ukraine,
36-b Vernadsky Blvd., Kyiv, 03142, Ukraine
e-mail: ksm@imag.kiev.ua

Materials with nontrivial topology of electronic band structure attracted much attention in the last decade. They host unusual transport properties such as ultra-high mobility, intrinsic Hall effect caused by Berry curvature, chiral anomaly etc. In our study, we found topological phases, which emerge in prospective Sr_2FeMoO_6 metal oxide combining DFT and Wannier interpolation methods. We showed that gaps opening between linearly crossing bands due to spin orbit coupling led to significant enhancement of Berry curvature. Intrinsic Hall and Nernst effects were calculated using maximally localized Wannier functions extracted from band structure. The effects of broken mirror and time reversal symmetries on topological characteristics of Sr_2FeMoO_6 were analyzed.

Effect of dysprosium trioxide on the structural and electrical properties of Tl-1223 HTS

I. R. Metskhvarishvili[1,2], G. N. Dgebuadze[1], D. L. Surmanidze[1,3], T. E. Lobzhanidze[3], cB. G. Bendeliani[1], V. M. Gabunia[1,4], M. R. Metskhvarishvili[5], D. A. Jishiashvili[1,6]

[1] Ilia Vekua Sukhumi Institute of Physics and Technology, Laboratory of Cryogenic Technique and Technologies, Mindeli St. 7, 0186 Tbilisi, Georgia
[2] Georgian Technical University, Faculty of Informatics and Control Systems, Department of Microprocessor and Measurement Systems, Kostava St. 77, 0175 Tbilisi, Georgia
[3] Ivane Javakhishvili Tbilisi State University, Faculty of Exact and Natural Sciences, Department of Chemistry, Chavchavadze Ave. 3, 0179 Tbilisi, Georgia
[4] Petre Melikishvili Institute of Physical and Organic Chemistry of the Iv. Javakhishvili Tbilisi State University, Jikia str 5, 0186, Tbilisi, Georgia
[5] "Talga" Institute of Georgian Technical University, Zurab Anjaparidze 5, 0186 Tbilisi, Georgia
[6] V. Chavchanidze Institute of Cybernetics of the Georgian Technical University, Zurab Anjaparidze 5, Tbilisi 0186, Georgia
e-mail: i.metskhvarishvili@gtu.ge

The Thallium-based cuprate is one of the high-temperature superconductor family members. The structurally related Tl–Ba–Ca–Cu–O high-temperature superconducting compounds are represented by the chemical formula $Tl_mBa_2Ca_nCu_nOy$, where m=1 or 2 and $1 < n \leq 5$. Among the members of the Tl-based series, the Tl-1223 show a superconducting transition temperature T_c above 118 K, while $T_c \approx 125$ K was found in Tl-2223. Both systems demonstrate suitable superconducting parameters (T_c, J_c), making these the phases of preferred material for practical application.

A review of numerous reports shows that the additives or substituents in superconducting materials by the appropriate metals or oxides can promote the formation of the superconducting phase, Improve structural stability or introduce effective pinning centers. Effects of RE oxides such as Gd, Er, Dy, Ho, Tb, Yb, and Y on the superconducting properties of the various superconductive materials have been reported as effective pinning centers to enhance the current-carrying capability of superconductivity materials.

Taking into account that the rare-earth oxides have sound effects on the physical-chemical properties of superconductor materials, the present study is devoted to the effects of doping of dysprosium (III) oxides on the $TlBa_2Ca_2Cu_3Dy_xO_{8+\delta}$ (x = 0.00–0.075 wt%) material.

Dysprosium-free and dysprosium-doped samples were synthesized using the two-step and sealed quartz tube techniques. Firstly, we synthesized dysprosium-free and dysprosium-doped precursors BCCO, and then Tl_2O_3 was added, and $TlBa_2Ca_2Cu_3Dy_xO_{8+\delta}$ superconducting materials were prepared.

X-ray powder diffraction patterns obtained on a Dron-3+PC diffractometer with CuKα radiation. The morphology and structure were studied using the FEI Quanta FEG 600 scanning electron microscope (SEM), equipped with an energy dispersive spectrometer (EDS): Oxford Instruments, AZtecOne. The critical temperature (T_c) was measured by the real part of the AC susceptibility (χ'), and transport critical current density (J_c) was determined using the high harmonics method.

Our results demonstrate that the presence of dysprosium oxide not only makes the Ba-Ca-Cu-O multiphase the precursor more reactive and enhances the kinetics of the reaction, but it also leads to the promotion of the high-T_c phase and enhancement of the transport critical current densities J_c.

New states of Fermi superliquid with conformational degrees of freedom

M. Yu. Kovalevsky[1], A. A. Rozhkov[2]

[1] NSC “Kharkiv Institute of Physics and Technology”
Akdemicheskaya, 1, Kharkiv 61108,Ukraine
[2] National Technical University Kharkiv Polytechnical Institute
Kirpichova str 2, Kharkiv 61108,Ukraine
e-mail: new.arz.yes777@gmail.com

Equations of the ideal superfluid hydrodynamics of a Fermi liquid with conformational degrees of freedom are constructed, which generalize the dynamics of the A-phase ^{3}He. The dynamic quantities of the reduced description associated with the broken symmetry are introduced in terms of the order parameter. A modified Mermin-Ho relation have been obtained, which takes into account the influence of conformational degrees of freedom. Expressions of the flux densities of additive integrals of motion in dissipativeless approximation in terms of the density of the energy functional are established. Spectra of collective excitations are found and their spatial anisotropy has been analyzed. It is shown that taking into account conformational degrees of freedom leads to positive anisotropic corrections in the acoustic spectra of the first and second sounds and their angular dependence is established. The appearance of the third sound, which has its origin from liquid crystal degrees of freedom, is clarified.

Influence of strong electron irradiation on fluctuation conductivity and pseudogap in $YBa_2Cu_3O_{7-\delta}$ single crystals

A. L. Solovjov[1,2], M. V. Shytov[1], E. V. Petrenko[1], L. V. Bludova[1], R. V. Vovk[3], K. Rogacki[2]

[1] B. Verkin Institute for Low Temperature Physics and Engineering of NAS of Ukraine, 47 Nauky Ave., Kharkiv, 61103, Ukraine
[2] Institute for Low Temperatures and Structure Research, Polish Academy of Sciences, Wroclaw 50-422, Poland
[3] Department of Physics, V. N. Karazin Kharkiv National University, Kharkiv 61022, Ukraine
e-mail: shytovnikita@gmail.com

At present, various superconducting devices based on HTSCs are widely used in technology. Quite often, such devices have to operate under conditions of strong electron irradiation, which creates numerous defects in HTSC due to the displacement of all atoms in the crystal under study. Strictly speaking, the role of defects in HTSC is still not completely clear [1]. To answer this questions, we measured the resistance of optimally doped (OD) untwinned $YBa_2Cu_3O_{7-\delta}$ (YBCO) single crystals irradiated with high-energy electrons (2.5 MeV). This approach makes it possible to obtain numerous defects in crystals in a controlled manner.

Twelve doses of irradiation φ=0, 1.3, 2.5, 3.9, 5.6, 6.9, 8.0, 8.7, 10.0, 11.2, 15.6 and $23\cdot10^{19}$ e/cm^2 are used. With increasing φ, T_c linearly decreases to $T_c = 0$ at $\varphi \geq 10\cdot10^{19}$ e/cm^2 while the resistivity also linearly increases and exhibits a metal-insulator transition above $\varphi_{10} \approx 11.2\cdot10^{19}$ e/cm^2. The slope dρ/dT in the normal state above T^* at all φ remained almost constant, which indicates the fulfillment of the Matthiessen's rule, characteristic of non-twinned YBCO [2]. The physics behind this behavior as well as linear dependencies of T_c and ρ on φ still remains uncertain.

To clarify the issues the temperature dependences of fluctuation conductivity (FLC) and pseudogap (PG) have been studied within the Local Pairs (LPs) model [1]. At φ = 0 FLC displays distinct crossover from 3D-AL to 2D-MT fluctuations which is typical for well-structured YBCO [1]. Then irradiation defects completely suppressed the 2D-MT fluctuation contribution. Unexpectedly, now the 2D fluctuations are well described by the 2D-AL theory. Simultaneously, the coherence length and the distance between the conducting CuO_2 planes increase more than twice. But, very surprisingly, the original FLC behavior restores at $\varphi = 5.6\cdot10^{19}$ e/cm^2. However, the absolute value of the FLP, measured at $T=T_G$ is constantly decreasing, most likely due to the pair-breaking effect of the irradiation. The similar "restoring" effect is observed for the PG $\Delta^*(T)$. At φ = 0 $\Delta^*(T)$ has the maximal $\Delta(T_{pair}) = 246.7$ K and $\Delta(T_G) = 243.9$ K and the shape characteristic of OD non-twinned single crystals [1]. At φ_2 $\Delta^*(T)$ decreases as expected, maintaining its shape. But at φ_3, when 2D-MT FLC changes to 2D-AL, $\Delta^*(T)$ suddenly increases, changing shape. At the same time, both T_{pair} and T^* increase. However, at φ_4 all parameters again sharply decrease, including the shape $\Delta^*(T)$. Finally, at $\varphi_5=5.6\cdot10^{19}$ e/cm^2 $\Delta^*(T)$ takes on a form typical for OD YBCO single crystals with defects, which are characterized by linear $\Delta^*(T)$ in the range from T_{pair} to T_{01}. The details of the unusual behavior of the FLP and PG under irradiation are discussed.

[1] R.V. Vovk and A.L. Solovjov, *Low Temp. Phys.* **44**, 81-113 (2018); https://doi.org/10.1063/1.5020905
[2] A. L. Solovjov, E. V. Petrenko, L. V. Omelchenko, R. V. Vovk, I. L. Goulatis & A. Chroneos, *Scientific Reports* **9,** 9274 (2019). https://doi.org/10.1038/s41598-019-45286-w
[3] F. Rullier-Albenque, H. Alloul, and R. Tourbot, *Phys. Rev. Lett.* **91**, 047001 (2003). https://doi.org/10.1103/PhysRevLett.91.047001

A detailed investigation of anomalies on the temperature dependences of the electrical resistance of $Bi_{88.08}Mn_{11.92}$ in fields up to 90 kOe

V. M. Yarovyi[1], K. Rogacki[2], A. V. Terekhov[1], E. Lähderanta[3], A. L. Solovjov[1,2]

[1] B. Verkin Institute for Low Temperature Physics and Engineering of NAS of Ukraine, 47 Nauky Ave., Kharkiv, 61103, Ukraine,
[2] Institute for Low Temperatures and Structure Research, Polish Academy of Sciences, P.O. Box 1410, 50-950 Wroclaw, Poland
[3] Lappeenranta University of Technology, School of Engineering Science, 53850 Lappeenranta, Finland
e-mail: yarovyi@ilt.kharkov.ua

Bi-Mn solid solutions are interesting due to their high coercive force at room temperature. With increasing temperature, it grows to values exceeding the coercive forces of rare-earth permanent magnets [1, 2]. It should be noted that electrical transport in these materials has hardly been investigated, but its behaviour may be as interesting as magnetic properties. Studies by our group have shown that the compound $Bi_{95.69}Mn_{3.69}Fe_{0.62}$ with a small amount of manganese has a colossal positive anisotropic magnetoresistance and anomalies on the temperature dependence of electric resistance $R(T)$ in magnetic field [3, 4]. The purpose of this work is to show what happens to the $R(T)$ in a magnetic field if the manganese content is increased. We examine in detail the behaviour of the temperature dependences in the $Bi_{88.08}Mn_{11.92}$ compound in magnetic fields up to 90 kOe.

The corresponding investigation of textured, polycrystalline $Bi_{88.08}Mn_{11.92}$ containing two phases (the bismuth matrix and magnetic inclusions of the α-BiMn phase) was carried out. Measurements of $R(T)$ for $\boldsymbol{H} \parallel \boldsymbol{I}$ and $\boldsymbol{H} \perp \boldsymbol{I}$ have been performed in the temperature range 2÷300 K and magnetic fields up to 90 kOe. In the absence of an external magnetic field, the metallic behaviour of $R(T)$ is observed, which is manifested by a decrease in resistance with decreasing temperature. In a magnetic field, the temperature dependence of the electrical resistivity changes significantly, demonstrating maxima T_{max} that shift towards higher temperatures with increasing field. Temperature dependences of magnetoresistance $MR = ([R(H) - R(0)]/R(0))*100\ \%$ for different magnetic fields have been plotted. It was found that the magnetoresistance increases with growing magnetic field and reaches a value of about 3300 % and 394 % in a magnetic field of 90 kOe for $\boldsymbol{H} \perp \boldsymbol{I}$ and $\boldsymbol{H} \parallel \boldsymbol{I}$, respectively. The analysis of temperature dependences of magnetoresistance for $Bi_{95.69}Mn_{3.69}Fe_{0.62}$ and $Bi_{88.08}Mn_{11.92}$ shows that as the manganese content grows, the magnitude of magnetoresistance also increases. For the case of $\boldsymbol{H} \perp \boldsymbol{I}$, we observe $MR \approx$ 3300 % and 2883 % in $Bi_{88.08}Mn_{11.92}$ and $Bi_{95.69}Mn_{3.69}Fe_{0.62}$, respectively. For the $\boldsymbol{H} \parallel \boldsymbol{I}$ configuration, it is established that $MR \approx$ 394 % and 235 % in $Bi_{88.08}Mn_{11.92}$ and $Bi_{95.69}Mn_{3.69}Fe_{0.62}$, respectively.

[1] Yong-Sheng Liu, Jin-Cang Zhang, Zhong-Ming Ren, Min-An Gu, Jing-Jing Yang, Shi-Xun Cao, and Zheng-Long Yang, Chin. Phys. Lett. **27**, 097502-1 (2010). DOI:10.1088/0256-307X/27/9/097502
[2] N.V. Rama Rao, A.M. Gabay, and G.C. Hadjipanayis, J. Phys. D: Appl. Phys. **46**, 062001-1 (2013). https://doi.org/10.1088/0022-3727/46/6/062001
[3] A.V. Terekhov, A.L. Solovjov, A. I. Prokhvatilov, A. I., V.V. Meleshko, I.V. Zolochevskii, J. Cwik, A. Los, A.D. Shevchenko, O.M. Ivasishin, and Z.D. Kovalyuk, East European Journal of Physics, **4**, 12 (2017). DOI:10.26565/2312-4334-2017-4-02
[4] A.V. Terekhov, K. Rogacki, A.L. Solovjov, A N. Bludov, A.I. Prokhvatilov, V.V. Meleshko, I.V. Zolochevskii, E.V. Khristenko, J. Cwik, A. Los, A.D. Shevchenko, Z.D. Kovalyuk, and O.M. Ivasishin, Low Temperature Physics, **44**, 1153 (2018). https://doi.org/10.1063/1.5060969

The acoustoelectric transformation in the mixed state in superconducting chalcogenides $FeSe_{1-x}S_x$ (x=0.075)

G. A. Zvyagina[1], V. D. Fil[1], I. V. Bilych[1], K. R. Zhekov[1], D. V. Fil[2,3]

[1] B. Verkin Institute for Low Temperature Physics and Engineering of NAS of Ukraine, 47 Nauky Avenue, Kharkiv, 61103, Ukraine
[2] Institute for Single Crystals, NAS of Ukraine, 60 Nauky Avenue, Kharkiv, 61072, Ukraine
[3] V.N. Karazin Kharkiv National University, 4 Svobody Square, Kharkiv, 61022, Ukraine
e-mail: bilich@ilt.kharkov.ua

In the literature devoted to discussing the properties of iron-based superconductors, it is proposed to classify FeSe-based superconducting chalcogenides into a separate class [1]. According to neutron data, structural transformation and nematicity occur in FeSe-based compositions, but there is no magnetic ordering and time-reversal symmetry is not broken. At the same time, it was suggested that the so-called "hidden magnetism" is realized in superconducting chalcogenides, which consists in the ordering of magnetic quadrupoles [2].

The acoustoelectric transformation (AET) experiments had shown that superconducting chalcogenides $FeSe_{1-x}S_x$ at temperatures below structural transformation temperatures T_s can be in a state of "hidden magnetism" with broken time-reversal symmetry [3, 4].

This work is devoted to the study of AET in the mixed state in superconducting chalcogenides $FeSe_{1-x}S_x$ (x=0.075). We investigated the dependence of the emitted electromagnetic field (phase and amplitude of the signal) on the magnetic field. The magnetic field is directed along the axis of sound propagation (z-axis). The measurements were done at the temperature $T = 0.9T_c$, that allows us to neglect the contribution of the normal component to the AET signal. The measurements were done in the range of H corresponding to the initial stage of magnetic flux penetration into the sample. The dependences were measured in a narrow range of magnetic fields to exclude possible capture of the residual field by the superconducting solenoid. From the amplitude measurements it can be concluded that the low critical field is equal to $H_{c1} \approx 15$ Oe. Above this field, the response amplitude varies linearly with the magnetic field, and the phases for the two directions of **H** are almost identical.

The dependence of the AET signal from the magnetic field we got at the initial stages of flux penetration has demonstrated a behavior that can be explained, in our opinion, only if the piezomagnetism is included in the consideration. The results obtained from the study of the piezomagnetic response in FeSe-based chalcogenides can be considered a direct confirmation of breaking of time-reversal symmetry in $FeSe_{1-x}S_x$ single crystals.

[1] T. Shibauchi, T. Hanaguri, and Y. Matsuda, J. Phys. Soc. Jpn. 89, 102002 (2020). https://doi.org/10.7566/JPSJ.89.102002.
[2] S. W. Lovesey, Phys. Rev. B 93, 085126 (2016). https://doi.org/10.1103/PhysRevB.93.085126.
[3] V. D. Fil, D. V. Fil, K. R. Zhekov, T. N. Gaydamak, G. A. Zvyagina, I. V. Bilich, D. A. Chareev and A. N. Vasiliev, EPL, 103, 47009 (2013). https://doi.org/10.1209/0295-5075/103/47009.
[4] V. D. Fil, D. V. Fil, G. A. Zvyagina, K. R. Zhekov, I. V. Bilich, D. A. Chareev, M. P. Kolodyazhnaya, A. Bludov, and E. Nazarova, Phys. Rev. B 104, 094424 (2021). https://doi.org/10.1103/PhysRevB.104.094424.

Combined electrical breakdown of a dielectric nanolayer between thin film electrodes

S. I. Bondarenko, A. V. Krevsun, V. P. Koverya

B. Verkin Institute for Low Temperature Physics and Engineering of NAS of Ukraine,
47 Nauky Ave., Kharkiv, 61103, Ukraine
e-mail: bondarenko@ilt.kharkov.ua

The goal of the research is to create a new type of a superconducting Josephson junction (JJ). To create it, the electrical breakdown (EB) of a dielectric layer (in the form of niobium oxide with a thickness of 30 nm) between two film electrodes was studied. In contrast to work [1], the EB was produced by the combined action of a DC voltage and a pulsed capacitor discharge on a dielectric [2]. Two features of this effect have been discovered. The first one concerns the possibility of obtaining a JJ with a reproducible resistance of more than 1 Ω. Figure 1 shows the dependence of the electrical resistance (R_b) arising after a breakdown of metal nanobridges (NB) between the electrodes on a value of the discharge resistance (R_2) in the capacitor circuit. It also shows the calculated dependence of a critical current of the NB at a temperature of 0 K on the R_b. It can be seen that the EB-method allows us to obtain NBs with a reproducible resistance of up to 8 Ω.

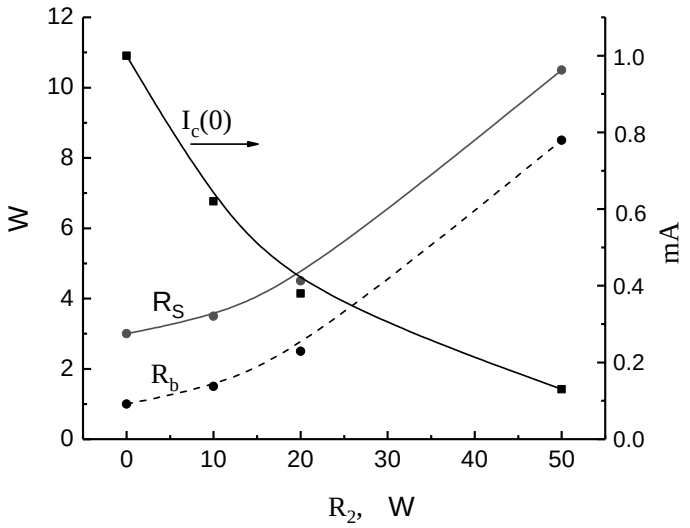

Fig.1. Dependences of the NB resistance (R_b) and the total measured resistance (R_Σ) with the supply wires, as well as the critical current ($I_c(0)$) on the discharge resistance (R_2).

The second feature concerns the unusual appearance of several (up to 10) oxidized point areas on a film cathode at certain values of the breakdown current. Calculations have shown that the cause of this phenomenon is a sequential multiple breakdown of the dielectric under different points of the film cathode. This may be caused by a spatial micro-inhomogeneity of the dielectric under the cathode film, as well as a high discharge current density sufficient to make successively arising NBs explode, and conditions for periodic charge-discharge cycles of the capacitor to the breakdown voltage.

[1] S. I. Bondarenko, A. V. Krevsun, V. P. Koverya, A. G. Sivakov, R. S. Galushkov, Low Temp. Phys. 48, 741 (2022). https://doi.org/10.1063/10.0013310
[2] A. V. Krevsun, S. I. Bondarenko, V. P. Koverya, Low Temp. Phys. 49, 83 (2023). https://doi.org/10.1063/10.0016479.

The formation of IV-characteristics of long Josephson junctions at zero-field steps

A. Grib, O. Chykina

V. N. Karazin National University, Svobody sq. 4, Kharkiv, 61022, Ukraine
e-mail: olena.chykina@student.karazin.ua

The so-called zero-field steps are formed in IV-characteristics of long Josephson junctions (i.e. junctions with the length larger than the double Josephson length of penetration of magnetic field) with inhomogeneous spatial distributions of critical currents in the absence of magnetic field [1]. Strong high-frequency radiation is observed at these steps. Steps appear at voltages which correspond usually to frequencies of even geometrical resonances of the junction. The formation of zero-field steps relates to the resonant interaction of Josephson generation with standing waves. On the other side, the inhomogeneity of the distribution of critical currents leads to the appearance of moving Josephson vortices. The IV- characteristic of the junction can be approximated with the use of parameters of these vortices [1]. In this report we check the validity of this approximation.

We modeled the long Josephson junction. The model is described elsewhere [2]. The long junction was divided to sections. It is supposed that in the center of each of the sections there is an "elementary" Josephson junction with parameters equal to parameters of the whole section. Parameters of all sections were identical except the critical current and the electrical resistance of one section, which was chosen at an arbitrary place of the junction. For each of the “elementary” junctions, the differential equation of the conservation of the current (the so-called dynamic equation) was solved together with the condition of quantization of magnetic flux. At the given bias current, the dependence of voltage over each of the “elementary” junctions on time was obtained and dc voltage was calculated by means of averaging of these dependences. The dc voltage over the whole long junction was calculated as averaged dc voltage over all “elementary” junctions.

Another approximation of the IV-characteristic of the long junction is proposed in Ref. [1]. In this approximation, the dc current is calculated from the equation of the balance of the input energy for some period and the energy of ohmic dissipation for the same time. The value of voltage is the integral of the propagating voltage pulse (i.e. of the Josephson vortex) over the length of the junction. This approximation contains characteristics of the Josephson vortex. Our goal was to compare the IV-curves obtained by two mentioned methods.

We calculated IV-characteristic of the junction with the length of 110 micrometers by means of the straightforward solution of dynamic equations (i.e. by the first method) and obtained zero-field steps. The depth of the penetration of magnetic field was 15.6 micrometers. The description of the zero-field step within ranges of the model of the motion of vortices (i.e. by the second method) includes direct measurements of the width of Josephson vortices, and the “Lorentz contraction” of the width at voltages close to the step. We visualized the movement of Josephson vortices and calculated widths of vortices directly from images. With the use of obtained data, we calculated velocities of vortices and the IV-curve at the first zero-field step by means of the second method. Though the IV-characteristic calculated by this method is in qualitative agreement with that obtained by means of the straightforward integration of equations of phase dynamics, values of the current obtained by the second method at the top of the step, exceed on above 30% those values calculated by means of the first method. The origin of this deviation and values of obtained coefficients of the approximation were discussed.

[1] T. A. Fulton and R. C. Dynes, Solid State Communications 12, 57 (1973). https://doi.org/10.1016/0038-1098(73)90345-1.
[2] A. Grib, P. Seidel, M. Tonouchi, Supercond. Sci. Technol. 30, 014004 (2017).
DOI 10.1088/0953-2048/30/1/014004

Experimental evidences for a favor of the staged nature of temperature evolution of the HTSC's pseudogap state

N. A. Azarenkov, V. A. Frolov, E. V. Karaseva, V. I. Sokolenko, A. V. Poida

National Science Center Kharkiv Institute of Physics and Technology, Kharkiv, 61108, Ukraine
e-mail: vsokol@kipt.kharkov.ua

Soon after the discovery of high-temperature superconductivity (HTSC) in copper cuprates, the existence of an extended temperature interval above the T_C was discovered, in which a state characterized by unusual behavior of kinetic coefficients is realized. Thus, when a pseudogap (PG) is "opened" in the electronic spectrum of cuprates (usually at $T_{PG} \sim 2T_C$), the material exhibits excess electrical conductivity, and with a subsequent decrease in T, the density of charge carriers decreases. Regarding the nature of PG, there are two most popular competing points of view. 1): starting from T_{PG}, the aggregations of Cooper pairs appear in the material; 2): the decrease in carrier density is due to the pairing of hole carriers into singlet local pairs (the electrical conductivity of HTSC is predominantly hole).

Using the method of planar-contact probing of the electronic subsystem of the interface formed upon contact of a normally conducting electron metal (Me) with a cuprate HTSC [1], it was shown in [2] that the interval T_{PG}.....T_C is a sequence of several close intervals, which, however, are not identical in kinetics. This conclusion was fully consistent with a non-monotonic behavior of the temperature dependences of both the absolute thermopower and the Hall coefficient of HTSC cuprates.

The work presents the results of further study devoted to the properties of the interface formed upon contact of Me=In with HTSC ceramics $Bi_{1.6}Pb_{0.4}Sr_2Ca_2Cu_3O_{10+x}$ and $Tl_2Ba_2Ca_2Cu_3O_x$. In the first group of experiments, the value studied, as in [2], was the electrical resistance r_{if} of the HTSC/In contacts. The second group of experiments was carried out using a new tool for studying PG, which we introduced into experimental practice. Its essence is a measurement of the temperature dependence of the thermopower coefficient s_{if} of the same interface between Me and HTSC.

According to both groups of experiments, the dependences of $r_{if}(T)$ and $s_{if}(T)$ in the case of $Bi_{1.6}Pb_{0.4}Sr_2Ca_2Cu_3O_{10+x}$/In and $Tl_2Ba_2Ca_2Cu_3O_x$/In contacts demonstrate non-monotonic correlations in the T_{PG}...T_C interval. From this, a conclusion was drawn about the stage-by-stage nature of the temperature evolution of the PG state in the cuprates studied. This result is qualitatively consistent with the observation [3] in the PG state of Y-123 cuprates with a superstructure of orbital magnetic moments directed at an angle of ~45° to the CuO_2 planes, the intensity of which varied non-monotonic and gradually with *T*. As for the phenomenon of the staged nature of the PG itself, it may indicate the influence on the PG expressed in changes in the ratio of electron and hole carriers.

[1] V.I. Sokolenko, V.A. Frolov. FNT, **39** 134 (2013).
[2] V.A. Frolov, V.I. Sokolenko. JETP Let. **107** 440 (2018).
[3] B. Faugué, Y. Sildis, V. Hinkov et. al. Phys. Rev. Lett. **96**, 197001 (2006).

Quantum capacitance of qubit-based systems

O. Y. Kitsenko[1,2], S. N. Shevchenko[1]

[1] B. Verkin Institute for Low Temperature Physics and Engineering of NAS of Ukraine, 47 Nauky Ave., Kharkiv, 61103, Ukraine
[2] V. N. Karazin Kharkiv National University, Kharkiv 61022, Ukraine
e-mail: kitsenko.sasha1212@gmail.com

If a classical resonator is coupled to a quantum system, its capacitance, inductance and resistance changes [1-3]. We investigate how different qubit-based systems (Fig. 1) interact with classical electric circuits and how to replace them with equivalent impedance which can be measured directly. The problem can be solved for the two-level approximation as well as for multi-level systems.

Our approach demonstrates how to strictly introduce quantum capacitance by quantizing the system and by applying the Krylov-Bogolyubov formalism [4]. The equations of motion for the classical and quantum subsystems then can be obtained and solved, so the correction terms for the circuit eigenfrequency as well as the effective impedance can be found.

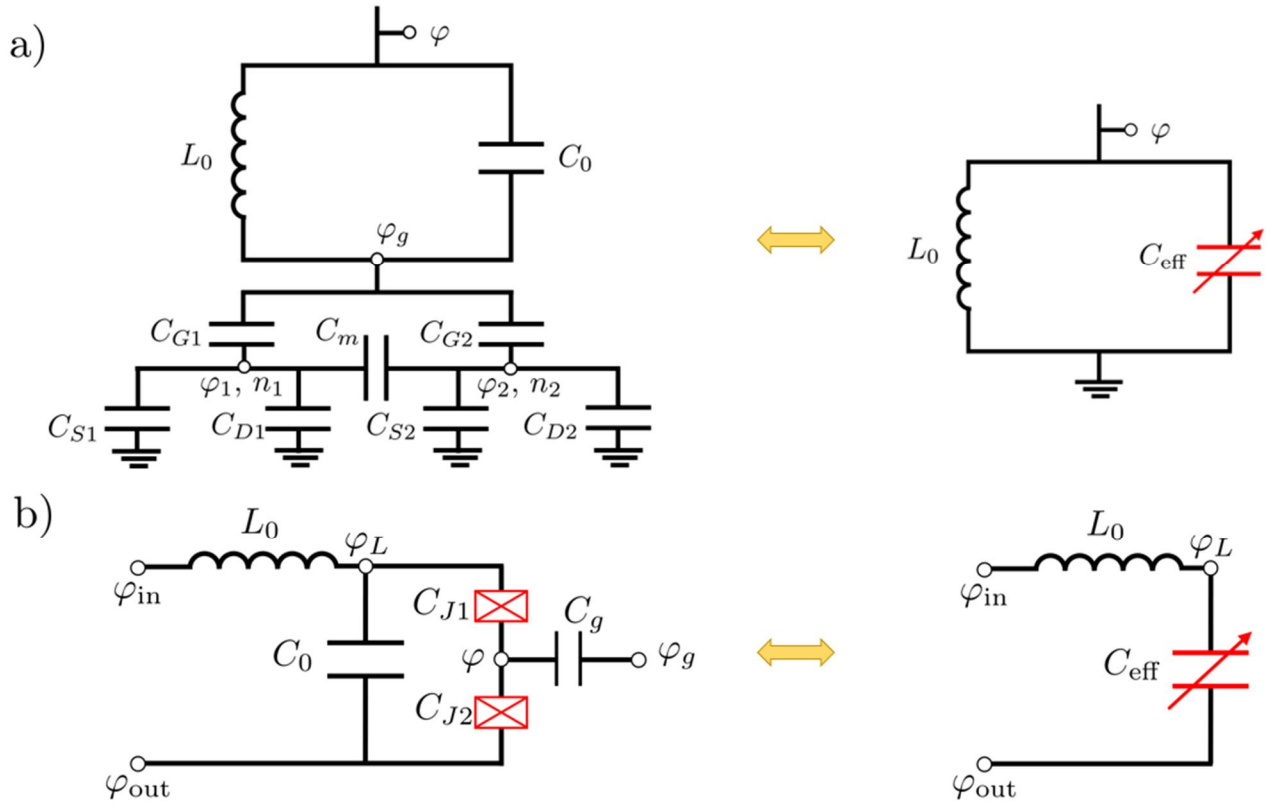

Fig.1 Examples of a double quantum dot [1] (a) and a single electron transistor [3] (b) coupled with classical LC circuit and respective equivalent circuits containing only effective capacitances.

[1] R. Mizuta, R. M. Oxtoa, A. C. Betz, M. F. Gonzalez-Zalba, Quantum and tunneling capacitance in charge and spin qubits, Phys. Rev. B **95**, 045414 (2017).
[2] S. N. Shevchenko, Impedance measurement technique for quantum systems, The European Phys. J. B **61**, 187-191 (2008).
[3] T. Duty, G. Johansson, K. Bladh, D. Gunnarsson, C. Wilson, P. Delsing, Observation of Quantum Capacitance in the Cooper-Pair Transistor, Phys. Rev. Lett. **95**, 206807 (2005).
[4] S. N. Shevchenko, A. N. Omelyanchouk, E. Ilichev, Multiphoton transitions in Josephson-junction qubits (Review Article), Low Temp. Phys. **38**, 360-381 (2012).

Electron transport in one dimensional disordered lattice

M. V. Klimov

V. N. Karazin Kharkiv National University, 4 Svobody Sq., Kharkiv, 61022, Ukraine
e-mail: klimovm19@gmail.com

We studied electron transport in one dimensional disordered lattice. We considered low electron limit where the number of electrons is much less then the number of host lattice sites. In this case one can neglect all the effects related to electron-electron interactions (i.e. Coulomb interactions, spin-spin interactions). Hamiltonian of this model has the form:

$$\hat{H} = -\sum_n \left[t_n c^+ c_{n+1} + h.c\right] + U_n c_n^+ c_n$$

here n enumerates lattice sites; c^+ and c_n are the creation/annihilation operators of electron on site n; t_n are the hopping constants and U_n are the constants of electron interaction with lattice. The parameters t_n and U_n are considered to be random. Their randomness is due to disorder of lattice sites positions. It is well known, that in one-dimensional systems the randomness of U_n (or t_n) leads to electrons localization [1]. Hence, electron transport is impossible even in the case of an arbitrary weak disorder.

We considered the model, where both U_n and t_n are random, but not independent. It was shown, that the correlations between random U_n and t_n can lead to delocalization of electrons states. As the result, electron transport becomes possible. Depending of the type of correlations between U_n and t_n several transport regimes were found: sub-diffusive, diffusive and super-diffusive. The areas of these regimes existences were established.

[1] I. M. Lifshits, S. A. Gredeskul, L. A. Pastur, Introduction to the Theory of Disordered Systems. Wiley-VCH, p.462 (1988).

Pressure effect on electronic structure and magnetic properties of LaFeAsO

A. S. Panfilov, I. P. Kobzar, G. E. Grechnev, A. V. Fedorchenko

B. Verkin Institute for Low Temperature Physics and Engineering of NAS of Ukraine,
47 Nauky Ave., Kharkiv, 61103, Ukraine
e-mail: zhhuravleva.irena@gmail.com

Following the discovery of the iron-pnictide high-T_C superconductors (SCs), a search for the new SCs extended to a variety of iron-based layered compounds like *R*OFeAs («1111», *R* = rare earth metal), AFe_2Se_2 («122», *A* = divalent alkaline earth metal), *B*FeSe («111», *B* = alkali metal), and simple FeSe(Te) materials («11»), which exhibited SC with transition temperatures T_C in the range of 8–55 K [1].

We expect that corresponding pressure (or volume) derivatives of χ are especially sensitive to the mechanism of magnetic interactions. The main objective of this study is to investigate atomic volume and pressure effects on magnetic properties of the LaFeAsO systems, which demonstrate a substantial pressure effect on T_C. The corresponding *ab initio* calculations of the electronic structure and magnetic susceptibility are supplemented by analysis of available experimental data.

In this work the polycrystalline $LaFeAsO_{0.85}F_{0.1}$ samples were obtained by conventional solid-state synthesis. The phase content of the samples was checked by the X-ray diffraction method.

In the following, polycrystalline and single-crystalline LaFeAsO samples will be designated by the letters P and S, respectively, indicating the series number. The dc magnetization studies were carried out in the magnetic field up to 50 kOe and the temperature range 4.2−300 K using a superconducting quantum interference device (SQUID) magnetometer. For single crystals the magnetic field was applied along the tetragonal *c*-axis. The studied sample $LaFeAsO_{0.85}F_{0.1}$ shows the superconducting transition at temperature $T_C \simeq 26$ K [2]. For the normal state, the $\chi(T)$ dependence, measured in $B \geq 1$ T, appears to be relatively flat and roughly described by the mean value of $\chi_{av} \sim 5 \cdot 10^{-4}$ emu/mol. The peculiar feature of the low-field magnetic susceptibility of $LaFeAsO_{0.85}F_{0.1}$ is a clear cusp at $T \simeq 135$ K with a sharp rise of χ with cooling from $T_M \simeq 135$ K to $T_C \simeq 26$ K.

To gain a further insight into magnetic properties of the iron-based SC systems in the normal state, the *ab initio* calculations of the electronic structure and paramagnetic susceptibility are carried out for LaFeAsO compounds within the density functional theory (DFT). The calculations were performed for varying atomic volume at the corresponding experimental lattice parameter ratios *c*/*a*. Under ambient conditions LaFeAsO compounds possess the tetragonal crystal structure (space group P4/nmm). The positions of As sheets are fixed by the internal parameter Z, which represents the height of these atoms above the iron square plane. This parameter also determines the chalcogen-Fe bond angles. Crystal structure parameters of LaFeAsO compounds were established in a number of works by means of X-ray and neutron diffraction studies.

[1] M.D. Lumsden, A.D. Christianson, *J. Phys.: Condens. Matter* **22**, 203203 (2010). https://doi.org/10.1088/0953-8984/22/20/203203.
[2] G.E. Grechnev, A.V. Logosha, A.O. Lyogenkaya, A.G. Grechnev, A.V. Fedorchenko, *Ukr. J. Phys* **59**, 284 (2014). https://doi.org/10.15407/ujpe59.03.0284.

Edge states at the boundary of hexagonal and Lieb lattices in a quantizing magnetic field

I. V. Kozlov, Yu. A. Kolesnichenko

B. Verkin Institute for Low Temperature Physics and Engineering of NAS of Ukraine,
47 Nauky Ave., Kharkiv, 61103, Ukraine
e-mail: kozlov@ilt.kharkov.ua

A boundary of two media with different topological order can be characterized by series of properties, the existence of which is protected. In the present work, the properties of such a boundary of two conductors are studied in a quantizing magnetic field: with charge carriers of the Dirac type and so-called spin-1 fermions, which are realized in graphene-like and Lieb lattices [1] respectively. Both lattices are characterized by the presence of a cone in the electron energy spectrum, the Klein paradox, but differ in Berry phase, which is equal to π in the graphene-like lattice, and trivial in the Lieb lattice.

A transmission coefficient is calculated. Spin-nonconserving Klein tunneling cannot occur, in contrast to the model proposed in [2]. It is shown that edge states arise that join the properties of conductors to the trivial and nontrivial Berry phase. An analogue of the area quantization rule is obtained. The systematics of energy levels for edge states can be described by the formula $S_L + 2\,S_G = 2\pi\dfrac{eB\hbar}{c}(n+\nu)$, where S_G and S_L are areas of segments of the edge state in the graphene-like lattice and the Lieb lattice respectively, the correction $\nu = \nu(S_L, S_G) < 1$ is a complicated oscillating function. Asymptotic behavior of energy levels contains information about the influence of the Berry phase on edge states.

These edge states lead to the appearance of a characteristic series of root singularities in the density of states $\nu(E)$, which are shown in the figure.

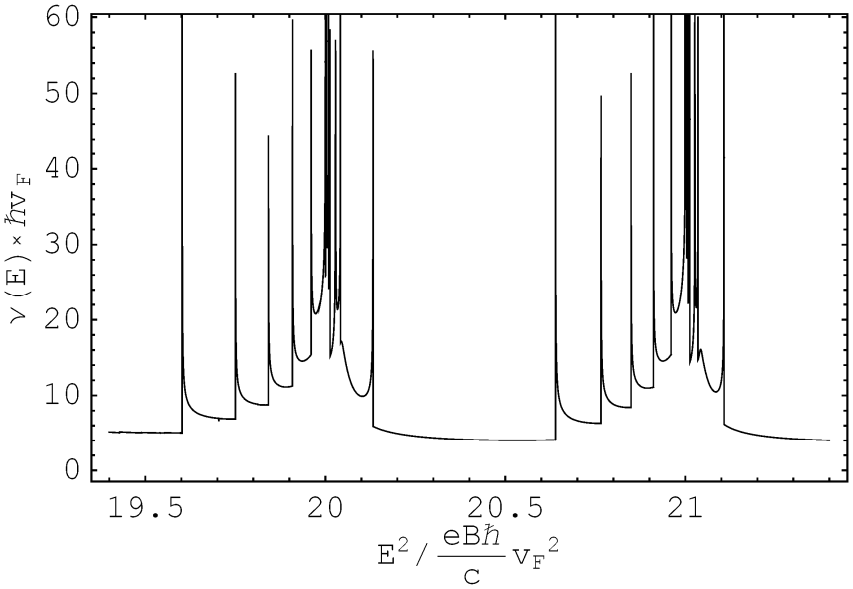

Fig.1. Edge part of the density of states $\nu(E)$.

[1] Elliott H. Lieb, Phys. Rev. Lett. 62, 10, 1201 (1989).
https://doi.org/10.1103/PhysRevLett.62.1927.5
[2] Luyang Wang and Dao-Xin Yao, Phys. Rev. B 98, 161403 (2018).
https://doi.org/10.1103/PhysRevB.98.161403

Manifestation of homogeneous superconductivity in single-crystalline [100] boron-doped diamond film near Superconductor-Insulator transition

O. Onufriienko[1], P. Szabó[1], V. V. Moshchalkov[2], P. Samuely[1], G. Zhang[3,4] and T. Samuely[1]

[1] Centre of Low Temperature Physics, Institute of Experimental Physics, Slovak Academy of Sciences and Faculty of Science, P.J. Šafárik University, 040 01 Košice, Slovakia
[2] Department of Physics and Astronomy, KU Leuven, B-3001 Heverlee, Belgium
[3] National Key Laboratory of Science and Technology on Advanced Composites in Special Environments, Harbin Institute of Technology, 150080 Harbin, China
[4] Zhengzhou Research Institute, Harbin Institute of Technology, 450000 Zhengzhou, China
e-mail: onufriienko@saske.sk

In ordinary life, diamonds are used as pieces of jewelry of the highest quality. In science and industry, they are also primarily known for their excellent dielectric properties and extremely high hardness. However, when diamonds are doped with boron, they can be converted into semiconductors and even superconductors. One interesting issue to study are the boundary conditions of transition from one state to another.

The transition from a superconductor to an insulator (SIT) in boron-doped diamond can be realized by reducing the concentration of charge carriers in two ways: either by directly reducing the boron concentration [1, 2], or by altering the orientation of crystal growth. The latter owes to the fact that the concentration of Hall carriers can exceed the actual doping concentration due to the distortion of the Fermi surface [3].

Here we present a scanning tunneling microscopy/spectroscopy (STM/S) study of superconductivity in a single-crystalline boron-doped [100] diamond film prepared by Chemical vapor deposition (CVD) with a low doping level of $n = 3\times10^{20}$ cm^{-3}. Homogeneous superconductivity with parameters $\Delta(0) = 0.13$ meV, $T_C = 0.85$ K, and H_{C2} between **1.5-1.6 T** was observed even at the boron concentration limit for SIT (Fig. 1).

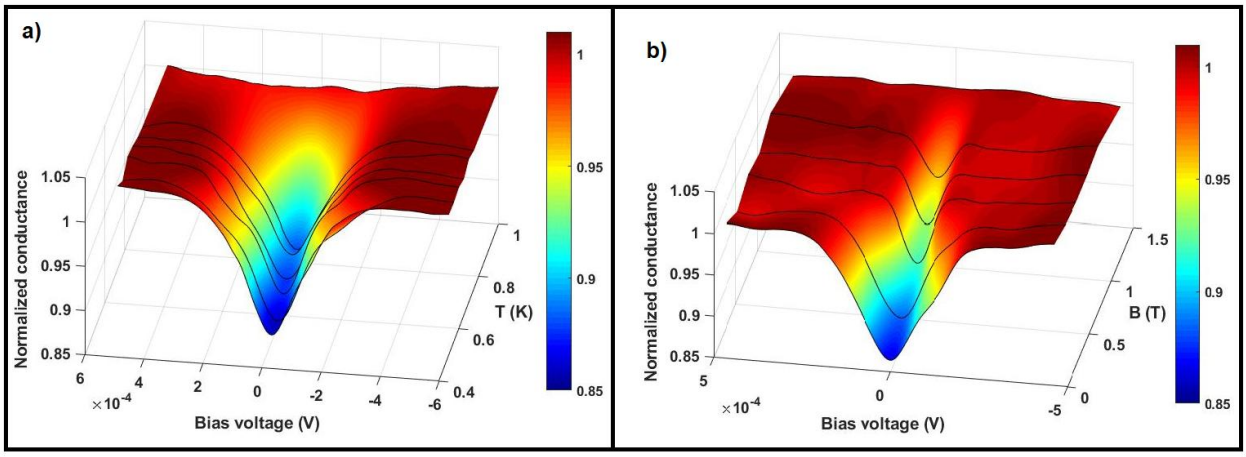

Figure 1. Normalized differential conductance vs. Bias voltage at temperature in range of 0.45-1 K (a) and in parallel magnetic field 0-1.5 T at temperature $T = 0.5$ K (b).

[1] E. Bustarret, J. Kačmarčik, C. Marcenat, E. Gheeraert, C. Cytermann, J. Marcus, and T. Klein Phys. Rev. Lett. 93, 237005 (2004).
[2] E Bustarret, P Achatz, B Sacépé, C Chapelier, C Marcenat, L Ortéga and T Klein, Phil. Trans. R. Soc. A, 366, 267–279 (2008).
[3] Akihiro Kawano, Hitoshi Ishiwata, Shingo Iriyama, Ryosuke Okada, Takahide Yamaguchi, Yoshihiko Takano, and Hiroshi Kawarada, Phys. Rev. B 82, 085318 (2010).

Study of the pseudogap temperature dependence in YBCO films in magnetic fields up to 8 T

E. V. Petrenko[1], L. V. Bludova[1], A. V. Terekhov[1], A. L. Solovjov[1], K. Rogacki[2]

[1] B. Verkin Institute for Low Temperature Physics and Engineering of NAS of Ukraine, 47 Nauky Ave., Kharkiv, 61103, Ukraine
[2] Institute for Low Temperatures and Structure Research, Polish Academy of Sciences, P.O. Box 1410, 50-950 Wroclaw, Poland
e-mail:petrenko@ilt.kharkov.ua

The number of works devoted to high-temperature superconductors (HTSCs) keeps growing steadily. It is believed that understanding the mechanism of electron pairing in HTSCs will indicate the direction of synthesis of superconductors with a desired high T_c. For this, it is necessary to study the properties of HTSCs in the normal state, especially in cuprates, where the pseudogap (PG) is opened at $T^*>>T_c$. It is worth noting that the PG state refers to a range of temperatures and energies where the density of states in a superconductor is suppressed, but superconductivity is not yet fully developed. This state is sensitive to the presence of a magnetic field, which can further modify the electronic and magnetic properties of the material. Obviously, applying of an external magnetic field is one of the excellent methods to study superconducting properties of cuprate HTSCs.

In our work, we studied a high quality 100 nm-thick YBCO film by having performed resistive measurements up to 8 T in $H||ab$ configuration.

Below the PG opening temperature T^*, the resistivity curves of studied sample deviate downward from linear dependencies at high temperatures that results in appearance of the excess conductivity $\sigma'(T)$. In our approach, in order to explicitly describe the PG temperature dependence $\Delta^*(T)$ under the influence of external magnetic fields, we utilized an equation proposed within the framework of the local pair (LP) model [1, 2], in which the equation is used for the experimentally measured $\sigma'(T)$:

$$\sigma'(T) = A_4 \frac{e^2 \left(1 - \frac{T}{T^*}\right) \exp\left(-\frac{\Delta^*(T)}{T}\right)}{16\hbar\xi_c(0)\sqrt{2\varepsilon^*_{c0}\sinh\left(2\frac{\varepsilon}{\varepsilon^*_{c0}}\right)}}, \qquad (1)$$

In this case, the dynamics of pair formation $(1 - T/T^*)$ and pair breaking $(\exp[-\Delta^*(T)/T])$ above T_c are taken into account. Here, e is an elementary charge of electron, T^* is a PG opening temperature, A_4 is a numerical factor, $\hbar$ is a reduced Planck constant, $\xi_c(0)$ is a coherence length along the c-axis, ε is a reduced temperature, ε^*_{c0} is a theoretical parameter.

Having obtained reliable data of $\sigma'(T,H)$, we plotted series of $\Delta^*(T,H)$ and compared the results in the vicinity of T_c with the Peters-Bauer (PB) theory. The further details will be presented directly at the conference.

[1] A. L. Solovjov and V. M. Dmitriev, *Low Temp. Phys.* **32**, 99 (2006). https://doi.org/10.1063/1.2171509
[2] A. L. Solovjov and V. M. Dmitriev, *Low Temp. Phys.* **35**, 169 (2009). https://doi.org/10.1063/1.3081150

Experimental verification of the occurrence of rectified voltage (“diode effect”) in multiply connected superconducting structures

A. G. Sivakov[1], O. G. Turutanov[2,1], A. S. Pokhila[1], A. V. Krevsun[1], A. E. Kolinko[1], and S. I. Bondarenko[1]

[1] B.Verkin Institute for Low Temperature Physics and Engineering of NAS of Ukraine, 47 Nauky Ave., Kharkiv, 61103, Ukraine
[2] Department of Experimental Physics, Comenius University, Mlynská dolina, 84248 Bratislava, Slovakia
e-mail:pokhila@ilt.kharkov.ua

Recent studies have increasingly focused on the superconducting diode effect, which is characterized by the nonreciprocity of the critical current and, consequently, the voltage rectification effect. Analogous to a semiconductor diode, a superconducting diode could become a fundamental component of superconducting electronics, relying on various quantum phenomena. The phenomenon of rectification, attributed to the asymmetry of the critical current, has been recognized for over 60 years. It was initially examined in [1] using a two-contact Josephson interferometer with clamping contacts (dc SQUID), where it was attributed to the difference in the contacts' critical currents. A similar effect results from the unequal inductances of Josephson contacts. In [2], it was demonstrated that in a doubly connected circuit without Josephson contacts, oscillations of the critical current emerge due to summing of the transport and circulating currents. Occasionally, this interaction causes a displacement of the critical current's peak in the magnetic field away from the zero value. Presumably, this anisotropy of the critical current is due to the inequality of the critical currents within the circuit's branches. Our work experimentally establishes that the rectified voltage (diode effect) correlates with the dissimilarity in the critical currents or the inductances of the circuit's branches. These measurements were conducted on the same structure, changing the critical current's value in the branches with a focused laser probe or modifying the geometric inductance by switching the current feed terminals. Thus, we have shown that a superconducting diode effect can be realized by using simple properties of critical currents in inhomogeneous structures and does not require involving complex quantum phenomena related to current nonreciprocity.

The work was supported in part by grant of the Science and Technology Center in Ukraine (Project Number 9918). O.T. acknowledges support of SPS Programme NATO under grant G5796 and the EU NextGenerationEU funded through the Recovery and Resilience Plan for Slovakia under the project No. 09I03-03-V01-00031.

[1] A. Th. A. M. De Waele and R. de Bruyn Ouboter, Physica 41, 225 (1969). https://doi.org/10.1016/0031-8914(69)90116-5
[2] A. G. Sivakov, A. S. Pokhila, A. M. Glukhov, S. V. Kuplevakhsky, A. N. Omelyanchouk, Low Temp. Phys. 40, 408 (2014). https://doi.org/10.1063/1.4876229

Hopping Hall effect in multi-walled carbon nanotubes

R. M. Rudenko[1], O. O. Voitsihovska[1], A. A. Abakumov[2], V. M. Poroshin[1]

[1] Institute of Physics, NAS of Ukraine, 46 avenu Nauky, 03680, Kyiv, Ukraine
[2] L.V. Pisarzhevskii Institute of Physical Chemistry, NAS of Ukraine,
31 Avenue Nauky, 03028, Kyiv, Ukraine
e-mail: rudenko.romann@gmail.com

Carbon nanotubes are promising material for applications in many fields, including electronic devices, due to their unique physical and electrical properties. Hall effect is a valuable tool for the investigation of charge transport in materials. Despite this, only a small number of works have studied the Hall effect in carbon nanotubes. This paper presents the results of an experimental study of the Hall effect in multi-walled carbon nanotubes (MWCNT, Arkema, France) in a wide temperature range of 12–300 K. The measurements of the Hall effect were performed by the van der Pauw method in a helium cryostat. The studied MWCNT samples had the shape of a rectangular parallelepiped with dimensions 5x5x0.3 mm^3, obtained under pressure conditions of ~100 MPa. In the studied temperature range, the Hall coefficient is positive and equal to 0.04 cm^3/C. The investigation of the temperature dependences of the Hall mobility indicates that the Efros-Shklovskii variable range hopping (ESVRH) conductivity provides the main contribution to the Hall effect in the entire studied temperature range of 12–300 K. Hall mobility shows a slight increase from 1 $cm^2/(V*s)$ to 2 $cm^2/(V*s)$ with increasing temperature. This behavior can be described by the exponential law (Fig. 1a) theoretically predicted for disordered semiconductors [1]:

$$\mu_H \sim \exp\left[-\left(\frac{T_0}{T}\right)^{1/2}\right] \quad (1)$$

where α is a numerical coefficient, T_0 is a characteristic temperature from the Efros-Shklovskii ESVRH conduction law $G \sim exp[-(T_0/T)^{1/2}]$. The investigation finds that T_0=11 K and $\alpha \approx 0.7$. It is interesting to note that the conductivity of MWCNTs follows ESVRH below 90 K (Fig. 1b). At the same time, the contribution of hopping conductivity to the Hall effect remains significant up to 300 K (Fig. 1a). Such behavior agrees with the data of investigation of the Hall effect in reduced graphene oxide that we reported previously [2].

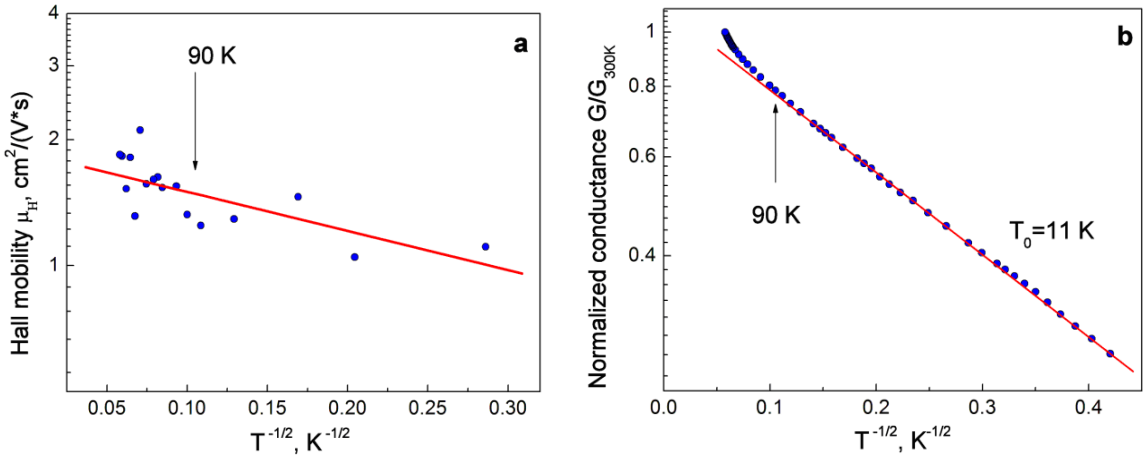

Fig. 1. Temperature dependence of conductance (a) and Hall mobility of charge carriers (b) in MWCNT.

[1] T. Holstein, Phys. Rev. 124 (1961) 1329. https://doi.org/10.1103/PhysRev.124.1329.
[2] R. Rudenko, O. Voitsihovska, A. Abakumov et al, Mater. Lett. 326 (2022) 132932.

Controlling the efficiency of the superconducting “diode effect” using microwave radiation

A. G. Sivakov[1], O. G. Turutanov[2,1], A. S. Pokhila[1], A. E. Kolinko[1], M. Grajcar[2,3]

[1] B. Verkin Institute for Low Temperature Physics and Engineering of NAS of Ukraine, 47 Nauky Ave., Kharkiv, 61103, Ukraine
[2] Department of Experimental Physics, Comenius University, Mlynská dolina, 84248 Bratislava, Slovakia
[3] Institute of Physics, Slovak Academy of Sciences, Dúbravská cesta, Bratislava, Slovakia
e-mail: sivakov@ilt.kharkov.ua

The superconducting diode effect, characterized by the nonreciprocity of superconducting currents, has garnered significant interest due to its demonstration of quantum physical phenomena with promising applications in superconducting electronics. The fundamental mechanisms that induce the superconducting diode effect include the simultaneous breaking of space-inversion and time-reversal symmetry, magnetochiral anisotropy, the interplay between spin-orbit interaction energy and the characteristic energy scale of supercurrent carriers, and finite-momentum Cooper pairing. Experimentally, the diode effect's efficiency is gauged by the asymmetry magnitude of critical currents in opposing directions. Meanwhile, most studies do not address the resistive state mechanisms or the nature of critical current emergence.

However, it is necessary to keep in mind that it is the superconducting current density that becomes critical locally, and is achieved at one of the sample’s edges of the when reaching the energy edge barrier. Since the perpendicular magnetic field components from the transport current have different directions at the sample's opposite edges, the magnetic field increase reduces the barrier where the external magnetic field and the current field coincide in sign and increases it at the opposite edge.

As shown in [1], the critical state occurs only at one “weaker” barrier. Therefore, by selecting the magnetic field and transport current directions, one can independently assess the critical current required to overcome each edge barrier. The critical currents will differ for opposite directions if the edge barriers' values are not equal, indicating a diode effect.

To induce a diode effect in superconducting tin strips, we introduced a local geometric inhomogeneity at one strip edge, increasing the local current density and reducing the critical current in one direction. Altering the magnetic field direction changes the diode effect's "sign" and efficiency (the difference in critical current for opposite directions) which reached 30%.

Besides the magnetic field, other external factors, such as microwave irradiation, can affect the edge barrier's value and the critical current. If the microwave field differently suppresses critical currents at the sample's edges, one can select a power level where the critical current becomes zero for one direction of transport current and finite for the other.

This scenario was realized in our experiment, allowing us to claim a 100% efficiency for the superconducting diode effect.

M.G. acknowledges support from SPS Programme NATO grant number G5796 and Slovak Research and Development Agency under the contracts APVV-20-0425. O.T. has been funded by the EU NextGenerationEU through the Recovery and Resilience Plan for Slovakia under the project No. 09I03-03-V01-00031.

[1] A. G. Sivakov, O. G. Turutanov, A. E. Kolinko, A. S. Pokhila. Low Temp. Phys. 44, 226 (2018). https://doi.org/10.1063/1.5024540

Josephson weak link based on proximity effect in long bimetallic thin-film bridge

O. G. Turutanov[1,2], A. G. Sivakov[2], A. S. Pokhila[2], M. Grajcar[1,3]

[1] Department of Experimental Physics, Comenius University, Mlynská dolina, 84248 Bratislava, Slovakia
[2] B. Verkin Institute for Low Temperature Physics and Engineering of NAS of Ukraine, 47 Nauky Ave., Kharkiv, 61103, Ukraine
[3] Institute of Physics, Slovak Academy of Sciences, Dúbravská cesta, Bratislava, Slovakia
e-mail: oleh.turutanov@fmph.uniba.sk, turutanov@ilt.kharkov.ua

Stationary and non-stationary Josephson effects are fundamental phenomena for the operation of nearly all modern superconducting electronics. Utilizing the Josephson tunnel junction (JJ), often with an external shunt to mitigate junction capacitance effects, yields the best device characteristics primarily due to a pure sine current-phase relation (CPR). However, their reproducible fabrication is complicated and costly, making them less suitable for small research projects. Various types of weak links, such as microbridges, exhibit non-sine CPR well below the critical temperature.

We studied the resistive state of long superconducting thin-film bridges with non-equilibrium regions called phase-slip centers (PSC) and lines (PSL), and the effect of shunting them by normal-metal covering as an additional channel for quasiparticle diffusion. We found that a bimetallic thin-film sandwich of Sn/Al, patterned as a 1x5 μm strip, showed "good" Josephson behaviour with the close-to-sine CPR. This was confirmed through the observation of at least the first 12 Shapiro steps in the current-voltage characteristics under 10 to 20 GHz microwave irradiation. Their voltage positions are 20% less than those following from the Josephson relation $V=hf/2e$. We propose a possible explanation for this fact. Notably, no subharmonic steps associated with non-sine CPR were observed while the oscillations of the n-th current step width with microwave field amplitude qualitatively follow the Bessel functions of n-th order. Thus, such a simple bimetallic bridge holds promise for use as a weak link in superconducting electronic devices, including SQUIDs and others.

Unexpectedly, we observed another set of small oscillations superimposed on the main oscillations. Simple modelling shows that this curve shape may arise from two parallel periodic processes: one with a 2π-periodicity and the other with a 4π-periodicity. The 4π-periodic CPR is typically associated with topological superconductors with a superconductor-semiconductor interface and Majorana states [1], which is not the case for our normal metal-superconductor interface. However, Landau-Zener transitions occurring at the anticrossing of highly transparent 2π-periodic Andreev states can induce 4π-periodic behavior, as discussed in [2]. These transitions can consequently result in the intriguing shape observed in the oscillating dependence of the Shapiro step width on the microwave field amplitude.

An interesting aspect of the discussed structure is that, due to the normal-metal layer, the entire long bridge behaves as a single weak link with a CPR close to sine, despite it may contain of up to four PSCs in it. Each PSC can be regarded as a "dynamic Josephson junction" [3].

The work was partially supported by SPS Programme NATO grant number G5796 and Slovak Research and Development Agency under the contracts APVV-20-0425. O.T. has been funded by the EU NextGenerationEU through the Recovery and Resilience Plan for Slovakia under the project No. 09I03-03-V01-00031.

[1] F. Dom'inguez, O. Kashuba, E. Bocquillon, et. al., Phys. Rev. B 95, 195430 (2017). https://doi.org/10.1103/PhysRevB.95.195430
[2] J. Wiedenmann, E. Bocquillon, R. S. Deacon, et al., Nature Comm. 7, 10303 (2016) . https://doi.org/10.1038/ncomms10303
[3] A. G. Sivakov, A. M. Glukhov, A. N. Omelyanchouk, Y. Koval, P. Müller, and A. V. Ustinov, Phys. Rev. Lett. 91, 267001 (2003). https://doi.org/10.1103/PhysRevLett.91.267001

MAGNETISM AND MAGNETIC MATERIALS

Effect of higher-order exchange interactions for skyrmion stability in monolayer MnSeTe

Megha Arya[1], Lionel Calmels[1], Rĭmi Arras[1], Soumyajyoti Haldar[2], Stefan Heinze[2], and Dongzhe Li[1]

[1] CEMES, Universitŭ de Toulouse, CNRS, 29 rue Jeanne Marvig, F-31055 Toulouse, France
[2] Institute of Theoretical Physics and Astrophysics, University of Kiel, Leibnizstrasse 15, 24098 Kiel, Germany
e-mail: meghaphy2@gmail.com

Magnetic skyrmions in atomically thin van der Waals (vdW) materials provide an ideal playground to push skyrmion technology to the single-layer limit. Here, we investigate the intrinsic magnetic skyrmions in a monolayer Janus vdW magnet, MnSeTe, by firstprinciples calculations combined with atomistic spin simulations. A very large Dzyaloshinskii-Moriya interaction (DMI) is observed due to the intrinsic broken inversion symmetry and strong spin-orbit coupling for monolayer MnSeTe, which is in agreement with the literature.

We will show that the interplay between the large DMI, the exchange coupling, and the magnetic anisotropy energy allows stabilizing zero-field nanoscale skyrmions in monolayer MnSeTe, becoming technologically competitive. We further show that the nanoscale skyrmions have moderate energy barriers protecting skyrmions against annihilation. Finally, we unravel the role of higher-order exchange interactions - which have so far been overlooked- as they can play an intriguing role in the stability of skyrmions.

Experimental analysis of magnetocaloric behavior of selected Laves phases compounds and their composites for low-temperature refrigerators performing an Ericsson cycle

J. Ćwik[1], Y. Koshkid`ko[1], K. Nenkov[2], B. Weise[2], A. Czernuszewicz[3]. K. Shinde[4], N. de Oliveira[5]

[1] Institute of Low Temperature and Structure Research, PAS, Okólna 2,Wrocław, 50-422, Poland
[2] Leibniz IFW Dresden, Institute for Complex Materials, Dresden, D-01069, Germany
[3] Ames National Laboratory, U.S. Department of Energy, Iowa State University, Ames, IA 50011, USA
[4] Department of Materials and Science and Engineering, Hanbat National University, Daejeon 34158, Republic of Korea
[5] Instituto de Física Armando Dias Tavares-Universidade do Estado do Rio de Janeiro, Rua São Francisco Xavier 524, 20550-013 Rio de Janeiro, RJ, Brazil
e-mail: j.cwik@intibs.pl

The magnetocaloric effect (MCE) is an exciting topic of investigation in the condensed matter physics field due to the link between magnetic and thermal properties of magnetic materials and its applicability in refrigeration technology. The compounds from the RNi_2 family, where *R* stands for rare earth metal, attracted a significant amount of attention due to their special properties associated with highly localized magnetic moments that originate from the incompletely filled 4*f*-electron shell of the lanthanide atoms. In those compounds, *Ni* atoms stay in the non-magnetic state. The 4*f*-4*f* interactions are weak since the wave functions derived from the lanthanides have a small range as compared to the interatomic distances. As a result, one can observe low magnetic ordering temperatures, which makes those materials ideal candidates for low-temperature refrigerants, since they exhibit a high magnetocaloric effect (MCE) [1-3].

The majority of reports on magnetocaloric subjects are concentrated in the experimental investigations that are usually performed by heat capacity measurements with and without an applied magnetic field or by magnetic methods. In this work, the influence of simultaneous substitution within the rare earth sublattice on the magnetic and magnetocaloric properties in a wide magnetic field range, up to 14 T, on $RR`Ni_2$ (*R*,*R`* = heavy rare earth elements) Laves phase solid solutions synthesized by the arc-melting method has been studied. To improve the knowledge of the properties of considered solid solutions, both direct and indirect methods were used to characterize the high-field properties of the adiabatic temperature change, ΔT_{ad}, and the magnetic entropy change, ΔS_M. The obtained values are high and close to each other in the specified temperature range, which allows us to conclude that studied solid solutions are promising candidates for magnetocaloric material at low temperatures, which is crucial for a regenerative cryocooler to reach a liquid-gases temperature. Composites with optimum proportions of the selected individual Laves phases components were obtained through the innovative high-pressure synthesis. The results indicate that the proposed composites are good candidates to be used as the refrigerant material in a magnetic refrigerator performing an Ericsson cycle at low temperatures.

The work was supported by the National Science Center, Poland through the OPUS Program under Grant No. 2019/33/B/ST5/01853.

[1] H. R. Kirchmayr, E. Burzo, in: H.P.J. Wijn (Ed.), Landolt-Börnstein, New Series III/19d2, Berlin (1990).
[2] W.E. Wallace, E. Segal, in: A.M. Alper, J.L. Margrave, A.S. Nowick (Eds.), Rare Earth Intermetallics, Academic Press, New York, (1973).
[3] K.A. Gschneidner Jr. et al., Adv. Cryog. Eng. 42, 465 (1996).

Ni-Fe-based layered double hydroxides: cluster glass and low-temperature magnetic phase separation

A. V. Fedorchenko[1], E. L. Fertman[1], Yu. G. Pashkevich[2], D. E. L. Vieira[3], E. Čižmár[4], V. Tkáč[4], R. Tarasenko[4], A. Feher[4], A. N. Salak[3]

[1] B.Verkin Institute for Low Temperature Physics and Engineering of NAS of Ukraine, 47 Nauky Ave., Kharkiv, 61103, Ukraine
[2] O. Galkin Donetsk Institute for Physics and Engineering of NASU, 03028 Kyiv, Ukraine
[3] Department of Materials and Ceramic Engineering, CICECO – Aveiro Institute of Materials, University of Aveiro, 3810-193 Aveiro, Portugal
[4] Institute of Physics, Faculty of Science, P.J. Šafárik University in Košice, 041 54 Košice, Slovakia
e-mail: fedorchenko.alexey@gmail.com

The low-temperature static and dynamic magnetic properties and heat capacity for Ni(II)-Fe(III) layered double hydroxides (LDH) with the nickel-to-iron ratio of n = 2, 3 have been studied in a wide range of magnetic fields up to 70 kOe. The cluster glass magnetic behavior in the high-temperature region (below about 100 K) was revealed for Ni_2Fe-based LDH, which is associated with the clustering of iron in metal layers. Below 5 K, these LDH demonstrate a step initial magnetization curves and wasp-waisted magnetization loops evident in magnetic phase separation. The effect is associated with a magnetic phase segregated state of Ni_2Fe LDH: at least two different magnetic phases coexist at low temperatures, at least below 5 K. At the same time, no effect is seen for the composition with cation ratio Ni/Fe=3.

The spontaneous magnetization appears for all the Ni-Fe LDH studied below 17 K; it is accompanied by magnetization loops of ferromagnetic type. Frequency-independent peak of the temperature dependent *ac* magnetic susceptibility curves is accompanied by the corresponding anomaly of the temperature dependent heat capacity.

To reveal the nature of the phase-segregated state found in Ni2Fe-based LDH XAS/XMCD experiment will be performed at the DEIMOS soft X-ray beamline (SOLEIL, France).

This work was supported by the EU H2020 project European Microkelvin Platform (EMP) - grant agreement No. 824109 and Slovakia-Portugal bilateral project FAST-LDH (2019-2020)/APVV-SK-PT-18-0019.

Nano-Oscillator Based on a 3D Non-Uniform Antiferromagnetic Spin Texture

V. S. Gerasimchuk[1], Yu. I. Gorobets[1,2], O. Yu. Gorobets[1], I. V. Gerasimchuk[1,2]

[1] National Technical University of Ukraine "Igor Sikorsky Kyiv Polytechnic Institute", Beresteisky Ave. 37, Kyiv 03056, Ukraine
[2] Institute of Magnetism, NAS of Ukraine and Ministry of Education and Science of Ukraine, Vernadsky Blvd. 36b, Kyiv 03142, Ukraine
e-mail: igor.gera@gmail.com

Topologically non-trivial two-dimensional magnetization configurations (solitons in magnets), such as skyrmions and vortices, are promising as information carriers for spintronics and magnonics [1]. Skyrmions exhibit several well-known dynamic regimes, among them are breathing modes when the skyrmion radius changes, and rotational modes when the position of the skyrmion core fluctuates. Various combinations of these modes and transitions between them, as well as inertial dynamics [2], can take place. To describe the oscillations of skyrmions and their translational motion, the Thiele equation is often used, in which inertial effects are taken into account when introducing the inertial mass of a skyrmion [2]. However, the real oscillations of spin textures, which take into account the non-uniform distribution of the density of solitons' inertial masses and the densities of driving forces, have not been sufficiently studied. Oscillations of spin textures as a physical process are almost not discussed.

In the present work, we proposed a model of the spatial distribution of magnetization, which is a confined spin configuration of the target skyrmion type in a two-sublattice AFM with perpendicular magnetic anisotropy. Using a 3D non-uniform AFM magnetization distribution and an energy approach, the *surface energy density* and *surface density* of the topological spin texture are calculated as functions of the radius of spin isosurface. Taking these characteristics into account, we derived the *equation of free oscillations of topological spin texture magnetization* in the form of a wave equation with variable coefficients, and found its quasi-classical solution. For a thin axisymmetric circular nanoscale spin configuration, the main characteristics of eigenexcitations are determined, viz., frequency, relative amplitude and period of oscillations. In addition, we found the *topological and inertial masses* of such a dynamical magnetization texture, which correlate with the known numerical and experimental results.

The localized oscillating spin texture is not only a source of rich physics, but also a promising candidate for advances in spintronics. Our results are applicable for finding the amplitude and spectra of oscillations of topological spin textures in confined geometry. We treat the self-oscillatory process of a localized spin texture as a *magnetic nano-oscillator* and can recommend it as a new tunable radio-frequency oscillation source [3].

In contrast to the well-known nano-oscillators driven by spin current such as STNOs or SHNOs, the *nano-oscillator based* directly *on a 3D non-uniform* AFM dynamical *spin texture* (NUST-NO) proposed by us has a different principle of operation and is not a technological structure. Therefore, its physical dimensions are the real dimensions of the spin texture itself (nanometers). It does not require spin currents, and its oscillations are a natural physical process of harmonic oscillations excited in the spin texture in one way or another. However, this does not exclude the use of the dynamical magnetization texture studied by us also as an active element of a high-frequency oscillator based on the spin-transfer torque.

[1] A. Fert, N. Reyren and V. Cros, Nat. Rev. Mater. 2, 17031 (2017). https://doi.org/10.1038/natrevmats.2017.31.
[2] F. Büttner et al., Nat. Phys. 11, 225 (2015). https://doi.org/10.1038/nphys3234.
[3] V. S. Gerasimchuk, Yu. I. Gorobets, O. Yu. Gorobets and I. V. Gerasimchuk, Sci. Rep. 13, 6613 (2023). https://doi.org/10.1038/s41598-023-33220-0.

Multiphonon Raman scattering in $BaBiO_3$

A. Glamazda[1,4], V. Gnezdilov[1,2], P. Lemmens[2,3]

[1] B. Verkin Institute for Low Temperature Physics and Engineering of NAS of Ukraine, 47 Nauky Ave., Kharkiv, 61103, Ukraine
[2] Institute for Condensed Matter Physics, TU-Braunschweig, D-38106 Braunschweig, Germany
[3] Laboratory for Emerging Nanometrology and International Graduate School of Metrology, TU-Braunschweig, D-38106 Braunschweig, Germany
[4] V. N. Karazin Kharkiv National University, 4 Svobody sq., Kharkiv, 61022, Ukraine
e-mail: glamazda@ilt.kharkov.ua

Perovskite oxides, ABO_3 have numerous functionalities, including superconductivity, magnetism, ferroelectricity, and multiferroicity. Such diverse functionalities of these versatile materials arise from the replacement of ions in A or B-site. Among perovskites, $BaBiO_3$ (BBO) is a fascinating compound that has begun to be intensively studied about five decades ago due to a wide variety of intriguing physical properties. BBO caused a lot of confusion when it was experimentally found to have the insulating properties despite theoretical predictions that it should be a metal. As a result, an extensive debate ensued about the mechanism responsible for the insulating properties of BBO. The two most commonly considered mechanisms are charge disproportion, when Bi ions have alternating 3+ and 5+ valence states forming a charge order on the BiO_6-octahedra network, and bond disproportion, when there is strong hybridization between the Bi 6s and O 2p orbitals.

Recent update of interest in $BaBiO_3$ is connected with theoretical predictions of a possible topological insulating state in it with a large topological gap (~0.7 eV). This, together with the natural stability against surface oxidation and defects, makes the bismuth-oxide family of special interest for possible applications in quantum information/computing and spintronics.

In spite of the wide variety of interesting properties of parent and doped BBO, the number of their spectroscopic studies has been limited and the conclusions drawn from these studies are questionable. Raman spectroscopy is a well-established technique to simultaneous probing of lattice, electronic, magnetic and orbital degrees of freedom as well as interaction between them. Here, we propose to re-examine the parent BBO compound to fill the existing gaps in understanding the interplay of lattice distortions and electronic properties using the unique capabilities of Raman spectroscopy. It is known that the phonon subsystem plays an essential role in the formation of mechanical and transport properties of the crystals, as well as being able to couple to other subsystems resulting in generation of new physical properties. The temperature-dependent Raman study of BBO can shed light on the quantum effects suppressed due to thermal-induced fluctuations at room temperature. In this paper, in order to obtain a deeper insight in physics of BBO we offer a comprehensive experimental and theoretical study, which will be studied the crystal lattice dynamics in a wide temperature range of 2 - 300 K, which will be accompanied by a group-theoretical analysis and a theoretical calculation of the phonon frequencies/vibrations and structural instabilities.

V. Gnezdilov and A. Glamazda thank the *Nanophotonic*s journal, De Gruyter, Sciencewise Publishing, and the Optica Foundation for the financial support through the Ukraine Optics and Photonics Researcher Grants.

Quasi-two-dimensional $S = 1/2$ antiferromagnet $Cu[C_6H_2(COO)_4][C_2H_5NH_3]_2$: evidence of field-induced Berezinskii–Kosterlitz–Thouless transition

I. Kozin[1], R. Tarasenko[1] A. Orendáčová[1], E. Čižmár[1], P. Danylchenko[1], V. Tkáč[1], and M. Orendáč[1]

[1] Institute of Physics, Faculty of Science, P.J. Šafárik University in Košice, Park Angelinum 9, 040 01 Košice, Slovakia
e-mail: illia.kozin@student.upjs.sk

The analysis of magnetic susceptibility, magnetization, and specific heat of the studied organo-metallic compound $Cu[C_6H_2(COO)_4][C_2H_5NH_3]_2$ was previously reported. The studied system was identified as a quasi-two-dimensional (quasi-2-D) $S = 1/2$ Heisenberg antiferromagnet with anisotropic exchange interaction forming rectangular lattice with the main intraplane coupling $J_1/k_B \approx 10$ K with the ratio $R=J_2/J_1 \approx 0.7$. No magnetic phase transition was observed at temperatures down to 1.8 K [1].

Our study extends the former investigation by low-temperature specific heat analysis down to 0.4 K under magnetic fields up to 9 T. Specific heat of a pellet-form powder sample was measured by commercial device Physical Property Measurement System (PPMS) using relaxation method. Without external field, long-range magnetic order was still not evident down to 0.4 K. However, such anomalies become observable under applied external magnetic field. Following these anomalies in the specific heat temperature dependence, we constructed a magnetic phase diagram for $Cu[C_6H_2(COO)_4][C_2H_5NH_3]_2$. We compared it with theoretical predictions for the Berezinskii–Kosterlitz–Thouless (BKT) transition in the $S = 1/2$ Heisenberg antiferromagnet on a square lattice. The experimental transition temperatures slightly exceeded those predicted for the square lattice due to interlayer interactions. Additionally, the field dependence of the magnetic entropy confirmed features characteristic of a field-induced BKT transition through the unbinding of bound vortex-antivortex pairs.

This work was supported by the Slovak Research and Development Agency Projects number APVV-18-0197, APVV-20-0324, APVV-22-0172, VEGA Grant No.1/0132/22 of the Scientific Grant Agency of the Ministry of Education, Science, Research and Sport of the Slovak Republic, the Czech Science Foundation Grant No. 21-02550S and the Development Operational Programme Research and Innovation for the project "New unconventional magnetic materials for applications ", ITMS: 313011T544, co-funded by the European Regional Development Fund (ERDF). Material support from U.S. Steel Košice s.r.o. is greatly acknowledged.

[1] R. Nath et al., Phys. Rev. B 91, 054409 (2015).

Locked domain structure of magnetostrictive FeTb/Fe multilayers via the Fe sublayers

Iryna Lukiienko[1,2], Vojtěch Uhlíř[1]

[1] Central European Institute of Technology, Brno University of Technology, Purkyňova 123, 62100 Brno, Czechia
[2] B. Verkin Institute for Low Temperature Physics and Engineering of NAS of Ukraine, 47 Nauky Ave., Kharkiv, 61103, Ukraine
e-mail: lukiienko@vutbr.cz

Alloys based on transition metal and rare-earth components are known as synthetic ferrimagnetic materials. Due to the property of fast spin reversal these compounds are attractive as media for ultrafast laser-induced magnetization switching [1] and spin-transfer-torque-induced domain wall or skyrmion propagation [2]. In case of stabilized stripe-domain structures these materials have been suggested also as media for spin-wave propagation [3]. Due to large magnetic polarization of the rare earth element caused by the transition metal, the synthetic ferrimagnets have giant magnetostrictive properties, which are pronounced not only at low temperatures but also at room temperature [4]. This property allows to use them in different equipment as a component that produces mechanical force, displacement, or torque [5].

Here we focus on complex multilayer structures consisting of ferrimagnetic alloy $Fe_{0.6}Tb_{0.4}$ (4.5 nm) and Fe sublayers. The Fe sublayers are functional here to decrease the total saturation field and, hence, to expand the applicability range. We found an unusual stabilized magnetic domain structure when the FeTb/Fe multilayer is deposited on top of an Fe epitaxial layer (Figure 1), while the Fe sublayers' thickness is close to 1.5-2 nm. Square- and triangle-like magnetic domains are observed (Figure 1) together with stabilized stripe domains, which are common but usually unstable for such kind of synthetic ferrimagnetic systems. These domains are "locked" and applying an in-plane magnetic field of 3 T is not enough to change the magnetic pattern. In the work we discuss how this peculiarity is reflected in magnetostrictive properties of these stacks and how it relates to perpendicular magnetic anisotropy.

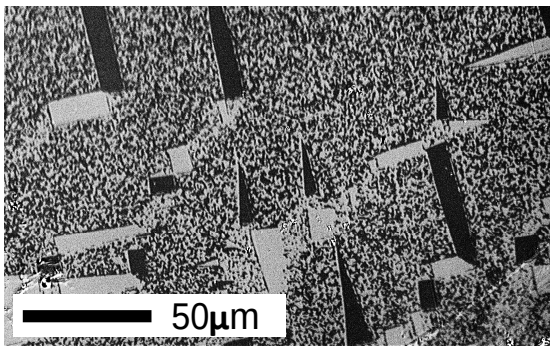

Figure 1. – Images of "locked" domain structure, observed in geometries of longitudinal (on the left) and polar (on the right) magnetooptical Kerr effect.

We acknowledge CzechNanoLab Research Infrastructure supported by MEYS CR (LM2023051). The work has been done in frames of the project IMPROVE VI, registration number CZ.02.01.01/00/22_010/0008114.

[1] C. D. Stanciu et al., Phys. Rev. Lett. 99 (2007) 047601; I. Radu et al., Nature 472 (2011) 205.
[2] A. Sergio, Montoya et al., Commun. Phys. 5 (2022) 293.
[3] C. P. Liu, S. Z. Wu, J. Y. Zhang, J. L. Chen et.al., Nature Nanotechnology 14, 691-697 (2019).
[4] A. Clark, H. Belson, Phys. Rev. B 5 (1972), 3642–3644.
[5] X. Liang, C. Dong, H. Chen, J. Wang, Y. Wei, M. Zaeimbashi, Y. He, A. Matyushov, C. Sun, and N. Sun. Sensors 20 (2020), 1532, https://doi.org/10.3390/s20051532

Single-layer methods for three-dimensional tensor networks

I. V. Lukin[1,2], A. G. Sotnikov[1,2]

[1] Karazin Kharkiv National University, 4 Svobody Square, Kharkiv, 61000, Ukraine
[2] Akhiezer Institute for Theoretical Physics, NSC KIPT, Kharkiv, 61108, Ukraine
e-mail: lukin.ilya@yahoo.com

Tensor networks based numerical methods are widely used to study strongly interacting quantum systems on the lattice in one and two dimensions. 3D systems are much more complex, as the straightforward generalization of two-dimensional approaches leads to very numerically costly algorithms, which makes it difficult to reach highly accurate results with 3D tensor networks. In this work, we present several algorithmic generalizations with single-layer corner-transfer matrix based methods, which allowed us to significantly lower the cost of 3D tensor network calculations and reach more accurate results than the previous studies. We have tested our algorithm on the cubic lattice Heisenberg model and found the results in excellent agreement with previous Monte-Carlo calculations. The proposed numerical algorithms open the door to extensive applications of tensor networks to complex 3D quantum systems.

The authors acknowledge support by the National Research Foundation of Ukraine under the call “Excellent science in Ukraine” (2024-2026).

Spectroscopic signatures of cross-Kerr coupling in a vibrating magnetic beam

A. M. Sokolov[1], T. T. Heikkilä[2]

[1] Institute of Physics of the National Academy of Sciences, Kyiv
[2] Department of Physics and the Nanoscience Center
of the University of Jyväskylä, Jyväskylä, Finland
e-mail: andriy145@gmail.com

We consider a doubly clamped magnetic microbeam [1,2], where both the ferromagnetic resonance (FMR) and the mechanical mode are driven. Surface anisotropy and magnetoelasticity mediate the interaction between the modes. Due to the symmetries in the system, the dominating interaction is of the cross-Kerr type. However, a beam specimen can buckle [1,2], thus breaking the symmetry and generating other coupling types. To facilitate experimental characterization of such beams and similar systems, we study the harmonic structure generated in the beam [1].

We consider the unbuckled case and assume that only the primary modes are excited. Apart from the cross-Kerr coupling, we still allow for a linear coupling. We expect that in the real systems the symmetries might be slightly broken, thus producing a small linear coupling. On the other hand, we assume no subharmonics generated, which we expect is a reasonable assumption for a relatively lossy FMR mode.

We show that the absence of the first sidebands indicates that there is no optomechanical-like coupling, which is the previous-order nonlinear interaction. Position of the second sidebands then convey the information about the cross-Kerr coupling. We provide analytical results in the limit of lossy FMR. First, resonance in the second FMR sideband shifts proportionally to the magnon number and the cross-Kerr coupling strength. Besides, the second sideband in the mechanical mode hybridizes with its primary harmonic. We predict an avoided crossing that is proportional to the phonon number and the cross-Kerr coupling strength.

Our results might be used for characterization of nonlinearities in a variety of hybrid systems [3] with application to quantum technologies. The result on the signature of dominating Kerr interaction is universal for systems of any nature where no subharmonics are generated. While we consider the cross-Kerr coupling specific to magnetic systems, our results on the second sideband positions can be generalized to other forms of interaction.

[1] A. M. Sokolov and T. T. Heikkilä, Phys. Rev. B 109, 014408 (2024). https://dx.doi.org/10.1103/PhysRevB.109.014408.
[2] K. S. U. Kansanen *et al.*, Phys. Rev. B 104, 214416 (2021). https://dx.doi.org/10.1103/PhysRevB.104.214416.
[3] G. Kurizki *et al.*, Quantum technologies with hybrid systems, Proceedings of the National Academy of Sciences 112, 3866 (2015). https://doi.org/10.1073/pnas.1419326112.

Electrical and magnetic properties of $(C_2H_5NH_3)_2CuCl_4$ magnetic multiferroic at low temperatures

O. I. Vira[1], Yu. Eliashevskyy[1], V. Kapustianyk[1], R. Tarasenko[2]

[1] Ivan Franko National University of Lviv, Faculty of Physics, Lviv 79005, Ukraine
[2] Pavol Jozef Safarik University, Institute of Physics, Faculty of Science, Kosice 04154, Slovakia
e-mail: olena.vira@lnu.edu.ua

Magnetic multiferroics are the materials combining the magnetic and ferroelectric types of ordering. The ferroelectrics which belong to this class of materials are of special interest for the scientists since they are characterized by the magnetoelectric coupling that implies the possibility to change the electric polarization by the applied magnetic field whereas the magnetization of a sample would be changed by the applied electric field [1]. Such materials are intensively investigated because the mechanism of these effects is not fully understood, and application of such materials in sensors, memory cells and nanoelectronics looks very prospective [2]. Unfortunately, very few magnetic multiferroics with a large magnetoelectric coupling at the high enough temperatures have been proved, because of the mutually exclusive requirements for the existence of magnetic and electric types of ordering.

The crystal of $(C_2H_5NH_3)_2CuCl_4$ is an organometallic compound belonging to the layered perovskite type multiferroics. This material possesses a quite high spontaneous polarization of 37 $\mu C/cm^2$ below the phase transition temperature of 247 K [3]. Therefore, this crystal is a good candidate for investigations of the magnetoelectric effect. Besides the ferroelectric transition, several other structural transitions also accompanied by different arrangements of hydrogen bonds in the organic chains occur at higher temperatures. The temperature dependence of the magnetization showed the presence of the antiferromagnetic transition at 10.2 K, which is transformed into the ferromagnetic one under the influence of applied magnetic field [4].

The electrical properties of this crystal were measured down to the liquid helium temperature. The anomalous behavior of the dielectric parameters as a function of temperature was observed in vicinity of the low-temperature phase transition at 10.2 K. Investigations of the dielectric parameters revealed the shift of the ferroelectric phase transition temperature under the influence of external magnetic field. There was observed increasing of the spontaneous polarization, measured using the pyroelectric current methods, with increasing of magnetic field up to 9 T. The magnetodielectric effect was also detected.

[1] M. Fiebig, Revival of the magnetoelectric effect, J. Phys. D: Appl. Phys. 38 (8) (2005) R123. https://doi.org/10.1088/0022-3727/38/8/R01.
[2] R. Ramesh, N.A. Spaldin, Multiferroics: progress and prospects in thin films, Nat. Mater. 6 (2007) 21. https://doi.org/10.1038/nmat1805.
[3] B. Kundys, A. Lappas, M. Viret, V. Kapustianyk, V. Rudyk, S. Semak, C. Simon, I. Bakaimi, Multiferroicity and hydrogen-bond ordering in $(C_2H_5NH_3)_2CuCl_4$ featuring dominant ferromagnetic interactions, Phys. Rev. B 81 (2010) 224434. https://doi.org/10.1103/PhysRevB.81.224434.
[4] Pavla Šenjug, Jure Dragović, Matija Kalanj, Filip Torić, Mirta Rubčić, Damir Pajić, Magnetic behaviour of $(C_2H_5NH_3)_2CuCl_4$ type multiferroic, J. of Magnetism and Magnetic Mater. 479 (2019) 144-148. https://doi.org/10.1016/j.jmmm.2019.02.020.

Features of magnetic properties of α-$Cr_3(PO_4)_2$ crystal

O. Bludov[1], Yu. Savina[1], V. Pashchenko[1], M. Kobets[1] T. Zajarniuk[2], M.U. Gutowska[2], A. Szewczyk[2]

[1] B.Verkin Institute for Low Temperature Physics and Engineering of NAS of Ukraine, 47 Nauky Ave., Kharkiv, 61103, Ukraine
[2] Institute of Physics of PAS, al. Lotników 32/46, 02-668, Warsaw, Poland
e-mail: bludov@ilt.kharkov.ua

Present work is devoted to the experimental investigations of magnetic and thermal properties of a single crystal α–$Cr_3(PO_4)_2$. The temperature and field dependences of magnetization ($M(T)$ and $M(H)$) have been measured by using a SQUID magnetometer MPMS–XL5 (Quantum Design) in the temperature range 2–350 K and external magnetic fields up to 5 T for three crystallographic axes. The $M(H)$ dependences have been measured in the range of field ±5 T at various temperatures in magnetically ordered state below T_N = 29 K. The temperature dependences of specific heat $C_p(T)$ have been measured by using a PPMS (Quantum Design) in the temperature range 2–300 K and external magnetic field up to 9 T directed along and perpendicular to the crystallographic *b* axis.

The chromium orthophosphate α–$Cr_3(PO_4)_2$ crystallizes in the orthorhombic system, space group $P2_12_12_1$ with a = 8.4849 Å, b = 10.3317 Å, c = 14.206 Å, Z = 8. The structure of this compound is quite complex and contains six crystallographically inequivalent positions of the Cr^{2+} ions. In the simple way, the structure of α–$Cr_3(PO_4)_2$ can be represented as a close packing of chromium helices directed along the *b* axis. The PO_4 groups are situated in the centers of the helices and between them [1].

Above T_N, the temperature dependences of susceptibility $\chi(T)$ can be described by using a Curie–Weiss law with the effective magnetic moments 4.41, 4.38, 4.49 μ_B per Cr^{2+} and Weiss temperatures 77, 76, 75 K for *a*, *c* and *b* axis, respectively. The magnetic ordering manifests itself by kink on $\chi(T)$ at 29 K and by the appearance of the spontaneous magnetization $M_S(T)$ in plane perpendicular to the *b* axis. The existence of a l –anomaly on the temperature dependences of specific heat $C_p(T)$ confirms the magnetic ordering at 29 K too. These results agree with those obtained in [2]. It was shown that α–$Cr_3(PO_4)_2$ is an antiferromagnet with an easy axis directed along the *b* axis.

The absolute value of $M_S(T)$ increases with decreasing of temperature, riches the maximum of 8.8×10^{-3} μ_B per Cr^{2+} at 18.8 K, then decreases to zero at 8.35 K and rises to the 1.3×10^{-2} μ_B per Cr^{2+} value down to 2.5 K. Peak on $C_p(T)$ for $H \wedge b$ near the compensation temperature has been discovered. It is evidence of the first-order phase transition happening in the crystal. Weak peculiarity on all $C_p(T)$ dependences near 17 K has been found.

[1] R. Glaum and A. Schmidt, *Z. anorg. Allg. Chem.* **623**, 1672 (1997).
[2] A.N. Vasiliev et al., *Phys. Rev. B* **85** 014415 (2012).

Temperature changes in magnetostatic properties of Al-doped yttrium iron garnets

V. Yu. Borynskyi[1], A. F. Kravets[1], D. L. Popadiuk[1], Yu. Yu. Shlapa[2], S. O. Solopan[2], A. G. Belous[2], A. I. Tovstolytkin[1]

[1] Institute of Magnetism of the NAS of Ukraine and MES of Ukraine, 36-b Akad. Vernadskogo blvd., Kyiv, 03142, Ukraine
[2] V.I. Vernadsky Institute of General and Inorganic Chemistry of the NAS of Ukraine, 32/34 Palladina ave., Kyiv, 03142, Ukraine
e-mail: vladislav.borinskiy@gmail.com

Yttrium iron garnets (YIG) and the garnet ferrites class of compounds, in general, have been among leading magnetic materials for many decades owing to their exceptional electromagnetic properties. Possessing high electrical resistance, high magnetization, and, at the same time, low dynamic losses, such ferrimagnetic insulators serve as essential parts in many microwave devices and other modern technologies, such as magnonics and magneto-optics [1]. Even though YIG's physical properties are well studied, there is a need for cheap mechanisms on reliable control and reproducibility of garnet final magnetic parameters. One way to tailoring their physical properties is doping initial mixture with non-magnetic cations, e.g., Al^{3+}. In this work, we have prepared a set of ceramic samples, sintered at 1350 °C using Al-doped YIG powders that were preliminarily synthesized via precipitation in aqueous solutions at different conditions [2]. The final garnet composition was $Y_3AlFe_4O_{12}$ for all samples.

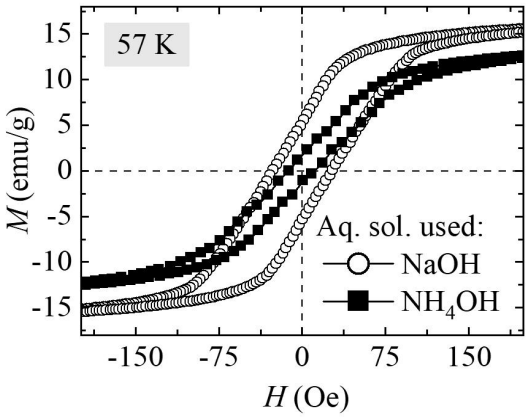

Fig. 1. Hysteresis curves at 57 K for the samples synthesized in different aqueous solutions.

Our magnetometry measurements show that the sample precipitated with ammonium hydroxide exhibits notably lower coercivity and saturation magnetization when compared to the sample synthesized with sodium hydroxide. Fig. 1 represents the hysteresis curves of the above-mentioned garnet samples at the selected temperature 57 K. It is also worth noting that the saturation magnetization and the coercive force of the sample prepared with NaOH reveal non-trivial behavior in the low-temperature range – both experience a slight increase (~4%) upon heating to 57 K. While the former can arise in a zero-field cooled measurements process likely due to magnetic moments of individual polycrystalline grains freezing along their specific anisotropic directions, the latter remains unclear. Elaborated discussion will be presented in forthcoming works.

This work was partially performed in the framework of the "Grants of the NAS of Ukraine to research laboratories/groups of young scientists of the NAS of Ukraine" (proj. No 0124U002212).

[1] V. Harris, IEEE Trans. Magn. 48, 1075 (2011). https://doi.org/10.1109/TMAG.2011.2180732.
[2] S. Solopan, A. Tovstolytkin, V. Zamorskyi, Yu. Shlapa, V.-A. Maraloiu, O. Fedorchuk and A. Belous, J. All. Comp. 968, 172248 (2023). https://doi.org/10.1016/j.jallcom.2023.172248.

Lattice dynamics in the thiospinel $CuIr_2S_4$: Raman spectroscopic studies across the metal-insulator transition

A. Glamazda[1,3], V. Gnezdilov[1,2], V. Tsurkan[4,5], P. Lemmens[2,6]

[1] B. Verkin Institute for Low Temperature Physics and Engineering of NAS of Ukraine, 47 Nauky Ave., Kharkiv, 61103, Ukraine
[2] Institute of Condensed Matter Physics, TU Braunschweig, D-38106 Braunschweig, Germany
[3] V. N. Karazin Kharkiv National University, 4 Svobody sq., Kharkiv, 61022, Ukraine
[4] Experimental Physics V, Center for Electronic Correlations and Magnetism, University of Augsburg, Augsburg, Germany
[5] Institute of Applied Physics, Moldova State University, 5 Academiei Str., Chisinau, 2028, Moldova
[6] Laboratory of Emerging Nanometrology LENA, Braunschweig D-38106, Germany
e-mail: glamazda@ilt.kharkov.ua

The AB_2X_4 spinel systems (A, B = transition metal ions; X = S, Se, Te) have attracted continuous research interests due to their rich physical properties relevant to the geometrical frustration. The geometrical frustration plays an important role in the coupling of different degrees of freedom.

Previous studies have shown that the thiospinel $CuIr_2S_4$ undergoes a metal-insulator transition at T_{MI} ~230 K upon cooling with a drop of the electrical resistivity by almost three orders of magnitude and a concomitant jump in the magnetic susceptibility from Pauli-like paramagnetism at high temperatures to diamagnetism in the low-temperature phase. Subsequent studies determined that $CuIr_2S_4$ undergoes a simultaneous charge-ordering (CO) and spin-dimerization (SD) transition [1]. Below T_{MI} the charge-ordering pattern consists of isomorphic octamers of $Ir_8^{3+}(\boldsymbol{S}=0)S_{24}$ and $Ir_8^{4+}(\boldsymbol{S}=1/2)S_{24}$. Orbitally-driven, three-dimensional Peierls-like spin dimerization between the magnetic ions in the $Ir_8^{4+}(\boldsymbol{S}=1/2)S_{24}$ octamers is responsible for the nonmagnetic nature of the insulating phase.

It is known that the symmetry of the crystal lattice is strongly related to the magnetic and transport properties of solids. At room temperature, $CuIr_2S_4$ has a normal cubic spinel structure. However, there is still debate in the literature about the symmetry of the low-temperature phase of this compound. This is due to the complexity of the superstructure formed as a result of the CO and SD transitions.

Here we report the results of the detailed analysis of the temperature evolution of the polarized-dependence Raman spectra of the high-quality $CuIr_2S_4$ single crystals. In the high-temperature Raman spectra we observed all five phonon modes allowed for a cubic normal spinel-type structure. To assign the observed Raman active phonon modes to the definite type of the atomic vibrations and symmetry we have performed the lattice dynamical calculations of the phonon spectra in the high-temperature phase. Below T_{MI}, we observed for the first time amazing changes in Raman spectra, an appearance of a large number of modes that strongly indicate an extraordinary change in symmetry of $CuIr_2S_4$ from cubic, $\boldsymbol{Fd\bar{3}m}$ to triclinic, $\boldsymbol{P\bar{1}}$.

V. Gnezdilov and A. Glamazda thank the *Nanophotonic*s journal, De Gruyter, Sciencewise Publishing, and the Optica Foundation for the financial support through the Ukraine Optics and Photonics Researcher Grants.

[1] P.G. Radaeli, Y. Horibe, M.J. Gutmann, H. Ishibashi, C. H. Chen, R. M. Ibberson, Y. Koyama, Y.-S. Hor, V. Kiryukhin, and S.-W. Cheong, Nature 416, 155 (2002). https://doi.org/10.1038/416155a.

Magnetic Properties of Low-dimensional Spin System Formed by Spin-1/2 XX Chains Coupled through Ising Spins

E. V. Ezerskaya, A. O. Kabatova, S. Ye. Kononenko

V. N. Karazin Kharkiv National University, 4 Svoboda Sq, Kharkiv, 61022, Ukraine
e-mail: kabatova.anna@ukr.net

This work is devoted to the theoretical study of quantum stationary states and thermodynamics of two exactly solvable quantum models based on open spin-1/2 XX chain [1, 2]. A set of finite XX chains connected by Ising spins S into the "bunch" via one intermediate site with the same number for each XX chain describing by the Hamiltonian

$$\hat{\mathbf{H}}_1 = -\sum_{l=1}^{L}\left[g_0\mu_B H s^z_{l,n_0} + J_0\left(s^z_{l,n_0} + s^z_{l+1,n_0}\right)S^z_{l,n_0} + \sum_{n=1}^{N} g\mu_B H S^z_{l,n} + J\sum_{n=1}^{N-1}\left(S^x_{l,n}S^x_{l,n+1} + S^y_{l,n}S^y_{l,n+1}\right)\right] \quad (1)$$

and a "cylinder" of XX chains connected by Ising spins S_1, S_2 at both ends

$$\hat{\mathbf{H}}_2 = -\sum_{l=1}^{L}\left[g_0\mu_B H s^z_{l,1} + g_0\mu_B H s^z_{l,N} + J_0\left(s^z_{l,1} + s^z_{l+1,1}\right)S^z_{l,1} + J_0\left(s^z_{l,N} + s^z_{l+1,N}\right)S^z_{l,N} + \sum_{n=1}^{N} g\mu_B H S^z_{l,n} + J\sum_{n=1}^{N-1}\left(S^x_{l,n}S^x_{l,n+1} + S^y_{l,n}S^y_{l,n+1}\right)\right] \quad (2)$$

These Hamiltonians have simple block form

$$\hat{\mathbf{H}}_1 = \sum_{l=1}^{L}\mathbf{H}(s_{l,n_0}, s_{l+1,n_0}); \quad \hat{\mathbf{H}}_2 = \sum_{l=1}^{L}\mathbf{H}(s_{l,1}, s_{l+1,1}, s_{l,N}, s_{l+1,N}),$$

which permits us to use standard transfer-matrix technique for numerical simulation of the thermodynamics. Here $\mathbf{H}(s_{l,n_0}, s_{l+1,n_0})$ and $\mathbf{H}(s_{l,1}, s_{l+1,1}, s_{l,N}, s_{l+1,N})$ are the Hamiltonians of finite spin-1/2 XX chain with the effective "impurity" spins (S = 1/2) at one of the intermediate sites n_0 (model (1)) or at the ends (model (2)). We can consider the eigenvalues of all Ising spins, as the parameters of the Hamiltonians (1) or (2) due to the commutation relations of Ising spins and model Hamiltonians.

We investigate the big effect of impurities localized levels on thermodynamics. For strong antiferromagnetic Ising interaction, the field dependence of the magnetization at very low temperatures demonstrates a jump associated with the spin-flip of impurity spins in sufficiently strong magnetic field for (1) and two jumps for (2).

The possibility of two-peak for model (1) and three-peak for model (2) at $J_0 \neq J$ behavior for zero-field temperature dependence of specific heat was found numerically.

We acknowledge support by IEEE via "Magnetism in Ukraine Initiative" (STCU project No. 9918).

[1] E. Lieb, T. Schultz, D. Mattis, Ann. Phys. 16, 407 (1961). DOI: 10.1016/0003-4916(61)90115-4.

[2] Zvyagin A.A., Quantum Theory of One-Dimensional Spin Systems, DOI : , Cambridge Scientific Publishers, Cambridge, 2010.

On the Energy Spectrum and Magnetic Properties of Quasi-One-Dimensional Branched Spin Chain

E. V. Ezerskaya, D. D. Kolesnyk

V. N. Karazin Kharkiv National University, 4 Svoboda Sq, Kharkiv, 61022, Ukraine
e-mail: iamdkolesnik@gmail.com

Theoretical study of the exact energy spectrum and low-temperature thermodynamics of two finite spin XX chains connected through an additional Ising spin at one point (T-chain) have been carried out. Model Hamiltonian has the form

$$\mathbf{H} = -g_1\mu_B H\sum_{n=1}^{N_1} S_{1,n}^z - J_1\sum_{n=1,n\neq n_1-1,n_1}^{N_1-1}\left(S_{1,n}^x S_{1,n+1}^x + S_{1,n}^y S_{1,n+1}^y\right) - g_2\mu_B H\sum_{n=1}^{N} S_{2,n}^z - J_2\sum_{n=1}^{N_2-1}\left(S_{2,n}^x S_{2,n+1}^x + S_{2,n}^y S_{2,n+1}^y\right)$$
$$- J_1'\left(S_{1,n_1-1}^x S_{1,n_1}^x + S_{1,n_1-1}^y S_{1,n_1}^y + S_{1,n_1}^x S_{1,n_1+1}^x + S_{1,n_1}^y S_{1,n_1+1}^y\right) - g_0\mu_B H S_0^z - J_0 S_0^z\left(S_{1,0}^z + S_{2,1}^x\right).$$

Here μ_B is the Bohr magneton, J_1, J_2 are the coupling constants between nearest neighboring spins along the XX chains, J_1' is the XX coupling constant for lattice site numbered $(1, n_1)$ with nearest neighbours, J_0 is the coupling constant between horizontal and vertical XX chains through impurity Ising spin-S, g_1, g_2, and g_0 are the *g*-factors of the spins of the XX chains and the impurity Ising spin, respectively, *H* is the permanent magnetic field directed along the axis *z*.

The above Hamiltonian can be reduced to the Hamiltonian of an ideal gas of spinless fermions. We performed analytical calculations of the corresponding spectrum of stationary states. For the states with one inverted spin this spectrum consists of two independent zones. The additional energy levels of the impurity spin can be split off from zones. We found the conditions for the appearance of localized impurity states.

Numerical simulation of the field and the temperature dependences of total magnetization, heat capacity and $\langle S_0^z\rangle$ at different values of system parameters was carried out. The possibility of additional oscillations of $\langle S_0^z\rangle$ with the increase of magnetic field for some values of model parameters (fig. 1) and the existence of several maxima in temperature dependence of heat capacity at zero field (fig. 2) are shown.

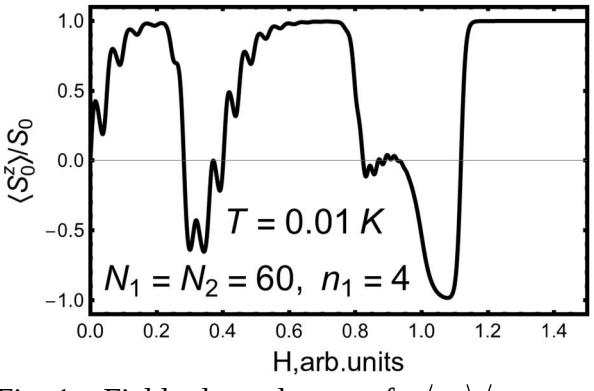

Fig. 1. Field dependence of $\langle S_0^z\rangle/S_0$ $g_0 = 0.5$, $g_1 = 1, g_2 = 2, J_0 = -1K, J_1 = 2K, J_2 = 10K$

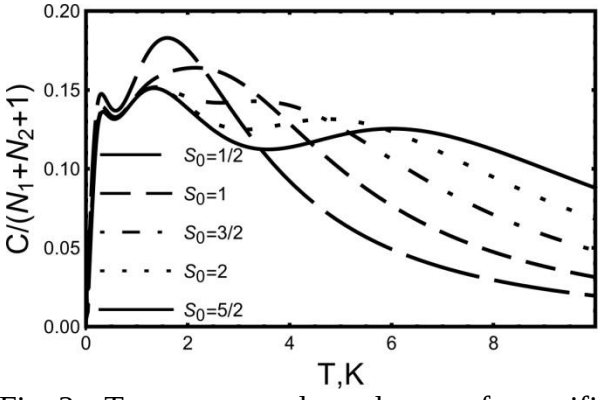

Fig. 2. Temperature dependence of specific heat in zero magnetic field $N_1 = N_2 = 8, n_1 = 4$, $J_0 = -10K, J_1 = 1K, J_2 = 5K$

E. V. Ezerskaya acknowledges support by IEEE via "Magnetism in Ukraine Initiative" (STCU project No.9918).

Low Temperature Magnetic Properties of Anisotropic Spin Ladder Systems

V. O. Cheranovskii, E. V. Ezerskaya, S. Ye. Kononenko

V. N. Karazin Kharkiv National University, 4 Svoboda Sq, Kharkiv, 61022, Ukraine
e-mail: semen.kononenko@student.karazin.ua

This work is devoted to the theoretical study of the decorated spin ladder built from two finite open spin-½ chains with XX interaction, connected vertically through additional Ising spins-S. This ladder structure has three spin unit cells.

The corresponding Hamiltonian has the following form:

$$\mathbf{H} = -g_1\mu_B H\sum_{n=1}^{N} S_{1,n}^z - g_2\mu_B H\sum_{n=1}^{N} S_{2,n}^z - g_3\mu_B H\sum_{n=1}^{N} S_{3,n}^z - \\ - J_1\sum_{n=1}^{N-1}\left(S_{1,n}^x S_{1,n+1}^x + S_{1,n}^y S_{1,n+1}^y\right) - J_3\sum_{n=1}^{N-1}\left(S_{3,n}^x S_{3,n+1}^x + S_{3,n}^y S_{3,n+1}^y\right) - J_2\sum_{n=1}^{N} S_{2,n}^z\left(S_{1,n}^z + S_{3,n}^z\right). \quad (1)$$

Due to Ising interactions in rungs of the model (1), each value of $S_{2,n}^z$, $n = 1, 2, \ldots N$ is a good quantum number s_n. This permits us to find the exact energy spectra of the lattice clusters formed by 3-4 unit cells in the analytical form. Some special cases of the set of above quantum numbers were studied analytically for arbitrary XX chain lengths. In particular, we considered two cases with periodical distribution of quantum numbers: equal quantum numbers s_n and alternating quantum numbers located on neighboring unit cells of the ladder. The corresponding energy spectra have two and four energy bands, respectively.

The partition function, free energy, internal energy, magnetization, magnetic susceptibility, and heat capacity for above ladder model were calculated using the exact diagonalization method. The algorithm for the numerical calculation of the partition function for an arbitrary number of unit cells was proposed and implemented in Wolfram Mathematica 14.0. Numerical simulation of the main thermodynamic characteristics such as the field and temperature dependences of the magnetization, magnetic susceptibility and heat capacity, were performed.

For the case of similar isotropic Heisenberg decorated ladder described by the Hamiltonian

$$\mathbf{H} = \sum_{i=1}^{L}\left[J_1\left(\mathbf{S}_{1,i}\mathbf{S}_{1,i+1} + \mathbf{S}_{3,i}\mathbf{S}_{3,i+1}\right) + J_2\left(\mathbf{S}_{1,i} + \mathbf{S}_{3,i}\right)\overline{\mathbf{S}}_{2,i}\right] - h\mathbf{S}_{total}^z, \quad (2)$$

where all g-factors have the same values for simplicity; $h = \mu_B g H$, S_{total}^z is a z-projection of total spin of the ladder.

We found that the mixed spin ladder model (2) with dominant coupling in rungs may have the intermediate plateaus in a low-temperature magnetization profile. At low temperatures zero magnetization plateau is present only for ladders with integer values of the decorated spins. The existence of the above plateaus was shown also in the case of some intermediate values of coupling in ladder rungs using an exact diagonalization study of small ladder clusters and by the density-matrix renormalization group (DMRG) calculations. We also found, that in contrast to isotropic spin model (2), for anisotropic spin ladder with Ising-type interactions in the ladder rungs one intermediate magnetization plateau may disappear in the case of dominant coupling in the rungs [1].

We acknowledge support by IEEE via “Magnetism in Ukraine Initiative” (STCU project No. 9918).

[1] V.O. Cheranovskii, E.V. Ezerskaya, S. Ye. Kononenko, Low Temp. Phys. 50, 152 (2024). https://doi.org/10.1063/10.0024327

Tunnel Magnetic Contacts with Perpendicular Anisotropy of Magnetic Electrodes as Promising Elements for Recording Information

M. M. Krupa

Institute of Magnetism National Academy of Science of Ukraine,
36 B Vernadsky's bul., Kiev, 03143, Ukraine
e-mail: krupa@imag.kiev.ua

Large values of tunneling magnetoresistance and tunnel magnetocapacitance, which were experimentally obtained in magnetic tunnel junctions [1], brought magnetic tunnel junctions to a prominent place in the perspective of their practical use for creating various spintronics devices. In this report are presented the results of experimental studies of tunnel magnetoresistance in magnetic tunnel contacts $Tb_{22-d}Co_5Fe_{73}/Pr_6O_{11}/Tb_{19-d}Co_5Fe_{76}$, in which the magnetic electrodes have perpendicular anisotropy and are magnetized perpendicular to the plane of the tunnel contact, and the barrier layer Pr_6O_{11} is high energy-gap semiconductor and paramagnet with low Curie temperature. It is shown, that in such magnetic tunnel contacts, with their antiparallel magnetization, a strong magnetic field gradient in the barrier layer near each electrode is created. The big gradient of a magnetic field arises only in in the direction of the magnetisation of magnetic electrodes. In the barrier layer arises an almost uniform magnetic field. This field is directed perpendicular to the direction of magnetization of the magnetic electrodes. Such strong changes in the distribution of the magnetic field lead to the appearance of an additional spin capacity near each magnetic electrode and an additional energy barrier for electrons with a major polarization, which makes it possible to obtain large values of tunnel magnetoresistance and tunnel magnetocapacitance in magnetic tunnel contacts $Tb_{22-d}Co_5Fe_{73}/Pr_6O_{11}/Tb_{19-d}Co_5Fe_{76}$, in which the magnetic electrodes have perpendicular anisotropy. This paper describes the mechanism of appearance of magnetic capacity in tunnel magnetic contacts with magnetic electrodes that have perpendicular anisotropy, presents the results of measurements of the value of tunnel magnetic resistance and tunnel magnetic capacity in tunnel contacts $Tb_{22-d}Co_5Fe_{73}/Pr_6O_{11}/Tb_{19-d}Co_5Fe_{76}$, where the value of tunnel magnetic resistance is almost 120%, and the value of the tunnel magnetic capacity is more than 110%. The work also provides a structural diagram of the construction of an information carrier based on tunnel magnetocapacitance and describes the principle of recording information in such a structure.

[1] H. Kaiju, S. Fujita, T. Morozumi and K. Shiiki. Magnetocapacitance effect of spin tunneling junctions. Journals of Applied Physic 91 (2002) 7430. https://doi.org/ 10.1063/1.1451754

The possibility of existence the magnetic field induced structural phase transition in $KEr(MoO_4)_2$

N. Nesterenko[1], K. Kutko[1], B. Bernáth[2], D. Kamenskyi[3]

[1] B.Verkin Institute for Low Temperature Physics and Engineering of NAS of Ukraine, 47 Nauky Ave., Kharkiv, 61103, Ukraine
[2] High Field Magnet Laboratory (HFML - EMFL) Radboud University Toernooiveld 7, ED 6525 Nijmegen, The Netherlands
[3] Experimental Physics V, Center for Electronic Correlations and Magnetism, Institute of Physics, University of Augsburg, 86159 Augsburg, Germany
e-mail: kkutko@ilt.kharkov.ua

Based on the investigation of double rare - earth (RE) molybdate $KEr(MoO_4)_2$ in [1] it was supposed that the peculiarities of the magnetic and magnetoresonance properties in vicinity of H_{cr} are the result of the phase transition induced by external magnetic field. Here we discuss the evolution of $KEr(MoO_4)_2$ FIR transmission spectra under the external magnetic fields up to 30 T (Zeeman effect), when $H||a$ at 1.4 K. Fig.1 (a) shows frequency-field dependences of the low energy electronic and phonon types excitations. The observed behavior of the transitions in low-field region can be described within linear approach. The energy levels (see Fig. 1(b)) have been calculated based on the slopes of observed branches below 4 T. When $H \sim H_{cr} \sim 5$T we observed the sharp changing of the behavior of electronic excitations: all branches have the linear dependences vs. magnetic field with the similar slope in contrast with the low-field region. These changes are the result of the RE ions local surrounding deformation. We suppose that in external magnetic field the weak rotations of tetrahedral anions around neighboring RE ions in $Er(MoO_4)_2$ layers, apparently, lead to energy nonequivalence of previously equivalent RE centers. To discuss the possible low–symmetry phase we use the data for others isostructural compounds.

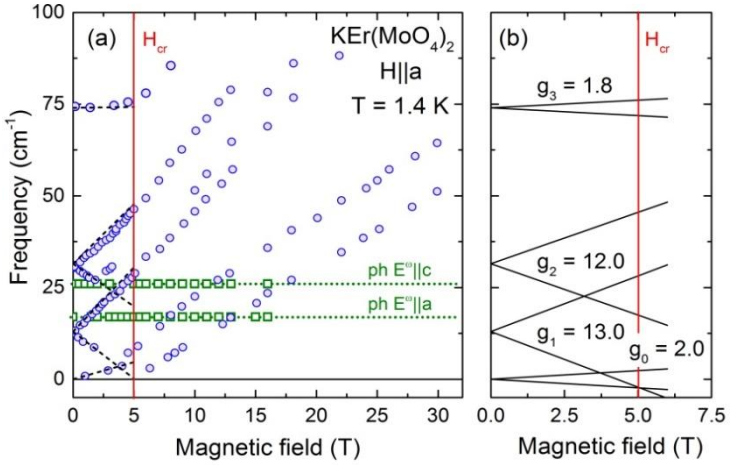

Fig.1. (a) The frequency – field dependences of the low energy excitations. Circles – electronic-type excitations and squares – phonon-type excitations. With the dashed lines showed calculated branches. (b) The calculated energy levels diagram in a low magnetic field. The vertical line locates the critical field, H_{cr}.

[1] V. I. Kut'ko, Fiz. Nizk. Temp. **31**, 3 (2005). [Low Temp. Phys. **31**, 1 (2005)]. https://doi.org/10.1063/1.1820349

Magnetic susceptibility as a tool for studying the phenomenon of mixed valence in SmB_6

A. A. Lyogenkaya[1], A. S. Panfilov[1], V. A. Desnenko[1], G. E. Grechnev[1], and N. Yu. Shitsevalova[2]

[1] B. Verkin Institute for Low Temperature Physics and Engineering of the NAS of Ukraine, 61103 Kharkiv, Ukraine
[2] Institute for Problems of Materials Science of the NAS of Ukraine, Kyiv 03680, Ukraine
e-mail: lyogenkaya@ilt.kharkov.ua

According to existing ideas, systems with intermediate valence (IV) of rare-earth ions are of interest because of their intermediate position between states with localized and collectivized electrons, between magnetic and non-magnetic states, and sometimes between metals and dielectrics. Few studies of the behavior of such IV systems under high pressure conditions show a general trend of increasing valence of rare-earth ions with increasing pressure, which leads to significant changes in physical properties.

SmB_6 is one of the most famous and widely investigated IV compounds. At ambient conditions, SmB_6 behaves as a heavy-fermion semiconductor, while at low temperatures it exhibits a narrow band gap related to the hybridization of nearly localized 4*f* electronic bands with a broad 5*d* conduction band, that classifies it as a Kondo insulator material. In this compound Sm ions display a fluctuating valence between Sm^{2+} ($4f^6$ configuration) and Sm^{3+} ($4f^5\,5d^1$ configuration) provided the bulk Sm valence z of about 2.6 at room temperature. The value of z appears to be quite sensitive to the pressure; z(P) dependence was studied in a number of works by different methods, and the general result of these investigations is the increase in Sm valence with increasing pressure. The values of the initial baric derivative dz/dP (P→0), estimated from the available literature data, are ambiguous and fall within the range dz/dP = 1–3.5 $Mbar^{-1}$. Moreover, the form of the z(P) dependence is inconsistent.

The above points to the need to improve existing methods for determining state IV under pressure, including the interpretation of experimental data and experimental conditions, taking into account the strong sensitivity of SmB_6 to pressure inhomogeneities. One of the effective tools for studying the IV state of rare-earth compounds under pressure is the study of their magnetic susceptibility, which is closely related to the valence of Re ions.

In the present work we report the results of a precise experimental study of the pressure effect on magnetic susceptibility χ of SmB_6 compound. The measurements χ(P) were carried out under helium gas pressure P up to 2 kbar at fixed temperatures 78 and 300 K using a pendulum-type magnetometer. The observed pressure effect value, $d\ln\chi/dP \approx 6$ $Mbar^{-1}$, demonstrates a noticeable decrease in susceptibility under pressure, which is weakly dependent on the temperature used. From the model analysis of the experimental data, combined with the supplemented LSDA + U calculations of the electronic structure and Van Vleck paramagnetism of the band states of SmB_6, we have estimated the value of the initial pressure derivative for the intermediate valence of Sm, $dz/dP = (2.5 \pm 0.15)$ $Mbar^{-1}$. It is consistent with the literature data obtained by other methods and indicates an increase in valence with increasing pressure. It was shown that the valence of Sm and its pressure dependence is closely related to the detailed characteristics of the conduction band and 4*f* states.

Position of optical axes of magnetized along tetragonal axis antiferromagnetic garnet $Ca_3Mn_2Ge_3O_{12}$

O. V. Bibik[2], O. V. Myloslavska[1], Yu. Kharchenko[1], M. Kharchenko[1]

[1] B.Verkin Institute for Low Temperature Physics and Engineering of NAS of Ukraine, 47 Nauky Ave., Kharkiv, 61103, Ukraine
[2] Georgia Institute of Technology | GT · School of Aerospace Engineering Atlanta, Georgia, USA
e-mail: olga.miloslav@gmal.com

The antiferromagnetic tetragonal crystal of calcium-manganese-germanium garnet $Ca_3Mn_2Ge_3O_{12}$ (CMG) belongs to the family of non-cubic garnets. The characteristic properties of this compound are related to the presence of the Jahn-Teller ion Mn^{3+} with degenerate ground energy state. During cooling, the Jahn-Teller distortions of $Mn^{3+}O^{2-}{}_6$ octahedra are ordered at T = 516 K and the symmetry of the crystal lattice decreases from cubic m3m to tetragonal as a result of the second order phase transition. The ferroelastic properties which appear in the crystal are accompanied by formation of deformation twins that can be switched by applying mechanical stresses. Under action of IR and visible light the manganese ion Mn^{3+} loses an electron by the charge transfer process and becomes the ion Mn^{4+}. It causes the new distortions of the $Mn^{3+}O^{4+}{}_6$ octahedra and emergence of photoinduced birefringence of linearly polarized light.

At temperatures lower 14 K, the CMG crystal loses its antisymmetry center as a result of antiferromagnetic ordering of magnetic moments of manganese ions. Due to this fact the magneto-optical effects which are forbidden in paramagnets are now allowed by symmetry and in CMG crystal one can observe the linear magneto-optical effect (a magnetic analogue of the electro-optical Pockels effect) and rotation of polarization plane of light quadratic with respect to magnetic field (quadratic Faraday effect [1]). The number of unique properties makes CMG garnet a promising model crystal for the creation of multifunctional materials [2]. But although $Ca_3Mn_2Ge_3O_{12}$ is a long-investigated compound, there are still many questions even about its crystal structure [3]. Very low degree of tetragonality and the presence of several types of crystal twins prevent a reliable determination of symmetry of both the ionic and magnetic crystal lattices. Polarization magneto-optical experiments allow visual control of the twin structure and can be also useful for more accurate establishing the point group of magnetic symmetry and clarifying the possibility of existence of certain symmetry elements.

Presented here results of linear magneto-optic effect measurements were obtained in a magnetic field H = 15 kOe directed along the beam of light and the tetragonal axis of the crystal C_4. Experimental studies are carried out for two pairs of homogeneous antiferromagnetic states prepared at special process of magnetic ordering in a magnetic field. For these magnetic states of a tetragonal CMG crystal the position of splitting plane of the optical axes in magnetic field was determined. The data obtained allow us to make a qualitative estimation of the optical anisotropy and can be considered as important for determining the magnetic point symmetry of antiferromagnetic garnet $Ca_3Mn_2Ge_3O_{12}$.

[1] N. F. Kharchenko and A. V. Bibik, Quadratic magnetic rotation of polarization plane of light in antiferromagnetic CaMnGe garnet, Low Temperature Physics, 20, 296 (1994). http:// DOI:10.3379/jmsjmag.11.S1_51.
[2] Martin Fally, The photo-neutronrefractive effect. arXiv:1706.03614v1 [physics.optics] (2017). https://doi.org/10.1007/s00340-002-1035-0.
[3] Stefan Heinemann and Ronald Miletich, Structure and twinning of tetragonal $Ca_3Mn_2Ge_3O_{12}$ garnet, American Mineralogist, 85, 993 (2000). http:// DOI:10.2138/am-2000-0714.

Spectroscopic peculiarities of a trigonal $TbAl_3(BO_3)_4$ single crystal

A. V. Peschanskii[1], A. Yu. Glamazda[1,2]

[1] B. Verkin Institute for Low Temperature Physics and Engineering of NAS of Ukraine, 47 Nauky Ave., Kharkiv, 61103, Ukraine
[2] V. N. Karazin Kharkiv National University, 4 Svobody sq., Kharkiv 61022, Ukraine
e-mail: alexei.peschanskii@gmail.com

The Raman spectra in the $TbAl_3(BO_3)_4$ single crystal were investigated in the frequency range of 3 – 1600 см$^{-1}$ and luminescence spectra were measured in the frequency range of 11800 – 21000 см$^{-1}$ in the temperature range of 5 – 300 K. The spectra were taken with Nd:YAG (neodymium-doped yttrium aluminum garnet) solid-state laser (λ_{exc}=532 nm) and He-Ne laser (λ_{exc}=632.8 nm). The using of the different excitation wavelengths made it possible to unambiguously separate Raman and luminescence spectra.

The analysis of Raman spectra of the single crystal has revealed 5 of 7 A_1 and all E phonon modes predicted by group-theory analysis. The splitting energy between the LO and TO components of polar E phonons was determined. Analysis of the phonon spectrum and its comparison with the isomorphic $TbFe_3(BO_3)_4$ compound were carried out.

A group of intense bands associated with the $^5D_4$ ® $^7F_0$ electronic transition was observed in the energy range of 14520–14680 cm^{-1} in the luminescence spectra (Fig.1). The intensity of these bands decreases upon heating. At the same time, the bands which can be assigned with the $^5D_4$ ® $^7F_6$, $^5D_4$ ® $^7F_5$ and $^5D_4$ ® $^7F_4$ transitions were revealed in the luminescence spectra at room temperature (Fig.1). The intensity of these bands is comparable to the intensity of Raman spectrum of $TbAl_3(BO_3)_4$. The observation of luminescence from the $^5D_4$ level (20600–20750 cm^{-1}) upon excitation with λ_{exc}=632.8 nm (15803 cm^{-1}) and λ_{exc}=532 nm (18797 cm^{-1}) indicates strong nonlinear properties of the studied crystal.

The structure of the main $^7F_6$ multiplet of the Tb^{+3} ion in the $TbAl_3(BO_3)_4$ single crystal has been studied by Raman spectroscopy at 5 K. The energies of the electronic levels of the $^7F_6$ and $^5D_4$ multiplets were determined by analyzing the luminescence spectra measured at 300 K.

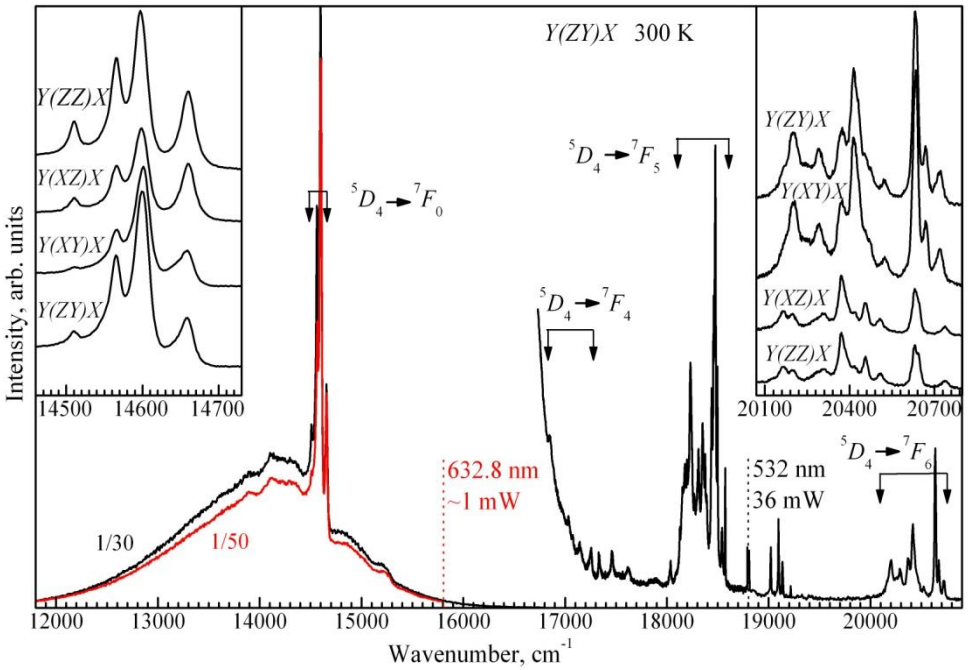

Fig.1. Raman spectra and luminescence of the $TbAl_3(BO_3)_4$ single crystal at 300 K; λ_{exc} = 532 nm (36 mW, ~1.2 mW (11800–16800 cm^{-1}) and λ_{exc} = 632.8 nm (~1 mW); the spectral resolution of 3.0 cm^{-1}.

Determination of Nd-Fe exchange interaction signs in excited states of Nd^{3+} in $NdFe_3(BO_3)_4$ crystal using optical spectroscopy

V. G. Piryatinskaya, V. S. Kurnosov, I. S. Kachur

B. Verkin Institute for Low Temperature Physics and Engineering of NAS of Ukraine,
47 Nauky Ave., Kharkiv, 61103, Ukraine
e-mail: piryatinskaya@ilt.kharkov.ua

Neodymium ferroborate $NdFe_3(BO_3)_4$ orders into easy-plane collinear antiferromagnetic structure at T_N » 30 K. At lowering temperature to T_{IC} » 13.5 K, the magnetic structure transforms to a long period spiral propagating along the C_3 axis; orientation of the magnetic moments remains parallel to the basal plane. The crystal structure of $NdFe_3(BO_3)_4$ is described by the space symmetry group $R32$; the rare-earth ion occupies a position with local symmetry D_3.

In the present work we study low temperature optical absorption spectra of $NdFe_3(BO_3)_4$ in the region of optical transition $^4I_{9/2}$ ® $^4G_{5/2}$ in Nd^{3+}. We perform a group-theoretic analysis of the transitions between the components of Nd^{3+} Kramers doublets split by Nd-Fe exchange interaction.

We consider the selection rules for transitions in C_2 symmetry, which is the maximum for easy-plane magnetic ordering. According to these rules, electric-dipole transitions between states of the same symmetry (G_3® G_3, G_4® G_4) can be observed only in s-polarization, while transitions G_3« G_4 can be observed both in s and in p-polarizations ($G_3(j_{+1/2})$ and $G_4(j_{-1/2})$ are one-dimensional irreducible representations of C_2 group). Hence, depending on arrangement of the excited doublet sublevels, different transitions can be observed in p-spectra (see schemes in Fig. 1).

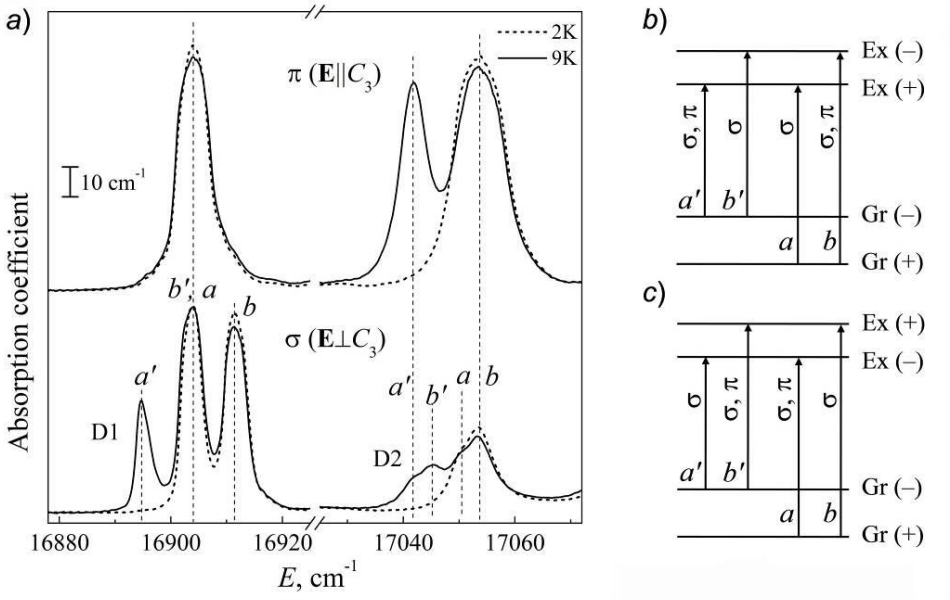

Fig. 1. Absorption spectra of $NdFe_3(BO_3)_4$ in the region of optical transition $^4I_{9/2}$® $^4G_{5/2}$ (*a*); schemes of transitions between the splitting components of ground and excited doublets (*b*,*c*).

In the region of optical transition $^4I_{9/2}$ ® $^4G_{5/2}$ (Fig. 1*a*), the absorption lines D1 and D2 demonstrate quite different polarization properties. In the case of D2 line, only transitions *a*' and *b* are observed in the p-spectra. This corresponds to the scheme (*b*) in which the order of levels in ground and excited doublets is the same. For D1 line, transitions *a* and *b*' appear in p-polarization, in accordance with the scheme (*c*) where the order of levels in excited state is reverse with respect to the ground state. Thus, in this case inversion of the sign of Nd-Fe exchange interaction in the Nd^{3+} excited state respectively to the exchange in the ground state takes place.

Impact of the magnetic Fe^{3+} ions substitution by nonmagnetic Ga^{3+} on the properties of holmium iron borate

Yu. Savina[1], O. Bludov[1], V. Pashchenko[1], T. Zajarniuk[2], A. Lynnyk[2], M.U. Gutowska[2], A. Szewczyk[2]

[1] B. Verkin Institute for Low Temperature Physics and Engineering of the NAS of Ukraine, 47 Nauky Ave., 61103 Kharkiv, Ukraine
[2] Institute of Physics, Polish Academy of Sciences, al. Lotników 32/46, 02-668 Warsaw, Poland
e-mail: savina@ilt.kharkov.ua

The holmium borate with the general formula $HoFe_3(BO_3)_4$ orders antiferromagnetically below 39 K and undergoes a spontaneous spin-reorientation phase transition from the easy-plane like (EP) antiferromagnetic state to the easy-axis like (EA) one at 5 K [1]. The present work is aimed at the study of influence of magnetic Fe^{3+} ions substitution by nonmagnetic Ga^{3+} on magnetic properties of the crystals $HoFe_{3-x}Ga_x(BO_3)_4$ with x=0.5, 1.5, 2.

Magnetic and heat capacity measurements of the samples have been performed by the SQUID magnetometer MPMS-XL7 and the PPMS system, respectively.

For all the investigated crystals, the slight anisotropy of susceptibility along the c axis and in basal plane of crystal, which appears due to anisotropy of Ho^{3+} g-factor value, have been observed. Above 100 K, the susceptibility of all studied crystals obeys the Curie-Weiss law.

Only for the holmium iron borate with x=0.5 two phase transitions have been detected. The first transition, at T_N = 28.6 K, is the transition to a magnetically ordered state. The spontaneous spin-reorientation phase transition has been found at T_{SR} = 7.5 K. Transition temperature T_{SR} strongly decreases with increasing of external magnetic field and it is suppressed by field higher than 1.5 T. The H-T phase diagrams for $HoFe_{2.5}Ga_{0.5}(BO_3)_4$ have been constructed for two principal field orientations (H along and perpendicular to the c axis).

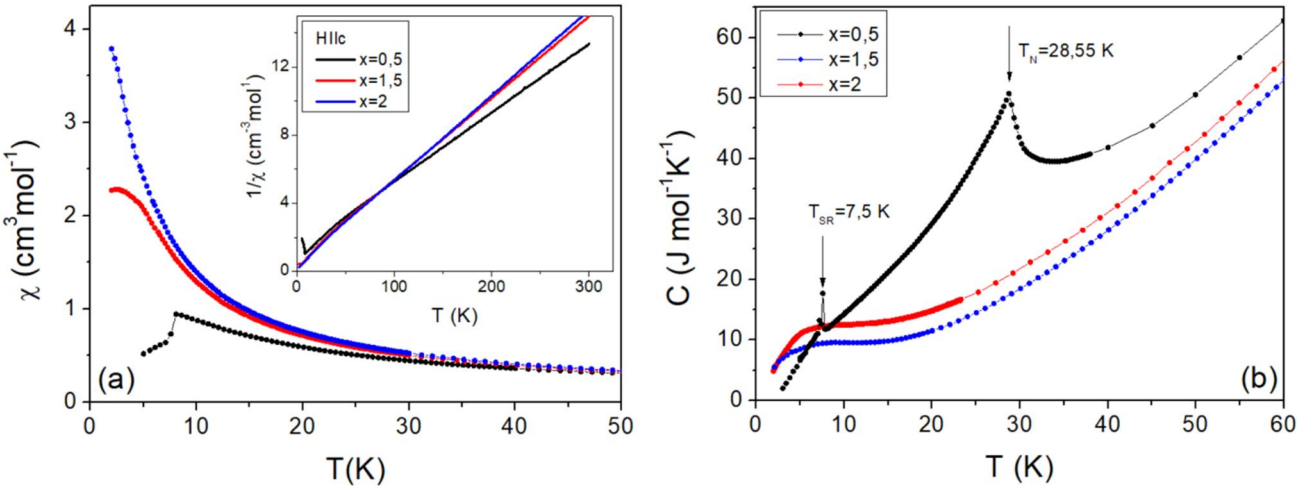

Fig.1. Magnetic susceptibility (a) and specific heat (b) of $HoFe_{3-x}Ga_x(BO_3)_4$ single crystal with x=0.5, 1.5, 2.

[1] C. Ritter, A. Vorotynov, A. Pankrats et al., Magnetic structure in iron borates $RFe_3(BO_3)_4$ (R = Y, Ho): a neutron diffraction and magnetization study, J. Phys.: Condens. Matter, V.20, 36, 365209, 2008.

Nickel-zinc spinel ferrites: Synthesis and magnetic characterization

V. O. Zamorskyi[1], A. F. Kravets[1], D. L. Popadiuk[1], Yu. Yu. Shlapa[2], S. O. Solopan[2], A.G. Belous[2], A. I. Tovstolytkin[1]

[1] Institute of Magnetism of the NAS of Ukraine and MES of Ukraine, 36b Academician Vernadsky Blvd., UA-03142 Kyiv, Ukraine
[2] V.I. Vernadsky Institute of General and Inorganic Chemistry of the NAS of Ukraine, 32/34 Academician Palladin Ave., UA-03142 Kyiv, Ukraine
e-mail: 0vl0ad0@gmail.com

Nickel-zinc spinel ferrite [1] ceramics are intriguing for safe remote heating applications. The reason is that on the one hand, substituting nickel with zinc [2] allows tuning Curie temperature down to room temperatures; on the other hand, nickel-zinc ferrites have increased specific loss power, which is also referred to as specific absorption rate that represents the power dissipation per unit mass, due to magnetization increase in a significant region of substitutions over nickel ferrite [3]. Essentially, it means that after putting such ceramics into media and turning on high frequency oscillating magnetic field (e.g. 100 kHz) the ceramics will heat up to its Curie temperature, but not higher. This way even using thermometer is not strictly necessary.

Our current work is concerned with different synthesis methods of nickel-zinc ferrite nanoparticles. Such investigation is necessary since properties of nanoparticles may significantly depend on the method of synthesis, and that directly affects properties of ceramics. Our current investigation is a work-in-progress, but as an example of difference in magnetic properties due to synthesis method for a pair of samples M(T) dependency is shown on figure 1. These samples were cooled to a temperature of 3 K and then heated in a magnetic field of 1 kOe. The difference between the samples is that S sample was obtained through solid-phase synthesis and P sample through co-precipitation synthesis.

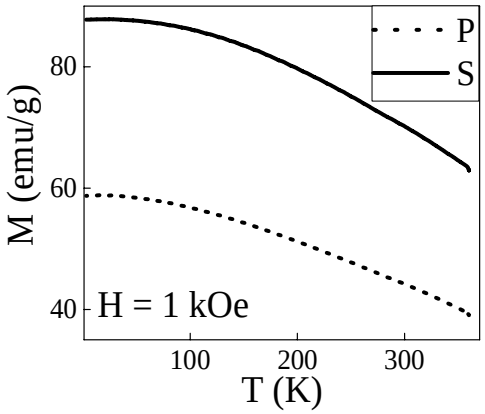

Fig. 1. Temperature dependencies of magnetization of samples S and P synthesized via solid-phase method and co-precipitation method respectively in a field of 1 kOe.

[1] S. Chikazumi, C. D. Graham / Physics of Ferromagnetism // Oxford University Press on Demand. – 2009. – 2e, – no. 94.
[2] Tovstolytkin A.I., Kulyk M.M., Kalita V.M., Ryabchenko S.M., Zamorskyi V.O., Fedorchuk O.P., Solopan S.O., Belous A.G. / Nickel-zinc spinel nanoferrites: Magnetic characterization and prospects of the use in self-controlled magnetic hyperthermia // J. Magn. Magn. Mater. – 2019. – V. – 473. – P. 422-427.
[3] Yelenich O.V., Solopan S.O., Kolodiazhnyi T.V., Dzyublyuk V.V., Tovstolytkin A.I., Belous A.G. Superparamagnetic behavior and AC-losses in NiFe2O4 nanoparticles // Solid State Sciences.-2013.-20.-P.115-119

.

OPTICS, PHOTONICS AND OPTICAL SPECTROSCOPY

Luminescent and scintillation properties of $CsPbCl_3$ perovskite crystal

V. Kolomiets, V. Kapustianyk

I. Franko National University of Lviv, Physics Department,
50 Dragomanova str., 79005, Lviv, Ukraine
e-mail: volodymyr.kolomiets@lnu.edu.ua

The emergence of halide perovskites as promising materials for high-energy radiation detection, owing to their high light yield and a very fast decay time, has sparked renewed interest in exploring of their scintillation properties [1]. Despite the challenges posed by thermal quenching [2], $CsPbCl_3$ exhibits remarkable luminescence characteristics at low temperatures, making it a compelling candidate for specialized applications in the particle physics experiments and nuclear imaging [3]. By delving into the X-ray luminescence and scintillation characteristics of $CsPbCl_3$ across a temperature range from room temperature down to 7 K, this study aims to comprehensively evaluate its suitability as a cryogenic scintillation detector. The investigation not only aims to assess its performance in detecting ionizing radiation but also seeks to shed light on the underlying mechanisms governing its luminescence behavior, thus contributing to the fundamental understanding of lead halide perovskites as scintillating materials. Furthermore, this study endeavors to provide valuable insights into the optimization of experimental conditions for maximizing the scintillation efficiency and stability of $CsPbCl_3$ at cryogenic temperatures, paving the way for its potential integration into the next-generation radiation detection systems. Through the rigorous experimentation and analysis, this research established $CsPbCl_3$ as a reliable and efficient scintillator for applications in cryogenic environments, thereby pushing the boundaries of current radiation detection technologies and opening up new avenues for scientific exploration and technological innovation.

The result of our research showed that $CsPbCl_3$ crystal demonstrates high light yield from an ^{241}Am source, which was estimated to be 47000±7000 ph/MeV and the sub-nanosecond response time at low temperatures, indicating its potential as a cryogenic scintillation detector. The obtained results are consistent with the previous theoretical and experimental studies and also complement the recent results of characterisation of other lead halide perovskites[4,5].

[1] M. Sytnyk, S. Deumel, S.F. Tedde, G.J. Matt, W. Heiss, Applied Physics Letters 115 (2019) 190501. DOI:10.1063/1.5125999
[2] M. Sebastian, J.A. Peters, C.C. Stoumpos, J. Im, S.S. Kostina, Z. Liu, M.G. Kanatzidis, A.J. Freeman, B.W. Wessels, Physical Review B 92 (2015) 235210. DOI:https://doi.org/10.1103/PhysRevB.92.235210
[3] S.E. Derenzo, E. Bourret-Courshesne, G. Bizarri, A. Canning, Nucl Instrum Meth A 805 (2016) 36. DOI: 10.1016/j.nima.2015.07.033
[4] V.B. Mykhaylyk, H. Kraus, M. Saliba, Materials Horizons 6 (2019) 1740. DOI:10.1039/c9mh00281b
[5] V.B. Mykhaylyk, H. Kraus, V. Kapustianyk, H.J. Kim, P. Mercere, M. Rudko, P. Da Silva, O. Antonyak, M. Dendebera, Scientific reports 10 (2020) 8601. DOI: 10.1038/s41598-020-65672-z6

Peculiarities of J-Aggregate Formation in Liquid Crystal Matrices: Enhancing Stability and Optoelectronic Characteristics

I. Yu. Ropakova[1], O. M. Samoilov[1], I. I. Grankina[1], S. L. Yefimova[1], O. V. Sorokin[1], N. A. Kasian[1], S. S. Hrankina[1,2], L. N. Lisetski[1]

[1] Institute for Scintillation Materials of NAS of Ukraine Kharkiv, Ukraine
60 Nauky Ave., Kharkiv 61072, Ukraine
[2] Kharkiv National Medical University, 4 Nauky Ave., 61022, Kharkiv, Ukraine
e-mail: adelma@ukr.net

In recent years, there has been a growing utilization of liquid crystals as host matrices for incorporating various inorganic and organic nanoparticles, serving both fundamental research and the development of novel composite nanomaterials. Luminescent liquid crystals (LLCs) have garnered significant interest due to their unique optical and anisotropic properties, holding promise for optoelectronic applications. However, conventional LLCs often encounter fluorescence quenching due to aggregation, imposing limitations on their practical utility. To address this challenge, innovative approaches have been employed to engineer intricate LC systems, such as those integrating luminescent polymer dots covalently linked to rod-shaped liquid crystal molecules.

A noteworthy class of luminescent aggregates is J-aggregates, comprising low-dimensional molecular crystals of certain organic dyes. Their excitonic electronic excitations and distinctive 1D or 2D structure result in optical properties differing markedly from individual molecules or bulk crystals. J-aggregates have been observed to form liquid crystal (LC) phases, offering potential for creating LLCs characterized by high anisotropy. Our study showcases successful J-aggregate formation of the anionic cyanine dye TDBC within the nematic LC matrix of 5CB, yielding LLCs with intriguing optical and electro-optical attributes.

Our findings indicate that the exciton coherence length of J-aggregates in LC environments is comparatively smaller than in aqueous media, suggesting increased static disorder. Nonetheless, enhancements in fluorescence quantum yield and lifetime signify suppressed non-radiative relaxation and notably prolonged radiative lifetime. Assessment of TDBC J-aggregate photostability in the LC matrix reveals substantial improvement compared to that in aqueous environments. These results hold promise for the advancement of novel luminescent liquid crystal materials, prompting further investigation and detailed exploration.

Engineering optical metasurfaces for far- and near-field applications

A. A. Hrinchenko[1], O. Yu. Demianyk[1], S. Yu. Polevoy[2], A. I. Ovcharenko[1], V. R. Tuz[1], K. E. Nemchenko[1], O. Y. Yermakov[1]

[1] V. N. Karazin Kharkiv National University, 4 Svobody Square, Kharkiv, 61022, Ukraine
[2] O. Ya. Usikov Institute for Radiophysics and Electronics NAS of Ukraine, 12 Ac. Proskura, Kharkiv, 61085, Ukraine
e-mail: oe.yermakov@gmail.com

Two-dimensional (2D) materials offer unique opportunities for photodetection, light emission, energy harvesting, and enhanced light-matter interactions. Even more interest brings the artificially engineered 2D micro- and nanostructures with on-demand properties paving the way towards a plethora of specific applications and devices including lensing, holography, imaging, polarimetry, biosensing, etc. The rapidly developing use of 2D nanostructures poses new challenges for their proper engineering and novel applications. Here, we focus on the metasurfaces, which are the periodic arrays of subwavelength scatterers.

In this work, we develop new approaches, generalizations and algorithms of the metasurfaces engineering based on the semi-analytical methods, numerical simulation and machine-learning-based inverse design [1]. Then, we study the properties of the plasmonic and all-dielectric metasurfaces in both far-field (Brewster's angle microscopy [2], antireflective coatings of solar cells) and near-field (ultrafocused in-plane transfer of electromagnetic signal [1], polarization degree of freedom [3] and chiral light-matter interactions), see Fig. 1. This work demonstrates the enhancement or modification of the mentioned phenomena using the specific design of metasurface and gives the connection between the properties and design of a metasurface.

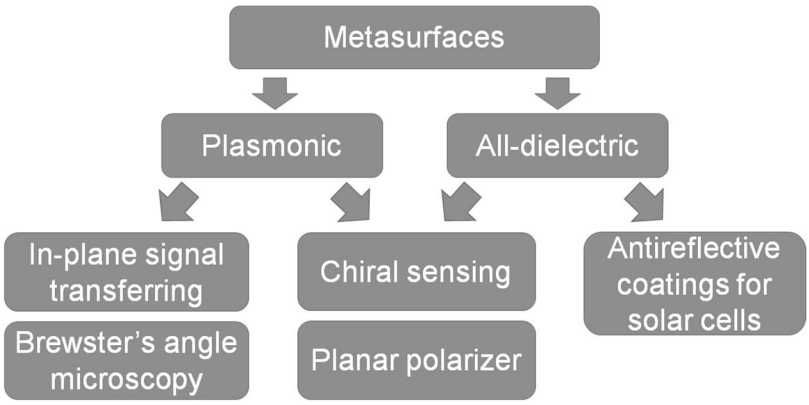

Figure 1. The applications of plasmonic and all-dielectric metasurfaces discussed in this work.

[1] A. Hrinchenko, and O. Yermakov, J. Phys. D: Appl. Phys. 56, 465105 (2023). https://doi.org/10.1088/1361-6463/acefde
[2] O. Yermakov, Phys. Rev. A 109, L031502 (2024). https://doi.org/10.1103/PhysRevA.109.L031502
[3] S. Polevoy, and O. Yermakov, IEEE Antenn. Wireless Propag. Lett. 22, 1962 (2023). https://doi.org/10.1109/LAWP.2023.3270456

Polaritons in the magnetic-«epsilon-near-zero» multilayers, with noncollinear orientation of magnetizations

A. F. Bukhanko

Donetsk Institute for Physics and Engineering Named after O.O. Galkin, NAS of Ukraine,
Nauki ave. 46, Kyiv, 03028, Ukraine
e-mail: metatem@ukr.net

We present a theoretical investigation of the polaritons propagation in the magnetic-«epsilon-near-zero» multilayer structure, with noncollinear orientation of magnetizations. In recent years large research efforts have been dedicated to artificial materials with extreme anisotropy, with particular attention devoted to so-called «epsilon-near-zero» media. Known work [1-3], which theoretically and experimentally studied materials with zero diagonal elements of permittivity tensor, however, manipulation of the magnetic-«epsilon-near-zero» multilayers remain elusive.

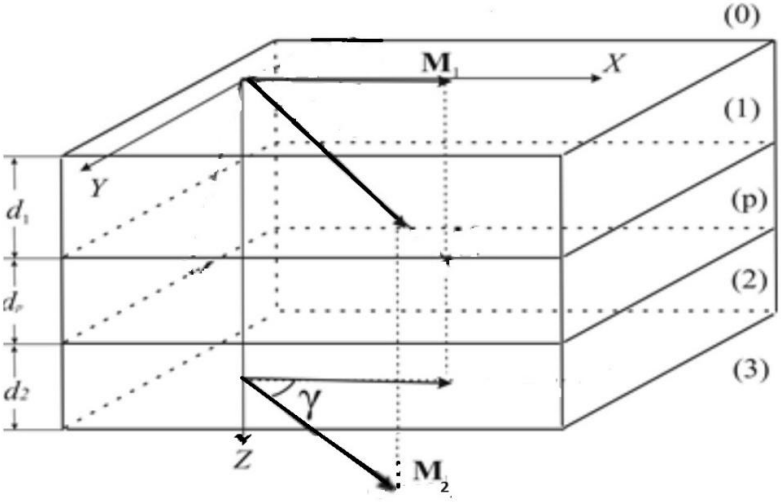

Fig.1. Film and magnetizations geometry.

In these studies, we are using the transfer matrix method to obtain analytical equations and analyse graphically dependencies from angle γ between the magnetizations for the polaritons in that structure. We study influence that external magnetic field can has on the optical properties of the magnetic-«epsilon-near-zero» multilayers. We show numerically, that characteristics of the polaritons can be controlled by the external magnetic field applied in the plane of the film, which leads to variations of the angle between the magnetization vectors γ. Special attention was paid to the possibility of surface waves in the epsilon-near-zero layer (p) (Fig.1).The presented results demonstrate that the properties of polaritons in this structure significantly depend on the angle γ between the magnetization vectors of magnetic layers (1) and (2). It was shown that, for such a configuration the non-reciprocal properties of the polaritons strong show themselves. This arises from the absence of time-reversal invariance, manifested by the off-diagonal permittivity tensor components, together with the reduction of spatial symmetry at the surface. Authors acknowledge the financial support from STCU grant # 9918.

[1] Mohammad H. Javani and Mark I. Stockman, Phys. Rev. Letters. 117. 107404 (2016). http://dx.doi.org/10.1103/PhysRevLett.117.107404.
[2] Vladimir R Tuz, Journal of Magnetism and Magnetic Materials. 419, 559 (2016) http://dx.doi.org/10.1016/j.jmmm.2016.06.070
[3] V. I. Fesnko, I.V. Fedorin, Vladimir R. Tuz, Optics Letters. 41, 2093 (2016). http://dx.doi.org/10.1364/OL.41.002093

Temperature-dependent operation of laser passive Q-switches based on polyurethane matrices

T. Bezrodna[1], V. Bezrodnyi[1], A. Negriyko[1], L. Kosyanchuk[2], O. Antonenko[2], V. Nesprava[1]

[1] Institute of Physics NAS of Ukraine,46 Nauky av., Kyiv, 03028, Ukraine
[2] Institute of Macromolecular Chemistry NAS of Ukraine,
48 Kharkivske shose, Kyiv, 02160, Ukraine
e-mail: tomaalone@yahoo.com

Among the various types of lasers, a special place belongs to the solid-state ones operating in a pulsed mode with the cavity Q-switching. The most widespread are the lasers with passive Q-switches based on bleachable filters. The generation parameters of such lasers depend not only on the active medium, but are also significantly determined by spectral and luminescent properties of the bleachable filter. Solid-state versions of passive Q-switches most fully meet modern operational requirements for elements of laser technology.

Polyurethane matrices used in our research for the development of dye-based active laser elements and passive Q-switches have a distinctive feature, namely, high mobility of polymer chain segments, which causes a highly elastic state of these polymers in a wide temperature range. Elastic properties of polyurethane matrices provide high resistance to the powerful laser radiation.

Our optimized multicomponent urethane polymer composition based on hexamethylene diisocyanate, polypropylene glycol and trimethylolpropane is a network elastomer, i.e. a continuous three-dimensional structure, where all constituent molecules are connected by various chemical bonds. An important property of this polymer is the ability to dissolve all main classes of organic dyes, which can provide passive Q-switches for the pulsed lasers of different spectral ranges. The radiation strength of this polymer composition is 18 J/cm^2 at a wavelength of 1.06 μm with a pulse duration of 10 ns.

The ambient temperature and thermal processes in the elements of solid-state lasers affect their generation characteristics; therefore, it is relevant to study the characteristic properties of passive Q-switches with temperature changes. In single-pulse solid-state lasers, the temperature effects on the energy parameters of generation are resulted from the redistribution of electrons across energy levels in the active medium, changes in the luminescence bandwidth, and consequently, changes in the effective cross section of the radiation transition.

This work deals with the investigations of how the ambient temperature influences the energy characteristics of solid-state lasers with the passive Q-switches. For this purpose, stable, highly efficient polymer Q-switches were developed based on a polyurethane composite and an organic dye, bis-(4-dimethylaminodithiobenzyl)-nickel (BDN). The specificity of lasers with the passive Q-switches is that their T_0 parameter (initial transmission) is the main factor determining the radiation energy regardless of the pump energy (within the single-pulse mode). Dependence of the T_0 value for the BDN dye in a polyurethane matrix has been studied at the ambient temperatures from -50 to +50 ℃.

According to literature data, temperature changes of the stimulated emission cross section for the Nd:YAG are minimal among solid-state laser Nd-doped materials. Therefore, in this work the energy parameters and threshold values of pump energy are investigated on a base of the Nd:YAG laser. Obtained experimental results indicate the possibility of passive Q-switches based on highly elastic polyurethane matrices to be used in the solid-state lasers, operating at ambient temperatures from -50 to +50 ℃.

First-principles investigation of optical features for gyrotropic α-$Hg_3S_2Cl_2$ polymorph

O. V. Bokotey[1], T. V. Vu[2], O. O. Bokotey[1], A. G. Slivka[1]

[1] Faculty of Physics, Uzhhorod National University, 3 Narodna Sqr., Uzhhorod, 88000, Ukraine
[2] Laboratory for Computational Physics, Institute for Computational Science and Artificial Intelligence, Van Lang University, Ho Chi Minh City, Vietnam
e-mail: obokotei@gmail.com

Corderoite family compounds present a class of functional materials with large nonlinearities. The main structural feature is the tendency to formation of various polymorphic modifications due to the great conformational capacity of mercury-chalcogen component. The α-$Hg_3S_2Cl_2$ compound is characterized by α- and β-polymorphism. Interest in corderoites is caused by such optical properties as photoconductivity, high refractive index, transparency in visible and IR-region, optical activity and electro-optic effect [1-4]. $Hg_3S_2Cl_2$ crystals are highly attractive materials because of their great potential for development of modern nonlinear optics, optoelectronics and nanophysics. They are expected to contribute in the development of nanobiophysics and personalized medicine for health monitoring and prevention.

The APW-LO technique as implemented in the WIEN2k package were employed to calculate the band structure, total and partial density of states, and the optical constants of α-$Hg_3S_2Cl_2$ polymorph.

The detailed analysis of the low-energy electronic states near the Fermi level was conducted. The main contributions of the sulfur and chlorine p states are located at the top of the valence band, while the S/p and Hg/s states give main contribution to the bottom of the conduction band. The direct optical band gap of 3.19 eV is at the Γ-points of Brillouin zone. All linear optical functions, such as the absorption coefficient α(ω), refraction index n(ω), extinction coefficient k(ω), reflectivity R(ω), and electron energy-loss function L(ω) were calculated from $\varepsilon_1(\omega)$ and $\varepsilon_2(\omega)$ spectra via well-known relationships.

Based on studies of optical activity in the $Hg_3S_2Cl_2$, it was found that the optical values and dispersion of rotatory ability are connected with the direct inter-band optical transitions. We can conclude that the band topology near the conduction band minimum is changed due to the spin-orbit coupling in the mercury orbitals at the Γ-point of the Brillouin zone. We analyzed some typical features in optical spectra of the $Hg_3S_2Cl_2$. Our calculations indicate that the main contribution comes from Hg/s, S/p and Cl/p electronic states near the Fermi level in DOS and strong reflectivity is occurred at higher energies. The reported structural and optical properties of α-$Hg_3S_2Cl_2$ polymorph make it a potentially interesting compound for nonlinear optical applications.

[1] O.V. Bokotey, Calculated optical properties of gyrotropic $Hg_3Te_2Br_2$, Optik, vol. 156 C, pp. 39-42, 2018.
[2] O.V. Bokotey, T.V. Vu, D. D. Vo, O.O. Bokotey, A.G. Slivka. Electronic and optical properties of gyrotropic α-$Hg_3S_2Cl_2$: insights from an ab initio study. Indian J. Phys., 2020.
[3] O.V. Bokotey, Theoretical calculations of refractive properties for $Hg_3Te_2Cl_2$ crystals, Nanoscale Res. Lett., 11:251, 2016.
[4] O.V. Bokotey, Investigation of gyrotropic properties for $Hg_3X_2Cl_2$ (X = Se, Te) crystals, J. Alloys Compd., vol. 678, pp. 444-447, 2016.

Spectral characteristics of three-particle ionic molecular system of the exotic Carbon atom in one-dimensional space

A. I. Haysak[1], M. I. Haysak[2]

[1] Uzhhorod National University, 3 Narodna sqr., Uzhhorod, 88000, Ukraine
[2] Institute of Electron Physics NASc of Ukraine, 21 Universitetska str., Uzhhorod, 88017, Ukraine
e-mail: mykhaylo.haysak@gmail.com

The work presents results of calculations of the spectral characteristics for three-particle molecular ions of the Carbon atom, which have the following form: $C^{6+}e^{\pm}\overline{C^{6+}}$.

Calculations for these systems had been carried out within the framework of the non-relativistic quantum-mechanical model for the three-body problem, which is based on relative collective Jacobian variables [1]. To find partial solutions of the non-relativistic Schrödinger equation (NRSh) of three independent variables, the problem is reduced to solving two boundary problems - finding adiabatic potentials - $U_v(R)$ and energy values (ε) of the ground and excited states of odd-even (oe) and even-even (ee) series of the given system. After separating the movement of the center of mass of the system, the NRSh depends only on two independent variables (R,α). The radial variable (R) belongs to the interval [0,∞), and the variable α is within the interval [0,β], where β is determined by the particle's mass [1].

The coordinates' values of the adiabatic potential energies minima for the considered series are respectively: $[-5.02076081003489*10^{16},[r=1.56250000000000*10^{(-8)}]]$ - for even-even and $[-1.2577263633462*10^{17},[r=1.22070312500000*10^{(-8)}]]$ - for odd-even series.

Numerical calculations of adiabatic potentials for series (ee) and (oe) and spectral parameters of the considered system were carried out using the Maple program (2017). Results of these calculations are presented in the table below.

States	Energy values of states ε (eV)	β	Average radius of the state, <r> (a.u)	Average radius of the system, (m)
$^1S^{ee}_{Ce\bar{C}}e_{00}$	$3.057105434\cdot10^{16}$	$9\cdot10^{-4}$	$2\cdot10^{-9}$	
$^1S^{ee}_{Ce\bar{C}}e_{01}$	$5.469531600\cdot10^{12}$	$2.95\cdot10^{-8}$	$2\cdot10^{-8}$	$1.058\cdot10^{-18}$
$^1S^{oe}_{Ce\bar{C}}e_{00}$	$6.382967840\cdot10^{15}$	$6.44\cdot10^{-9}$	$3.5\cdot10^{-9}$	
$^1S^{oe}_{Ce\bar{C}}e_{01}$	$2.721160000\cdot10^{14}$	$4\cdot10^{-8}$	$125\cdot10^{-10}$	$6.6125\cdot10^{-19}$

The obtained energy values of the ground and excited states of the considered system lie in the range of ~[3.06·1016, 5.47·1012] eV. The average radii values of these states allow us to assert that all doublet states belong to nanoparticles. It should be noted that the Hamiltonian of this system is invariant, since when the charge of each particle of a given ion is replaced by corresponding antiparticle, we receive the same parameters for negative ions. Positive ions, attracting negative ions, will form neutral molecules of six-particle type $\left(C^{6+}e^{\pm}(\overline{C^{6+}})\right)2$, that is, it is a six-particle neutral Carbon molecule [2].

So, received data allow us to assume the existence of molecular Carbon ions, and the applied mathematical approach can be used in performing calculations for other systems.

[1] M. I. Haysak, I. I. Haysak, M. Nagy, V. V. Onysko, Acta Physica Polonica A, 142 (4), 549 (2022). http://dx.doi.org/10.12693/APhysPolA.142.549.
[2] J. Wolfe & A. Mysyrowicz, Excitonic Matter. Scientific American, 250(3), 98-107 (1984) Retrieved October 12, 2020, from http://www.jstor.org/stable/24969326.

Emission of monochromatic sub-THz radiation by IR-active phonons in KY(MoO4)2

D. Kamenskyi[1,2,3], K. Vasin[3], K. Kutko[4], V. Khrustalyov[4], S. G. Pavlov[1], H.-W. Hübers[1,2]

[1] Institute of Optical Sensor Systems, German Aerospace Center (DLR), Rutherfordtstr. 2, 12489 Berlin, Germany
[2] Department of Physics, Humboldt-Universität zu Berlin, Newtonstr. 15, 12489 Berlin, Germany
[3] Experimental Physics V, Center for Electronic Correlations and Magnetism, Institute of Physics, University of Augsburg, 86159 Augsburg, Germany
[4] B. Verkin Institute for Low Temperature Physics and Engineering of the NAS of Ukraine, 47 Nauky Ave., Kharkiv, 61103, Ukraine
e-mail: khrustalyov@ilt.kharkov.ua

Time-domain spectroscopy (THz-TDS) is a relatively new method to study optical properties of materials in THz range. The method is based on electromagnetic transients optoelectronically generated by femtosecond laser pulses. Here we report the observation of a re-emission of the sub-THz monochromatic radiation from $KY(MoO_4)_2$ pumped by a broadband THz excitation pulse. Crystal structure of this compound is formed by $[K]^+$ and $[Y(MoO_4)_2]^-$ layers which are responsible for the phonon modes with energies below 1 THz [1]. Fig.1 presents experimental data for 80 μm thick single crystal sample when THz radiation pulse propagating along the *b*-axis in two polarizations: $E^{\omega}||a$ (red) and $E^{\omega}||c$ (blue). The waveforms of THz pulses passed the sample showed in Fig.1 (b, c). The long extended emission tail (highlighted by yellow and zoomed in insets) is a manifestation of the electromagnetic wave emission by coherent phonons in $KY(MoO_4)_2$. The transmittance spectra, after Fast Fourier Transform (FFT), with sharp absorption lines at phonon frequencies S_a and S_c (0.568 and 0.860 THz consequently), and peaks correspond to re-emission at these frequencies, have shown at Fig.1 (d, e). The splitting of re-emission peak for $E^{\omega}||c$ (Fig.1 (e), blue curve) is a consequence of strong intensity of S_c phonon. The temperature and sample thickness dependencies of THz-TDS spectra would be also discussed.

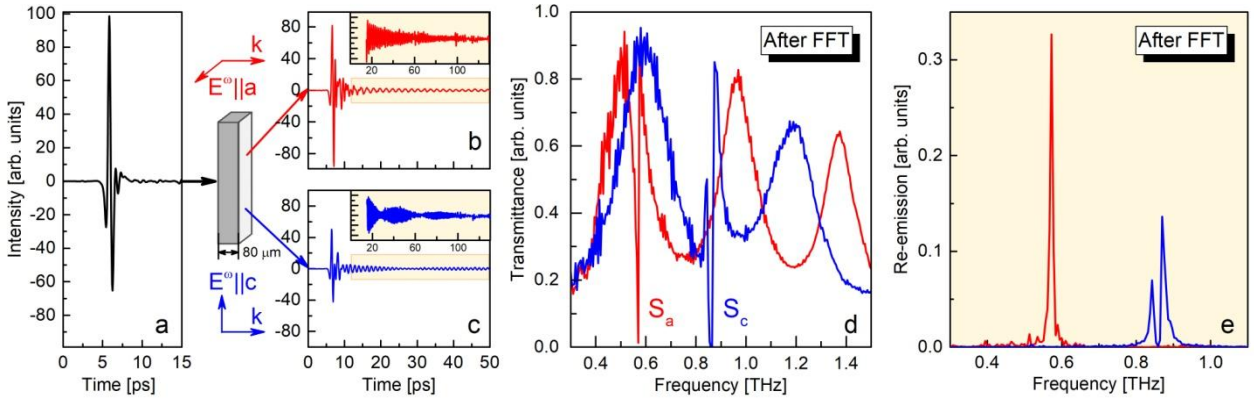

Fig.1. (a) The electric field waveform of the THz pulse before the sample. (b, c) Waveforms of the THz pulse passed the sample (for the case of 80 μm thick sample plate and T = 4 K). Inserts show zoomed waveforms in the time range 10 – 120 ps after the start of the pulse. (d) Squared FFT spectra (transmittance) for $KY(MoO_4)_2$. The periodic fringes in the spectra are caused by multiple reflections within the plane-parallel sample (Fabry-Perot type modulation). (e) Squared FFT of the waveforms shown in the inserts of the Fig.1 (b, c). The spectra obtained at polarizations $E^{\omega}||a$ and $E^{\omega}||c$ denoted by red and blue colors respectively.

[1] Poperezhai, P. Gogoi, N. Zubenko, et al., J. Phys.: Condens. Matter 29, 095402 (2017). https://doi.org/10.1088/1361-648X/aa55a8.

Enhancement of local fields in the vicinity of biconic and bipyramidal metal nanoparticles

A. V. Korotun[1,2]

[1] National University Zaporizhzhia Politechnic, 64 Zhukovsky Str., Zaporizhzhya, 69063, Ukraine
[2] G.V. Kurdyumov Institute for Metal Physics of the NAS of Ukraine,
36 Academician Vernadsky Blvd., Kyiv, 03142, Ukraine
e-mail: andko@zp.edu.ua

Research in recent years [1] has shown that metal nanoparticles of biconical and bipyramidal shapes significantly enhance the signals of surface-enhanced Raman spectroscopy (SERS). In turn, high sensitivity to changes in dielectric constant, photothermal effect, and photothermal stability are related to the features of the geometry of these nanoparticles. Despite the above, the issue of field enhancement around biconic and bipyramidal nanoparticles remains unexplored, and therefore very relevant.

Due to the anisotropy of the shape of biconic and bipyramidal (we assume that the base of the bipyramid is a pentagon) nanoparticles, the amplification of local electric fields in their vicinity is given by a diagonal tensor of the second rank, the components of which are determined by the expressions

$$G_{\hat{\alpha}} = \left| 1 + \left(1 - L_{\hat{\alpha}}\right) \frac{\varepsilon_{\hat{\alpha}}(\omega) - \varepsilon_m}{\varepsilon_m + L_{\hat{\alpha}} \left[\varepsilon_{\hat{\alpha}}(\omega) - \varepsilon_m\right]} \right|^2, \quad (1)$$

where $L_{\hat{\alpha}}$ are depolarization factors; ε_m is the permeability of the surrounding dielectric medium, and the diagonal components of the dielectric tensor of the nanoparticle material are described by the Drude model

$$\varepsilon_{\hat{\alpha}}(\omega) = \varepsilon^{\infty} - \frac{\omega_p^2}{\omega\left(\omega + i\gamma_{\text{eff}}^{\hat{\alpha}}\right)}. \quad (2)$$

In formula (2) ε^{∞} is the contribution of the crystal lattice to the dielectric constant; ω_p is the plasma frequency, and $\gamma_{\text{eff}}^{\hat{\alpha}}$ is the effective rate of electron relaxation, which is the sum of volume and surface relaxation and radiation attenuation. It should be noted that $\gamma_{\text{eff}}^{\hat{\alpha}}$ is calculated within the framework of the equivalent spheroid approach [2], and therefore $L_{\hat{\alpha}}$ will have the same appearance as for prolate and oblate spheroids (depending on the ratio of geometric parameters of the particles of the studied forms).

Calculations of the frequency dependences of the longitudinal and transverse components of the field amplification tensor indicate the presence of one maximum in these dependences, which corresponds to the longitudinal (transverse) surface plasmon resonance. It was also established that the results of calculations for biconical and bipyramidal nanoparticles are close and practically do not differ quantitatively, which allows us to consider bipyramidal particles, which are most often synthesized by various methods, biconical.

[1] S. Xu, L. Jiang, Y. Nie, J. Wang, H. Li, Y. Liu, W. Wang, G. Xu, and X. Luo, ACS Appl. Mater. Inter. 10, 26851 (2018). https://doi.org/10.1021/acsami.8b05447.
[2] A.V. Korotun, Ukr. J. Phys. 68, 695 (2023). https://doi.org/10.15407/ujpe68.10.695.

Frequency splitting of surface plasmon resonance in a cylindrical shell of variable thickness

R. O. Malysh[1], A. V. Korotun[1,2], I. M. Titov[1]

[1] National University Zaporizhzhia Politechnic, 64 Zhukovsky Str., Zaporizhzhia, 69063, Ukraine
[2] G.V. Kurdyumov Institute for Metal Physics of the NAS of Ukraine,
36 Academician Vernadsky Blvd., Kyiv, 03142, Ukraine
e-mail: andko@zp.edu.ua

The spectral position of surface plasmon resonances (SPR) depends on the size, shape of nanoparticles, their composition, and the dielectric constant of the environment. Therefore, the number and position of surface plasmon resonance peaks can be easily adjusted by manipulating the size and shape of nanoparticles, as well as their composition. The use of layered structures of the "core-shell" (A@B) type, in which the core of material A is covered with a shell of material B, where material B can act either a dielectric or the other metal, is more promising. Among the various forms of nanoparticles, cylindrical nanoshells attract great attention [1] due to their high spectral rearrangement in the windows of biological transparency, as well as the existence of a large number of new synthesis methods that allow controlling the size, morphology, and surface area of such structures. Note that it is technologically very difficult to obtain shells of constant thickness during the synthesis of such structures. In this regard, the study of the optical properties of metallic cylindrical shells of variable thickness is of great practical interest and is an urgent task.

Consider the interaction of light with a two-layer cylindrical nanostructure placed in a dielectric medium, and this structure consists of two non-reciprocal cylinders. The dielectric constant of the shell material is equal to ε_s.

In the case when dissipation can be neglected, we have four branches of SPR frequencies

$$\omega_{sp}^{(1,2)(\pm)} = \frac{\omega_p}{\sqrt{\varepsilon^{\infty} - \varepsilon_s^{(1,2)(\pm)}}}, \qquad (1)$$

where ω_p is the plasma frequency; ε^{∞} is the contribution of the crystal lattice to the dielectric constant.

Since $\varepsilon_s^{(1,2)(\pm)}$ is a dimension-dependent function (depends on the radii of the cylinders and the distance between their axes), the corresponding SPR frequencies will also be dimension-dependent.

It was established that, unlike the case of a shell of constant thickness, where there are two branches of SPR frequencies, in the case of a shell of variable thickness, there are four branches of these frequencies due to the additional splitting of SPR frequencies due to the misalignment of the cylinders.

It is shown that for one pair of SPR frequencies there is an increase in the splitting with increasing distance between the cylinder axes, while for the second pair this splitting is a constant value. In addition, the nature of the dimensional dependence of the SPR frequencies for shells of different metals is qualitatively similar, and the differences are quantitative.

[1] S.A. Scherbak, A.A. Lipovskii, J. Phys. Chem. C, 122, 15635 (2018).

Optical response of chains of oblate metal nanospheroids on a dielectric substrate

M. S. Maniuk[1], A. V. Korotun[1,2], V. P. Kurbatsky[1]

[1] National University Zaporizhzhia Politechnic, 64 Zhukovsky Str., Zaporizhzhia, 69063, Ukraine
[2] G.V. Kurdyumov Institute for Metal Physics of the NAS of Ukraine,
36 Academician Vernadsky Blvd., Kyiv, 03142, Ukraine
e-mail: andko@zp.edu.ua

Currently, a targeted search is being carried out for nano-sized structures of different geometries, characterized by certain possibilities for adjusting their optical properties. These structures include nanogrooves on a flat surface, stripes, ridges, and chains of spherical and spheroidal nanoparticles. Chains of metal nanoparticles of different shapes are of particular interest because they can be used to transmit modulated optical signals with a high degree of spatial confinement. Therefore, studying the optical properties of chains of spheroidal nanoparticles on a dielectric substrate is an urgent task.

Let us consider a chain of oblate metal nanospheroids oriented on a dielectric substrate with permeability ε_d in such a way that their minor axes lie in the plane of the substrate. In the local field approximation, taking into account the interaction of nanospheroids with each other and with image dipoles, under the condition of normal light incidence on the substrate, the transverse component of the chain polarizability tensor is determined by the relation

$$\alpha_{\perp}^{\text{chain}} = \frac{\alpha_{\perp}(\omega)}{1 - \dfrac{\alpha_{\perp}(\omega)}{d^3 \varepsilon_m}\left(S_{\perp}^{d} + \dfrac{\varepsilon_d - \varepsilon_m}{\varepsilon_d + \varepsilon_m} S_{\perp}^{i}\right)}, \qquad (1)$$

where d is the distance between the centers of neighboring spheroids (a chain period); ε_m is permeability of an environment; $\alpha_{\perp}$ is the transverse component of the polarizability tensor of a spheroidal nanoparticle; $S_{\perp}^{d}$ and $S_{\perp}^{i}$ are chain sums determined by the contributions of other particles of the chain and image dipoles.

The results of calculating the frequency dependence of the chain polarizability are compared with the calculation results for a single oblate nanospheroid, which made it possible to identify the manifestation of collective effects in a chain of the spheroids. A strong size dependence of the chain plasmon resonance frequency has been established in the case when the values of the chain period and the minor axis of a spheroid are close.

Radiation efficiency of an ensemble of disk-shaped plasmonic nanoparticles

N. I. Pavlyshche[1], A. V. Korotun[1,2], V. P. Kurbatsky[1]

[1] National University Zaporizhzhia Politechnic, 64 Zhukovsky Str., Zaporizhzhia, 69063, Ukraine
[2] G.V. Kurdyumov Institute for Metal Physics of the NAS of Ukraine,
36 Academician Vernadsky Blvd., Kyiv, 03142, Ukraine
e-mail: andko@zp.edu.ua

Ensembles of metal nanoparticles of various shapes are widely used nowadays, in particular, to increase the efficiency of light absorption by thin film solar cells due to the excitation of localized surface plasmon resonance. Therefore, the study of the optical properties of ensembles of metal nanoparticles of different shapes, compositions, and morphologies is an urgent task.

An important characteristic of ensembles of nanoparticles is the radiation efficiency, i.e., a value that indicates how much absorption capacity of the ensemble is.

The radiation efficiency is determined by the expression

$$\mathsf{x}_{\text{rad}} = \frac{\langle Q_{\text{abs}} \rangle}{\langle Q_{\text{abs}} \rangle + \langle Q_{\text{sca}} \rangle}, \tag{1}$$

where $\langle Q_{\text{abs}} \rangle$ and $\langle Q_{\text{sca}} \rangle$ are averaged efficiencies of absorption and scattering of an ensemble, directly proportional to the averaged absorption and scattering cross sections $\langle C_{\text{abs}} \rangle$ and $\langle C_{\text{sca}} \rangle$, so

$$\langle Q_{\text{abs}} \rangle = \frac{\langle C_{\text{abs}} \rangle}{S}, \langle Q_{\text{sca}} \rangle = \frac{\langle C_{\text{sca}} \rangle}{S}, \tag{2}$$

where S is the equivalent cross-sectional area.

The results of calculations show that ensembles of disc nanoparticles are characterized by radiation efficiency close to unity in almost the entire frequency range and sharp minimums that correspond to absorption minimas. The location of the maxima depends significantly on the aspect ratio (the ratio of the diameter of the disc to its height), in contrast to ensembles of spherical nanoparticles, when the position of the maxima of the radiation efficiency does not depend on the size of the particles.

Thus, ensembles of disc nanoparticles compared to ensembles of spherical particles have improved optical characteristics with additional possibilities for adjustment when used in plasmonic photovoltaics.

Color centers in undoped lithium fluoride LiF

O. M. Pop, V. I. Roman, I. H. Megela, V. T. Maslyuk, I. V. Pylypchynets, E. V. Olejnikov, O. O. Papp

Institute of Electron Physics of NAS of Ukraine, 21 Universytetska Str., Uzhhorod 88017, Ukraine
e-mail: pop.ksenja@gmail.com

Today, ultra-high dose dosimetry is of great interest in such fields as space dosimetry, medical dosimetry, and dosimetry on high-energy accelerators. Thermoluminescent (TL) dosimeters are used for such tasks as lithium fluoride LiF doped with Mg, Ti.

It is known that when broad-band alkali-halide crystals are irradiated, color centers are formed. A halogen vacancy that has captured an electron creates the well-known F-center. Such color centers increase when crystals are heated in alkali metal vapors. In addition, F-centers are also formed when exposed to low-energy radiation, in particular, X-rays. This indicates that the decay of electronic excitations into radiation defects can explain F-centers' formation.

The paper investigated the formation of color centers of radiation defects in undoped LiF crystals. The studied samples were irradiated with electrons with an energy of 18 MeV at room temperature on the M-30 microtron of the Department of Photonuclear Processes of the Institute of Electronic Physics of the NAS of Ukraine. Irradiation with electrons was accompanied by integral bremsstrahlung gamma radiation. The fluence at the place of installation of the samples was determined by the current of accelerated electrons, which was measured by a Faraday cylinder with a calibrated inlet hole.

The optical absorption of irradiated samples was measured with a SF-46 spectrophotometer. It was established that the following color centers are observed upon irradiation with high-energy electrons: 240 nm (F-centers) – at low doses and 450 nm (M-center) – at higher doses.

The concentration of color centers, depending on the radiation dose, was determined using the Smakula-Dexter ratio. The obtained number of coloration centers is not related to the formation of radiation defects but only to filling existing vacancies.

Time limits for measurement of gravitational waves with dynamical Casimir effect in solid-state detectors

A. M. Sokolov

Institute of Physics of the National Academy of Sciences, Kyiv, Ukraine
e-mail: andriy145@gmail.com

Detection of gravitational waves with frequencies above 10 kHz may hint on the existence of some exotic astrophysical objects, indicate new physics beyond the Standard Model, and provide a glimpse into the processes in the early Universe [1]. However, both the currently functioning detectors and most of the proposed ones were tailored for the lower frequencies, where less exotic sources are known to exist [1]. On the other hand, modern quantum technologies promise measurement resolution high enough to study the gravity-related effects in a lab [2]. Coincidentally, to avoid thermal noise, quantum devices often operate in this higher frequency range that is now interesting for the gravitational wave detection. We theoretically explore the limits of one such detection scheme based on quantum squeezing in solid-state devices.

A passing gravitational wave modulates a resonator length—and hence its resonance frequency—due to the change of space-time metric [3]. Vigorous modulation of the resonance can even create resonator photons by parametric amplification of the vacuum fluctuations, a process that is known as the dynamical Casimir effect [4]. Luckily, the changes of metric that we can evidence on Earth are not so strong to induce photons.

We study a measurement that uses the Casimir effect in a more general sense. We use the change in the resonator quantum state induced by the modulation in its frequency. More precisely, we consider how a change in a squeezed resonator state evidences the gravitational wave. Advancing the results of Ref. [3], we obtain simple limits on the squeezing and the measurement time required to detect a gravitational wave in some interesting frequency ranges. We focus on use of the solid-state resonators, for which we provide numerical estimates.

[1] N. Aggarwal, O. D. Aguiar, A. Bauswein, G. Cella, S. Clesse, A. M. Cruise, V. Domcke, D. G. Figueroa, A. Geraci, M. Goryachev, *et al.*, Living Rev. Relativ. 24, 4 (2021). https://dx.doi.org/10.1007/s41114-021-00032-5.
[2] Y. Liu, J. Mummery, J. Zhou, M. A. Silanpää, Phys. Rev. Applied 15, 034004 (2021). https://dx.doi.org/10.1103/PhysRevApplied.15.034004.
[3] C. Sabín, D. E. Bruschi, M. Ahmadi, and I. Fuentes, New J. Phys. 16, 085003 (2014). https://dx.doi.org/10.1088/1367-2630/16/8/085003.
[4] P. Lähteenmäki, G. S. Paraoanu, J. Hassel, and P. J. Hakonen, Proceedings of the National Academy of Sciences 110, 4234 (2013). https://dx.doi.org/10.1073/pnas.1212705110.

Methodology for studying the properties of gas discharge plasma in mixtures of inert gases with chalcogen atoms vapours

A. General, E. Svitlichnyi

Institute of Electron Physics of NAS of Ukraine, Universitetska str., 21, Uzhhorod, 88017, Ukraine
e-mail:bercheni14@gmail.com

Due to its multifaceted properties, sulfur is included in the composition some amino acids (cysteine, methionine), vitamins (biotin, thiamin) and enzymes [1], and redox reactions of sulfur are a source of energy in chemosynthesis. It is important to emphasize that sulfur is contained in the atmosphere of some spaceships objects and is a very common element in the universe and interstellar space environment [2]. This determines the constant interest in the study of various physical and chemical properties of sulfur.

The results of the first measurements of the spectral characteristics of the emission of a mixture of sulfur vapor with argon and helium in a gaseous pulse-periodic discharge in the ultraviolet and visible spectral regions are presented.

The longitudinal pulse-periodic discharge in the gas discharge device was excited using a thyratron generator with a commutator ТГИ1-2000/35 and resonant recharging of the storage capacity 1650 nF.

In the experiments, the voltage on the high-voltage rectifier was up to 5 kV, the average discharge current was up to 1 A, and the frequency of the pumping pulses was up to 10 kHz. Argon was used as a buffer gas, the pressure of which was 30 Torr. Crystalline sulfur was in the gas discharge chamber. The temperature of the mixture during the operation of the installation did not exceed 300 °C.

The time-integrated emission characteristics of the discharge were recorded using the MS 7504i spectrometer. The MS 7504i also included two optical radiation detectors: a HS 101H CCD camera and an R928 photomultiplier. Recording information from these detectors and its analysis was carried out using a personal computer.

In the course of the first experiments, the spectral composition of discharge radiation in a vapor mixture of sulfur and argon was studied. It was established that the luminescence spectrum contains radiation in the UV region, which consists of emissions of low intensity, where bands of S_2 molecules are observed, and in the region of 600-1000 nm, which includes emissions of sulfur and argon.

[1] Greenwood N., Earnshaw A. / Chemistry of the Elements, 2nd ed.Butterworth−Heinemann. Oxford, 1997. P. 645−662.
[2] Feaga L.M., McGrath M.A., Feldman P.D. // Astrophys. 2002. Vol. 570. P. 439.

Experimental setup for spraying chalcogens onto a surface in a gas discharge

A. Minya[1], E. Svitlichnyi[2]

[1] Uzhgorod National University, Voloshin str. 56, 88000 Uzhgorod, Ukraine
[2] Institute of Electron Physics of NAS of Ukraine Universitetska str., 21, Uzhhorod, 88017, Ukraine
e-mail:bercheni14@gmail.com

Plasma spraying is an innovative technology that is widely used in various industries.

Its exceptional properties such as high adhesion, surface density, fast application, wide material selection and environmental friendliness are essential for protection, coverage and surface coatings and components. Plasma spraying is a spraying in which the energy source is plasma. As a rule, the inert gas argon and/or helium is used to form plasma. The material in powder form is then fed into the plasma where it is melted and atomized. The sprayed material is deposited on the surface of the product, where a thin and dense layer is formed.

The technology of plasma spraying is widely used in various industries due to its properties and capabilities. Plasma spraying has found its application:

wear protection, corrosion protection, thermal insulation, electrical insulation, decorative coatings, medical industry, electronics and semiconductors.

Plasma spraying offers a number of advantages that set it apart from other technologies:
high adhesion, unique protection properties, uniform coating application, wide range of materials, environmental safety.

Based on all above, research in this direction is relevant. For experiments we designed a universal gas discharge chamber shown on Fig.1 which consist of quartz tube 15 cm long and diameter 4 cm, vacuum gasket, dielectric flanges, universal high-voltage inputs, metal electrodes with adjustable interelectrode distance, heating element(optional), pins for fixation. For sputtering we will use chalcogens (such as sulfur) located in the interelectrode space. It should be noted that we used neon as a buffer gas. In our experiment rectifier voltage was 2.5 kV and the 0.24 A average rectifier current. The storage capacitance value was 1,650 pF at the repetition frequency from 1 to 10 kHz.

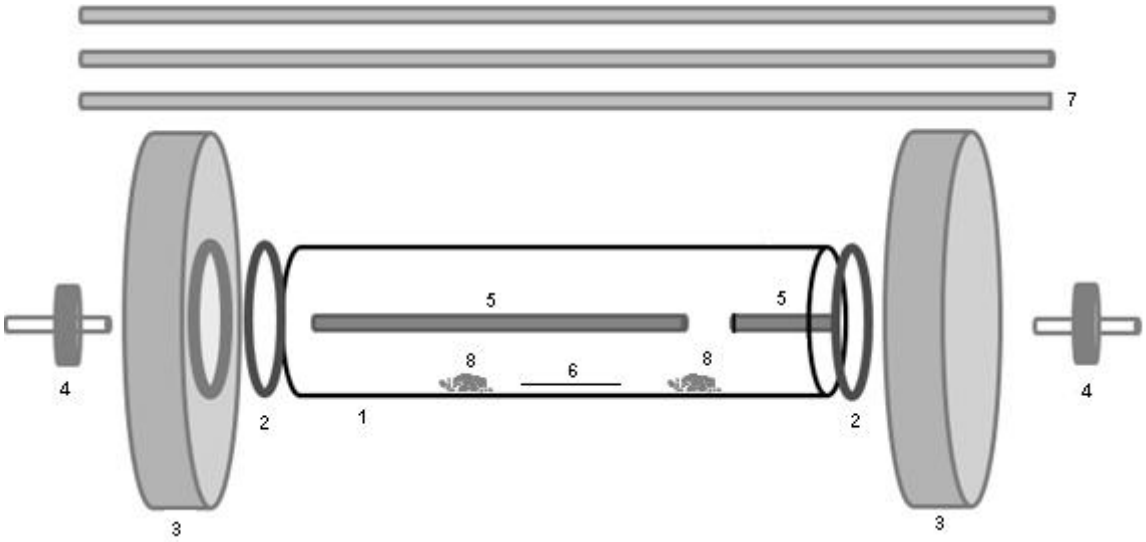

Fig. 1. General view of the universal discharge chamber. 1 – quartz tube, 2 – vacuum gasket, 3 – dielectric flanges, 4 – universal high-voltage inputs, 5 – metal electrodes, 6 – slide, 7 – pins for fixation, 8 – sulfur.

Relevance and prospects for studying low-temperature photoluminescence of GO of various morphologies and its derivatives with impurities

V. N. Zoryansky, P. V. Zinoviev

B. Verkin Institute for Low Temperature Physics and Engineering of NAS of Ukraine,
47 Nauky Ave., Kharkiv, 61103, Ukraine
e-mail: zoryansky@ilt.kharkov.ua

Recording the temperature dependences (20-300 K) of the integral radiation intensity in the mode of continuous quantum counting is a powerful tool for studying the dynamics of electronic excitations, their features and changes with temperature, in carbon structures regardless of the quantum yield of materials. Such experiments help clarify the presence and specificity of various phase transformations and record changes in the energy spectrum of a nanomaterial in the presence of impurities with different chemical activity. Thus, for the C_{60}+H_2 and C_{60}+N_2 systems, which have the limits of the adsorption crossover (transition from the diffusion mechanism of intercalation - physisorption, to the chemical interaction - chemisorption), respectively 300°C and 420°C [1,2], spectral-luminescence studies confirmed the formation of new chemical compounds - hydrofullerite $C_{60}H_x$ and biazafulerite $(C_{59}N)_2$. At the same time, it was the registration of the temperature dependence of the integral intensity of luminescence from low to room temperatures according to the indicated method that showed that for $C_{60}H_x$ there is no orientational phase transition and the transition to the glassy state, and for $(C_{59}N)_2$ quenching of photoluminescence at low temperatures was found [3].

According to the literature, some carbon nanocompounds based on graphene oxide at room temperature also demonstrate a change in optical properties in the presence of impurities. For example, in [4] the quenching of photoluminescence of GO by metal ions in an aqueous medium was discovered, and in [5] determined the influence of carbohydrate saturation of graphene suspension (GS), which also leads to a decrease in the quantum yield of the substance. As a result, the similarity of the observed changes in the luminescent properties of various compounds of the graphene group with those of fullerite compounds has been established, which may indicate the similarity of both the emission mechanisms in such carbon nanostructures and the response of their energy spectrum to the presence of impurities. The conclusion from this is that the study of spectral-luminescent properties by the method of continuous recording of the integral luminescence intensity in the temperature range of 20-300 K may make it possible to identify new optical or structural properties for these compounds.

[1] K. A. Yagotintsev, I. V. Legchenkova, Yu. E. Stetsenko, P. V. Zinoviev, V. N. Zoryansky, A. I. Prokhvatilov, and M. A. Strzhemechny, Low Temperature Physics 38, 952 (2012) https://doi.org/10.1063/1.4758781
[2] I. V. Legchenkova, K. A. Yagotintsev, N. N. Galtsov, V. V. Meleshko, Yu. E. Stetsenko, A. I. Prokhvatilov, Low Temp. Phys. 40, 685 (2014) https://doi.org/10.1063/1.4894316.
[3] P. V. Zinoviev and V. N. Zoryansky, Low Temp. Phys. 48, 268 (2022) https://doi.org/10.1063/10.0009547
[4] D.-Y. Wang, D.-W. Wang, H.-A. Chen, T.-R. Chen, S.-S. Li, Y.-C. Yeh, T.-R. Kuo, J.-H. Liao, Y.-C. Chang, W.-T. Chen, et al. Photoluminescence quenching of graphene oxide by metal ions in aqueous media. Carbon, 82, 24, (2015). https://doi.org/10.1016/j.carbon.2014.10.017
[5] Y.V. Pakharukov, F.K. Shabiev, R.F. Safargaliev, S.S. Volkova, Quenching of graphene suspension photoluminescence with saturated hydrocarbons. Colloid Interface Sci. Commun., 42, 1, 100431, (2021). http://dx.doi.org/10.1016/j.colcom.2021.100431

QUANTUM LIQUIDS AND QUANTUM CRYSTALS, CRYOCRYSTALS

Influence of acoustic emission on the resonance properties of a quartz tuning fork vibrating in superfluid ^{3}He - ^{4}He mixtures

V. K. Chagovets, V. E. Syvokon, S. S. Sokolov

B. Verkin Institute for Low Temperature Physics and Engineering of NAS of Ukraine,
47 Nauky Ave., Kharkiv, 61103, Ukraine
e-mail: chagovets@ilt.kharkov.ua

Recently, in studies of various properties of superfluid ^{4}He and mixtures of ^{3}He in ^{4}He, miniature quartz tuning forks have been applied, which have replaced other mechanical resonators traditionally used for this purpose. However, the complicated geometrical form of the tuning forks and the occurrence of acoustic resonances in the cell filled by the studied liquid with frequencies close to the resonance frequency of the tuning fork strongly affect the measurement results. The purpose of this work is to study the influence of acoustic processes and cell geometry on the vibrational properties of a tuning fork immersed in the liquid.

The work includes the measurements of the resonant frequency of a tuning fork under vibrations in normal and superfluid ^{4}He and concentrated mixtures of ^{3}He in ^{4}He and the estimates of the acoustic mode contribution arising in these liquids. Figure 1 shows the temperature dependences of the resonant frequency of a tuning fork connected with outer space (an open tuning fork) in superfluid ^{4}He (a) and the resonances of the first sound in the cell (b). The cell is considered as a cylinder, the first resonance index corresponds to the mode of radial vibrations, the second to tangential vibrations, and the third to the mode of vibrations along the cylinder axis.

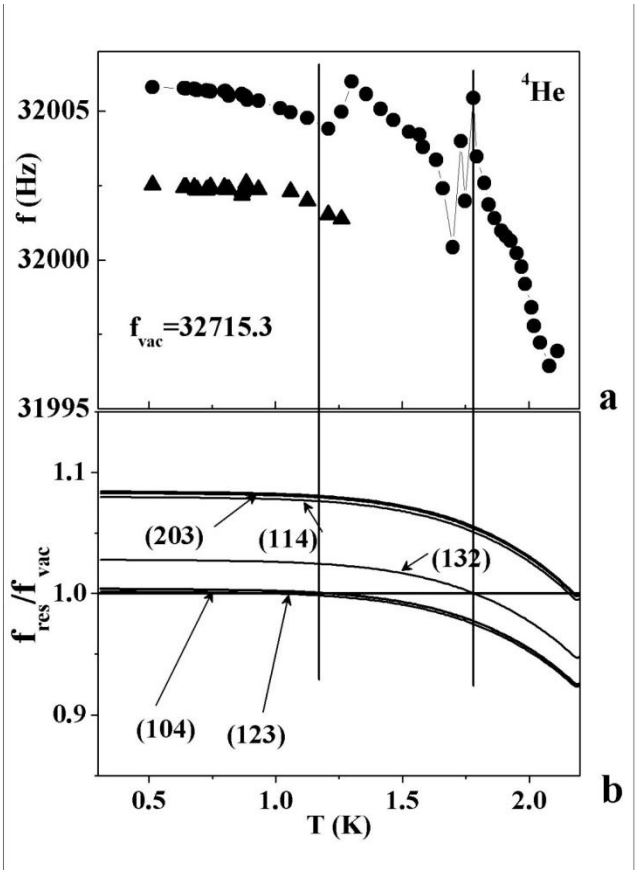

Fig. 1. Frequency of oscillations of a tuning fork in superfluid ^{4}He (a) and relative frequencies of acoustic resonances in the cell (b).

Vertical lines illustrate the conditions for the coincidence of the frequencies of acoustic resonances with the frequency of the tuning fork. One can clearly see how the sound resonance affects the frequency of the tuning fork. At temperature $T < 1$ K, mode (104) has a frequency close to that of the tuning fork, which manifests itself in measurements as an additional resonance (triangles in Fig. 1a). If the tuning fork is located in a closed capsule the influence of acoustic processes in ^{4}He decreases. However, in the mixtures with 5 and 15% ^{3}He such an influence is available not only in open, but also in closed tuning forks.

Thus, when using quartz tuning forks, it should be kept in mind that the size and geometry of the surrounding environment can affect their properties and, in particular, the shape and center frequency of their resonances. The reason is the coupling of the tuning fork oscillation modes to acoustic standing wave modes in the surrounding environment.

Two-step energy dissipation of oscillating tuning fork in ^{3}He-^{4}He superfluid mixtures

J. Amrit[1], N. Herashchenko[2], K. Nemchenko[2], S. Rogova[2], T. Vikhtinskaya[2]

[1] LISN, CNRS, Université Paris-Saclay, 91405, Orsay, France
[2] V. N. Karazin Kharkiv National University, 4 Svobody Sq.,61022, Kharkiv, Ukraine
e-mail: n.gerashchenko@karazin.ua

In this report we present the results of theoretical studies of the possible mechanism of energy dissipation that take place in the experiments [1-2] on study of a vibrating quartz fork in superfluid ^{3}He–^{4}He mixtures with enough high concentration.

Along with known mechanisms of energy loss from a vibrating quartz fork such as first and seconds sound radiation [3-4], interaction with thermal excitations, and radiation of thermal wave [5] we consider the two-step mechanism of heat radiation.

The main idea of the work is that the viscosity of such concentrated solutions is quite high, and a fairly large part of the tuning fork energy is lost when a viscous wave is excited. The presence of a viscous wave leads to heat dissipation in the boundary region of the fork walls. This local heated region in the solution, in turn, relaxes throughout the entire volume of the solution by the second sound wave and via the thermal conductivity of the solution. We examine the effectiveness of this mechanism, compare it with experimental results, and determine the conditions under which such a mechanism is most effective.

This work was supported by the project “Remote Research Grants for Ukrainian Researchers” that has received funding through the EURIZON project, which is funded by the European Union under grant agreement No.871072.

[1] E. M. Pentti, J. T. Tuoriniemi, A. J. Salmela, A. P. Sebedash, J. Low Temp. Phys. 150, 555 (2007). https://doi.org/10.1007/s10909-007-9583-7.
[2] V. A. Bakhvalova, V. K. Chagovets, I. A. Gritsenko, et al., J Low Temp. Phys. 187, 413 (2017). https://doi.org/10.1007/s10909-016-1712-8.
[3] N. Herashchenko, K. Nemchenko, S. Rogova, T. Viktinskaya, Low Temp. Phys. 49, 171 (2023). https://doi.org/10.1063/10.0016841.
[4] T. Vikhtinskaya. N. Herashchenko, K. Nemchenko, Low Temp. Phys. 48, 117 (2022). https://doi.org/10.1063/10.0009290.
[5] K. Nemchenko, S. Rogova, T. Vikhtinskaya, J Low Temp Phys. 187, 324 (2017). https://doi.org/10.1007/s10909-017-1761-7.

Phase composition of large substrate-free binary Ar-Kr clusters

O. P. Konotop, O. G. Danylchenko

B. Verkin Institute for Low Temperature Physics and Engineering of NAS of Ukraine,
47 Nauky Ave., Kharkiv, 61103, Ukraine
e-mail: konotop@ilt.kharkov.ua

The prediction of crystal structures is one of the popular tasks in solid state physics. In the case of finite crystals, the preferred crystal structure is dependent on the size of aggregation. The simplest object to study crystal growth with size-dependence of the structure is rare gas solids (RGS). However, in spite of simple interatomic interactions described by two-body Lennard-Jones potential, the preference of the heavy rare gases for the fcc crystal structure is not understood [1].

The fcc/hcp dilemma is also actual in the studies of free single-component and binary rare gas clusters produced by adiabatic expansion of supersonic jets. The hcp structure peaks were fixed by electron diffraction data for the first time on a large free Ar clusters [2]. Further, the transformation from the fcc to the two-phase fcc-hcp structure with a change in the size of these clusters was traced in [3]. Finally, in [4] we studied the fcc-hcp structural transition in heterogeneous Ar-Kr clusters of equimolar component composition and compared it with the one in Ar clusters.

In present work, we continue the research begun in [4] and add to the investigation the phase composition of both large pure Kr clusters and large binary Ar-Kr clusters for two values of krypton mole fraction in clusters (0.25mf and 0.8mf). The average cluster size $\overline{N}$ ranged from $2{\cdot}10^3$ to $1{\cdot}10^5$ at./cl. (i.e. the average linear cluster size δ was varied from 60Å to 200Å). The results of THEED quantitative phase analysis are shown in the figure. It was found that the threshold cluster size for the formation of fcp phase has the same value for both homogeneous and heterogeneous clusters and equals to $\delta \approx 90$ Å ($\overline{N} \approx 1.1{\cdot}10^4$ at/cl). As clusters grow, the relative volume of hcp phase increases substantially to reach its maximum in large ($\delta \approx 150$–160 Å, $\overline{N} \approx 4.3{\cdot}10^4$ at/cl) polycrystalline aggregations. A further increase in cluster size has almost no effect on the relative volume of hcp phase and even the largest clusters we studied ($\delta \approx 200$ Å, $\overline{N} \approx 1{\cdot}10^5$ at/cl) have a two-phase fcc-hcp structure. In the case of clusters having the same size, it was found that: firstly, the volume of hcp phase in heterogeneous clusters significantly exceeds that in homogeneous ones; secondary, the volume of hcp phase depends on the krypton content in clusters, and the maximum fraction of hcp phase is observed at equimolar contents of argon and krypton.

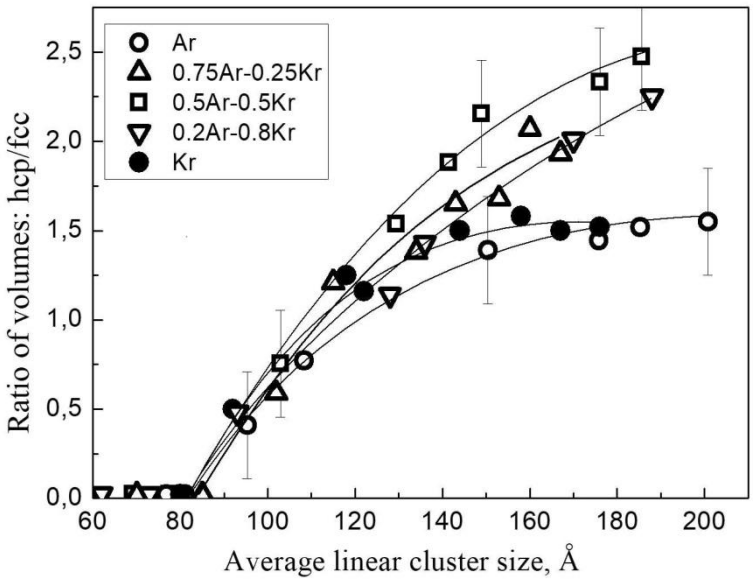

[1] B.W. van de Waal, The FCC/HCP dilemma (University of Twente, Enschede 1997).
[2] O. G. Danylchenko, S. I. Kovalenko, V. N. Samovarov, Low Temp. Phys. 30, 166 (2004). https://doi.org/10.1063/1.1645170.
[3] O. G. Danylchenko, S. I. Kovalenko, V. N. Samovarov, Low Temp. Phys. 34, 966 (2008). https://doi.org/10.1063/1.3009597.
[4] O. G. Danylchenko, S. I. Kovalenko, O. P. Konotop, V. N. Samovarov, Low Temp. Phys. 40, 1083 (2014). https://doi.org/10.1063/1.4904000.

Thermal conductivity of ABS polymer composite with 0.5 wt% of the thermally reduced graphene oxide

V. V. Sagan, A. I. Krivchikov, V. A. Konstantinov

B. Verkin Institute for Low Temperature Physics and Engineering of NAS of Ukraine,
47 Nauky Ave., Kharkiv 61103, Ukraine
e-mail: sagan@ilt.kharkov.ua

The processes of heat transfer are a rather complex and intriguing problem in the physics of condensed matter. It is well-known that in simple, crystalline, orientationally ordered solids, the temperature dependence of thermal conductivity $\kappa(T)$ exhibits a crystalline-like pattern: starting from the lowest temperatures, as the temperature increases, the thermal conductivity grows, and then the curve $\kappa(T)$ has a phononic maximum [1].

A fundamentally different picture is observed in the behavior of $\kappa(T)$ in amorphous substances. The nature of $\kappa(T)$ behavior is glass-like: the thermal conductivity is low, it increases with temperature, passing through a thermal conductivity plateau κ_{pl}, which is practically located in the range of approximately 5–10 K for all amorphous substances. With further temperature increase, $\kappa(T)$ also continues to increase slowly until saturation is reached. The dependence of $\kappa(T)$ is determined by energy transfer mechanisms in a solid. These mechanisms are characterized by ballistic propagation and thermal diffusion of collective excitations in a disordered solid.

The thermal conductivity of pure ABS (Acrylonitrile Butadiene Styrene, chemical formula $(C_8H_8 \cdot C_4H_6 \cdot C_3H_3N)_n$) polymer and ABS polymer composite with 0.5 wt% of the thermally reduced graphene oxide (trGO) was measured in a wide temperature range from 2 to 100 K [1, 2].

From the experimental results it is clear that glass-like behavior $\kappa(T)$ takes place. The thermal conductivity of both samples increases sharply at low temperatures, then growth slows down between 30 and 100 K. Adding 0.5 % trGO enhanced the thermal conductivity of ABS polymer by 1.5 times over the entire temperature range.

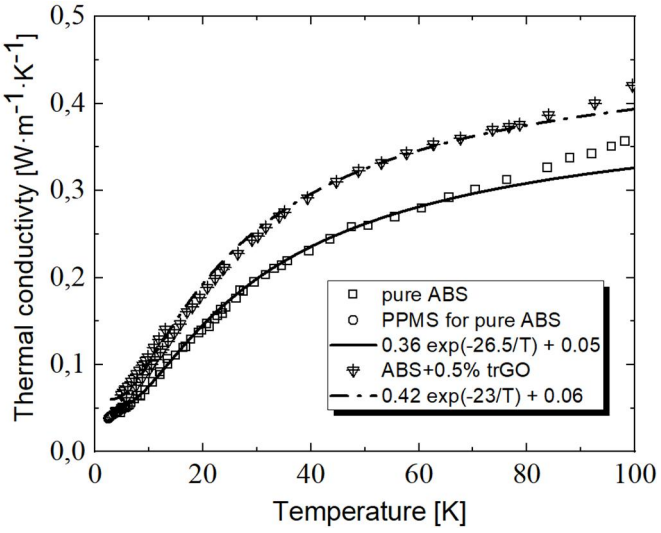

An approximation has been proposed, according to which the experimentally observed thermal conductivity can be well described by an Arrhenius-type exponential function:

$$\kappa(T) = \kappa_{pl} + \kappa_0 \exp(-E/T)$$

where κ_0 is the value of the high-temperature limit of thermal conductivity, and representing the maximum value of the diffusion contribution by the excitation system referred to as diffusions, and E denotes the characteristic energy associated with the dominant diffusions, expressed in K, and a constant term κ_{pl}, most likely related to the lower limit of thermal conductivity [3].

[1] A. Jezowski, J. Mucha, and G. Pompe, J. Phys. D, Appl. Phys. 20, 1500 (1987). https://doi.org/10.1088/0022-3727/20/11/022.
[2] A. Jeżowski, B. A. Danilchenko, M. Boćkowski, I. Grzegory, S. Krukowski, T. Suski, and T. Paszkiewicz, Solid State Communication 128, 69 (2003). http://dx.doi.org/10.1016/S0038-1098(03)00629-X.
[3] A. I. Krivchikov, A. Jeżowski, V. A. Konstantinov, V. V. Sagan, O. A. Korolyuk, and D. Szewczyk, Thermochimica Acta 733, 179696 (2024). https://doi.org/10.1016/j.tca.2024.179696.

Structural characteristics of solid nitrogen. Isotopic effect

N. A. Aksenova[1], D. E. Hurova[2], N. N. Galtsov[2]

[1] V. N. Karazin Kharkiv National University, 6 Nezalezhnosti Ave, Kharkiv 61022, Ukraine
[2] B.Verkin Institute for Low Temperature Physics and Engineering of NAS of Ukraine, 47 Nauky Ave., Kharkiv, 61103, Ukraine
e-mail: aksenova@karazin.ua

Most isotopes of molecular crystals (H_2O/D_2O and $^{14}N_2/^{15}N_2$) in the solid phase have the same crystal lattice and different molar volumes [1]. Consequently, in the diffraction patterns obtained from isotopes, the diffraction peaks are shifted relatively to each other.

As was shown in [2], the scattering amplitude from linear molecules is proportional to the amplitude of librational vibrations. The use of such a technique for analyzing the intensity of X-ray diffraction patterns can make it possible to observe new effects in molecular crystals.

The purpose of this work is to analyze the intensity of diffraction maxima of solid nitrogen $^{14}N_2$ and $^{15}N_2$.

Structural studies of solid nitrogen $^{14}N_2$ and $^{15}N_2$ were carried out on a DRON X-ray diffractometer in Kα radiation from an iron and copper anode, respectively. The X-ray diffraction patterns were carried out in the temperature existence range for orientationally ordered phases of solid nitrogen $^{14}N_2$ - $^{15}N_2$ [3].

Using X-ray diffraction patterns obtained from solid nitrogen $^{14}N_2$ and $^{15}N_2$ in the orientationally ordered phase, the temperature dependences for the angles of variation by a linear molecule from the <111> direction of the cubic lattice were determined.

Using the Rietvelds approach described in [3], we determined the distances between nuclei in a linear molecule $^{15}N_2$.

[1] V. G. Manzhelii, A. I. Prokhvatilov, V. G. Gavrilko, and A. P. Isakina, Structure and Thermodynamic Properties of Cryocrystals (Begell House Inc., New York 1996).
[2] N. N. Galtsov, O. A. Klenova, and M. A. Strzhemechny, Fiz. Nizk. Temp. 28, 517 (2002) [Low Temp. Phys. 28, 365 (2002)].
[3] R. A. Young, The Rietveld Method (Oxford University Press Inc., New York 1993).

Observation of new band in stimulated luminescence of solid nitrogen

M. A. Bludov, I. V. Khyzhniy, S. A. Uyutnov, E. V. Savchenko

B. Verkin Institute for Low Temperature Physics and Engineering of NAS of Ukraine,
47 Nauky Ave., Kharkiv, 61103, Ukraine
e-mail: M.Bludov@ilt.kharkov.ua

Radiation effects in solid N_2 up to very recently were explored and considered mainly in terms of neutral electronic excitations and their interactions. Active research of the problem of charged species dynamics and their role in a variety of radiation-induced phenomena has been undertaken in recent years and its trends were reviewed in [1]. One of the related questions concerns identification of, the so-called γ-line, situated in the near infrared (NIR) range. Connection of this line with interaction of nitrogen species with electrons was established in [2, 3]. According to [2] the γ–line appears as a result of the electron attachment to the metastable $N(^2D)$ atom forming nitrogen anion in the excited state N^- (^1D). However, this suggestion does not explain the red satellite of the γ–line. Moreover, finding the second satellite of the γ–line in the spectrum of spontaneous luminescence excited with an electron beam [3] calls into question the identification of the γ–line as the emission of nitrogen anion N^-.

Here we present new results on the study of spontaneous and stimulated luminescence in nitrogen solids in NIR range. Irradiation was performed in dc regime with an electron beam of subthreshold energy. Relaxation dynamics was monitored by emission spectroscopy – cathodoluminescence (CL), along with optical and current activation spectroscopy. The CL of nitrogen films of different thicknesses when excited by electrons with energies of 0.5, 1, and 1.5 keV was studied. On completion of irradiation real-time correlated measurements of thermally stimulated luminescence (TSL) and exoelectron emission (TSEE) were carried out.

The CL spectrum in NIR range registered at 5 K consists of three line: 794, 802 and 810 nm in agreement with [3]. A comparison of the CL spectra obtained under different conditions showed that there is no correlation in the behavior of emission from the ^2D state of the N atom and the γ-line, which could be expected in the case of the formation of the γ-line emitting centers via electron attachment to the $N(^2D)$ atom. Increasing the irradiation time made it possible to register a new NIR band at 810 nm (the second satellite of the γ-line) in the spectra of TSL. The positions of all three spectral features coincide in the spectra of spontaneous and stimulated luminescence, as evidenced by a comparison of the CL spectrum recorded at 5K with the TSL spectrum recorded at the TSL maximum at 16K. Measurement of the TSL curves at 802 and 810 nm showed a correlation with the TSL curve measured on the γ-line at 794 nm and the yield of the TSEE. The similar behavior of all these lines in the stimulated luminescence and the correlation with the stimulated current indicate their common origin and connection with the neutralization reaction. Note that the position of the γ-line (1.56 eV) is quite close to the theoretically found transition of the N_4 isomer of (D_{2h}) symmetry from the lowest excited state 1^1B_{3u} to the ground state ^1A_g (1.6 eV) [4]. However, the distances between the lines do not coincide with the vibrational structure predicted in [4]. The origin of the γ-group and connection with the neutralization reaction $N_4^+ + e^- \rightarrow N_4^* \rightarrow N_4 + h\nu + \Delta E$ are discussed.

[1] E. Savchenko, I. Khyzhniy, V. Bondybey, Low Temp. Phys. 45, 975 (2019). http://dx.doi.org/10.1063/1.5121267.
[2] R. E. Boltnev, I. B. Bykhalo, I. N. Krushinskaya, A. A. Pelmenev, S. Mao, A. Meraki, P. T. McColgan, D. M. Lee and V. V. Khmelenko, PCCP, **18**, 16013 (2016). http://dx.doi.org/10.1039/C6CP01080F.
[3] E. V. Savchenko, I. V. Khyzhniy, S. A. Uyutnov, M. A. Bludov, Low Temp. Phys. 50**,** 89 (2024). http://dx.doi.org/10.1063/10.0023897.
[4] M. Bittererova, H. Östmark, and T. Brinck, Chem. Phys. Lett. 347**,** 220 (2001). http://dx.doi.org/10.1016/S0009-2614(01)01002-8.

The influence of a point impurity on the phonon spectrum of a chain of noble gas atoms adsorbed on a carbon nanobundle

E. V. Manzhelii, S. B. Feodosyev, E. S. Syrkin

B. Verkin Institute for Low Temperature Physics and Engineering of NAS of Ukraine,
47 Nauky Ave., Kharkiv, 61103, Ukraine
e-mail: emanzhelii@ilt.kharkov.ua

The synthesis and experimental study of long chains of inert gas atoms adsorbed in grooves on the surface of carbon nanotube bundle aroused interest in the theoretical study of the vibrational and thermodynamic properties of these chains [1-5]. The linear and periodic nature of these objects is directly confirmed by neutron diffraction studies [6]. The linear and periodic nature of these chains is indirectly confirmed by studying their low-temperature heat capacity [7,8].

The stability of the adsorbed chains of atoms is determined by the interaction of the atoms of the chain with the substrate. As a result of this interaction, the spectrum of the adsorbed chain starts with a nonzero frequency. Localized vibrations generated by a substitution impurity can occur both below the initial frequency and above the maximum frequency of the quasi-continuous spectrum of the chain. We considered a point impurity that differs from the atoms of the chain in mass, in interaction with the atoms of the chain, and in the interaction with the substrate. We consider a chain of adsorbed atoms as a chain in a periodic external field. In this approximation, we obtained analytical expressions for the oscillation frequencies as functions of these three parameters. Analytical expressions for the thresholds for the occurrence of localized oscillations and the intensity of localized oscillations were also obtained. These results make it possible to further theoretically study in the effect of point impurities on the low-temperature heat capacity of chains of inert gas atoms adsorbed in grooves on the surface of carbon nanobundles.

[1] E. V. Manzhelii, S. B. Feodosyev, I. A. Gospodarev, E. S. Syrkin and K. A. Minakova, Low. Temp. Phys. 41, 557 (2015). https://doi.org/10.1063/1.4927047.
[2] E. V. Manzhelii, JLTP 187, 105 (2017). https://doi.org/10.1007/s10909-016-1699-1.
[3] E. V. Manzhelii, S. B. Feodosyev, I. A. Gospodarev, Low Temp. Phys. 45, 355 (2019). https://doi.org/10.1063/1.5090095.
[4] S. B. Feodosyev, I. A. Gospodarev, E. V. Manzhelii, V. A. Sirenko, E. S. Syrkin, Low Temp. Phys. 45, 763 (2019). https://doi.org/10.1063/1.5111304.
[5] V. E. Syvokon, S. S. Sokolov, Low Temp. Phys. 49, 1148 (2023). https://doi.org/10.1063/10.0020869.
[6] M. Bienfait, P. Zeppenfeld, N. Dupont-Pavlovsky, M. Muris, M. Johnson, T. Wilson, M. De Pies, O.E. Vilches, Physica B 350, E423 (2004). https://doi.org/10.1016/j.physb.2004.03.130.
[7] M. I. Bagatskii, V. G. Manzhelii, V. V. Sumarokov, and M. S. Barabashko, Low Temp. Phys. 39, 618 (2013). https://doi.org/10.1063/1.4816120.
[8] M. S. Barabashko, M. I. Bagatskii, A. V. Dolbin, V. V. Sumarokov, Low Temp. Phys. 49, 979 (2023). https://doi.org/10.1063/10.0020166.

Observation of dynamic- and thermo- anomalies at surface electron to surface anions transition over helium film on structured substrate

V. A. Nikolaenko, A. V. Smorodin, E. Ya. Rudavskii and S. S. Sokolov

B. Verkin Institute for Low Temperature Physics and Engineering of NAS of Ukraine,
47 Nauky Ave., Kharkiv, 61103, Ukraine
e-mail: nikolaenko@ilt.kharkov.ua

The exchange interaction of electron with the neutral matter is nontrivial and the condensed matter researchers are challenged. The surface electrons over liquid helium (SEs) is widely used here as a research tool. At large electric field or/and at dense surrounding gas SE forms dimple in helium - a surface anion (SA) [1-2]. In this work the electro- and the thermo- dynamic anomalies of SE/SA transition over the super-flow helium film on a structured substrate were investigated.

The transport method and the temperature monitoring are used for research. Substrate is a mono- crystalline silicon plate with ~1 cm^2 in square and 0.3 mm in thickness with the periodical grid of pores 2 μm in diameter and 60 μm in depth on surface. Substrate is placed on the cell measurement electrodes and for the conductivity definition, σ, used the capacitive coupling of charge on substrate with electrodes. The cell situated in a vacuum chamber as in diameter as in height 30mm, the "Mutsuhito" brand thermometer mounted under cell. The chamber elements were covered by the super-flow helium film ~ 20 nm in thickness. The saturated electron layer with $N \sim 10^{10}$ e was emitted from the glow thread on substrate with a developed square ~ 25cm^2. (According the electrostatic picture the electrons localized predominant above film on the pore walls).

The experiment had shown the slowly heating chamber from 1.75K to 2.04K causes the value σ decreases according the SE interaction with the growing density atoms in gas. But at 2.04 K was observed both the sharp drop electron conductivity from ~ $5.5 \cdot 10^{-9}$ sim to $7 \cdot 10^{-10}$ sim (the left figure) and the thermo-dip about ΔT~5 mK in size (the right figure).

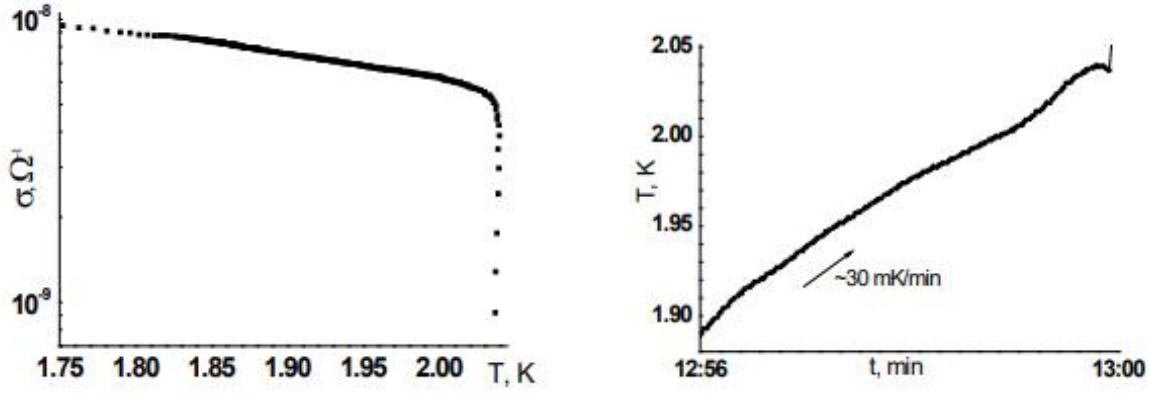

The analyze. From electro- and thermo- energy balance the value ΔT is ~ $e \cdot \Delta V \cdot N / C \cdot m$ (here C_{He} and m are the specific heat capacity and the He-film mass, accordingly). The experimental parameters are next: $m \sim 2.5 \cdot 10^{-5}$ g on surface near 10^2 cm^2; C ~ C_{He} ~1J/g·K; $\Delta V \sim 10^2$ V at transition SE-SA [3]. So anomalies are caused the SE/SA transition on the super-flow helium film.

[1] Yu. P. Monarkha, Phys. Nizk. Temp. 1, 526 (1975).
[2] V. B. Shikin, JETP Lett. 80, 417 (2004). https://doi.org/10.1134/1.1830660.
[3] Yu. Z. Kovdrya, F. F. Mende, and V. A. Nikolaenko, Phys. Nizk.Temp. 10, 1129 (1984).

Four-particle states of low-dimensional fermions with three-body interaction

V. Polkanov, V. Pastukhov

Professor Ivan Vakarchuk Department for Theoretical Physics,
Ivan Franko National University of Lviv, 12 Drahomanova str., Lviv, Ukraine
e-mail: cogersum92@gmail.com

Inspired by the narrow Feshbach resonance in systems with the two-body interaction, we propose a two-channel model of three-component fermions with a three-body interaction that considers finite-range effects in low dimensions.

Applying this effective description to the three-component Fermi system with the suppressed two-body interactions in the fractional dimension above d = 1, we have predicted the emergence of the Efimov-like physics in the p-wave channel of the four-body sector. Analytic estimations in the scaling limit are supported by numerically exact calculations for finite effective ranges at unitarity. The detailed analysis of the one-dimensional problem revealed the necessary conditions for the occurrence of negative eigenvalues in the four-body spectrum both in the case of broad and narrow resonances. Particularly, it is shown that depending on the mass ratios of fermions with three-body interactions, one can in principle observe an arbitrarily large number of the tetramer levels. The effect is suppressed for the non-zero effective ranges towards larger mass imbalance.

Heat capacity features of epoxy-based composites with different graphene oxide contributions at low temperatures

O. O. Romantsova[1,2], D. Szewczyk[2], A. Jeżowski[2], Yu. Horbatenko[1], O. Krivchikov[1,2], M. Vinnikov[1], S. Cherednichenko[1]

[1] B. Verkin Institute for Low Temperature Physics and Engineering of NAS of Ukraine, 47 Nauky Ave., Kharkiv, 61103, Ukraine
[2] Institute of Low Temperatures and Structure Research, Polish Academy of Sciences, 2 Okólna str., 50-422 Wroclaw, Poland
e-mail: romantsova@ilt.kharkov.ua

The study of the properties of materials with impurities is of current interest and has important scientific and technical implications. The introduction of impurities makes it possible to obtain a new material with completely different unique properties, which depend on both the type of impurity and its amount. In recent years, a considerable amount of work has been devoted to the study and preparation of epoxy composite nanomaterials. [1]

In this work, samples of epoxy with graphene oxide (GO) impurity at concentrations of 0.25%, 0.5%, 3%, 6% and pristine epoxy have been studied. The heat capacity of the epoxy-based samples was measured using Quantum Design Physical Property Measurement System (PPMS) in the temperature range from 2 K to 50 K.

The “boson peak” is observed in the heat capacity data for epoxy with GO impurity and pristine epoxy, the position and height of which varies with filler loading. This peak slightly decreases with increasing filler content. In addition, a shift as a function of temperature is observed. The experimental data were analysed in comparison with literature data, where the eventual decrease of the peak was related to inherited “crystalline” characteristics of the material due to the high graphene content [2].

O. Romantsova gratefully acknowledges the support from the Visegrad Fellowship under the International Visegrad Fund in 2024.

[1] D. E. Hurova, S. V. Cherednichenko, N. A. Aksenova, N. A. Vinnikov, A. V. Dolbin, and N. N. Galtsov, Low Temperature Physics, 50, 2, 177 (2024). https://doi.org/10.1063/10.0024329.
[2] Z. E. Nataj, Y. Xu, D. Wright, J. O. Brown, J. Garg, X. Chen, F. Kargar & A. A. Balandin, Nature Communications, 14, 3190 (2023). https://doi.org/10.1038/s41467-023-38508-3.

NANOPHYSICS AND NANOTECHNOLOGIES

Rate-equation approach for a driven two-electron four-level double-quantum dot

M. P. Liul[1,2], A. I. Ryzhov[1,2], S. N. Shevchenko[1]

[1] *B.Verkin Institute for Low Temperature Physics and Engineering of NAS of Ukraine, 47 Nauky Ave., Kharkiv, 61103, Ukraine*
[2] *Theoretical Quantum Physics Laboratory, Cluster for Pioneering Research, RIKEN, Wakoshi, Saitama 351-0198, Japan*

In the research, a driven two-electron four-level double-quantum dot (DQD) tunnel coupled to a fermionic sea is theoretically described by applying the rate-equation formalism [1]. The main advantage of this approach is its relative simplicity, compared to other methods [2]. The solution of the corresponding system of rate-equations is probabilities to occupy a given energy level of the DQD. The system was experimentally studied [3], so one can compare the obtained dependencies with the experimental ones. The DQD is driven by a strong excitation signal, therefore it shows Landau–Zener–Stuckelberg–Majorana interferometry patterns. Particularly, the experimental interferogram shows four different regimes: single-passage, double-passage, multi-passage, incoherent one. Figure 1 shows the results of theoretical calculations: dependence of the parametric capacitance C of the DQD on the excitation field amplitude A and the energy detuning ε. The theoretical picture obtained by using the considered formalism shows the same interferometry regimes as the experimental one: single-passage (yellow triangle), double-passage (green circle), multi-passage (red star), and incoherent one (blue star). The operation regime depends on the excitation signal parameters, so one can achieve the necessary quantum state most efficiently by adjusting such parameters. So, obtained results can provide useful information about characterizing, initializing, and controlling quantum systems states.

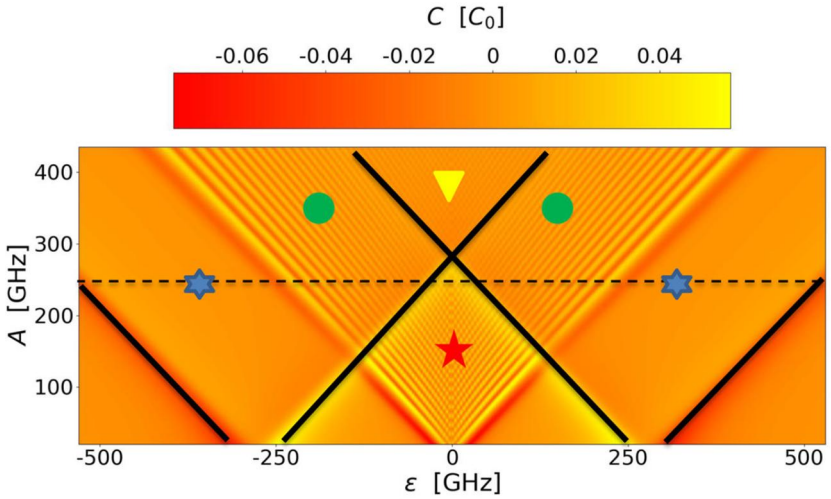

Fig. 1. Parametric capacitance C of the DQD as a function of the excitation field amplitude A and the energy detuning ε. This value is calculated in units of C_0. The results are presented in [1].

Acknowledgements: M. P. L. was partially supported by the grant from the National Academy of Sciences of Ukraine for research works of young scientists (0123U103073). A. I. R. was supported by the RIKEN International Program Associates (IPA).

[1] M.P. Liul, et al., Eur. Phys. J.: Spec. Top. **223**, 3227 (2023).
[2] M.P. Liul, S.N. Shevchenko, Low Temp. Phys. **49**, 102–108 (2023).
[3] A. Chatterjee, et al., Phys. Rev. B **97**, 045405 (2018).

Selective uptake and desorption of carbon dioxide in carbon honeycombs

D. G. Diachenko, N. V. Krainyukova

B. Verkin Institute for Low Temperature Physics and Engineering of NAS of Ukraine,
47 Nauky Ave., Kharkiv, 61103, Ukraine
e-mail: dyachenko@ilt.kharkov.ua

Amidst growing environmental concerns, carbon honeycombs (CHs), built from graphene ribbons forming the 3D architecture, offer a novel solution for carbon dioxide (CO2) capture and storage, showing superior uptake and desorption capabilities [1-3]. Through high-energy electron diffraction and advanced structural analysis, which includes various structural modeling [3], this study explores CO2 sorption in CH matrices at low and elevated temperatures, highlighting a strong correlation between the sizes of the CH channels and the temperatures of gas release (Fig. 1).

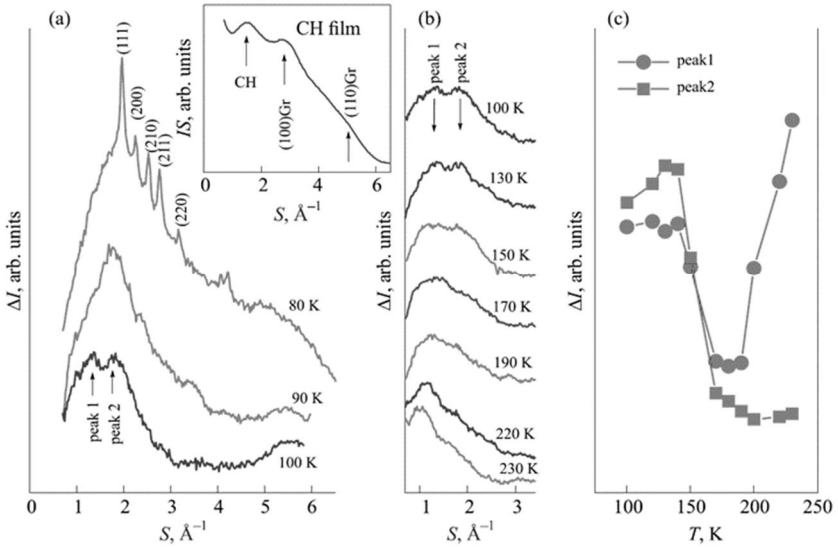

Fig. 1. Electron diffraction intensities *I* on the scattering wave vector *S* from carbon dioxide absorbed in CH matrices and warmed up to 230 K (a, b). The diffraction curve for the CH substrate (see inset) is subtracted. The maximal intensities of two peaks ascribed to sorbed CO_2 in the different CH channels are shown vs temperature T in Fig. 1c.

In the thinnest channels of the structures A2 and C0 [3] carbon dioxide can be kept even at temperatures about three times higher as compared with the CO_2 sublimation from flat solid surfaces in vacuum, whereas from wider channels gas release occurs at much lower temperatures. Since typical vacuum conditions in our experiment reduce the condensation temperatures of classical gases by ~3 times, we can expect the same capturing mechanism at ambient pressures at about room temperatures. This breakthrough presents new pathways for reducing atmospheric CO_2 and leveraging it in sustainable energy solutions.

[1] N.V. Krainyukova and E.N. Zubarev, Phys. Rev. Lett. 116, 055501 (2016). https://doi.org/10.1103/PhysRevLett.116.055501
[4] N.V. Krainyukova, B. Kuchta, L. Firlej, and P. Pfeifer, Low Temp. Phys. 46, 219 (2020). https://doi.org/10.1063/10.0000705
[3] D. G. Diachenko and N. V. Krainyukova, Low Temp. Phys. 48, 232 (2022). https://doi.org/10.1063/10.0009542

Aluminum uptake in carbon honeycomb

M. A. Kabanenko, D. G. Diachenko, N. V. Krainyukova

B. Verkin Institute for Low Temperature Physics and Engineering of NAS of Ukraine,
47 Nauky Ave., Kharkiv, 61103, Ukraine
e-mail: kabanenko@ilt.kharkov.ua

In quest of possible sorption of aluminum in a novel structure - carbon honeycomb (CH) [1] we studied Al films deposited onto appropriate carbon substrates applying high energy electron diffraction at elevated temperatures. But in contrast with noble gasses and CO_2 only physically sorbed in carbon honeycomb and explored previously [1,2] we can expect in the case of aluminum that physical sorption can precede the formation of chemical compounds.

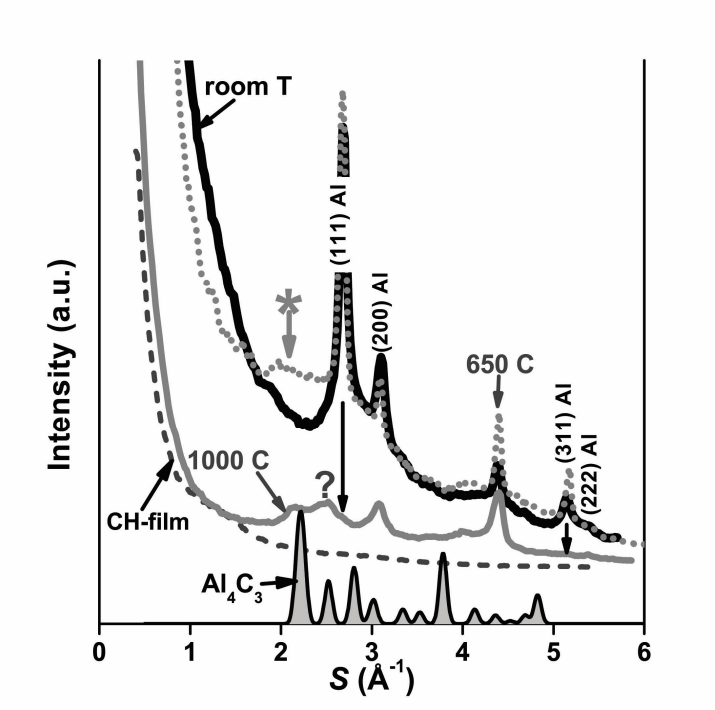

The carbon honeycomb films were prepared by carbon sublimation in the vacuum from thinned graphite rods heated by electric current and further deposited onto a room-temperature polycrystalline NaCl substrate [1-3]. Such carbon films in our experiment were covered by thick aluminum films produced by Al sublimation from a crucible and deposition in a vacuum. Further, we studied either such sandwiches as prepared or investigated the films, which were heated in two steps up to ~650 C and then to 1000 C. The films were put on the holder inside the high energy electron diffraction setup EMR-100.

At room temperature *T* we can see only a superposition of CH (dash line) and thick Al films (black line). At elevated temperatures up to ~650 C (close to the melting point of Al) the Al film contribution is still large but a distinctly seen wing marked by a star at smaller angles for the (111) Al peak appears and can be presumably associated with physically sorbed aluminum. At further heating up to ~1000 C Al films mostly sublimate in vacuum and form a texture reducing the peak (111), but a wing formed at lower 650 C becomes even clearer splitting in the former peak (marked by a star) and a new one (with a sign "?"). To elucidate if these new structural features are associated with fragmentary Al filling the channels of carbon honeycomb or there exists the possibility of the formation of aluminum compounds like carbide Al_4C_3 we built the models for both cases and compared them with experimental diffraction curves. The diffraction pattern of Al_4C_3 is also shown in the lower part of the figure.

Our findings open many prospects for potential applications in making composites based on CH filled with metallic species with tunable properties such as strength, flexibility etc.

[1] N.V. Krainyukova and E.N. Zubarev, Phys. Rev. Lett. 116, 055501 (2016). https://doi.org/10.1103/PhysRevLett.116.055501
[2] N.V. Krainyukova, B. Kuchta, L. Firlej, and P. Pfeifer, Low Temp. Phys. 46, 219 (2020). https://doi.org/10.1063/10.0000705
[3] D.G. Diachenko and N.V. Krainyukova, Low Temp. Phys. 48, 232 (2022). https://doi.org/10.1063/10.0009542

Low-temperature ultrasonic investigation of severe deformed high-purity titanium

V. S. Klochko, A. V. Korniiets, V. I. Sokolenko, V. I. Spitsyna, M. A. Shulgin, I. F. Kislyak, I. V. Kolodiy, O. O. Kondratov, T. M. Tikhonovska

National Scientific Center "Kharkov Institute of Physics and Technology" of NAS of Ukraine, 1 Academichna St., UA-61108 Kharkiv, Ukraine
e-mail: korniets@kipt.kharkov.ua

Titanium and titanium-based alloys are actively being used in the industry and medicine. High-purity titanium is an excellent material for medical implants according to criteria such as biocompatibility, corrosion resistance, hypoallergenicity, and absence of toxic impurities. It is known that the high level of metals mechanical properties is achieved by creating a nanostructure using the severe plastic deformation methods. The technology of deposition-extrusion and extrusion at cryogenic temperatures were used to create nanostructured titanium in this work. Severe plastic deformation is known to generate a high dislocation density and to form a structural state of high-energy non-equilibrium grain boundaries with anomalously accelerated grain-boundary diffusion, at least for several hours after deformation. Non-equilibrium grain boundaries make the main contribution to diffusion phenomena during recovery and recrystallization [1].

In this regard, this work aimed to detect a possible transformation of the defect structure of severe deformed titanium after aging at room temperature.

The researches were made on cylindrical (Ø6.5 mm, length 6.6 mm) samples of nanostructured titanium. The starting material was iodide titanium with the impurities content O - 0.01, N - 0.01, C - 0.01, Si - 0.009, Fe - 0.005, Ni - 0.005, Mg - 0.004, Mn - 0.004 , Al - 0.005, Cr - 0.005 (wt%). The starting material was subjected to double re-melting using electron beam melting in a high ($1.3\cdot10^{-4}$ Pa) vacuum. The hardness of the resulting titanium ingot was HB≈1.13 GPa. The electrical resistance ratio was R_{293}/R_{77}=9.6.

Severe plastic deformation of titanium ingot was carried out using upsetting extrusion at 523, 648, and 703 K temperatures. The value of true deformation was ~1.3. The deformed material was further subjected to extrusion by 52% in liquid nitrogen. According to structural studies, the average grain size of fragmented titanium was ~150 nm, while the feature of grain boundary regions characteristic of nano-sized materials was noted, due to the high density of structural defects. Axial texture {10.0}<10.0> was noted in all samples. The further aging of severely deformed material at room temperature covered a period of time up to a year.

Low-temperature (77-300 K) ultrasonic investigations were performed using a pulsed phase-sensitive method. Excitation and detection of ultrasonic oscillations was carried out using the broadband (±2 MHz) lithium niobate piezotransducers with a natural resonant frequency of 50 MHz. Acoustic contact was achieved with silicone oil. The silicone oil effect was not taken into account. Measurements were performed in the amplitude-independent region of internal friction during heating at a heating rate of 40 K/h. Both the velocity (V_L) and the change in attenuation ($\Delta\alpha_L$) of longitudinal ultrasound were measured simultaneously.

As a result of ultrasonic investigations, characteristic deflections on $V_L(T)$ and three peaks on $\Delta\alpha_L(T)$ at 125 (P_1), 175 (P_2), and 275 K (P_3) temperatures were revealed. It is suggested that these anomalies are caused by relaxation resonance of the Bordoni (P_1, P_2) and Hasiguti (P_3) type. During aging at room temperature, peaks P_1 and P_2 decreased, and peak P_3 shifted towards low temperatures. At the same time, the steepness of the inclination of $V_L(T)$ temperature dependences was reduced as a result of the intensification of the recovery processes in non-equilibrium grain boundaries. The results of the studies are discussed on the basis of the non-equilibrium grain boundaries theory where the non-equilibrium degree is the grain boundaries free volume.

[1] A.V. Norhin, JETP Letters, 38(13), 71 (2012).

Modification of transmission gaps by an optical field in a molecular field-effect transistor

V.O. Leonov, E.G. Petrov, Ye.V. Shevchenko

Bogolyubov Institute for Theoretical Physics of NAS of Ukraine,
14-b Metrolohichna str. Kyiv, 03143, Ukraine
e-mail: leogluck@gmail.com

In a molecular transistor, its current-voltage characteristics are controlled by the gate voltage V_G. This voltage affects the position of the molecular orbitals, bringing the orbital energy levels into resonance with the Fermi levels of the electrodes or shifting the orbital levels away from resonance with the Fermi levels. The conditions under which resonance occurs, and thus electron transport through the molecular transistor becomes most efficient, is given by equation [1,2].

$$V_b = \frac{k_a \Delta E_{aj}^{(0)} + |e| V_G}{|e|(d_{r,2} - h_c)},$$

where V_b and V_G are the bias and gate voltages, respectively, and $\Delta E_{aj}^{(0)}$ is the basic transmission gap for the charge neutral state of the molecule and its cationic ($a = +$, $k_+ = +1$) or anionic ($a = -$, $k_- = -1$) forms. This condition defines a diamond, the edges of which indicate at which pair of voltages V_b and V_G the current-voltage characteristics of the molecular transistor experience identical jumps. In a molecular field-effect transistor, a molecule can absorb or emit a quantum of light, thereby matching the energy of the molecule with the resonant transfer of an electron through the molecule. We showed that in this case the resonance conditions now look like

$$V_b = \frac{k_a \Delta E_{aj}^{(0)} + |e| V_G + E_{ph}}{|e|(d_{r,2} - h_c)},$$

where $E_{ph} = \pm \hbar\omega$ is the photon energy at the frequency ω of intramolecular optical transition.

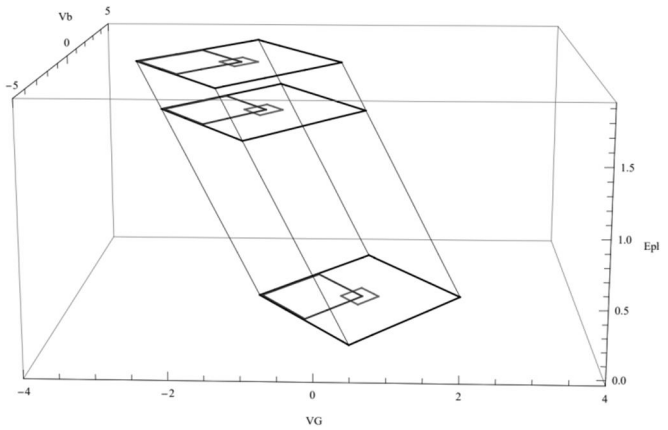

The figure shows an example of a parallelepiped, the surface of which corresponds to those V_b, V_G and E_{ph} values, resonant transmission through a molecular field-effect transistor is possible. The planes correspond to diamonds, which are realized at fixed photon energy E_{ph}.

[1] E.G. Petrov, V.V. Gorbach, A.V. Ragulya, A. Lyubchik. and S. Lyubchik, J. Chem. Phys. 153, 084105, 1-15 (2020).
[2] E.G.Petrov and V.I. Teslenko, Low Temp. Phys. (Fiz. Nizk. Temper.) 48, 1175-1186 (2022).

Interpolation expressions for dependencies of heat transfer parameters on the boundary diffusivity factor in nanoribbons

J. Amrit[1], K. Nemchenko[2], Ye. Nemchenko, S. Rogova[2], M. Spotar[2], T. Vikhtinskaya[2]

[1] LISN, Université Paris-Saclay, CNRS, 91405, Orsay, France
[2] V. N. Karazin Kharkiv National University, 61022, Kharkiv, Ukraine
e-mail: nemchenko@karazin.ua

In this report we analyze the features of heat transfer in nanoribbons of arbitrary size depending on the degree of phonon boundary scattering diffusivity. We start from the numerical solutions of the system of integral equations for the distribution function of incident phonons:

$$F_{inc}(z,\varphi) = g_h(z,\varphi) + F_{ref}(z - W\mathrm{ctg}\varphi, \varphi)\Theta(L - z + W\mathrm{ctg}\varphi)\Theta(z - W\mathrm{ctg}\varphi) \quad (1)$$

and the distribution function of reflected phonons at a definite point on the conductor boundary:

$$F_{ref}(z,\varphi) = pF_{inc}(z,\varphi) + \tfrac{1}{2}(1-p)\int_0^{\pi} F_{inc}(z,\tilde{\varphi})\sin\tilde{\varphi}\,d\tilde{\varphi}\,. \quad (2)$$

The coordinate axis z is directed along the axis of the conductor, the φ is the angle between the direction of motion of the phonon and this axis, Θ is the step-function, W is the width, and L is the length of the nanoribbon. The value p determines the degree of diffusivity during boundary reflection and is equal to 1 for completely mirror scattering and 0 for purely diffuse scattering [1, 2]. The function $g(z, \varphi)$ describes the flow of phonons that arrive at a given point on the boundary directly from the heater.

This work presents the results of a numerical solution conducted for ratios of the width to length of the nanoribbon ranging from 10 to 0.01, and for values of the degree of specularity p varying from 0 to 1. The resulting solutions describe the temperature profile along the conductor, the dependence of the heat flow on the parameters of the problem, and the influence of the degree of specularity on the value of the thermal conductivity coefficient.

The results obtained made it possible to derive simple analytical interpolation dependencies for the temperature profile, heat flow and thermal conductivity coefficient. These functions describe the dependence of these parameters on the values of p, and relate to each other the known analytical results [3] for limiting cases for the purely diffuse scattering [4] and purely specular reflection.

The derived expressions provide not only explicit analytical dependences on the parameters of the problem, but also make it possible to describe complex phonon systems with different polarizations and at different temperatures without carrying out cumbersome numerical solutions.

This work was supported by the project “Remote Research Grants for Ukrainian Researchers” that has received funding through the EURIZON project, which is funded by the European Union under grant agreement No.871072.

[1] H.B.G. Casimir, Physica 5, 495 (1938).https://doi.org/10.1016/S0031-8914(38)80162-24]
[2] J. M. Ziman, *Electrons and Phonons: The Theory of Transport Phenomena in Solids* (Oxford University Press, Oxford, 2001).
[3] J. Amrit, T. Medintseva, Ye. Nemchenko, K. Nemchenko, M. Spotar, S. Rogova, T. Vikhtinskaya, Low Temp. Phys. **49**, 961 (2023). https://doi.org/10.1063/10.0020163
[4] J.Amrit,K. Nemchenko,T.Vikhtinskaya, J. Appl. Phys. 129,085105(2021). https://doi.org/10.1063/5.0036935.

Heat transfer in 3D samples of definite cross-section at diffusive boundary scattering

J. Amrit[1], K. Nemchenko[2], Ye. Nemchenko[2], S. Rogova[2], T. Vikhtinskaya[2]

[1] LISN, Université Paris-Saclay, CNRS, 91405, Orsay, France
[2] V. N. Karazin Kharkiv National University, 61022, Kharkiv, Ukraine
e-mail : egor.nemchenko@karazin.ua

This report discusses the results of a study of thermal conductivity in three-dimensional dielectric thermal conductors in the ballistic regime of phonon propagation. The problem is considered in the radiative approximation of phonon emission by a heater at a given temperature; and the interaction with the walls is assumed to be completely diffusive. The main goal of the study is to determine the temperature profile along the conductor, the features of its formation, and the conditions for the deviation of the temperature dependence from the linear profile. The heat flow and thermal conductivity coefficient are also determined, and the difference between the obtained results and another generally accepted formulation of the problem, when a linear temperature gradient is created by external sources [1], is discussed. The problem is considered for several cases of conductor cross-section and compared with known results for a cylindrical conductor [2, 3].

The main idea of the method follows the work of the authors for nanoribbons [4] and is reduced to a numerical and approximate analytical solution [5] of the generalized integral equation for the temperature profile $t(\mathbf{r})$:

$$t(\mathbf{r}) = t_{out}(\mathbf{r}) + \hat{G}(\mathbf{r},\mathbf{r}\phi t(\mathbf{r}\phi \qquad (1)$$

Here $\mathbf{r}$ is the radius-vector of a point on the boundary of the conductor, $g(\mathbf{r})$ describes the temperature profile created at the boundary by phonons emitted by external sources, for example, a heater. The integral operator $\hat{G}(\mathbf{r},\mathbf{r}\phi$ describes the contribution of phonons that arrives at a given point $\mathbf{r}$ after diffuse reflection from a point $\mathbf{r}\phi$on the boundary.

The solution to this problem makes it possible to determine the thermal properties of conductors with an arbitrary ratio between their length and transverse dimensions, as well as with different cross-sectional shapes of the conductor. A comparison is made with experimental results and with the results of numerical calculations of the authors from previous works.

This work was supported by the project “Remote Research Grants for Ukrainian Researchers” that has received funding through the EURIZON project, which is funded by the European Union under grant agreement No.871072.

[1] H.B.G. Casimir, Physica 5, 495 (1938).https://doi.org/10.1016/S0031-8914(38)80162-2
[2] T. Klitsner, J. E. VanCleve, H. E. Fischer, and R. O. Pohl, Phys. Rev. B 38, 7576 (1988). https://doi.org/10.1103/PhysRevB.38.7576
[3] M. Perlmutter, R. Siegel, J. Heat Transfer, 85, 55-62 (1963). https://doi.org/10.1115/1.3686010.
[4] J.Amrit, K. Nemchenko, T.Vikhtinskaya, J. Appl. Phys. 129,085105(2021). https://doi.org/10.1063/5.0036935.
[5] J. Amrit, T. Medintseva, Ye. Nemchenko, K. Nemchenko, M. Spotar, S. Rogova, T. Vikhtinskaya, Low Temp. Phys. **49**, 961 (2023). https://doi.org/10.1063/10.0020163.

Iterative analytical solution to the problem of heat flow in a two-dimensional conductor

J. Amrit[1], K. Nemchenko[2], M. Spotar[2], T. Vikhtinskaya[2]

[1] LISN, Université Paris-Saclay, CNRS, 91405, Orsay, France
[2] V.N.Karazin Kharkiv National University, 61022, Kharkiv, Ukraine
e-mail: xa12283354@student.karazin.ua

In the report, we present an iterative analytical approach for solving the integral equation that describes the temperature profile of heat flow in two-dimensional conductor [1] :

$$t(z)=\frac{1}{2}\left[1-\frac{z}{\sqrt{w^2+z^2}}\right]+\frac{1}{2w}\int_0^1 dz_1\,\frac{1}{\left[1+(z-z_1)^2\right]^{3/2}}t(z_1), \tag{1}$$

where $w = W/L$ is the ratio of the width W to the length L of the conductor, $t(z)$ is the normalized temperature and z is the normalized coordinate along the conductor. Equations similar to this arose both in problems on the flow of rarefied gases through tubes [2] and in problems on radiative heat transfer by phonons in the ballistic regime [3, 4]. In the proposed approach, we begin to solve the problem from the linear dependence [2, 5] for temperature

$$t^{(1)}(z)=\left[1+a(w)(1-2z)\right]/2, \tag{2}$$

where $a(w)=\left\{1+4w\left[1+(1+w)/\sqrt{1+w^2}\right]^{-1}\right\}^{-1}$. The parameter $a(w)$ is found from the fact that dependence (2) satisfies the original equation (1) at the ends of the sample. This approximate linear solution (2) describes the temperature profile quite accurately, but it can be improved using further iterations in the integral equation (1).

The iteration method is quite well known and consists in the fact that the result of the next step is determined by relation (1), in which the result of the previous iteration is substituted on the right side. This iterative procedure is most often used for numerical solutions of integral equations of type (1). In this work, we propose to use this procedure to obtain a solution in an analytical form. For example, the second approximation for the temperature profile will be

$$t^{(2)}(z)=\frac{1}{2}\left[1-\frac{z}{\sqrt{w^2+z^2}}\right]+\frac{1}{2w}\int_0^1 dz_1\,\frac{1}{\left[1+(z-z_1)^2\right]^{3/2}}t^{(1)}(z_1) \tag{3}$$

A simple form of the first linear approximation (2) allows one to carry out integrations in (3) and thereby obtain an explicit analytical dependence for a more accurate, second approximation for desired solution of Eq. (1):

$$t^{(2)}(z)=\frac{1}{2}\left[1-\frac{z}{2\sqrt{w^2+z^2}}+\frac{1-z}{2\left[w^2+(1-z)^2\right]^{1/2}}\right]+\frac{a(w)}{2}\left[\frac{z}{2\left[w^2+z^2\right]^{3/2}}+\frac{1-z}{2\left[w^2+(1-z)^2\right]^{1/2}}\right](1-2z)-\left[\frac{w^2}{\left[w^2+z^2\right]^{3/2}}-\frac{w^2}{\left[w^2+(1-z)^2\right]^{3/2}}\right]. \tag{4}$$

The resulting solution conveys the features of the exact solution to equation (1) with a much higher accuracy, such that it describes small deviations from the linear solution (2). If necessary, the iterative procedure can be repeated the required number of times. It is worth noting, that this method, in particular, allows us to get rid of the shortcomings of methods that use Taylor series expansions near the middle of the segment [4], which leads to asymptotic series.

This work was supported by the project “Remote Research Grants for Ukrainian Researchers” that has received funding through the EURIZON project, which is funded by the European Union under grant agreement No.871072.

[1] J.Amrit,K. Nemchenko,T.Vikhtinskaya, J. Appl. Phys. 129,085105(2021).
[2] D. Clausing, Ann. D. Physik, 404, 961 (1932). https://doi.org/10.1002/andp.19324040804
[3] T. Klitsner, J. E. VanCleve, H. E. Fischer, and R. O. Pohl, Phys. Rev. B 38, 7576 (1988).
[4] M. Perlmutter, R. Siegel, J. Heat Transfer, 85, 55-62 (1963). https://doi.org/10.1115/1.3686010.
[5] J. Amrit, T. Medintseva, Ye. Nemchenko, K. Nemchenko, M. Spotar, S. Rogova, T. Vikhtinskaya, Low Temp. Phys. **49**, 961 (2023). https://doi.org/10.1063/10.0020163.

Aluminium doped ZnO thin films

V. V. Zaika, N. K. Shvachko, I. V. Sukhenko, V. L. Karbivskyy

G. V. Kurdyumov Institute for Metal Physics of NAS of Ukraine, Kyiv, Ukraine
e-mail: zaikavladimir228@gmail.com

Recently, ZnO thin films have attracted significant attention of researchers due to their complex of unique properties, such as a wide bandgap of 3.37 eV [1], good transparency in the visible range, high exciton binding energy (60 meV) [2], cost effectiveness, and environmental safety.

In our study, ZnO thin films were prepared by radio frequency magnetron sputtering from a target of pressed ZnO powder. The aluminium doping was carried out by placing different numbers of aluminium slabs on the pressed powder target (Table 1).

Table 1: Ratio of the areas of Al and ZnO targets used to obtain AZO films.

Sample name	Slab area (cm^2)	Ratio of areas (%)
ZnO	0.0	0.00
Al05	0.5	3.98
Al10	1.0	7.96
Al25	2.5	19.89

Insignificant changes in the surface morphology of the obtained films after aluminium doping were observed. The analysis showed an increase in the maximum size of clusters with increasing aluminium concentration compared to the pure ZnO sample. The average cluster size was 35.0, 37.5, and 42.0 nm for ZnO, Al05, and Al10 samples, respectively. Also, using a scanning electron microscope, cross-sectional images of ZnO thin films showed that the films grow along the c-axis perpendicular to the substrate.

With an increase in the aluminium concentration, an increase in the transparency of the films obtained in the visible and near-infrared range was observed. Using the Tauc method [3], an enlargement of the band gap from 3.42 eV to 4.00 eV was detected. The broadening of the band gap can be explained by the fact that the states at the bottom of the conduction band are populated by free electrons from aluminium, and as a result, the optical gap increases: thus, the Moss-Berstein effect is observed [4]. On the basis of the results obtained, the films can be recommended for use as protective coatings against ultraviolet radiation, which require good transparency in the visible range.

[1] C. F. Klingshirn, B.K. Meyer, A. Waag, A. Hoffmann, J. Geurts. Zinc Oxide. Springer Series in Materials Science (2010). https://doi.org/10.1007/978-3-642-10577-7
[2] M. Dvorak, S.-H. Wei, Z. Wu. Origin of the Variation of Exciton Binding Energy in Semiconductors. Physical Review Letters, 110(1) (2013).
https://doi.org/10.1103/physrevlett.110.016402
[3] J. Tauc, Mater. Res. Bull, 3, No.1: 37–46(1968). https://doi.org/10.1016/0025-5408(68)90023-8
[4] T.S. Moss. The Interpretation of the Properties of Indium Antimonide. 67(10), 775–782) (1954). https://doi.org/10.1088/0370-1301/67/10/306

Modeling and calibration of the electrical features of submicron p-n and p-i-n junction structures based on Si and GaAs over a broad temperature.

J. Sh. Abdullayev, I. B. Sapaev

National Research University TIIAME, st. Kori Niyazov, house 39, 100000 Tashkent, Uzbekistan
e-mail: j.sh.abdullayev6@gmail.com

The p-n junction based on silicon is the most successful structure to date. In this article, we advocate and research submicron p-n and p-i-n junction structures, which have unique features, unlike conventional p-n junction structures. The successful implementation of electrical features in p-n and p-i-n junction structures proves that they are the next generation of semiconductor devices. Silicon (Si) and Gallium arsenide (GaAs) based devices are widely used in almost all industries. Due to the high sensitivity of Si and GaAs to changes in temperature, the development of temperature-resistant devices or photodiodes is an important task. For this reason, in this paper, the effect of temperature from 250 K to 500 K on the characteristics of Si and GaAs p-n and p-i-n homojunction structure with various base the i-layer region doping concentrations (10^{13}, 10^{14}, 10^{15}, 10^{16} cm^{-3}) was studied by modeling. The influence of the i-layer thickness (in the range from 100 nm to 5 μm on the distributions of potential, electric field, and minority charge carriers was also studied. The Si and GaAs p-n and p-i-n homojunction structures were calibrated using experimental results to determine the appropriate model.

On the Energy Spectrum and Magnetic Properties of low-dimensional spin systems of complex topology

K. S. Dzhenzherova, O. S. Dzhenzherov, E. V. Ezerskaya, V. O. Kovalenko

V. N. Karazin Kharkiv National University, 4 Svoboda Sq, Kharkiv, 61022, Ukraine
e-mail: kovalenko2020.8954539@student.karazin.ua

Low dimensional effective spin models of nanomagnets are permanently attracting big interest of the investigators due to their interesting physics and possibly applications in nanoelectronics. Some of these models can be solved exactly. This gives the very important opportunities for the verification of different approximate methods in quantum theory of low-dimensional magnetism [1].

We propose two exactly solvable quantum models based on finite spin-1/2 XX chains with additional Ising spin-S, connecting XX chains at fixed lattice sites, describing by such Hamiltonians

$$\hat{\mathbf{H}} = -g_1\mu_B H\sum_{n=1}^{N_1} S_{1,n}^z - J_1\sum_{n=1}^{N_1-1}\left(S_{1,n}^x S_{1,n+1}^x + S_{1,n}^y S_{1,n+1}^y\right) - g_2\mu_B H\sum_{n=1}^{N_2} S_{2,n}^z - J_2\sum_{n=1}^{N_2-1}\left(S_{2,n}^x S_{2,n+1}^x + S_{2,n}^y S_{2,n+1}^y\right) - \\ - g_0\mu_B H\hat{S}_0^z - \left[J_{01}\left(S_{1,1}^z + S_{1,N_1}^z\right) + J_{02}\left(S_{2,1}^z + S_{2,N_2}^z\right)\right]\hat{S}_0^z \qquad (1)$$

$$\hat{\mathbf{H}} = -g_1\mu_B H\sum_{n=1}^{N_1} S_{1,n}^z - J_1\sum_{n=1}^{N_1-1}\left(S_{1,n}^x S_{1,n+1}^x + S_{1,n}^y S_{1,n+1}^y\right) - g_2\mu_B H\sum_{n=1}^{N} S_{2,n}^z - J_2\sum_{n=1}^{N_2-1}\left(S_{2,n}^x S_{2,n+1}^x + S_{2,n}^y S_{2,n+1}^y\right) - \\ - g_0\mu_B H\hat{S}_{n_1}^z - g_0\mu_B H\hat{S}_{n_2}^z - J_0\hat{S}_{n_1}^z\left(S_{1,n_1}^z + S_{2,1}^z\right) - J_0\hat{S}_{n_2}^z\left(S_{1,n_2}^z + S_{2,N_2}^z\right). \qquad (2)$$

The Hamiltonian (1) describes two finite XX chains forming two coupled "rings" connected via Ising spin-S. The Hamiltonian (2) corresponds to finite open XX chain combined with other XX chain by additional Ising spins at intermediate lattice sites numbered $(1,n_1)$, $(1,n_2)$. Z-projections of Ising additional spins commute with models Hamiltonians and are the good quantum numbers. This property permits us to consider Hamiltonians (1) and (2), as the Hamiltonians of the finite XX-chain with an effective impurity spin S = 1/2 at some lattice sites.

We derive exact dispersion equations for the stationary states with one inverted spin for all cases. These spectra consist of two quasi-continuous zones and several localized impurity levels. We obtain and analyzed the analytical inequalities for the values of critical parameters of the models describing the appearance of local energy impurity levels above and below the quasi-continuous zones.

Field and temperature dependencies of the main thermodynamic characteristics of the models were investigated numerically. It is shown that the appearance of localized levels near impurities may effects significantly on the thermodynamics properties at low temperatures, leading to additional features in the field and temperature dependences of the main thermodynamic characteristics. For example, the field dependence of the average z-projection of total spin and the field dependence magnetization at zero temperature should have finite jumps associated with both the quasi-continuous spectrum and impurity levels. Remnants of these jumps are clearly visible at very low temperatures.

EVE acknowledges support by IEEE via "Magnetism in Ukraine Initiative" (STCU project No. 9918).

[1] A. A. Zvyagin, Quantum Theory of One-Dimensional Spin Systems (Cambridge Scientific Publishers, Cambridge, 2010).

Influence of the defects on the behavior of the heat capacity of MWCNTs with Ø9.4 nm

M. I. Bagatskii[1], V. V. Sumarokov[1], M. S. Barabashko[1], A. I. Krivchikov[1], A. Jeżowski[2], D. Szewczyk[2,3]

[1] B. Verkin Institute for Low Temperature Physics and Engineering of NAS of Ukraine, 47 Nauky Ave., Kharkiv, 61103, Ukraine
[2] W. Trzebiatowski Institute for Low Temperatures and Structure Research, Polish Academy of Sciences, P.O. Box 1410, 50-950 Wroclaw, Poland
[3] Low Temperature Laboratory, Condensed Matter Physics Department, Universidad Autónoma de Madrid, Madrid, Spain
e-mail: msbarabashko@gmail.com

The influence of defects and geometrical sizes on the heat capacity of the multi-walled carbon nanotubes (MWCNTs) with an average outer diameter of Ø9.4 nm was studied by the relaxation method using PPMS in the temperature range from 1.8 to 275 K. The initial MWCNTs were obtained by the CVD method. The length of MWCNTs and parameters of defects (number and types) in MWCNTs were changed: 1) grinding of the initial nanotubes in a ball mill; 2) the initial nanotubes were first oxidized and then milled. The figure shows low-temperature experimental heat capacity curves of ground (S_m), ground-oxidized (S_{m-o}) MWCNTs with outer diameters of Ø9.4 nm, as well as, for comparison, original nanotubes (S_i), bundles of SWNCTs (Ø1.1 nm) and graphite. The analysis of the low-temperature behavior of the heat capacity of carbon materials below 3 K was carried out under the assumption that C(T) is determined primarily by phonons with sufficiently long wavelengths (deformation waves). The specific heat C(T), described by the equation $C(T) = A*T + B*T^3$, are represented by straight lines in the Figure. The coefficients A and B were calculated and analyzed. The decrease in the length of nanotubes and the appearance of defects as a result of both grinding and oxidation with subsequent grinding lead to an increase in heat capacity in the low-temperature region.

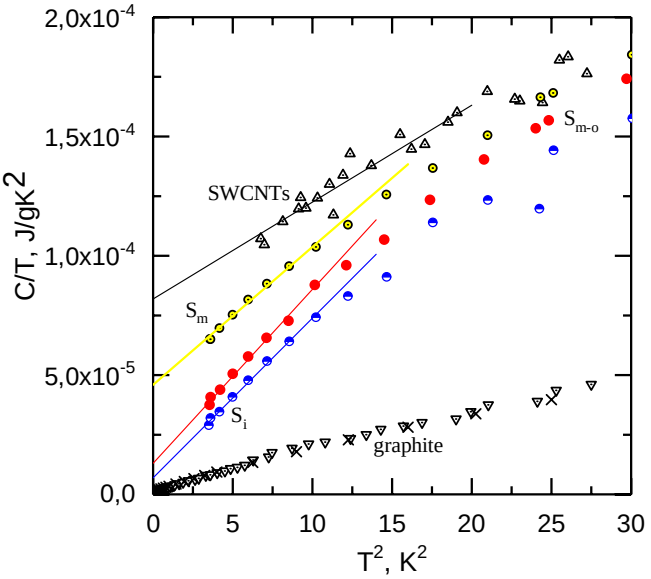

Fig.1. Low-temperature specific heat in C/T vs T^2: initial (S_i), milled (S_m), milled-oxidized (S_{m-o}) MWCNTs with outer diameters of Ø9.4 nm, bundles of SWNCTs (Ø1.1 nm) and graphite.

Acknowledgments: This work has been supported by the National Research Foundation of Ukraine

Raman, UV-Vis, MS and IR Characterization of Molecular-Colloidal Solution of Hydrated Fullerenes C_{60} Obtained Using Vacuum-Sublimation Cryogenic Deposition Method

R. M. Basnukaeva[1], S. V. Cherednichenko[1], G. V. Andrievsky[2], N. A. Vinnikov[1], A. V. Dolbin[1], M. V. Kosevich[1], V. S. Shelkovsky[1], L. M. Buravtseva[1], G. I. Dovbeshko[3,4], O. P. Gnatyuk[3], O. Bezkrovnyi[4], M. Ptak[4], M. Chaika[4], P. O. Kuzema[5]

[1] B. Verkin Institute for Low Temperature Physics and Engineering of NAS of Ukraine, 47 Nauky Ave., Kharkiv, 61103, Ukraine
[2] Institute of Physiologically Active Compounds LLC, Nauky Ave., 58, Kharkiv, Ukraine,
[3] Institute of Physics of the National Academy of Sciences of Ukraine, Nauky Ave., 46, Kiev 03028, Ukraine
[4] Institute of Low Temperatures and structural Research PAS, Wroclaw, 50-422, Poland
[5] Chuiko Institute of Surface Chemistry of the National Academy of Sciences of Ukraine, 17, General Naumov str., Kyiv, 03164, Ukraine
e-mail: basnukaeva@ilt.kharkov.ua

In this study, we introduce a novel approach using the vacuum-sublimation cryogenic deposition (VS-CD) method to produce fullerene water colloidal solution (FWCS). The melting process of the solid phase of the mixture obtained by combined condensation of C_{60} fullerene and water vapors onto a surface cooled with liquid nitrogen results in the formation of a stable colloidal solution. The results of characterization of FWCS via Raman, IR, and UV-Vis spectroscopy with a comparison with literature data on hydrated fullerenes, revealed the presence of $C_{60}@\{H_2O\}_n$ complexes of hydrated C_{60} fullerene within the solution. Furthermore, transmission electron microscopy revealed predominantly small C_{60} clusters from 2 to 5 nm size within the VS-CD-produced material. Mass spectrometry with laser desorption/ionization further confirmed the existence of pure fullerene C_{60} while ruling out any transformation. Our analysis reveals the close similarity between the stable $C_{60}@\{H_2O\}_n$ complexes generated by VS-CD and the previously known highly hydrophilic hydrated fullerene obtained by ultrasonication method, highlighting the potential of VS-CD as a promising technique in the synthesis of colloidal fullerene solutions.

Electron excitation energy transfer in mixed krypton-xenon clusters

Yu. S. Doronin, A. A. Tkachenko, V. L. Vakula, G. V. Kamarchuk, O. G. Danylchenko and O. P. Konotop

B. Verkin Institute for Low Temperature Physics and Engineering of NAS of Ukraine, 47 Nauky Ave., Kharkiv, 61103, Ukraine
e-mail: doronin@ilt.kharkov.ua

We present the first experimental study of the energy transfer of electronic excitations in heterogeneous krypton-xenon clusters.

Two-component Kr-Xe clusters were formed in a supersonic gas jet flowing into a vacuum. The measurements were made for clusters with average sizes of 2000-4000 at/cl at two concentrations of xenon impurity in the working gas mixture: 1% and 2% [1]. At a distance of 30 mm from the nozzle, the cluster jet was excited by electrons with an energy of 1 keV and a current of 20 mA. Cathodoluminescence spectra were recorded in the VUV range, in the wavelength interval of 100 to 200 nm.

Earlier studies of heterogeneous Ar-Kr clusters [2] revealed that the processes of energy transfer of electronic excitations in two-component clusters significantly depend on the cluster size, structure, number of impurity atoms, and their location within the cluster.

The registered VUV spectra of Kr-Xe clusters, despite the low initial concentration of xenon impurity, have no trace of the molecular bands of krypton Kr_2^* and $(Kr_4^+)^*$, suggesting a high efficiency of the energy transfer process of electronic excitations in clusters from krypton centres to xenon ones. The presence of an exciplex band $(Kr\text{-}Xe)^*$ in the spectrum at a krypton concentration of 1% indicates that mainly two-component Kr-Xe clusters are formed during the heteronucleation process in the supersonic jet.

An analysis of the features of energy transfer of electronic excitations in two-component Kr-Xe clusters is carried out, presenting a general scheme of occupation and relaxation of excited molecular centres and their spatial distribution within the cluster volume.

[1] O. P. Konotop, S. I. Kovalenko, O. G. Danylchenko, and V. N. Samovarov, J. Clust. Sci. 26, 863 (2015). https://doi.org/10.1007/s10876-014-0773-6
[2] Yu. S. Doronin; V. N. Samovarov; E. A. Bondarenko, Low Temp. Phys. 32, 251 (2006). https://doi.org/10.1063/1.2178482

Mechanical stability and electronic properties of heterostructures based on β-InSe/$MoSe_2$

O. I. Korolov, K. E. Glukhov, L. Yu. Kharkhalis

Institute for Physics and Chemistry of Solid State, Uzhhorod National University,
54 Voloshin Str., Uzhhorod, 88000, Ukraine
e-mail: oleh.korolov@uzhnu.edu.ua

As is known, the crystal β-InSe is characterized by its layered structure and unique electronic properties, making it quite valuable for applications in electronics and optoelectronics. On the other hand, $MoSe_2$, is also a material with a quasi-two-dimensional structure, which has a wide range of potential applications, especially in the field of semiconductor devices and photodetectors. Consequently, studying the electronic properties of the created heterostructures β-InSe/$MoSe_2$ is of interest. Particularly relevant is the question of their mechanical stability, as only mechanically stable heterostructures can open up new opportunities for the development and optimization of devices based on such materials.

In the bulk phases of β-InSe and $MoSe_2$, weak interlayer van der Waals interaction allows for different stacking sequences along the OZ direction. Accordingly, this study considered two simplest models of β-InSe/$MoSe_2$. The studied heterostructures consist of two pairs of translationally non-equivalent layers with Se-Mo-Se and Se-In-In-Se structures, which are arranged perpendicular to the hexagonal axis OZ. Both models are described by the spatial group P-3m1, which is hexagonal.

Investigations were conducted on the energy spectra, spatial distribution of valence electrons, and Mulliken charges for bulk crystals of β-InSe and $MoSe_2$, as well as for heterostructures based on them [1]. For both heterostructure models, the bandgap remains indirect, with the main extremum of the conduction band shifted to the high-symmetry K point of the Brillouin zone for hexagonal symmetry. Additionally, there is a reduction in the bandgap compared to the Eg for β-InSe and $MoSe_2$ crystals, resulting in states overlapping between the bottom of the conduction band and the top of valence band. It has been demonstrated that there is no significant difference in the formation of valence band states for the two models of the studied heterostructures.

Mechanical characteristics (elastic moduli, Young's moduli, Poisson's ratios) were calculated for bulk crystals of β-InSe and $MoSe_2$, as well as for InSe/$MoSe_2$ heterostructures. It was found that the elastic constants C_{11}, C_{12}, C_{13}, C_{33}, C_{44}, and C_{66} for both heterostructure models are nearly identical in numerical value, except for the elastic constants C_{13} and C_{44}, which characterize the bonding between the layers [1-2]. Both β-InSe/$MoSe_2$ heterostructures were determined to be mechanically stable based on the assessment of the Born criterion.

The reduced parameter of generalized anisotropy for the heterostructure β-InSe/$MoSe_2$ in one of models indicates a lower degree of property anisotropy in this heterostructure. The minimal energy and interlayer bonding also confirm the higher stability of this model.

Therefore, based on the mentioned results, we can conclude the mechanical stability and energy efficiency of the considered models of heterostructure β-InSe/MoSe2, making it promising for further research and potential applications in high-tech fields of physics.

[1] He X. The tunability of electronic and transport properties of InSe/$MoSe_2$ van der Waals heterostructure: A first-principles study /Xiao He, Jieshi Chen, Shuai Li, Meng Lin, Yajie Wang, Yi Zheng, Hao Lu// Surfaces and Interfaces.-2023.- Vol. 36.- P. 102634-11.
[2] Mouhat F. Necessary and Sufficient Elastic Stability Conditions in Various Crystal Systems/ F. Mouhat and F.-X, Coudert//Phys.Rev.B.-2014.-V.90.-P.224104-1-4.

Electronic and Sensing Properties of ZnO Nanoribbons: a DFT Analysis

M. Kovalenko, O. Bovgyra, D. Malanchuk

Ivan Franko National University of Lviv, 8, Kyrylo and Mefodiy, 79005 Lviv, Ukraine
e-mail: mariya.kovalenko@lnu.edu.ua

Gas sensing technologies are attracting increasing attention in industry and academic research due to their widespread use in industrial manufacturing, automotive, medicine, indoor air quality control, and environmental monitoring. The increased demand for susceptible, selective, low-cost, low-power, reliable, stable, and portable sensors has stimulated extensive research into developing new sensor materials. Semiconducting metal oxides have long been considered promising candidates for gas-sensing applications due to their high sensitivity, simple fabrication methods, low cost, and high compatibility with other parts and processes. As is known, when the structural dimensions are reduced to a few nanometers, the surface-to-volume ratio increases tremendously; therefore, a large active area for interaction with the gas is provided.

Zinc oxide (ZnO) is an n-type semiconductor with a wide bandgap (3.37 eV at 0 K) due to its unique optical and electronic properties, besides attracting considerable attention for potential applications such as solar cells, optoelectronic devices, nanogenerators, and catalysts, is one of the most studied sensitive materials for gas sensors. Due to their high sensitivity, stability, and low-cost advantages, ZnO nanostructures are widely used to detect gases. The synergistic combination of excellent sensing characteristics of ZnO with the potential of 1D nanostructures leads to high detection efficiency, reduced operating temperature, fast response and recovery, and improved selectivity. Therefore, in this work, we presented the study of the electronic and sensor properties of ZnO nanoribbons (ZnO_{NRs}) with armchair and zigzag edges within the density functional theory (DFT) under the adsorption of various gases (CO, CO_2, NO, NO_2).

The geometry optimization of the structure ZnO nanoribbons with width n = 8 with different edges, armchair (8a-ZnONR), and zigzag (8z-ZnO_{NR}), and the study of the electronic and sensor properties of ZnO_{NRs} were carried out within DFT. ZnO_{NR} configurations with hydrogen edge passivation were also considered. The exchange-correlation potential is described using the GGA(PBE) approximation. To evaluate the weak intermolecular interaction during gas adsorption, a semi-empirical dispersion correction for van der Waals' interaction with DFT was used according to the scheme proposed by Grimm. The Hubbard corrections method to the GGA approximation, the DFT+U method, was used to describe the structural and electronic properties accurately.

Different adsorption configurations of molecules were considered to study the sensor properties of ZnO_{NRs}, and the adsorption energy was calculated for all considered molecules' positions to establish thermodynamically stable adsorption configurations. The calculations showed that, regardless of whether the NRs are of the armchair or the zigzag edges, the most energetically favorable case is when the molecule is adsorbed only on one side of the ZnONRs.

Investigations of the electronic properties of different adsorption configurations of molecules on ZnO_{NRs} showed that the molecule's adsorption leads to a radical change in the electronic spectrum of NRs. For example, the adsorption of CO, CO_2, NO, and NO_2 molecules on zigzag nanoribbons leads to the appearance of a magnetic ground state in some configurations. Also, under the adsorption of CO and NO, the Fermi level shifts to the conduction band in some armchair nanoribbons. Meanwhile, for the adsorption of the NO2 molecule on 8a-ZnONHC-H, the electronic spectra show that nanoribbons exhibit semiconducting properties in all configurations of edge adsorption.

Thus, the adsorption of CO, CO_2, NO, and NO_2 molecules on the 8a-ZnO_{NR} and 8z-ZnO_{NR} leads to significant changes in the electronic spectrum compared to pure nanoribbons, and our results can be used for further research of such nanoribbons for possible application in sensor and spintronic devices.

Magnetotransport properties of carbon nanotubes decorated with magnetic alloys

I. Ovsiienko[1], D. Shpylka[1], D. Zaiatc[1], T. Len[1], L. Matzui[1], I. Mirzoiev[2], E. Beliayev[2]

[1] Taras Shevchenko National University of Kyiv, Departments of Physic, Volodymyrska Str., 64/13, 01601 Kyiv, Ukraine
[2] B. Verkin Institute for Low Temperature Physics and Engineering of NAS of Ukraine, 47 Nauky Ave., Kharkiv, 61103, Ukraine
e-mail: talen148@gmail.com

This work is devoted to studying the magnetoresistance of multiwalled carbon nanotubes (MWCNTs) decorated with magnetic alloys ($Fe_{80}Ni_{20}$, $Co_{93}Fe_{07}$, and $Ni_{20}Co_{80}$). The particles of a magnetic alloy of the appropriate composition were formed on the MWCNTs' surface. Magnetic particles were evenly distributed over the MWCNT surface. The particle size was 20-40 nm. The method of obtaining decorated MWCNTs, the structural and morphological state of decorated MWCNTs, and the character of metal particles' distribution on the MWCNTs surface were described in detail in [1]. For electron transport measurements, bulk specimens of rectangular parallelepiped form have been made from decorated MWCNT powder by cold pressing using polyvinyl acetate (20 % mass) as a binder. The magnetoresistance measurements were carried out in the temperature range 77 – 293 K for an external magnetic field (sweeping up to 2.5 T) applied at different angles to the direction of current flowing through the specimens.

Figure 1 presents the field dependences of transverse and longitudinal magnetoresistance $\Delta\rho/\rho(B)$ for a bulk specimen decorated with $Ni_{20}Fe_{80}$ MWCNTs at room temperature T = 293 K.

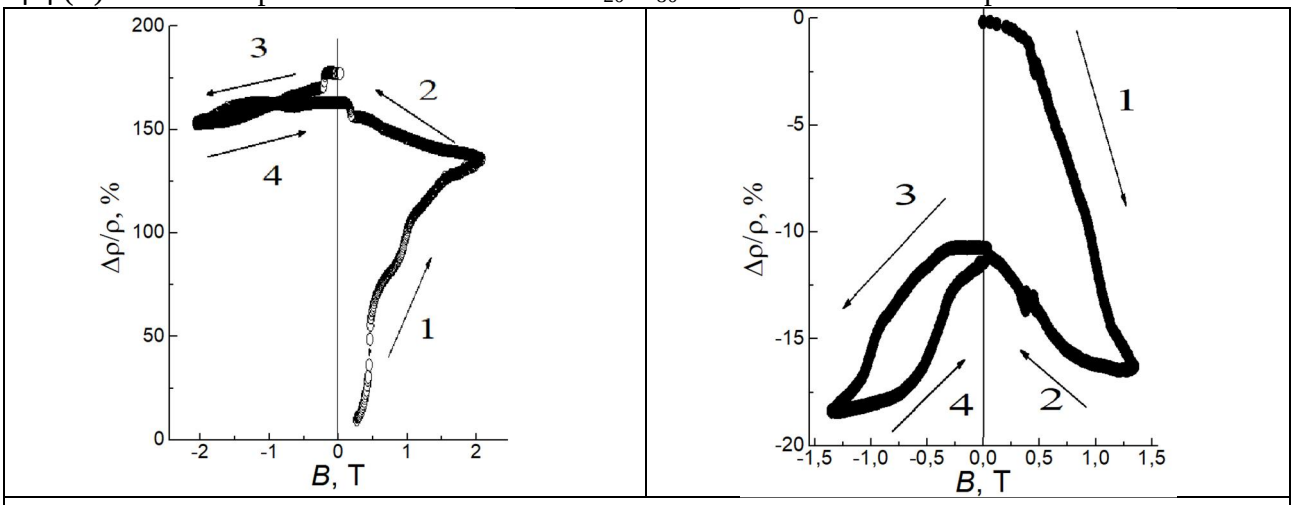

Figure 1. Dependences of transverse (a) and longitudinal (b) magnetoresistance for bulk MWCNT specimen decorated with $Ni_{20}Fe_{80}$. Arrows indicate changes in the external magnetic field.

As seen from the Figures, transverse and longitudinal magnetoresistance dependences are significantly different. For transverse magnetoresistance, there is a significant, up to 200% increase in resistance at initial magnetization, and magnetoresistance saturation is not observed in a magnetic field up to 2.3 T. For longitudinal magnetoresistance, saturation occurs already in magnetic fields of ~ 1.3 T, and pronounced hysteresis in $\Delta\rho/\rho(B)$ dependence was found. The experimental results are analyzed in terms of manifestation of the effects of giant anisotropic magnetoresistance.

[1] L. Yu. Matzui , V. V. Vovchenko , O. A. Syvolozhskyi , O. S. Yakovenko , M. O. Borovoy , O. O. Gomon , A. G. Dyachenko , O. V. Ishchenko , A. V. Vakalyuk , A. V. Bodnaruk , V. M. Kalita Mol. Cryst. Liq. Cryst. 752(1), 77 (2023). DOI: 10.1080/15421406.2022.2091275.

Reversible luminescent hydrogen peroxide sensors based on CeO_{2-x} and $CeO_{2-x}:Eu^{3+}$ nanocrystals

P. Maksimchuk[1], Ye. Neuhodov[1], K. Hubenko[1], A. Onishchenko[2], S. Yefimova[1], V. Seminko[1]

[1] Institute for Scintillation Materials NAS of Ukraine, 60 Nauky Ave., Kharkiv, 61072, Ukraine
[2] Kharkiv National University of Radio Electronics, 14 Nauky Ave., Kharkiv, 61166, Ukraine
e-mail: pavel.maksimchuk@gmail.com

Hydrogen peroxide (HP) is a widespread industrial chemical widely used for bleaching, cleaning, and disinfection. HP also plays an indispensable role in living organisms being a ubiquitous cell signaling molecule [1] and a substrate or byproduct of a number of enzymes (including catalase, superoxide dismutase, and a number of oxidases and peroxidases) [2]. So, HP sensing is required for reliable quantification of HP content in these systems.

HP sensors based on luminescent inorganic nanoparticles can be considered as a perspective alternative to traditional dye- and enzyme-based sensors which usually are unstable and non-reversible. Undoped (CeO_{2-x}) and Eu^{3+}-doped ($CeO_{2-x}:Eu^{3+}$) colloidal ceria nanoparticles provide HP detection by reversible quenching of Eu^{3+} (590 nm) and Ce^{3+} (430 nm) luminescence bands [3]. The dynamics of Eu^{3+} and Ce^{3+} luminescence quenching and recovery during HP-nanoceria interaction provides an insight into the microscopic mechanisms of HP sensing by CeO_{2-x} and $CeO_{2-x}:Eu^{3+}$ nanoparticles.

Both CeO_{2-x} and $CeO_{2-x}:Eu^{3+}$ luminescent sensors are reversible and their recovery rates can be sufficiently increased by temperature and continuous UV irradiation. At the same time, Eu^{3+} ions deteriorate the catalase-mimetic activity of CeO_{2-x} NPs and worsen their antioxidant properties that should be keep in mind while using these sensors in biological media.

[1] D. R. Gough, T. G. Cotter, Hydrogen peroxide: a Jekyll and Hyde signalling molecule. Cell Death Dis. 2011, 2(10), e213-e213.
[2] 2.Copeland, R. A. Enzymes: a practical introduction to structure, mechanism, and data analysis. John Wiley & Sons: 2000.
[3] V. Seminko, P. Maksimchuk, V. Klochkov, Ye. Neuhodov, L. Demchenko, S. Yefimova. Reversible CeO_{2-x} and $CeO_{2-x}:Eu^{3+}$ Luminescent Hydrogen Peroxide Sensors with Recovery Rates Controlled by Temperature and UV Irradiation, The Journal of Physical Chemistry C, 2023, 127 (22), 10662-10669.

Impact of pressure on electrical properties of silver nanofilms

S. Udachan[1], S. B. Kolavekar[1], N. H. Ayachit[1], L. A. Udachan[2], S. Siddanna[2], S. S. Kolkundi[3], K. N. Kumar[4], S. Ramya[5], S. Veeresh[5]

[1] Department of Physics, School of Advanced Sciences, KLE Technological University, Hubballi-580031, India
[2] S. S. Tegnoor Degree College, Kalaburagi-585105, India
[3] Government First Grade College, Shahapur-585223, Yadgir, India
[4] Department of Physics and Center for Nanomaterials and MEMS, Nitte Meenakshi Institute of Technology, Yelahanka, Bangalore-560064, India.
[5] Shree Sangam Vidya Mandir, Kalburagi, Karnataka, India.
e-mail: shivaudachan8@gmail.com, sangeeta_k@kletech.ac.in

Silver nanoparticles are the subject of immense interest because of their distinct chemical and physical properties that are different from their bulk counterpart. This makes these nanoparticles very important in many fields including antimicrobial applications, biosensor materials, composite fibers, cryogenic superconducting materials, cosmetic products and electronic components. The silver nanoparticle research continues to grow, drawing the attention of researchers. It is known that silver has very high electrical conductivity [1,2]. Silver has been widely used as a conductor wire in circuits that require low dissipation, and high conductivity [3,4]. Pressure plays a key role in determining the electrical characteristics of silver nanoparticles. Hence, we have undertaken a study on the electrical properties.

[1] Dr. Lide CRC Handbook of Chemistry and Physics: A Ready-Reference Book of Chemical and Physical Data. New York: CRC Press; (2008).
[2] R. Ma, B Kang, S. Cho, M. Choi, S. Baik. Extraordinarily high conductivity of stretchable fibers of polyurethane and silver nanoflowers. ACS Nano.;9:10876 (2015). DOI:10.1021/acsnano.5b03864.
[3] D. Basak, S. Karan, B. Mallik. Significant modifications in the electrical properties of poly(methyl methacrylate) thin films upon dispersion of silver nanoparticles. Solid State Communications. 141:483-487, (2007). DOI: 10.1016/J.SSC.2006.12.014.
[4] K. Gupta, P.C. Jana, A. K. Meikap. Optical and electrical transport properties of polyaniline-silver nanocomposite, Synthetic Metals, 160:1566-1573, (2010).
DOI: 10.1016/J.SYNTHMET.2010.05.026.

BIOPHYSICS AND PHYSICS OF MACROMOLECULES

Characterization of graphene oxide by Raman spectroscopy and atomic force microscopy

A. Glamazda[1,2], A. Linnik[1], O. Lytvyn[3], V. Karachevtsev[1]

[1] B.Verkin Institute for Low Temperature Physics and Engineering of NAS of Ukraine, 47 Nauky Ave., Kharkiv, 61103, Ukraine
[2] V. N. Karazin Kharkiv National University, 4 Svobody sq., Kharkiv, 61022, Ukraine
[3] Borys Grinchenko Kyiv University, 18/2 Bulvarno-Kudriavska Str., Kyiv, 04053, Ukraine
e-mail: glamazda@ilt.kharkov.ua

The carbon low-dimensional materials are a new class of multifunctional materials that can change the approach in the development and design of the novel element base for advanced technologies and electronic devices. For such materials, a number of requirements are put forward, which are related to their homogeneity and the possibility to tune the electrical properties and change the carrier density. Graphene is a two-dimensional carbon monolayered nanomaterial with a "honeycomb" lattice structure. The carbon 2D graphene monolayer has a number of unique physical characteristics, such as an extremely high surface/mass ratio, high thermal conductivity (almost ten times higher than the thermal conductivity of copper), optical transparency in the visible range, high electronic mobility, etc. Chemical modification of the graphene surface leads to new interesting physicochemical properties. For example, oxidation of the graphene surface with covalently linked different types of oxygen-containing functional groups (epoxy, hydroxyl, carboxyl) introducing sp^3 defects changes the optoelectronic properties of graphene and gives rise to a bandgap between its valence and conduction bands with width depending on the number of defects on the surface. The modified graphene material is called graphene oxide (GO). The linked oxygen-containing functional groups can serve as anchors for the further multi-stage process of functionalization of graphene. Thus, it is very important to certify the individual components of nanohybrids for defects that can significantly change the physical properties of nanohybrids through the appearance of the inputting barrier limiting the wave propagation. The low-temperature studies can shed light on the quantum effects suppressed due to thermal fluctuation at room temperature. The low-temperature Raman study gives an understanding of the phonon dynamics because the phonons play an essential role in thermal conductivity and mechanical properties of materials, as well as they can couple to other excitations that significantly expand the field of their study. In addition, the graphene family includes nanomaterials with different amounts of oxidation groups and defects that affect Raman spectra.

The present work is devoted to the low-temperature Raman studies of the GO film in the range of 5 - 325 K. The performed analysis of the temperature evolution of the peak positions as well as linewidths of two Raman modes D (~1300 cm^{-1}) and G (~1600 cm^{-1}) was described in terms of the anharmonic model. The temperature behavior of G mode demonstrated a slight deviation from the anharmonic model below ~100 K in contrast to the D mode that could be explained in terms of involving an additional phonon decay channel [1]. The analysis of the linewidth of the Raman modes showed that the distribution of defects in GO is inhomogeneous and surface functionalization effectively separates neighbouring layers. The average value of the distance between defects and the defect density was estimated. The obtained results can be useful for understanding phonon dynamics for the development of nanodevices based on 2D materials where confinement of propagation of phonon excitations plays a key role.

[1] A. Glamazda, A. Linnik, O. Lytvyn, V. Karachevtsev, AIP Advances 14 (2), 025033 (2024). https://doi.org/10.1063/5.0188838.

Mathematical modeling of the freezing zone temperature dynamics of the hydrogel for cryoablation and cryotherapy applications

O. V. Ivakhnenko[1,2], S. N. Shevchenko[1], and O. F. Todrin[3]

[1] *B.Verkin Institute for Low Temperature Physics and Engineering of NAS of Ukraine, 47 Nauky Ave., Kharkiv, 61103, Ukraine*
[2] *Theoretical Quantum Physics Laboratory, Cluster for Pioneering Research, RIKEN, Wako, Saitama 351-0198, Japan*
[3] *Institute for Problems of Cryobiology and Cryomedicine, 61016 Kharkiv, Ukraine*
e-mail: olegiv333@gmail.com

Cryoablation is common in medicine to remove abnormal tissue from the body with minimal damage to healthy tissues. One of the principal problems is to define the time of cryogenic impact, since on the one hand, it should be enough to kill all abnormal cells, like tumours, and on the other hand, a cryogenic application should not be too long to minimize damage to healthy tissues. This problem can be solved by using a temperature detector. But it is impossible to insert such a detector into dense tissue without damaging living cells. In addition, any detector will distort the temperature field. There is a non-invasive technique of measuring temperature by thermal vision camera [1], but it gives only a surface temperature field.

Physical and mathematical modeling methods are widely used to test cryoapplication regimes. For physical modeling of the cryoapplication process, instead of biological tissue, various gels are used as a model medium [2]. Temperature detectors can be easily placed inside the gel. Mathematical modeling of this process [2,3] allows one to predict the temperature field of the frozen region. This makes it possible to determine the cryoapplication time sufficient to destroy target cells and minimize damage to healthy cells under various experimental conditions.

The problem with moving phase border is known as the Stefan problem. There are several ways to numerically solve that problem, one of them is gradually changing thermodynamic parameters close to the phase change border, which is good to describe the freezing dynamics of the hydrogel, because the appearance of solutes in water in hydrogel the freezing temperature changes in a range of temperatures (-14C..-0.1C) due to change of solute concentration, so we can use effective thermal capacity by combining usual thermal capacity with latent heat. That allows us to solve the heat equation in 2D cylindrical geometry see Fig. 1.

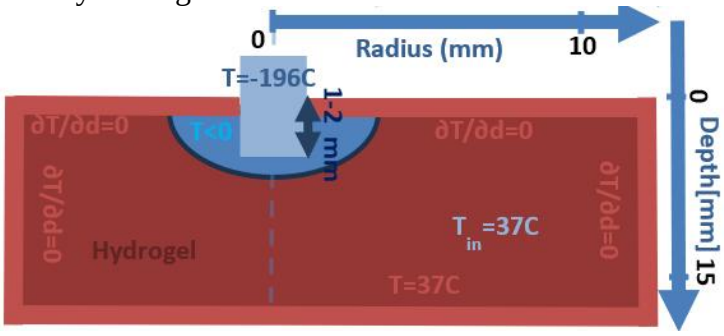

Fig. 1. Principal scheme of the cryo-application problem for 2D cylindrical geometry with radial symmetry, where is cryo-applicator with a temperature of liquid Nitrogen pressed 1-2mm inside the hydrogel.

We neglect temperature transfer from the air and the sides, assuming the freezing spot is much smaller than the simulated size, and put a constant temperature deep in the hydrogel. After finishing freezing time, we replace the cryo-applicator with air border conditions.

Acknowledgments: This research is sponsored by the National Research Foundation of Ukraine (Grant No. 2022.01/0094).

[1] G. Kovalev et al., Problems of Cryobiology and Cryomedicine, 2020, 30, 359-368
[2] M. Rossi and Y. Rabin, Proc. Int. Conf. "Modeling, Simulation & Visualization Methods" (MSV 2007), CSREA Press, 187-193.
[3] Y. Rabin and A. Shitzer, J. Biomech. Eng., 1997, 119, 146-152.

Electronic transport in composite film of reduced graphene oxide with molybdenum disulfide

N. V. Kurnosov[1], A. M. Plokhotnichenko[1], V. A. Karachevtsev[1]

B. Verkin Institute for Low Temperature Physics and Engineering of NAS of Ukraine,
47 Nauky Ave., Kharkiv, 61103, Ukraine
e-mail: nick.kurnosov@gmail.com

Composites that contain low-dimensional nanostructures currently attract the great attention of researchers. The possible application areas include nanoelectronics, nanophotonics, and sensors. Graphene and related carbon nanostructures (graphene oxide (GO), reduced graphene oxide (rGO)) are among the well-established two-dimensional (2D) nanomaterials used in composites. The transition metal dichalcogenides (TMDs) also emerge as promising 2D nanomaterials, as the bulk TMDs crystals can be exfoliated into individual layers or few-layered flakes.

The composite material studied in this work was formed by semiconducting TMD molybdenum disulfide (MoS_2) and rGO. We should note that the rGO used for composite preparation had ~87% fraction of carbon which means a large amount of conductive sp^2 domains. The film was obtained by vacuum filtration from suspension of rGO-MoS_2 hybrids in methanol. Preparation of the suspension was based on ultra-sound treatment (60 min, 22 kHz) with the following centrifugation (3000g, 15 min) of rGO and MoS_2 with a weight ratio of 1:2.

In order to assess the electronic transport properties of rGO-MoS_2 composite, the temperature dependence of resistance (R(T)) was measured in the range of 5–312 K. Derivative analysis of R(T) dependence has confirmed that the low-temperature electronic transport of rGO-MoS_2 composite is governed by Efros-Shklovskii variable-range hopping (ES VRH) mechanism, which relies on electron tunneling between localized states and accounts for Coulomb gap phenomenon [1]. We also confirmed that in our composite there is a transition from ES VRH to the two-dimensional Mott VRH mechanism [2] at higher temperatures as the thermal energy becomes essentially larger than the Coulomb gap. The transition temperature is ~160 K while the Mott VRH mechanism persists up to the room temperature. Overall, our present results as well as comparison with those already published for rGO film and rGO composite with single-walled carbon nanotubes [3] show that the rGO essentially provides the electronic conductivity in rGO-MoS_2 composite.

[1] B. I. Shklovskii and A. L. Efros, Electronic Properties of Doped Semiconductors (Springer-Verlag, Berlin 1984).
[2] N. F. Mott and E. A. Davis, Electronic Processes in Non-Crystalline Materials (Oxford: Clarendon Press, New York 1979).
[3] N. V. Kurnosov, A. S. Linnik, and V. A. Karachevtsev, Low Temp. Phys. 46, 285 (2020). https://doi.org/10.1063/10.0000700.

Metal-dielectric metasurface sensoring structure for IgG/glucose concentration determination in solutions

K. S. Kuznetsova[1], V. A. Pashynska[1, 2], Z. E. Eremenko[1,3]

[1] Usikov Institute for Radiophysics and Electronics of the NAS of Ukraine, 12 Academ. Proskury Str., Kharkiv 61085, Ukraine
[2] B. Verkin Institute for Low Temperature Physics and Engineering of the NAS of Ukraine, 47 Nauky Ave., Kharkiv, 61103, Ukraine
[3] Leibniz Institute for Solid State and Materials Research, Helmholtzstraße 20, Dresden 01069, Germany
e-mails: tkachenkok89@gmail.com, vlada.pashynska@gmail.com, zoya.eremenko@gmail.com

The current research is devoted to the development of the metal-dielectric metasurface based sensoring structure for determination of Immunoglobulin G (IgG) or glucose concentration in water solutions basing on the results of the combined study by differential microwave dielectrometry method and by numerical modelling using COMSOL software. Dependences of the values of complex permittivity (CP) of IgG/glucose water solutions on the analyte concentration were experimentally obtained at 31.82 GHz frequency using original microwave dielectrometer setup. It was shown that increase of IgG (or glucose) concentration resulted in decrease in the CP values of the solutions studied. The experimentally obtained CP data were used for microwave metal-dielectric metasurface sensing unit cell numerical modelling. The optimal metasurface structure (Fig.1a) consisted of two Teflon layers with four rectangular copper plates placed between them, and with the dielectric well which was used as a tested liquid samples holding volume. Numerical modelling of the metasurface with optimal thickness L of the tested solution layer was carried out. The results of the numerical calculations demonstrated that with increase of the analyte (IgG or glucose) concentration in the solutions, the reflection coefficient resonance frequency shifts towards the area of the lower frequencies (Fig.1 b, c). In our previous study, we also employed similar metasurface structure as a sensing element for detecting the Human Serum Albumin concentration [1] in water solutions and the data of the current study is in a good correlation with the previous ones. The calibration graphs were proposed for the analytes concentration determination in water solutions using the proposed metasurface sensoring structure (Fig.1 b, c). The obtained data confirms the applicability of such metasurface based biosensors for medical diagnostic purposes related with the examining of the glucose or IgG levels in biological liquid samples.

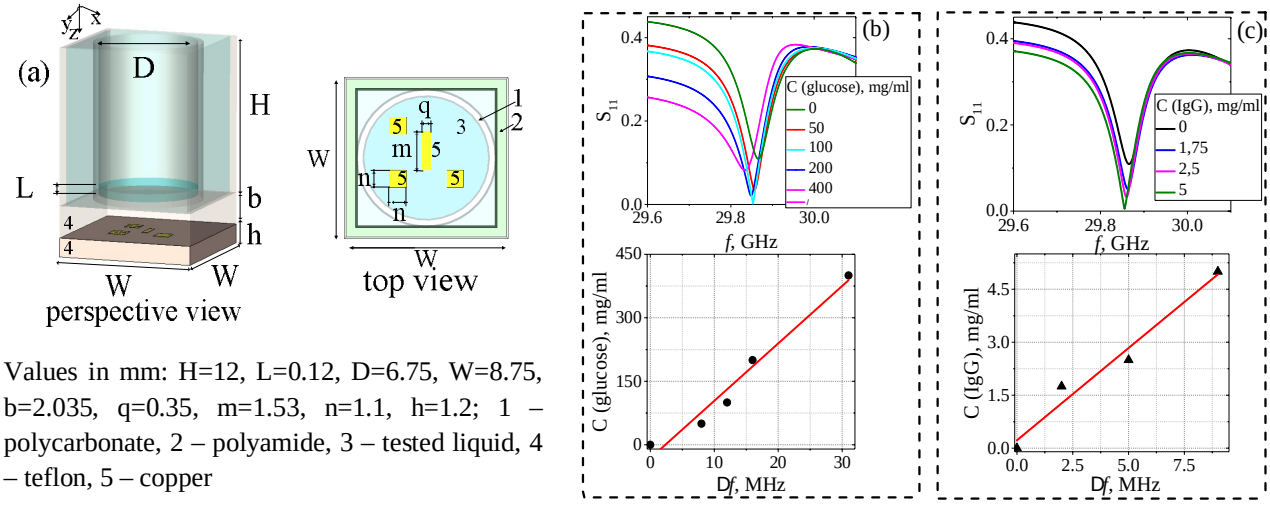

Values in mm: H=12, L=0.12, D=6.75, W=8.75, b=2.035, q=0.35, m=1.53, n=1.1, h=1.2; 1 – polycarbonate, 2 – polyamide, 3 – tested liquid, 4 – teflon, 5 – copper

Fig. 1. Metal-dielectric metasurface unit cell structure (a). Dependence of the reflection coefficient (S_{11}) of the metal-dielectric metasurface unit cell with water solutions of glucose (b) and IgG (c) (up) on frequency and calibration curves for glucose (b) and IgG (c) concentration determination (down).

[1] K. S. Kuznetsova, V. A. Pashynska, and Z. E. Eremenko, Low Temp. Phys. 50, pp. 18-23 (2024).

Biologically significant intermolecular interactions of doxorubicin with phospholipids and supporting drug molecules

V. A. Pashynska[1], V. O. Karachevtsev[1], A. Gomory[2], L. Drahos[2]

[1] B. Verkin Institute for Low Temperature Physics and Engineering of NAS of Ukraine, 47 Nauky Ave., Kharkiv, 61103, Ukraine
[2] Institute of Organic Chemistry of the HUN-REN Research Center for Natural Sciences, Budapest, Hungary
e-mail: pashynska@ilt.kharkov.ua, vlada.pashynska@gmail.com

Doxorubicin (DOX) is an effective antitumor medication, which is widely used for about 50 years as a first-line chemotherapeutic drug in combination or alone for the treatment of a large number of cancer diseases including breast cancer, ovarian cancer, some types of leukemia and lymphoma, Kaposi`s sarcoma etc. [1]. Similarly to other cytotoxic agents, DOX along with a significant antitumor effect can cause serious undesired side effects such as high cardiotoxicity, an acute life-threatening inflammation of bowel and some others. To reduce the side effects and to avoid the formation of chemoresistance to DOX by providing the site-specific drug transportation, a number of nanoscale drug delivery systems for DOX have been developed [2]. One of the effective strategies of DOX encapsulation is the use of liposomes as the drug delivery systems, which provide the prolongation of the DOX circulation time in an organism and decrease the drug toxicity [3]. Such DOX liposomal formulations as Doxil and Myocet liposomal [2] are already successfully used in medical practice, and the development of new liposomes-based DOX nanoformulations attracts the attention of scientists [2]. In the framework of the problem of ensuring the effective DOX delivery and functioning, the study of intermolecular interactions of the DOX with phospholipids (main components of liposomal and biological membranes) as well as with some supporting drugs (such as anti-inflammatory or antioxidative agents, which are often used during the cancer treatment) is considered as an actual research task.

In the current study the electrospray ionization (ESI) mass spectrometry (MS) method was applied to examine the intermolecular interactions of DOX with dipalmitoylphosphatidylcholine (DPPC, which is biomembrane phospholipid widely used for liposomes production), and with acetylsalicylic acid (aspirin, ASP) or ascorbic acid (ASC, vitamin C). Aspirin and vitamin C can be used as supporting drugs in antitumor therapy or can be affiliated with the patients` nutrition. The formation of stable noncovalent complexes of DOX with DPPC in the polar solvent methanol was revealed by the ESI MS experiments that proves the possibility of stable encapsulation of the DOX molecules in the liposomes till the beginning of the drug release from the delivery nanosystems. The drug release can be regulated by temperature, pH and other factors [2]. The following ESI MS examination of the model systems containing DOX and ASP (or ASC) confirmed the probability of the noncovalent complexation between DOX and the supporting acidic drug molecules in the polar solvents. Such biologically significant intermolecular interactions between the molecules of DOX and ASP or ASC can modify the activity of the drugs in the case of their co-administration in medical practice. The data obtained are of practical importance since they demonstrate the role of intermolecular interactions between the DOX molecules and the active molecules of the surrounding for realization of the DOX antitumor activity.

The research was supported by the Grant N 0123U100628 of the National Academy of Sciences of Ukraine and Ukrainian-Hungarian inter-academy research program (2019-2022 years).

[1] S. Sritharan and N. Sivalingam, Life Sciences. 278, 119527 (2021). https://doi.org/10.1016/j.lfs.2021.119527
[2] N. D'Angelo, M. Noronha,M. Câmara, I. Kurnik, C. Feng, V. Araujo, J. Santos,V. Feitosa, J. Molino, C. Rangel-Yagui, M.Chorilli, E. Ho and A. Lopes, Biomaterials Advances. 133, 112623 (2022). https://doi.org/10.1016/j.msec.2021.112623

Influence of structural defects in MoS_2 on interaction with biological molecules

T. Piddubnyi[1], S. Stepanian[1], L. Adamowicz[2]

[1] B. Verkin Institute for Low Temperature Physics and Engineering of NAS of Ukraine, 47 Nauky Ave., Kharkiv, 61103, Ukraine
[2] Department of Chemistry and Biochemistry, University of Arizona, 85721 Tucson AZ, USA
e-mail: piddubnyi@ilt.kharkov.ua

Transition metal dichalcogenides, including molybdenum disulfide (MoS_2), have attracted considerable attention as promising materials for biosensing and biomedical applications. Monolayer two-dimensional (2D) MoS_2 consists of three atomic layers. The middle layer contains molybdenum atoms. Above and below this layer are sulfur atoms that form two surface layers. The surfaces formed by sulfur atoms are chemically relatively inert and are analogous to the carbon surface of graphene. However, unlike graphene, the edges of MoS_2 fragments have a much more complex structure, which depends on the method used to produce monolayer MoS_2. When using chemical or physical vapor deposition methods, these edges are almost completely terminated by sulfur atoms and are inert like the MoS_2 surface. At the same time, the edges of the fragments obtained by ultrasonic exfoliation have molybdenum atoms. These atoms have unfilled valences and can form coordination covalent bonds with biomolecular atoms that have electron lone pairs. In biomolecules, such atoms are most often oxygen and nitrogen atoms.

The various types of structure defects of MoS_2 are commonly observed. The most frequent defects are vacancies of surface sulfur atoms, as well as more complex ones resulting from the replacement of one or more sulfur atoms by molybdenum atoms and vice versa. The type of defects also varies depending on the method used to produce single-layer MoS_2. Ultrasonic exfoliation and chemical sputtering result in sulfur atom vacancies dominating the structure, while physical sputtering leads to the replacement of sulfur atoms with molybdenum atoms and vice versa. The deficiency of the structure of MoS_2 is affected by the method of preparation. Defects on the MoS_2 surface alter its electronic structure and can significantly impact its interaction with guest biomolecules. The defects can act as carrier donors, scattering centers, traps and recombination centers, modifying the electronic and spectral properties.

The main aim of this study is elucidation how the defects change vibrational spectra and electronic structure of the MoS_2 monolayers as well as their interaction energies with important biological molecules using the quantum-mechanical DFT/M06-2X method. Totally we examined eight types of defects: three vacancy defects and five substitution defects. The simulation results showed that the greatest changes in the spectral characteristics and energies of interaction with guest molecules are observed for defects associated with the substitution of a sulfur atom by molybdenum atom. As a result of this substitution, a molybdenum atom appears on the MoS_2 surface. Such an atom can form coordination bonds with a guest molecule and this significantly increases the interaction energy and spectral changes. For example, when an uracil molecule interacts with such defect, the interaction energy reaches about -25 kcal/mol as compared to -16 kcal/mol in the case of the pristine MoS_2 surface. The analysis of the obtained data allowed us to detect spectral markers for each type of the structural defects.

Biopharmaceutical studies of a novel sedative drug based on glycine and tryptophan in model membrane medium: revealing of bioavailability and synergistic properties

O. V. Vashchenko[1], R. Ye. Brodskii[2], I. O. Davydova[3], P. V. Vashchenko[1], O. I. Ivaniuk[3], O. A. Ruban[3]

[1] Institute for Scintillation Materials of NAS of Ukraine, 60 Nauky Ave., Kharkiv, 61072, Ukraine
[2] Institute for Single Crystals of NAS of Ukraine, 60 Nauky Ave., Kharkiv, 61072, Ukraine
[3] National University of Pharmacy, 53 H.Skovorody Str, Kharkiv, 61002, Ukraine
e-mail: olga_v@isma.kharkov.ua

Various disorders of central nervous system, such as insomnia, emotional overstrain, chronic stress, depression, neurosis, *etc*., are a common problem growing year by year [1]. A promising way to develop effective sedative drugs is pharmacological properties improvement, *i.a.* due to synergistic effects and bioavailability optimization. Lipid medium is believed to be pivotal to assessment drug bioavailability, so membrane permeability improvement is thought to be a direct reason of improve drug delivery [2].

In the present study, biopharmaceutical properties and drug-excipient interactions of a novel sublingual lozenge based on amino acids Gly and Trp as sedative agents were explored in a lipid membrane medium of hydrated dimyristoylphosphatidylcholine (DMPC) to reveal. A kinetic differential scanning calorimetry (DSC) approach [3] was involved to address the challenge. DSC parameters of DMPC "gel to liquid crystal" phase transition were collected and used as an effective marker for tracing drug distribution over membrane medium. Time dependences of the DSC parameters allowed us to obtain both kinetic and equilibrium parameters of membrantotropic action of selected drug components and their combinations.

It was shown that manipulating the drug formulation causes essential changes in its membranotropic effect. In particular, lactose as an excipient noticeably facilitates Trp release providing its ability to get into the bloodstream simultaneously with Gly, i.e. Gly-Trp synergism. A number of mucoadhesive agents was alternatively involved in the drug formulation in order to prolong the time of contact between a drug and the mucous membrane of human oral epithelium. Mucoadhesive agents were found to impact both equilibrium membranotropic drug effect and kinetic parameters of drug-membrane interactions, up to an order of magnitude for various mucoadhesive agents, which directly affect the drug bioavailability. Generally, a clear correlation was shown between the interaction parameters and the viscosity of a mucoadhesive agent.

A dynamic mathematical model was developed to give the physical reasons to some experimental findings, including two-exponential dependence of DSC kinetic profiles. The model describes two simultaneous processes, namely, drug release in surrounding water phase and further drug diffusion into lipid vesicles in various cases. For the case under consideration, the model suggests that the drug release is the limiting (slower) process.

We suppose that both the dynamic model and the experimental approach developed are quite applicable to characterize the processes of release and distribution for wide range of drug substances and could be helpful in revealing variety of their biopharmaceutical properties.

[1] M. Moitra, D. Santomauro, P.Y. Collins, et al., PLoS Med., 19(2), e1003901 (2022). http://dx.doi:10.1371/journal.pmed.1003901.
[2] B. Gorain, H. Choudhury, M. Pandey, et al., Drug – excipient interaction and incompatibilities. In: Rakesh K., Ed. Dosage form design parameters. Vol. II, Chapt. 11, p. 363-402. (Academic Press, 2018). https://doi.org/10.1016/B978-0-12-814421-3.00011-7.
[3] O.V. Vashchenko, O.A. Ruban, I.V. Zupanets, et al., Biophys. Bull., 50, 25–35 (2023). https://doi.org/10.26565/2075-3810-2023-50-03.

Binding characteristics of systemic glucocorticoids with the SARS-CoV-2 spike glycoprotein: in-silico evaluation

N. V. Khmil[1,2], V. G. Kolesnikov[1], A. O. Boiechko-Nemovcha[2]

[1] O. Ya. Usikov Institute for Radiophysics and Electronics of NAS of Ukraine, 12 Acad. Proskura str., Kharkiv, 61085, Ukraine
[2] Kharkiv National University of Radio Electronics, Nauky ave., 14, Kharkiv, 61166, Ukraine, e-mail: khmilnatali@gmail.com

Severe acute respiratory syndrome coronavirus 2 (SARS-CoV-2) poses a serious threat to people worldwide causing a variety of diseases, manifesting with intestinal, respiratory, hepatic, and neurological symptoms. SARS-CoV-2 predominantly focuses on the lower parts of the respiratory system, infiltrating the epithelial cells of the lungs. It releases the nucleocapsid component which then arrogates the host cell to replicate the viral genome. The therapeutic strategy to counteract SARS-CoV-2 encompasses antiviral drugs, monoclonal antibodies, as well as immunomodulatory drugs, such as systemic glucocorticoids, which may benefit patients with middle and severe COVID-19. In the treatment of COVID-19, systemic glucocorticoids exhibit anti-inflammatory activity by suppressing the cytokine storm mitigating the systemic inflammatory response caused by SARS-CoV-2. In addition, the spike glycoprotein (S protein), which recognizes the host cell receptor and initiates the attachment of SARS-CoV-2 to it, can be considered a potential target for glucocorticoids [1]. However, the mechanism of glucocorticoid inhibitory action against the S protein is currently unclear due to insufficient study of the ligand-binding sites on the S protein.

The aim of the study was to evaluate the binding characteristics of systemic glucocorticoids with the SARS-CoV-2 S protein and to elucidate the topological features of non-covalent ligand-protein complexes.

Molecular docking was performed to study the binding affinity and type of interactions between ligands and the protein targets. AutoDock Vina was used for docking studies against SARS-CoV-2 S protein with ligands [2]. Dexamethasone, methylprednisolone, triamcinolone, and prednisone were selected as ligands to perform molecular docking studies to identify favorable binding sites on S protein. The structures of the ligands were downloaded from PubChem, an open chemistry database at the National Institutes of Health. AutoDock tool was used to prepare ligand structures in the PDB format. Two 3D structures of S protein which have open (RBD-up) and closed (RBD-down) conformations in the receptor-binding domain (PDB ID: 6VYB, and PDB ID: 6VXX), respectively, were used as docking targets (www.rcsb.org). Water molecules were removed and hydrogen atoms were added. Ligand interactions with amino acid residues were identified using the PLIP web tool (https://plip-tool.biotec.tu-dresden.de). Visualization of docking results was implemented in PyMol 2.5.

In silico docking study demonstrated that all glucocorticoids can bind to multiple sites on the SARS-CoV-2 S protein, including the receptor-binding fragment (S1) and the fusion fragment (S2). Methylprednisolone showed the best affinity with S protein in RBD-up conformation than other glucocorticoids, with a binding free energy of -9,7 kcal/mol and an inhibition constant value of $0{,}08 \times 10^{-6}$ M. Triamcinolone demonstrated a high affinity with S protein in RBD-down conformation, at which the binding free energy was -8,8 kcal/mol and an inhibition constant value was $0{,}36 \times 10^{-6}$ M. Our results showed that Tyr369, Lys417, and Ser514 are mainly involved in the stabilization of complexes through the hydrogen bonds. Hydrophobic interactions are primarily mediated by Phe464, Asn1023, and Leu1024. These results are an important basis for the development of potential drugs against SARS-CoV-2.

[1] H. G. Toor et al., European journal of pharmacology. 890, 173720 (2021).
[2] O. Trott, and A. J. Olson, Journal of computation chemistry. 31, 2 (2010).

Intermolecular interactions of glutathione with molybdenum disulfide probed by laser desorption/ionization mass spectrometry

O. A. Boryak[1], V. A. Pashynska[1], M. V. Kosevich[1], P. O. Kuzema[2], V. A. Karachevtsev[1]

[1] B. Verkin Institute for Low Temperature Physics and Engineering of the NAS of Ukraine, 47 Nauky Ave., Kharkiv, 61103, Ukraine
[2] Chuiko Institute of Surface Chemistry of the NAS of Ukraine, 17 General Naumov Str., Kyiv 03164, Ukraine
e-mail: boryak@ilt.kharkov.ua

In the search for nanomaterials promising for drug delivery applications, molybdenum disulfide MoS_2 nanoparticles are actively studied. Among the requirements to drugs carriers there is a sufficiently strong noncovalent binding of drug molecules to the carriers, avoiding noticeable chemical modification. In our studies of interactions of MoS_2 with biomolecules and biologically active compounds our attention was attracted by a peculiar case of redox active sulfur-containing compound Glutathione (GSH), which may interact both non-covalently and covalently with sulfur atoms of MoS_2. The GSH-MoS_2 nanocomposite was prepared by sonication of aqueous mixture of GSH and MoS_2 and examined by laser desorption/ionization (LDI) mass spectrometry.

In the positive ion LDI mass spectra of pure GSH, it was present in the cationized form as GSH•Na^+, *m/z* 330, and GSH•K^+, *m/z* 346; a fragment ion at *m/z* 279, $[GSH - 28]^+$ was observed as well. Characteristic LDI mass spectrum of MoS_2 in the negative ion mode contained envelopes of peaks of clusters of general formula $Mo_xS_yO_z$. In the positive ion mass spectrum of dried GSH-MoS_2 nanocomposite sample only one noticeable peak related to GSH monomer was present at *m/z* 279; at the same time a cationized dimer $[GSSG + Na]^+$, *m/z* 635, was recorded. In the negative ion mode the deprotnated GSH, $[GSH - H]^-$, *m/z* 306 was identified and it was accompanied by several peaks which can be attributed to $[GSH + H_2O]^-$, *m/z* 325, $[GSH + S]^-$, *m/z* 339, and $[GSH + 47]^-$, presumably $[GSO_3]^-$, *m/z* 354, ions (Fig. 1). Such a set of peaks different from solely molecular ions of GSH, points to a possibility of both physical and chemical nature of interactions of GSH with MoS_2. The clarification of a question, whether the relevant reactions are initiated by the laser irradiation under LDI or proceed spontaneously on the surface of MoS_2, necessitates further checks by independent techniques.

From the point of view of mass spectrometry basics, it is of interest that in the obtained spectra the organic-related peaks are well resolved from the peaks of MoS_2 origin (compare with the spectrum of the neat MoS_2 in Fig. 1). For example, the calculated monoisotopic mass value of the $[GSH + S]^-$ - 339.056 a. u. (or $[GSH + 2O]^-$ - 339.073 a. u.) is located between two peaks of Mo_2S_4O cluster distribution, namely 338.694 and 339.694 a. u.

Possible pathways of interactions of GSH with MoS_2 are discussed in the report.

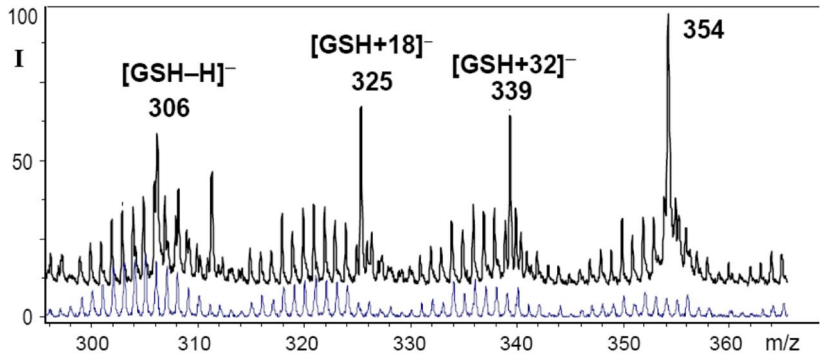

Fig. 1. Fragment of LDI mass spectra of negative ions of GSH-MoS_2 nanocomposite (upper line) and pure sonicated MoS_2 (bottom line).

This work was supported by a grant № 0123U100628 of the NAS of Ukraine.

Analysis of cholinomimetic pharmacological properties of a new agonist of muscarinic cholinergic receptors

T. O. Fedirko[1], O. V. Tsymbalyuk[1], I. S. Voiteshenko[1], S. A. Starosyla[2], V. G. Bdzhola[3], A. O. Prykhod'ko[3], A. Yu. Nyporko[1]

[1] Taras Shevchenko National University of Kyiv, 64/13, Volodymyrska St., Kyiv 01601, Ukraine
[2] Receptor AI Inc., 20-22 Wenlock Road, London N1 7GU, United Kingdom
[3] Institute of Molecular Biology and Genetics of NAS of Ukraine, 150, Zabolotnogo Str., Kyiv 03143, Ukraine
e-mail: tetiana.fedirko@knu.ua

Muscarinic cholinergic receptors (mAChRs) of the M2-subtype predominate in visceral smooth muscles. The most successful strategy for normalizing hypofunction of visceral smooth muscles is the use of drugs - selective agonists of mAChRs of the M2 subtype. Therefore, there is an urgent need to develop such selective drugs to modulate the functional activity of M2 receptors. The work aimed to study the effect of compound with the code 146539, for which the ability to activate mAChRs was predicted by *in silico* methods, on the contractile activity of the smooth muscles of the large intestine of rats.

Compound 146539 was used in concentrations of 10^{-9} - 10^{-6} M. Acetylcholine-induced (concentration of acetylcholine was 10^{-5} M) contractions were studied tensometrically in isometric and isotonic modes on preparations of circular smooth muscles of the rat caecum. The kinetic properties of the contractions were estimated with the calculation of the normalized maximum speeds of the contraction and relaxation phases.

Compound 146539 heterogeneously modulated the phasic and tonic components of isometric contractions. In the case of phasic contraction, a biphasic effect was observed: an increase of force under the background of concentrations of 10^{-9} – 10^{-7} M (the greatest effect under the action of 10^{-8} M of the compound) and inhibition under the action of 10^{-6} M of compound 146539. The absolute values of the force of the tonic components of acetylcholine contractions were dose-independently enhanced by compound 146539.

In contrast to the isometric mode of registration, in the case of isotonic shortening, activation of acetylcholine responses was observed only against the background of 10^{-9} M concentration of compound 146539. Against the background of 10^{-8} and 10^{-7} M of compound 146539, acetylcholine-induced shortening remained at the control level, and under the action of 10^{-6} M of this compound, shortening was significantly suppressed.

Since substance 146539 significantly increases not only the tonic but also the phasic component of acetylcholine contraction, it is reasonable to predict that this compound does not exhibit specific M2-cholinomimetic properties. Also, it cannot be excluded that, in addition to mAChRs, higher concentrations of compound 146539 may affect other important cellular targets that regulate the processes of excitability and contractility in intestinal smooth muscle tissue.

The influence of the type of charged particles on the parameters of zigzag patterns in BSA films

D. Glibitskiy[1], O. Gorobchenko[2], O. Nikolov[2], T. Dzhimieva[2], I. Zaitseva[2,3], A. Roshal[4], M. Semenov[1], G. Glibitskiy[1]

[1] O. Ya. Usikov Institute for Radiophysics and Electronics, NAS of Ukraine, 12 Academician Proskura Str., Kharkiv 61085, Ukraine;
[2] V. N. Karazin Kharkiv National University, 4 Svobody Sq., Kharkiv 61022, Ukraine;
[3] O. M. Beketov National University of Urban Economy in Kharkiv, 17 Marshal Bazhanov Str., Kharkiv 61002, Ukraine;
[4] Institute for Chemistry, V. N. Karazin Kharkiv National University, 4 Svobody Sq., Kharkiv 61022, Ukraine
e-mail: dima.glib@gmail.com

Previously, an analysis of changes in the parameters of zigzag patterns on the surface of BSA (bovine serum albumin) films was carried out [1], relating those changes to the presence of colloidal particles, aggregates and negatively charged associates of flavin mononucleotide (FMN), as well as to a decrease in the surface potential and hydration of negatively charged BSA particles in solution. The relations were studied by adding FMN or $AlCl_3$ to BSA solutions, drying them and analyzing the films, as well as measuring the changes in the state of BSA and its environment via microwave dielectrometry, pH-metry, ultraviolet spectroscopy of absorption and fluorescence, and dynamic light scattering methods. This led to the observations that (1) the zigzag segment count and specific length drop from the range of control values to almost zero when the relative concentration of FMN to BSA goes from 1:1 to 4:1; (2) increasing concentrations of $AlCl_3$ result in the gradual decline in zigzag parameters as the zeta potential of BSA grows neutral and then positive; (3) adding $FeCl_3$ affects zeta potential less, but also results in the formation of large colloidal particles of iron hydroxide, which start reducing zigzag parameters at $FeCl_3$:BSA concentration ratios of 25:1 or above.

In light of a recent study [2] that brings attention to the mutually attracting and clustering behavior of negatively charged particles in aqueous solutions, it is worth considering the possibility that such phenomena may contribute to the above observations. Specifically, clusters can be formed even from dissimilar particles, so long as the sign of their zeta potential is the same, and negatively charged biomolecules can gather into droplet-like condensates even in the presence of salt ions [2]. Since both FMN and BSA have a negative potential, they would likely be located nearby in those droplets, and upon drying, this might quickly violate the crystallization conditions. Also, traditionally, one would expect BSA to be stable when having either positive or negative potential, and precipitate when its potential is neutralized by Al^{3+}. However, a minimum of zigzag parameters at those concentrations is not observed. Instead, the parameters' gradual decline appears to correlate with the potential becoming more positive, which in the study [2] is shown to reduce the tendency to form clusters and cause the particles to be more uniformly distributed throughout the solution. Unlike the negatively charged FMN, the colloidal aggregates of $Fe(OH)_3$ are neutral and, therefore, will not tend to form droplets with BSA, but instead precipitate; as such, it might take a greater amount of this "random debris" to interfere with the crystallization to the same extent as the FMN particles located right beside BSA.

[1] O. A. Gorobchenko, D. M. Glibitskiy, O. T. Nikolov, T. A. Cheipesh, T. N. Dzhimieva, I. S. Zaitseva, A. D. Roshal, M. A. Semenov and G. M. Glibitskiy, Low Temp. Phys. 50, 48 (2024). https://doi.org/10.1063/10.0023892
[2] S. Wang, R. Walker-Gibbons, B. Watkins, M. Flynn and M. Krishnan, Nat. Nanotechnol. (2024). https://doi.org/10.1038/s41565-024-01621-5

Immobilization of glucose oxidase on graphene using 1-pyrenebutanoic acid succinimide ester: molecular dynamics study

M. V. Karachevtsev, V. A. Karachevtsev

B.Verkin Institute for Low Temperature Physics and Engineering of NAS of Ukraine,
47 Nauky Ave., Kharkiv, 61103, Ukraine
e-mail: mkarachevtsev@ilt.kharkov.ua

In an elaboration of biological sensors involving graphene one of the important problems that needs to be solved is related to the immobilization of the recognizing molecule on the carbon surface. As enzymes are often exploited as possible recognition elements in biosensors, their immobilization on the nanotube surface needs to be investigated in detail. The simple method of enzyme adsorption using direct immobilization on graphene cannot be applied as its interaction with the carbon surface significantly decreases the enzyme activity. One of the real ways to solve this problem is related to the use of molecular interfaces. Earlier an effective noncovalent way to functionalize carbon nanotube by organic molecules was suggested a bifunctional molecule containing succinylimide ester and a pyrene moiety to bind proteins to the nanotube surface [1, 2]. Pyrene attaches to the nanotube surface employing the π-π stacking and hydrophobic interactions and does not significantly disturb the electronic structure of the nanotube.

In this work, we present results of simulating an immobilization of glucose oxidase (GOX) on graphene using 1-pyrenebutanoic acid succinimide ester (PSE) in an aqueous environment by exploiting molecular dynamics study. The structures of the nanobiohybrid and the interaction energy between components were determined.

In the graphene-PSE-GOX complex, the interaction energy between graphene and GOX with PSE ranges from -27 to -32 kcal/mol. Note that this energy is mainly determined by the contribution of the interaction energy of pyrene with graphene. This value is essentially lower than the interaction energy of GOX and graphene without the interface (~-110 kcal/mol). The molecular dynamics simulation also shows that only one PSE molecule used as a linker between graphene and GOX is enough to keep GOX near the carbon surface in the water surrounding and prevent the strong interaction between graphene and GOX. We also simulated the more complex formed by two sheets of graphene and two molecules of GOX. In this complex, the energy value of GOX binding with two sheets when the enzyme is placed between two graphene sheets is almost doubled. The obtained results can be used in the biosensor elaboration for the detection of glucose, lactate, and other compounds.

This work has been partly supported by funding from the National Academy of Sciences of Ukraine (Grant 0123U100628).

[1] R. J. Chen, Y. Zhang, D. Wang, H. Dai, J. Am. Chem. Soc. 123, 3838 (2001) https://doi.org/10.1021/ja010172b
[2] V. A. Karachevtsev, S. G. Stepanian, A. Yu. Glamazda, M.V. Karachevtsev, V. V. Eremenko, O. S. Lytvyn, L. Adamowicz, J. Phys. Chem. C 115, 21072 (2011) https://doi.org/10.1021/jp207916d

Fluorescence responses of silica gel films with two coumarin dyes measured on a portable endogenous acetone analyzer in the microconcentration range

Ya. P. Lazorenko, V. P. Mitsai

Institute of Magnetism NAS of Ukraine and MES of Ukraine,
36-b Akad. Vernadskogo blvd., Kyiv, 03142, Ukraine
e-mail: lazorenko85@gmail.com

Quantitative determination of metabolites-biomarkers in human exhaled air is promising for non-invasive diagnosis and monitoring of human diseases. The complexity of the task is due to the multi-component nature of exhaled air, very low concentrations of metabolites, and high humidity. For example, in diabetics, there is an increase in exhaled acetone levels above 1.8 ppm (molecules per million) [1]. An interesting solution to this problem from the point of view of practical application may be the use of fluorescent sensors, especially due to the high sensitivity of fluorescent analysis methods and compact dimensions. In our previous work [2], the fluorescence quenching of one of the coumarin fluorophores (coumarin 4) immobilized in porous silica films upon interaction with acetone molecules adsorbed from air was revealed. The purpose of this work was to create a portable fluorescent analyzer of endogenous acetone and to detect with its help the fluorescent response of sensor films to the microconcentrations of acetone in model mixtures of exhaled air.

Mesoporous silica films with two immobilized organic fluorescent dyes, 7-(diethylamino)-4-methylcoumarin or 7-hydroxy-4-methylcoumarin, were studied as samples of sensor films. The films were created by fixing a monolayer of silica gel particles on a glass substrate with a thin layer of an alkaline solution of sodium and potassium silicates, followed by dehydration. The model exhaled air mixtures were synthesized by the static volumetric method of preparation of calibration gas mixtures.

A portable fluorimetric acetone analyzer with film sensing elements was developed and produced. Based on the spectrometric measurements of the investigated film samples, the analyzer was designed to have fluorescence excitation wavelengths of 360-370 nm and registration wavelengths of 420 nm and more. A UV light-emitting diode was used as an excitation source and a photodiode as a photodetector, also appropriate light filters were used. The samples were placed in the quartz cell of the analyzer, through which one liter of the model exhaled air mixture was pumped during the measurement at a certain period. The signal from the photodiode was transmitted to the amplifier and the analog-to-digital converter, with subsequent transmission from the microcontroller to a computer in real-time using specially developed programs.

Measurements of fluorescence kinetics on the developed analyzer for films with these two coumarins showed a change in fluorescence intensity upon absorption of acetone molecules in the range of 0-10 ppm, which was proportional to the concentration. When pumping clean air, fluorescence was restored. For samples with 7-(diethylamino)-4-methylcoumarin, the changes ranged from 0.09% to 0.25%, with 7-hydroxy-4-methylcoumarin from 2.7% to 3.7%, for 2.5 ppm and 10 ppm, respectively. The root mean square error is estimated to be 12.9% for N = 5 measurements for 10 ppm. The change in the fluorescence of organic dye molecules is explained by the dynamic quenching of fluorescence caused by the formation of exciplexes with acetone molecules.

[1] M. R. Jadhav, P.R. Wankhede, S. Srivastava, H. N. Bhargaw, and S. Singh, Diabetes Metab. Syndr.: Clin. Res. Rev. 18(1), 102931 (2024). https://doi.org/10.1016/j.dsx.2023.102931.
[2] V. P. Mitsai, Ya. P. Lazorenko, A. G. Misyura, and S. O. Mamilov, Nanosistemi, Nanomateriali, Nanotehnologii 19(4), 941 (2021). https://doi.org/10.15407/nnn.19.04.941.

Study of fluorescent responses of film polymer structures with dyes and quantum dots using a model of a portable analyzer of endogenous ammonia trace concentrations

V. P. Mitsai, Ya. P. Lazorenko

Institute of Magnetism NAS of Ukraine and MES of Ukraine,
36-b Akad. Vernadskogo blvd., Kyiv, 03142, Ukraine
e-mail: vitapok@i.ua

Today, much attention is paid to the study of hybrid nanostructures, consisting of semiconductor nanocrystals and organic molecules, and their application in various fields. One of the areas of application of similar structures can be considered as means of non-invasive diagnosis of diseases based on the analysis of exhaled air, which contains a large number of various volatile substances. For some of them, a correlation of their defined concentrations with specific diseases was found. One such substance is endogenous ammonia (NH_3), which is a biomarker of a number of diseases, such as kidney failure, liver cirrhosis, lung cancer, etc. However, the use of these materials for the detection of volatile substances in human exhalation requires certain characteristics, first of all, it is quite high sensitivity of such sensory materials to analyte substances, since the concentration of such substances lies in the range of ppm units (parts per million). In particular, the concentration of ammonia in the breath of a sick person is usually more than 1.5 ppm [1]. Among other characteristics the selectivity in relation to other substances and compactness, as an alternative to complex laboratory analytical equipment, is not less important.

In previous work [2], we have discovered the sensitivity of the organic fluorescent coumarin dye (coumarin 7 from [2]) in a complex with a CdTe nanocrystal to ammonia molecules in a gas-air sample. This paper presents the results of the study of fluorescent responses of hybrid polymer structures with a fluorescent complex quantum dot – the coumarin dye molecule in adsorbate matrices, to volatile ammonia molecules obtained using a model of a portable fluorescent ammonia analyzer developed by us.

The layout of the analyzer was developed by analogy with the principle of operation of the fluorimeter, as an exciting source of radiation an LED with a wavelength of l_{fl} = 450 nm was used. The layout uses an orange (OS-12) and a purple (PS-11) color filters, which ensured the maximum sensitivity of the analyzer to ammonia. Fluorescence was recorded in the wavelength range of 540-600nm. The fluorescence optical signal was read by a BPW21R photodiode, amplified by an analog signal amplifier, then fed to an AD7793 ADC and processed by an STM-32F103 microcontroller and displayed on a PC screen using the developed software. The film polymer structure was formed on glass substrates in a layer-by-layer manner. Ethylene vinylacetate (EVA) polymer covered with a layer of silicon dioxide was used as a polymer matrix. A fluorescent complex of the coumarin dye (l_l = 508 nm) with colloidal semiconductor nanocrystals CdTe (l_{fl} = 530 nm) was used as a signal element. The kinetics of the sample fluorescence intensity was measured at the following concentrations of ammonia vapors in the air sample: 10ppm, 7.5ppm, 5ppm. As a result of the experiment, the response of the film sample to the specified concentrations of ammonia was obtained, which had the form of a drop in the fluorescence intensity of the sample: for 10ppm NH_3, the fluorescence signal (intensity) of the sample dropped by 1.17% relative to the initial signal, for 7.5ppm it dropped by 1.04% and for 5ppm fell by 0.61%. Therefore, there is an increase in response, i.e., a drop in the fluorescence signal of the sample with an increase in the concentration of ammonia in the sample. The decrease in the fluorescence intensity of the coumarin-CdTe complex upon interaction with ammonia is probably related to the formation of non-fluorescent complexes between them, which occurs with fluorescence static quenching.

[1] S. Kumar et al., Sens. Diagn. 2, 1256 (2023).
[2] V. P. Mitsai et al., J. NanoElectron. Phys., 8(4), 04032-1 (2016).

Binding of Pheophorbide-*a* and its Derivatives to Biopolymers of Different Composition and Secondary Structure: a Spectroscopic Study

O. A. Ryazanova[1], I. M. Voloshin[1], L. V. Dubey[2], I. Ya. Dubey[2], and V. A. Karachevtsev[1]

[1] B.Verkin Institute for Low Temperature Physics and Engineering of NAS of Ukraine, 47 Nauky Ave., Kharkiv, 61103, Ukraine
[2] Institute of Molecular Biology and Genetics of NAS of Ukraine, 150 Zabolotnogo str., Kyiv, 03143, Ukraine
e-mail: ryazanova@ilt.kharkov.ua

Pheophorbide-*a* (Pheo-*a*, Fig. 1) is a natural anionic chlorophyll *a* catabolite characterized by the chlorine-type visible absorption spectrum with high molar extinction coefficient in the red region where the transparency of the tissues to the light increases considerably. It is selectively accumulated in the tumor cells and actively generates singlet oxygen when irradiated with red light that determines its strong photodynamic therapy (PDT) effect on the cancer cells *in vitro* and *in vivo*. Pheo-*a* also can be also applied for the molecular recognition of G-quadruplexes. Since the dimerization and aggregation of the dye in aqueous solutions substantially reduce its photodynamic activity, the peculiarities of the structure and physical properties of complexes formed by Pheo-*a* and its derivatives with different biological macromolecules found in the blood and body tissue cells are of great interest being subject of intensive study for last many years.

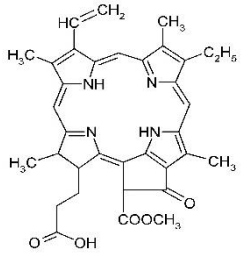

Fig. 1. Structure of Pheo-*a*.

Results of a comprehensive spectroscopic study on binding of Pheo-*a*, its cationic (CatPheo-*a*) and neutral (MePheo-*a*) derivatives, as well as Pheo-*a* conjugate with cationic intercalative aminophenazinium dye linked via polymethylene chain (Pheo-Pzn) to inorganic polyphosphate (poly(P)), poly-L-lysine (PLL) and nucleic acids of various primary and secondary structures (*ds*-poly(A)×poly(U), *ds*-poly(G)×poly(C), *fs*-poly(G), antiparallel telomeric DNA quadruplex Tel22) in solutions of low (1 mM Na^+) and near-physiological (0.15 M Na^+) ionic strengths [1-6] are summarized. Investigations were carried out in a wide range of *P/D* ratios using techniques of absorption, polarized fluorescence, fluorimetric titration, absorption and fluorescence melting, and resonance light scattering. Types of the dye binding to the biopolymers and the features of its aggregation were established. As much as Pheo-Pzn discriminates between duplex and quadruplex polynucleotides exhibiting 50-fold emission increase upon binding to quadruplex poly(G) and quenched fluorescence in the case of *ds*-polymers, it is proposed as efficient fluorescent probe for the recognition of G-quadruplex structures.

[1] O. Ryazanova, I. Voloshin, I. Dubey, L. Dubey, V. Zozulya, Ann. N. Y. Acad. Sci. 1130, 293 (2008), https://doi.org/10.1196/annals.1430.033.
[2] O. Ryazanova, V. Zozulya, I. Voloshin, V. Karachevtsev, Mol. Cryst. Liq. Cryst. 749(1) 33 (2022) https://doi.org/10.1080/15421406.2022.2068469
[3] O.A. Ryazanova, I.M. Voloshin, I.Ya. Dubey, L.V. Dubey, V.N. Zozulya, IFMBE Proc. (Springer) 20, 397 (2008). https://doi.org/10.1007/978-3-540-69367-3_107.
[4] O.A. Ryazanova, I.M. Voloshin, L.V. Dubey, V.N. Zozulya, Biophys. Bull. 23(2), 20 (2009)
[5] O.A. Ryazanova, V.N. Zozulya, I.M. Voloshin, L.V. Dubey, M.M. Ilchenko, I.Ya. Dubey, V.A. Karachevtsev, J. Mol. Struct. 1214 (19) (2020) https://doi.org/10.1016/j.molstruc.2020.128218
[6] O.A. Ryazanova et al., Biopolym. Cell 35(2), 129 (2019) http://dx.doi.org/10.7124/bc.00099E.

Mass spectrometric probing of nanocomposite of methylene blue with molybdenum disulfide flakes

V. S. Shelkovsky[1], O. A. Boryak[1], M. V. Kosevich[1], P. O. Kuzema[2], V. A. Karachevtsev[1]

[1] B. Verkin Institute for Low Temperature Physics and Engineering of the NAS of Ukraine, 47 Nauky Ave., Kharkiv, 61103, Ukraine
[2] Chuiko Institute of Surface Chemistry of the NAS of Ukraine, 17 General Naumov Str., Kyiv 03164, Ukraine
e-mail: shelkovsky57@gmail.com

Recently, in the search of new nanotechnology-based oncotherapy approaches, it was proposed to evaluate multifunctional nanoplatforms which would provide several different mechanisms of anticancer action simultaneously [1]. Guided by this trend, in this study we considered a combination of methylene blue (MB) dye applied in photodynamic therapy (PDT) with MoS_2 promising in photothermal therapy (PTT). The MB-MoS_2 nanocomposite was prepared by sonication of the components mixture in water, which is known to exfoliate MoS_2 to flakes available for adsorption of organic compounds. Thus produced sample was probed by laser desorption/ionization (LDI) mass spectrometry which selection was justified by our earlier observations of the sensitivity of certain mass spectral parameters to the state of MB at the nanostructured substrates, its aggregation and redox transformations [2, 3].

In the LDI mass spectra of the MB-MoS_2 dried sample, recorded in positive ion mode, a single abundant peaks envelope with isotopic distribution characteristic of intact cation of MB (the first monoisotopic peak at m/z 284) was present. This spectral feature correlates with the monomeric adsorption of MB cations on the nanostructured surfaces [2, 3]. It is known that namely monomeric form of MB is required for realization of a PDT mechanism of singlet oxygen production, while redox processes in the aggregates of MB prevent this mechanism. It is presumed that MB cations are adsorbed on the partially negatively charged surface of MoS_2 (loosing the chlorine anion of the MB organic salt). Existence of the “preformed” cations provides their easy desorption by laser irradiation under LDI conditions. The efficiency of the cations desorption increased dramatically with increase of the irradiating laser power, which was caused, obviously, by increase of heating of the exfoliated MoS_2 flakes. This thermal effect may correlate with PTT potential of MoS_2 nanomaterial. Thus, two above described features of the LDI mass spectra may be used for evaluation of some properties of the MB-MoS_2 nanoplatform.

For comparison, a composite of MB with graphene oxide (GO) was tested by LDI at similar conditions. The LDI mass spectra of the MB-GO composite were qualitatively different: the spectra contained products of fragmentation of MB and no significant increase of MB cations abundance was observed. Obviously, the fragmentation was facilitated by MB interactions with oxygen-containing groups of GO, since it was not recorded earlier under LDI of MB from pure carbon surfaces of carbon nanotubes [3]. The examples presented demonstrate approaches to mass spectrometric examination of nanocomposites.

This work was supported by a grant № 0123U100628 of the NAS of Ukraine.

[1] Q. Wang, G. Xia, J. Li, L. Yuan, S. Yu, D. Li, N. Yang, Z. Fan, and J. Li, Int. J. Mol. Sci. 24, 16949 **(**2023). https://doi.org/10.3390/ijms242316949
[2] V.S. Shelkovsky, M.V. Kosevich, O.A. Boryak, V.V. Chagovets, I.V. Shmigol, and V.A. Pokrovskiy V.A. RSC Advances. 4(104) 60260 (2014). https://doi.org/10.1039/c4ra09592h
[3] V.V. Chagovets, M.V. Kosevich, S.G. Stepanian, O.A. Boryak, V.S. Shelkovsky, V.V. Orlov, V.S. Leontiev, V.A. Pokrovskiy, L. Adamowicz, and V.A. Karachevtsev, J. Phys. Chem. C. 116, 20579 (2012). https://doi.org/10.1021/jp306333c

The comparative characterization of DNA:TiO_2 nanoparticle and DNA:MoS_2 nanoparticle nanoassemblies colloidal solutions investigated by dynamic light scattering method

A. Yu. Svidzerska[1], V. A. Valeev[1], A. N. Lahuta[2,3], S. I. Petrushenko[2], A. Yu. Glamazda[1], V. A. Karachevtsev[1]

[1] B.Verkin Institute for Low Temperature Physics and Engineering of NAS of Ukraine, 47 Nauky Ave., Kharkiv, 61103, Ukraine
[2] V.N. Karazin Kharkiv National University, 4 Svobody Square, Kharkiv, 61022, Ukraine
[3] Aston University, Birmingham B4 7ET, U.K.
e-mail: sviderska@ilt.kharkov.ua

The present work is dedicated to compare of nanopaticle (NP) size and temperature stability characteristic of three different colloidal solutions contained DNA and inorganic nanoparticles. As a method the dynamic light scattering (DLS) measurements were performed in the temperature range of 25–90 ^{0}C in the cacodylate buffer. Accordingly to previous investigation [1] it seems reasonable that we need used the DLS size distribution by number.

The first one of colloidal system was the DNA:TiO_2 NP nanoassemblies solution at pH 5.0 (Fig.1a). We suppose that addition of TiO_2 NPs and heating of colloidal system leads to appearance of untwisted strands which capture the neighboring nanoassemblies. This leads to formation of larger nanoaggregates which can consist of more than one TiO_2 NP or large amount of DNA molecules are associated with TiO_2 NPs. The number-based average diameter of the DNA:TiO_2 NP nanoassemblies is of about 80 nm at 25 ^{0}C and of about 210 nm at 90 ^{0}C.

In the case of pH 7.0 the distribution by number for DNA:TiO_2 NP nanoassemblies system is different (Fig.1b). The number-based average diameter of the DNA:TiO_2 NP nanoassemblies is ~ 100 nm at 25 ^{0}C and ~ 110 nm at 90 ^{0}C. There are observed minor peaks (~ 20 nm) but the main peak looks similar to that one for pure TiO_2 NP and DNA:TiO_2 NP nanoassemblies (pH 5.0) colloidal solutions at 25 ^{0}C. So, at pH 7.0 we didn't observed formation of larger nanoaggregates as in the case of pH 5.0. In turn it may be related to strong binding of DNA macromolecules to TiO_2 NPs.

As regards DNA:MoS_2 NP nanoassemblies colloidal solution at pH 7.0 (Fig.1c), the number-based average diameter of the DNA:MoS_2 NP nanoassemblies is of about 90 nm in all temperature range. So, for this system at pH 7.0 we didn't observed larger nanoaggregates.

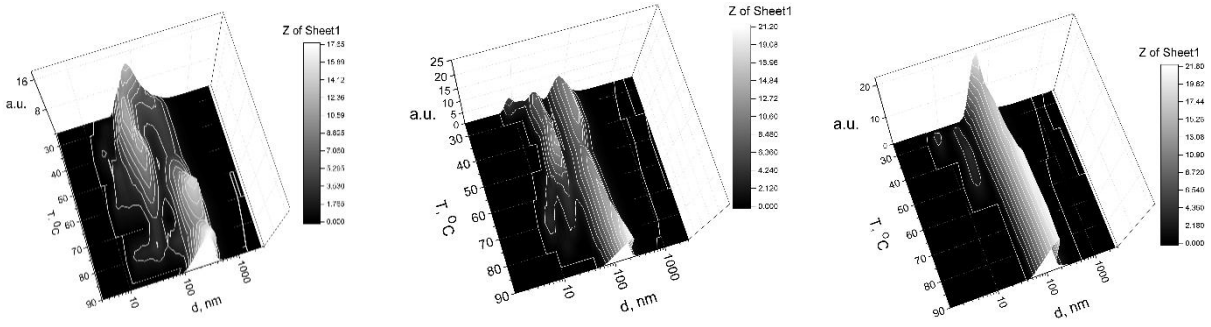

a) b) c)

Fig. 1. The size distributions by number at the different temperatures (T = 25–90 ^{0}C – distribution map) for a) DNA:TiO_2 NP nanoassemblies colloidal solution at pH 5.0, at the temperature of about 60 ^{0}C the surface of map gradually "turns into" larger nanoaggregates; b) DNA:TiO_2 NP nanoassemblies colloidal solution at pH 7.0; c) DNA:MoS_2 NP nanoassemblies colloidal solution at pH 7.0.

[1] B. Krause, T. Meyer et al., RSC Adv. 8, 14377 (2018).

Effect of TiO_2 nanoparticles on the thermal stability of native DNA under conditions close to physiological ones

E. L. Usenko, A. Yu. Glamazda, V. A. Valeev, V. A. Karachevtsev

B. Verkin Institute for Low Temperature Physics and Engineering of NAS of Ukraine,
47 Nauky Ave., Kharkiv, 61103, Ukraine
e-mail: usenko@ilt.kharkov.ua

At the present, TiO_2 nanoparticles (NPs) are quite intensively used in the environmental engineering, cosmetology, pharmaceuticals, and medicine [1]. But, despite the growing demand for these NPs in production and medicine, numerous works are currently appeared, indicating their possible negative impact on human health, as well as their genotoxicity [2].

The present work is devoted to the study of the thermostability of native DNA upon its binding to TiO_2 NPs depending on their concentration at near physiological ionic conditions (0.1 M Na^+, pH 7) using thermal denaturation method.

The analysis of the DNA melting curves in the presence of TiO_2 NPs revealed a temperature range where the DNA absorption decreases. The effect observed can be explained by the availability of unwound DNA regions which can bind to NPs and form a more ordered structure on the NP surface as compared with initial double-stranded DNA. The injection of 2.5×10^{-5} M of TiO_2 NPs into DNA suspension leads to a decrease in the DNA melting temperature by ~ 6°C. It is assumed that the effect is caused by the predominant interaction of the DNA nitrogenous bases with these NPs. It should be noted that in our previous studies performed at pH 5, minor changes in the DNA melting temperature were observed in the entire studied range of TiO_2 concentrations [3]. The difference in the binding of DNA to TiO_2 NPs at pH5 and 7 are discussed.

The results obtained can be used to design hygiene products, as well as in medicine and pharmacology.

[1] S. Shabbir, M. Fakhar-e-Alam Kulyar, Z. A. Bhutta, P. Boruah, and M. Asif, BioNanoScience. 11, 621 (2021). https://doi.org/10.1007/s12668-021-00836-3.
[2] S. Patel, P. Patel, and S.R. Bakshi, Cytotechnology. 69, 245 (2017). https//doi.org/10.1007/s10616-016-0054-3.
[3] E. Usenko, A. Glamazda, V. Valeev, A. Svidzerska, A. Laguta, S. Petrushenko, and V. Karachevtsev, Appl. Phys.A. 128, Article number: 900 (2022). https://doi.org/10.1007/s00339-022-06043-5.

PEGylation of cytosine nucleic acid base: experiment and modeling

V. G. Zobnina, M. V. Kosevich

B. Verkin Institute for Low Temperature Physics and Engineering of the NAS of Ukraine,
47 Nauky Ave., Kharkiv, 61103, Ukraine
e-mail: valezobnina@gmail.com

Organic polymers polyethylene glycols (PEG), polydispersed polyethers which chains are built from different number (n) of monomers $HO{-}(CH_2{-}CH_2{-}O)_n{-}H$, find versatile applications as green solvents, cryoprotectos, excipients, components of nanosomes, hydrogels, biobetters, and as PEGylation agent. PEGylation, that is binding of PEGs to biomolecules or nanoparticles, is used for drug delivery, in particular in elaboration of anti-SARS-CoVID vaccines.

In our previous investigations, using combination of experimental mass spectrometric technique and molecular dynamics computer simulations we have demonstrated that molecular mechanism of action of PEGs consists in their wrapping over both positively and negatively charged monoatomic ions and amino acids ions [1]. Here we apply the same approach to study PEGylation of nucleic acid nitrogen base Cytosine (Cyt). Three aspects of the problem are addressed. Firstly, formation of stable complexes of PEG-400 oligomers (labeled as M_n) with a set of Cyt derivatives – Cyt, m^1Cyt, m^5Cyt, Br^5Cyt - was demonstrated experimentally by means of electrospray ionization mass spectrometry. As an example, in the spectrum of PEG-Br^5Cyt system shown in Fig. 1 a set of $M_n{\bullet}Br^5Cyt{\bullet}H^+$ noncovalent complexes was detected. Characteristic isotopic distribution of $^{79}Br/^{81}Br$ unambiguously evidenced the inclusion of Br^5Cyt into the clusters.

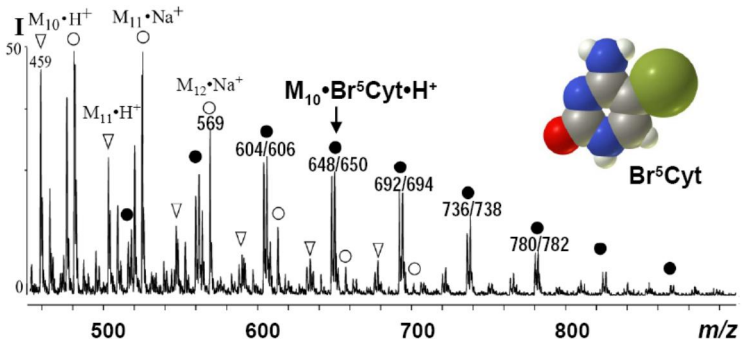

Fig. 1. Positive ion electrospray mass spectrum of PEG-Br^5Cyt system. ● - $M_n{\bullet}Br^5Cyt{\bullet}H^+$ clusters, Ñ - $M_n{\bullet}H^+$, o – $M_n{\bullet}Na^+$.

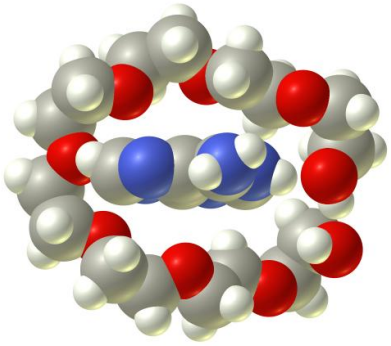

Fig. 2. Complex of Cytosine (centered) with M_8 of PEG.

Secondly, interaction of neutral or protonated Cyt with small PEG oligomers in the gas phase was modeled by molecular dynamics (CHARMM force field). Similar to other studied systems, wrapping of the PEG chains over the nitrogen base occurs with time of modeling; a typical structure of Cyt-PEG_n complex is presented in Fig. 2.

Thirdly, more complicated task of modeling of desolvation of a cluster-containing methanol droplet, which mimics electrospray process, was performed. It was shown that the "wrapped" cluster structure is preserved on transfer of the Cyt-PEG complex from the liquid to the gas phase.

The acquired knowledge on the self-assembling of the complexes of PEG_n oligomers with small biomolecules is in demand for further development of PEGylation procedures.

[1] V. G. Zobnina, M. V. Kosevich, V. V. Chagovets, and O. A. Boryak. Study of nanocomposites of amino acids and organic polyethers by means of mass spectrometry and molecular dynamics simulation. In: Nanomaterials Imaging Techniques, Surface Studies, and Applications. Springer Proceedings in Physics. 146 (Springer Science, New York 2013).
https://doi.org/10.1007/978-1-4614-7675-7_22

The effect of glycocalyx on the partitioning of antimicrobial peptides into plasma membrane of erythrocytes

O. Yu. Borikov, D. A. Liadov, V. P. Berest

V.N. Karazin Kharkiv National University, 4 Svobody Sq., Kharkiv, 61022, Ukraine
e-mail: biophysics@karazin.ua

The glycocalyx is a layer of carbohydrate-rich molecules, including glycoproteins and glycolipids that covers the outer surface of the cell membrane. In red blood cells (RBCs), the glycocalyx plays a significant role in various cellular functions, including influencing the electrophoretic mobility and zeta potential of the cells. The glycocalyx contributes to the overall negative charge on the RBC surface and the zeta potential due to the presence of sialic acid residues and other negatively charged molecules. A higher density of negatively charged molecules in the glycocalyx increases the absolute value of zeta potential, leading to greater electrostatic repulsion between cells. This repulsion helps to keep the RBCs suspended and prevents cell aggregation. A thicker glycocalyx can also influence mobility. While it increases the surface charge, it can also introduce additional drag, potentially balancing out the increased mobility from the higher charge density. The glycocalyx attracts a layer of water molecules, forming a hydration shell around the RBCs. This shell contributes to the effective zeta potential by stabilizing the negative charges and influencing the ionic environment near the cell surface. The glycocalyx can interact with plasma proteins, which can either shield or enhance the surface charge, thereby affecting the zeta potential.

Changes in the glycocalyx can affect how cells interact with each other and their environment. For example, a reduced zeta potential may increase cell adhesion, influencing processes like blood clotting or immune cell recruitment. In endothelial cells, changes in the glycocalyx can impact the vascular barrier function, affecting fluid and molecule exchange between blood and tissues. Understanding how the glycocalyx affects electrophoretic mobility and zeta potential can inform the design of drug delivery systems, especially those targeting specific cell types or tissues. The charges on molecules of glycocalyx could directly affect the way small molecules or active pharmaceutical ingredients adsorb on and partition into the plasma membrane of RBCs. The interplay between the cell surface charge and the redistribution efficiency is of particular importance for charged amphipathic molecules of antimicrobial membrane active peptides.

In this work to determine the role of sialic acids in the formation of the total surface charge of erythrocytes and its influence on antimicrobial peptide gramicidin S insertion into plasma membrane of RBCs, the electrokinetic indicators, the electrophoretic speed and ζ-potential of intact human erythrocytes and those after enzymatic modification of the membrane surface with trypsin and neuraminidase were measured. It was shown that after treatment with trypsin, the ζ-potential of erythrocytes decreases by almost 40% compared to intact cells and is 12.33±0.61 mV. Incubation of trypsin-modified erythrocytes with gramicidin S led to a further decrease in ζ-potential regardless of concentration in the range from 5 to 20 μg/ml. The latter may indicate that under conditions of loss of a part of sialic acids and a decrease in the overall negative charge of the surface of erythrocytes, the number of adsorbed gramicidin S molecules necessary for its neutralization also decreases.

In summary, it was shown that the negative ζ-potential of erythrocytes is primarily caused by the presence of carboxyl groups of sialic acids, which are part of the carbohydrate part of glycoproteins and glycolipids. Gramicidin S, which contains positively charged amino groups of ornithine residues, being adsorbed on the membrane, reduces the ζ-potential of erythrocytes due to partial neutralization of the negative surface charge.

MATERIALS SCIENCE

First-principles study of point defects in C-doped yttrium aluminum garnet

K. V. Hermash[1], D. V. Fil[1,2]

[1] Institute for Single Crystals of NAS of Ukraine, 60 Nauky Avenue, Kharkiv, 61072, Ukraine
[2] Karazin Kharkiv National University, 4 Svobody Square, Kharkiv, 61022, Ukraine
e-mail: kostiantyn.hermash@gmail.com

This work is devoted to the investigation of isolated and complex defects in yttrium aluminum garnet ($Y_3Al_5O_{12}$, YAG). We consider oxygen, aluminum, and yttrium site vacancies, carbon substitution of oxygen and aluminum, and interstitial carbon. Aluminum atoms in YAG occupy two distinct positions: one within a tetrahedral oxygen environment, and the other within an octahedral oxygen environment. Both positions are taken into account. The following complex defects are considered: 1) a C substitution of O and an oxygen site vacancy; 2) a C substitution of Al and an oxygen site vacancy. The defect formation energies and the concentrations of different types of defects in several charge states are calculated.

Our main tool for doing this work is the SIESTA computer program [1]. It is based on the density functional theory. To use this program, one can take a unit cell and set coordinates of all atoms. Defects are modeled by adding/removing some atoms to/from the unit cell and then the structure optimization is fulfilled.

The formation energy of a defect, where an atom of x is removed from the unit cell, and an atom of y is added to the unit cell, is given by the formula

$$E_i = E_{def.\ cell} - E_{perf.\ cell} + \mu_x - \mu_y + q\mu_e + E_M.$$

Here i stands for a defect type, $E_{def.\ cell}$ is the total energy of a defective cell, $E_{perf.\ cell}$ is the total energy of a perfect cell, μ_x is the chemical potential of an atom of x, μ_y is the chemical potential of an atom of y, μ_e is the chemical potential of electrons, E_M is the Madelung energy, and q is the charge of a defect (in units of e, the elementary charge). Total energies of defective and perfect unit cells are calculated by the SIESTA program.

Concentration of defects of type i is evaluated by the formula:

$$n_i = (1/\Omega_0)N_i \exp(-E_i/[k_B T]),$$

where Ω_0 is the unit cell volume, N_i is the number of ways to place a defect of type i into the unit cell, and T is the temperature of sintering or annealing.

The chemical potential of electrons is found from the charge neutrality equation

$$\sum_i q_i n_i + n_h - n_e = 0,$$

where n_e and n_h are the concentrations of free electrons and holes, correspondingly, and the sum is taken over all kinds of defects.

We demonstrate how doping with C changes the concentration of anion and cation vacancies in YAG. We find that the concentration of C_O-V_O complex defects is the highest one under the reducing conditions, while the concentration of C_{Al}-V_O complex defects reaches its maximum at an intermediate value of the oxygen chemical potential. The defect energy levels in the band gap caused by different types of point defects are calculated.

This work was performed using computational facilities of the Joint computational cluster of State Scientific Institution "Institute for Single Crystals" and Institute for Scintillation Materials of National Academy of Sciences of Ukraine incorporated into Ukrainian National Grid.

[1] J. M. Soler, E. Artacho, J. D. Gale, A. García, J. Junquera, P. Ordejón and D. Sánchez-Portal, The SIESTA method for ab initio order-N materials simulation, J. Phys.: Condens. Matter. 14, P. 2745–2779 (2002). https://doi.org/10.1088/0953-8984/14/11/302.

Ring and linear structures of CdTe clusters

I. V. Semkiv[1], M. Y. Rudysh[2, 3], R. S. Yavorskyi[4], N. Y. Kashuba[1], P. A. Shchepanskyi[2], A. I. Kashuba[1]

[1] Lviv Polytechnic National University, Bandera Str. 12, 79013 Lviv, Ukraine
[2] Ivan Franko National University of Lviv, Dragomanov Str. 19, 79000 Lviv, Ukraine
[3] Jan Długosz University in Częstochowa, Armii Krajowej Al.,13/15, 42-200 Częstochowa, Poland
[4] Vasyl Stefanyk Precarpathian National University,
Shevchenko Str. 57, 76018 Ivano-Frankivsk, Ukraine
e-mail: andrii.i.kashuba@lpnu.ua

We report the results of an *ab initio* study of the linear and ring structures of cadmium telluride clusters $[CdTe]_n$ (Cd_nTe_n) $n \leq 10$ using the density functional GGA+PBE with Hubbard corrections (GGA+*U*). We optimize linear and ring isomers for each size to obtain the lowest energy structures and to understand the growth behavior. The convergence criteria for energy and force are set to $\sim 3 \cdot 10^{-4}$ eV and $\sim 5 \cdot 10^{-2}$ eV/Å, respectively, for all calculations. To accurately describe the electronic spectrum, two Hubbard corrections were selected for the studied objects: for *d*-orbitals Cd (U_{4d}= 5.80 eV) and *p*-orbitals Te (U_{5p}= 2.55 eV).

The gap between the highest occupied molecular orbital (HOMO) and the lowest unoccupied molecular orbital (LUMO), binding energy and electronegativity of the stoichiometric Cd_nTe_n clusters have been calculated. These results for the different properties of CdTe clusters will give clear information enabling the design of new materials with potential importance in thin-film solar cells [1]. Cd_nTe_n clusters are found to have a small (linear clusters)/high (ring clusters) highest-occupied–lowest unoccupied molecular orbital (HOMO-LUMO) gap (see Fig. 1). Ring structures are not planar suggesting that the bonding nature in Cd_nTe_n clusters has some covalent character. The ring type structure of the Cd_nTe_n cluster with n = 3 is found to be the most favorable (n= 6 for linear structure of the Cd_nTe_n cluster).

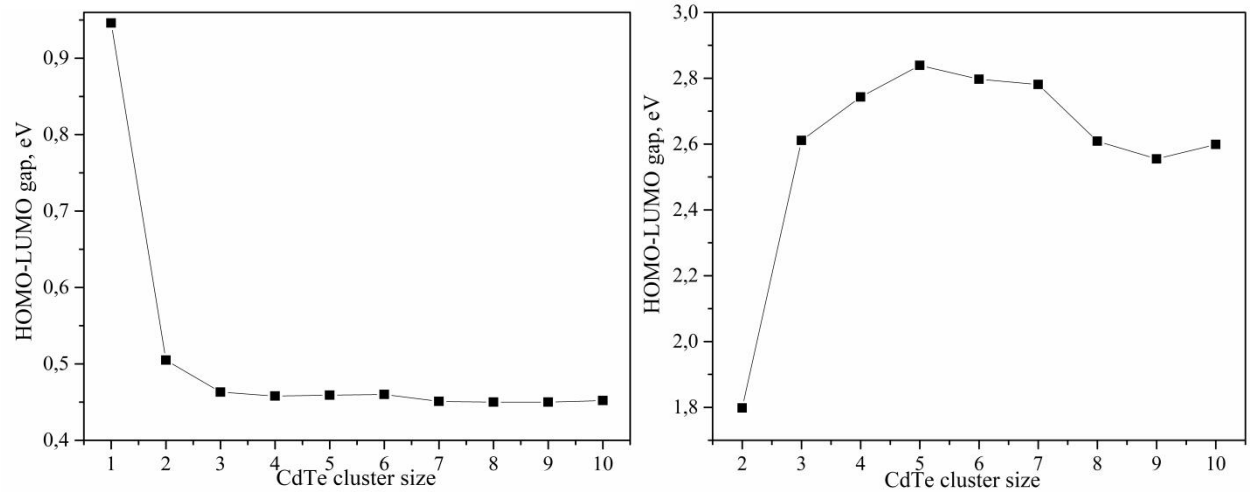

ab

Fig. 1. HOMO–LUMO gaps for the linear (*a*) and ring (*b*) CdTe clusters.

[1] S. Sriram and R. Chandiramouli, Res. Chem. Intermed. 41, 2095 (2015). https://doi.org/10.1007/s11164-013-1334-6.

Mechanical properties of high-entropy $CoCrFeNiC_x$ alloys at 77 K and 300 K

A. V. Levenets, V. S. Okovit, M. A. Tikhonovsky, O. M. Velikodnyi

National Science Center "Kharkiv Institute of Physics and Technology" of NAS of Ukraine
Akademichna str. 1, Kharkiv, 61108, Ukraine
e-mail: avlevenets@gmail.com

A new class of materials, so-called high entropy (HEA), is actively developed at last time [1]. For use in cryogenic technique HEAs with an fcc lattice are especially promising, in particular the four-component equiatomic alloy CoCrFeNi, which has high ductility and toughness in the region of nitrogen and helium temperatures. However, the strength characteristics of this alloy need significant improvement. In this work, an attempt was made to increase the strength characteristics of the $Co_{25-x}Cr_{25}Fe_{25}Ni_{25}C_x$ HEA by alloying with an interstitial element, namely carbon.

Alloys with different carbon concentrations x (x = 0, 1, 3 and 5 at. %) were produced by argon-arc melting [2] subjected to homogenizing annealing at 1100 °C for 5 hours and rolled into a strip 0.5 mm thick with intermediate annealing at 1050 °C /1 h after reduction thickness by 50%. Dogbone-shaped samples for mechanical tensile tests at 300 K and 77 K were cut from the strips in the direction of rolling using the electric spark method (the cross-section of the working part of the samples was 0.5 mm^2, the length of the working part was 8 mm). The samples were annealed at 1050 C/1 h, the deformation rate during testing was 10^{-3} s^{-1}. The figures show the concentration dependences of the limits of proportionality σ_0 (curves 1,2) and strength σ_B (curves 3,4), as well as uniform ε_e (curves 1,2) and maximum elongation ε_{max} (curves 3,4) for samples tested at 300 K (curves ●, ○) and 77 K (curves ■, □).

As you can see, the optimal combination of strength and plastic characteristics for a temperature of 77 K is observed at a carbon concentration x = 1 at.%. The relationship between mechanical characteristics and previously studied microstructure features [2] is discussed.

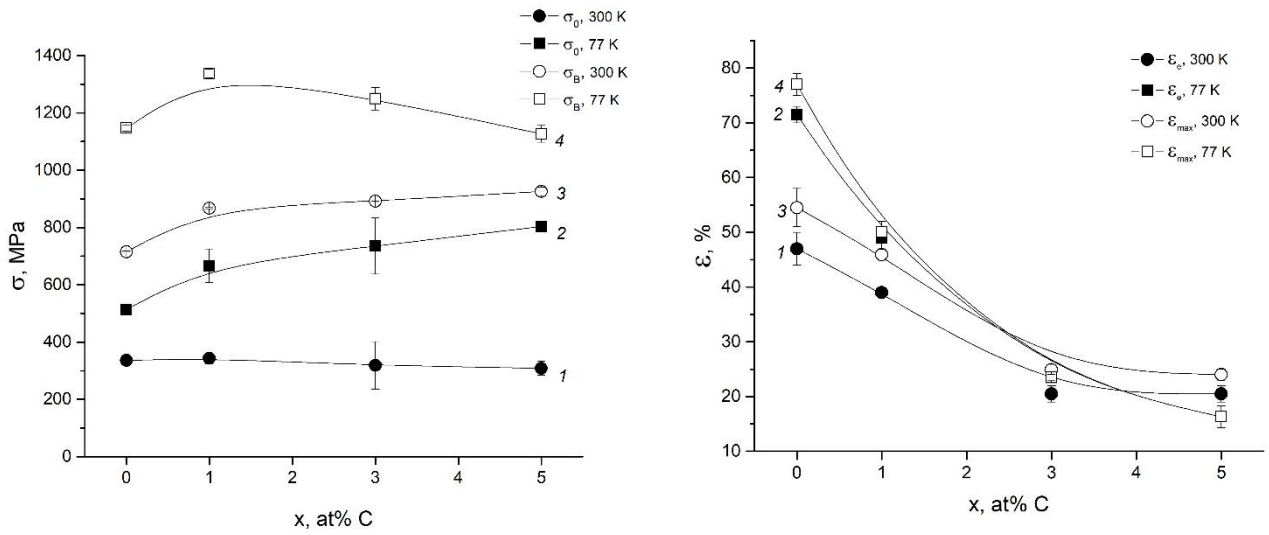

[1] A.V. Levenets, M.A. Tikhonovsky, V.N. Voyevodin et al. PAST. 132, 3 (2021). http://dx.doi.org/10.46813/2021-132-003
[2] A.V. Levenets, H.V. Rusakova, L.S. Fomenko et al. Low Temperature Physics, 48, 560 (2022). http://dx.doi.org/10.1063/10.0011605

Influence of Long-Term Exposure on Mechanical Properties of Polyimide Kapton H Films

V. A. Lototskaya, L. F. Yakovenko

B. Verkin Institute for Low Temperature Physics and Engineering of NAS of Ukraine,
47 Nauky Ave., Kharkiv, 61103, Ukraine
e-mail: lototskaya@ilt.kharkov.ua

It is known that polymers of this type in the manufacturing process acquire a non-isotropic oriented structure - amorphous or partially crystalline, depending on the thickness and technology. It was found in [1], that after the deformation of films by uniaxial tension, even at room temperature, a noticeable relaxation of the film structure occurs over several days. So far, the work of investigation the nature of the change in the mechanical properties of the initial undeformed polymer after a long exposure time has not been carried out. This material have been operating in orbit as thermoregulating coatings on the surfaces of near-Earth satellites, the duration of which reaches 10-15 years. So, it is important to know the degree and direction of change in the mechanical properties of the polymer during operation.

Mechanical properties (forced elasticity limit, fracture stress, deformation before fracture and the values of its components, modules of elasticity and forced elasticity at individual stages of deformation) of polypyromellitimide $C_{22}H_{10}N_2O_5$ films of different thicknesses (25, 75 and 125 μm) produced in China and 25 μm thick, manufactured in the USA, Dupont, obtained in 2013 and 2012 years, respectively, were studied. The films were carried out under uniaxial tension conditions at room temperature after preparation and several years later.

It has been found that the mechanical properties of “fresh” films of the kapton H type made in PRC and kapton H made in the USA differ significantly. The relative deformation before fracture and the highly elastic component of deformation reversible upon removal of the load of a "fresh" film with 25 μm thickness made in the USA is significantly higher than that of a similar film made in PRC. It has been established that exposure polyimide films of the Kapton H type from both manufacturers at room temperature for several years leads to a change in the all studied mechanical characteristics. The strongest change in all characteristics was found in the most amorphous film 25 μm manufactured by Dupont (USA). After exposure during for 9 years at room temperature, the limit of forced elasticity increased by 1.5 times, the fracture stress by 5- deformation before fracture 7%, and the strain to fracture decreased by almost 3 times.

It has been established that the nature of the change with the exposure time of such characteristics as the physical limit of forced elasticity, relative deformation before fracture and its components, the number of stages on the deformation curve, the elastic modulus depends on the thickness and structure of the film (amorphous or partially crystalline).

From a practical point of view, an unfavorable consequence of the relaxation of the films structure of both manufacturers as a result of long exposure is a decrease in the contribution of the highly elastic component of deformation, which is reversible upon removal of the load, which is especially pronounced in the thinnest amorphous films with 25 μm thickness. However, the available margin of elasticity and the amount of relaxation of other mechanical characteristics of the exposured films leaves them suitable for use at room temperature

.

[1] V.A. Lototskaya, L.F. Yakovenko, E.N. Aleksenko, V.V. Abraimov, and Wen Zhu Shao, East. Eur. J. Phys. **4,** 44-52 **(**2017), https://doi.org/10.26565/2312-4334-2017-2-06.

Radiation-Induced Effects in Polyimide Kapton H Films of Different Thicknesses. Influence on Mechanical Properties

V. A. Lototskaya, L. F. Yakovenko, G. I. Saltevskiy, I. P. Zaritskiy, Yu. S. Doronin, A. A. Tkachenko

B.Verkin Institute for Low Temperature Physics and Engineering of NAS of Ukraine,
47 Nauky Ave., Kharkiv, 61103, Ukraine
e-mail: lototskaya@ilt.kharkov.ua

The mechanical characteristics (forced elasticity limit σ_{forc}, fracture stress σ_r, relative strain to fracture ε_r and its components, modules of elasticity and forced elasticity at individual stages of deformation) of polyimide films of the kapton H type (manufactured in China) of different thicknesses (25, 75 and 125 μm) have been studied. Deformation was carried out under conditions of uniaxial tension along the film drawing direction at room temperature and a strain rate of 10^{-4} s^{-1}. Films were studied in the initial state and after separate irradiation by fluxes of corpuscular radiation from the Earth's radiation belts (protons or electrons) and electromagnetic radiation from the transatmospheric Sun in the range of vacuum ultraviolet (VUV) and ultrasoft x-rays (UMX), simulated in a laboratory.

It was found that in deformed irradiated films the forced elastic state ($\sigma_{forc} < \sigma_r$) is preserved, as in the original one. The influence of corpuscular and electromagnetic irradiation on a number of characteristics is different and with thickness they change in the opposite way.

The most significant change in all mechanical characteristics is caused by proton irradiation. There is an increase in the forced elasticity limit σ_{forc}, a decrease in the fracture stress σ_r and a decrease in the relative strain to fracture ε_r. All changes increase with decreasing film thickness. A similar tendency for changes in properties is observed after exposure by electrons. Irradiation of VUV and UMX radiation leads to the opposite nature of the change in the forced elasticity limit - a decrease σ_{forc} with increasing thickness.

After exposure to all types of irradiation, a redistribution of the values of various contributions to the total deformation to fracture occurs. The nature and magnitude of the redistribution also depend on the type of irradiation and film thickness. Irradiation with protons and electrons leads to a significant reduction in the contribution of irreversible deformation. The magnitude of the reduction increases to 90% with a decrease in thickness to 25 microns, while the elasticity of the film is generally maintained. Irradiation with VUV and UMX radiation, on the contrary, reduces the contribution of highly elastic deformation, which is reversible at the test temperature. The degree of reduction increases with increasing film thickness. The change in the contribution of irreversible deformation is insignificant and has the same trend with a change in film thickness as with corpuscular irradiation.

The modules of elasticity and forced elasticity at the first linear stage after irradiation with protons and electrons increase slightly and depend weakly on thickness. At the second linear stage of deformation, the forced elasticity modulus of samples irradiated with protons is lower than the values in the initial films of all thicknesses, or the second stage is completely absent. In the case of irradiation with VUV and UMX radiation, both the modules of elasticity and forced elasticity at both stages increase and show a dependence on thickness. The greatest increase was found in the thinnest films (25 μm).

Hysteresis phenomena in $Cd_2P_2S_6$ layered crystals

H. Ban, D. Gal, S. Motrja, A. Molnar

Uzhhorod National University, Department of the Physics of Semiconductors,
54 Voloshina Str., Uzhhorod, 88000, Ukraine
e-mail: alexander.molnar@uzhnu.edu.ua

Cadmium hexathiohypodiphosphate, also known as $Cd_2P_2S_6$, has received considerable attention in recent decades due to its ease of intercalating with various inorganic and organic substances [1]. Its exceptional chemical and physical properties make it a promising candidate for composite materials. $Cd_2P_2S_6$ has been used as a window material in heterojunction solar cells to prevent recombination of light-generated carriers, and as quantum dots to increase the efficiency of solar cells. A flexible memristor for artificial synapse and logic operations was also created based on 2D Cadmium Phosphorus Trichalcogenide [2].

Despite recent advancements in synthesizing and studying the physical and chemical properties of $Cd_2P_2S_6$, there is currently no available detailed data on its electrophysical properties. From [3], we only know the bandgap of $CdPS_3$ crystals, which is ~ 3.3-3.5 eV. Therefore, we have investigated the temperature dependence of the dielectric spectra of $Cd_2P_2S_6$ single crystals.

The dielectric susceptibility was measured using GW Instek/Goodwill LCR-815 high-end digital LCR meter at frequency intervals 10 - 10^5 Hz. Measurements were performed in the temperature range 80-400K at heating and cooling rates of 0.1-0.05 K/min.

The temperature dependence of the dielectric constant indicates the discontinuous change of $\varepsilon'(T)$ at 228 K in cooling mode, and at 265 K in heating mode. Such behavior and a great temperature hysteresis of phase transitions indicate a first-order phase transition in $Cd_2P_2S_6$ crystals. As for us, this explains the discrepancy of the phase transition temperatures indicated in the previous works.

However, despite the large bandgap of $Cd_2P_2S_6$ crystals, both the real and imaginary parts of the dielectric constant exhibit semiconductor-like behavior in the high-temperature phase. The temperature dependence of the parameters is manifested in their activation nature (increase in conductivity with increasing temperature, which is reflected in the growth of components $\varepsilon^*(T)$). Moreover, at repeated cycles of change of temperature, i.e. change of a mode of heating or cooling, $\varepsilon^*(T)$ increases. Most materials in the $Me_2P_2S(Se)_6$ family also exhibit the activation-induced conductivity growth in the high temperature region, but the dielectric constant decreases with time (e.g., in $Sn_2P_2S_6$ due to shielding), or remains unchanged (as in the case of $CuInP_2S_6$) when the temperature stabilizes. Therefore, this behavior can be considered atypical, especially for wide-gap materials.

The opposite behavior, a decrease in $\varepsilon^*(T)$ during temperature cycling, can be observed at low temperatures (80-90K), but the nature of this hysteresis phenomenon has not yet been established and needs further investigation. Since the amplitude of hysteresis decreases with repeated cycling, the conclusion about the influence of intercalated materials (atmospheric gases or water) in the interlayer space on this phenomenon is reasonable. Most likely, they leave the interlayer space during repeated heating, reducing the polar contribution to the dielectric constant.

[1] X. Yu, W. Ren, Nature Communications, 14 (2023). https://doi.org/10.1038/s41467-023-39725-6
[2] Z. Peng, Z. Cheng, S. Ke, Y. Xiao, Z. Ye, Z. Wang, T. Shi, C. Ye, X. Wen, P.K. Chu, X. Feng, J. Wang, Advanced Functional Materials 33, (2023). https://doi.org/10.1002/adfm.202211269.
[3] D. Yang, P. Westreich, R.F. Frindt, Journal of Solid State Chemistry 166, (2002). https://doi.org/10.1006/jssc.2002.9618.

Multiple phase transitions in thin ethanol films obtained by physical deposition from the gas phase

A. Aldiyarov[1], D. Yerezhep[1,2,3], D. Yu. Sokolov[1,4], E. Korshikov[1], A. Nurmukan[1]

[1] Al-Farabi Kazakh National University, Al-Farabi Av., 71, 050040 Almaty, Kazakhstan
[2] Satbayev University, Satbaev str., 22, 050040 Almaty, Kazakhstan
[3] Institute of Physics and Technology, Satbayev University, Ibragimov str., 11, 050032 Almaty, Kazakhstan
[4] Almaty Technological University, Tole Bi av., 100, 050012 Almaty, Kazakhstan
e-mail: assel.nurmukan@gmail.com

Glasses are easily formed when a supercooled liquid phase of ethanol is cooled below the temperature T_g = 97 K. Such glasses were formed by the method of physical gas-phase deposition of ethanol molecules into thin films at temperatures below the mentioned one [1]. These films were grown on a cooled copper substrate coated with a thin layer of gold in a high-vacuum chamber. The estimated thickness of about one micron and the density of studied films were measured using a two-beam laser interferometer.

The thin film of ethanol exhibits a fascinating polymorphism, representing various solid phases below the melting point (T_c = 159 K): "structural glass" is similar to glass obtained by quenching a supercooled liquid below the glass transition temperature (T_g = 97 K); "plastic crystal" has the volume-centered cubic (VCC) structure, also it becomes an orientationally disordered crystal with glassy properties (sometimes called a "vitreous crystal") and completely ordered (monoclinic) crystals when quenched below the glass transition temperature. In this report, we discuss the nature of the crystallization process of glassy ethanol into a "plastic crystal". We also present the results of experimental study of Fourier-transform infrared (FTIR) spectrometry and measurement of the specific heat capacity of various ethanol phases in the corresponding temperature range close to the glass transition and melting temperatures. In addition, we conducted experiments on the thermal desorption of the aforementioned crystalline phases, both fully ordered and orientationally disordered ones, complementing our earlier studies of glass phases.

[1] A. Aldiyarov, A. Drobyshev, E. Korshikov et al. Phys. Solid State 54, 1475–1479 (2012). https://doi.org/10.1134/S1063783412070025

Thermal conductivity of epoxy resin polymer composites with thermally reduced graphene oxide

V. V. Sagan[1], A. I. Krivchikov[1], A. Jeżowski[2]

[1] B. Verkin Institute for Low Temperature Physics and Engineering of NAS of Ukraine
47 Nauky Ave., Kharkiv 61103, Ukraine
[2] Institute of Low Temperature and Structure Research, Polish Academy of Sciences,
Wroclaw,50-422, Poland
e-mail: sagan@ilt.kharkov.ua

The thermal conductivity of polymers is an interesting aspect that can be crucial in developing new materials and technical applications. Decreasing temperature often means reducing the thermal conductivity of polymers, but the relationship is more complex than it may seem. The temperature dependence of thermal conductivity is related to many factors, such as molecular structure, crystallinity, and the presence of various impurities.

In particular, at low temperatures, especially below the glass transition temperature, the molecular structure plays a key role. Amorphous polymers, where long-range order is absent, may have reduced thermal conductivity due to phonon scattering at structural defects such as molecular irregularities or chain ends. This effect can be exacerbated by the presence of impurities or additives.

On the other hand, adding fillers or additives can increase the thermal conductivity of polymers [1]. Here, not only the nature of the filler is important, but also the morphology of the composite and the interaction between the filler and the polymer matrix. Understanding these processes can pave the way for creating new materials with defined thermal properties, and the ability to regulate thermal conductivity opens up broad prospects for innovation in materials science.

In this work, the change in the nature of the temperature dependence of thermal conductivity of epoxy resin-based polymer composites was investigated. Thermally reduced graphene oxide (trGO) was used to create the composites [2]. The thermal conductivity of the compounds was measured over a wide temperature range using an experimental setup [3]. The temperature gradient along the sample was typically 0.2-0.3 K in the steady-state regime when measuring the thermal conductivity at a specific temperature. The maximum experimental systematic error was less than 15%, mainly due to uncertainties in sample geometry. The error estimated from the dispersion of the experimental points did not exceed ± 2% [3].

From the experimental data obtained during the study, it can be seen that the thermal conductivity $\kappa(T)$ of polymer composites exhibits glass-like behavior, which is characteristic of various types of amorphous solids and disordered crystals. Moreover, an increase in the concentration of carbon filler leads to an increase in the effective thermal conductivity of the composite material.

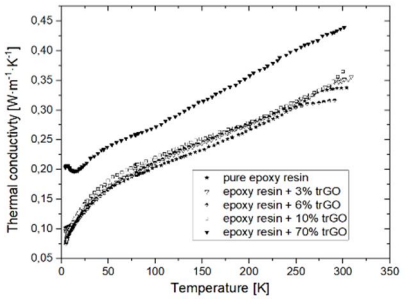

[1] A.I. Krivchikov, A. Jeżowski, V.A. Konstantinov, V.V. Sagan, O.A. Korolyuk, and D. Szewczyk, Thermochimica Acta 733, 179696 (2024). https://doi.org/10.1016/j.tca.2024.179696
[2] A. V. Dolbin, M. V. Khlistyuck, V. B. Esel'son, V. G. Gavrilko,N. A. Vinnikov, R. M. Basnukaeva, I. Maluenda, W. K. Maser, and A. M. Benito, Appl. Surf. Sci. 361, 213 (2016). https://doi.org/10.1016/j.apsusc.2015.11.167
[3] A. Jeżowski, B.A. Danilchenko, M. Boćkowski, I. Grzegory, S. Krukowski, T. Suski, and T. Paszkiewicz, Solid State Communication 128(2-3), 69-73 (2003). http://dx.doi.org/10.1016/S0038-1098(03)00629-X

Peculiarities of lattice dynamics of cadmium iodide and its appearance in photoelectric effects

M. Rudka[1], M. Orendáč[2], R. Tarasenko[2], M. Karkuliovska[1], N. Tovstyuk[1], B. Seredyuk[3]

[1] Lviv Polytechnic National University, 12 Bandery street, Lviv, Ukraine, 79013
[2] Institute of Physics, Faculty of Science, P.J. Šafárik University, Park Angelinum 9, 044 54 Košice, Slovakia
[3] Hetman Petro Sahaidachnyi National Army Academy, Faculty of Rocket Troops and Artillery, 32 Heroes of Maidan street, Lviv, 79026 Ukraine,
e-mail: ntovstyuk@gmail.com

Peculiarities of lattice dynamics of cadmium iodide are caused by its structure which defines a certain arrangement of defects and in turn determines the behavior of heat capacity [1]. Features of the structure, namely a different order of interaction forces both between atoms within a layer and between layers, lead to anomalies in the electronic (due to a strong anisotropy of the effective mass of charge carriers) and vibrational spectra of the layered crystal (the appearance of low-energy bending modes in the vibrational spectrum of the crystal). An important feature inherent only to this type of oscillations is their strict polarization along the main axis of a crystal.

In our work, we study the behavior of the temperature dependence of heat capacity of both pure cadmium iodide and doped one with different impurities (Cu and Au). Peculiarity of CdI_2 structure causes the possibility: of displacement of a specific "nodal" Cd atom either into the adjacent unfilled octahedral void inside the package, or outside the package into the van der Waals gap; of impurities entering during intercalation or activation of crystals both into van der Waals gaps and voids in structural packages. This is how the associated donor-acceptor (DA) complex of the intrinsic structural defects in the form of cation vacancy and interstitial Cd are formed. These DA complex pairs of two types are oriented in different ways: "cation vacancy –interstitial Cd" within an atomic plane (axis of DA1 pair is normal to the anisotropy axis C_6) as well as "cation vacancy – interstitial Cd" in van der Waals gap (axis of DA2 pair coincides with the anisotropy axis C_6). Such combination of pairs of DA complexes generates a trimer DADi – like ($Donor_i^0$-$Acceptor_{Cd}^-$ - $Donor_i^+$). For doped CdI_2 crystals, we receive different type of trimmers: intrinsic defects, own-impurity defects or impurity defects depending on impurity concentration [2,3].

Specific heat of both pure CdI_2 crystals and doped ones with Cu and other impurities of the I-st group have been studied in temperature range from nominally 2 K to 300 K in zero magnetic field using the Quantum Design Physical Properties Measurement System (PPMS) using a relaxation technique. The samples were pressed into the form of a pellet. Subsequently, a piece of the pellet of nominal weight of 4 mg was glued to a microcalorimeter with GE 7031 varnish. The contribution of varnish and the calorimeter itself to the total specific heat was investigated in a separate run and the data were subtracted from the total signal.

Estimation of Debye and Einstein temperatures based on the experimental data allows us to identify the influence of impurities on lattice dynamics, photoelectric properties, and to evaluate changes in the molar mass of crystals when alloyed with different concentrations of impurities.

[1] M. Rudka, I. Matviishyn, B. Seredyuk, N. Tovstyuk, M. Karkulovska, I. Kravchuk. Luminescence centers in low-dimensional layered cadmium iodide crystals and nanostructures. 2020 IEEE 40th International Conference on Electronics and Nanotechnology, ELNANO 2020 - Proceedings, 2020, pp. 268-271, 9088922.
[2] M.M. Rudka, "Spectroscopy of copper activated low-dimensional cadmium iodide layered crystals", Visnyk Physical and Mathematical Sciences, vol. 566, 2006, pp. 97-102.
[3] M.M. Rudka, "Centers of green-yellow and red luminescence in crystals of cadmium iodide", Physical and Mathematical Sciences, vol. 687, 2010, 181-187.

Conditions for the formation of new structural phases in BEDT-TTF

Y. M. Trotskyi[1], E. S. Syrkin[1], V. O. Lykah[2]

[1] B.Verkin Institute for Low Temperature Physics and Engineering of the NAS of Ukraine, 47 Nauky Ave., Kharkiv, 61103, Ukraine
[2] National Technical University "Kharkiv Polytechnic Institute", Kharkiv 61002, Ukraine
e-mail: trotskyi@ilt.kharkov.ua

In our report, we review the conditions under which we can observe the mechanism of the structural transition in the TTF type organic layered π-donor conductors [1] known to be classified as highly anisotropic molecular crystals. The aforementioned transition consists in the inclination of molecules, leading to a formation of α- and θ-type structures. That may also include the pairing of donor molecules and the formation of the κ-type structure [2]. It was found that the main reason for the rearrangement of molecules is the combination of two types of interaction: 1) van der Waals forces between donor molecules within the stack and between adjacent stacks; 2) electrostatic force between the donor and anion layers. Among the estimated reasons responsible for the pairing of BEDT-TTF (ET) molecules are the large size of the anion molecule and the great value of the negative charge of the anion sub-compound, like SCN in NaSCN or KSCN.

We provide a method of calculating the ground state energy of a molecular arrangement, which is known as a density functional theory (DFT) comparative analysis, analogically to [3]. This method allows us to study the structural and electronic properties of condensed molecular structures like ET-based (semi)conductors. Our first goal is to find the bonding energy between the donor and anion layers and to compare the interaction of in-stack molecules to the one between adjacent stacks. The considered system demonstrates stability in case of the anion layer's placement near the hydrogen side of the ET molecule rather than near the sulfur one. The dimensions of the crystallographic unit cell are defined by the X-ray diffraction analysis. The interaction between molecules is the strongest between the donor and anion layers and the weakest between the donor stacks. Therefore, an increase in the distance, Δr_0, due to the anion's electrostatic field has the greatest value between the donor and anion layers and the smallest one between the donor stacks. It is worth noting that the temperature also contributes to the value of Δr_0.

[1] Misaki, Y. (2009). Tetrathiapentalene-based organic conductors. Science and technology of advanced materials, 10(2), 024301. https://doi.org/10.1088/1468-6996/10/2/024301
[2] Mori, T., Mori, H., & Tanaka, S. (1999). Structural genealogy of BEDT-TTF-based organic conductors II. Inclined molecules: θ, α, and κ phases. Bulletin of the Chemical Society of Japan, 72(2), 179-197. https://doi.org/10.1246/bcsj.72.179.
[3] Alzahrani, A. Z. (2011). Structural and electronic properties of graphene upon molecular adsorption: DFT comparative analysis. Graphene Simulation, *1*, 21–38. https://doi.org/10.5772/20356.

In situ video recording of crystallization of amorphous Sb_2Se_3 films

A. G. Bagmut

National Technical University "Kharkiv Polytechnic Institute",
2, Kyrpychova str., 61002, Kharkiv, Ukraine
e-mail: agbagmut@gmail.com

During thermal evaporation in vacuum of a powder weight of antimony selenide, an amorphous film is formed on a substrate at room temperature. Electron irradiation of a free-standing amorphous film with a dose rate ~ $6 \cdot 10^4$ $e^-/Å^2 \cdot s$ inside the column of the electron microscope causes its crystallization (Fig. 1) due to Joule-Lenz heating. In situ electron microscopy studies with the video recording method demonstrated, that the amorphous-crystalline phase transformation is described with the island polymorphous crystallization mode with the relative length $\delta_0 \approx 196$ [1].

The time dependence of the crystallized volume fraction $x(t)$ in an amorphous Sb_2Se_3 film has an exponential character, described by the Johnson-Mehl-Avrami-Kolmogorov (JMAK) formula [2]. The formation of the polycrystalline film occurs at the constant crystal growth rate and constant nucleation rate, which corresponds to the α-version of the Kolmogorov model (continuous nucleation process). According to (1), the Avrami exponent $n = 2.16$ (the nearest integer = 2).

$$x(t) = 1\text{-}\exp(-0.08733t^{2.16}). \quad (1)$$

These values of n are typical for the crystallization process in which grain growth occurs with nucleation. Values of n, where the nearest integer = 2, took place during crystallization of thin amorphous films of Ta_2O_5, Yb_2O_2S, V_2O_3 [3].

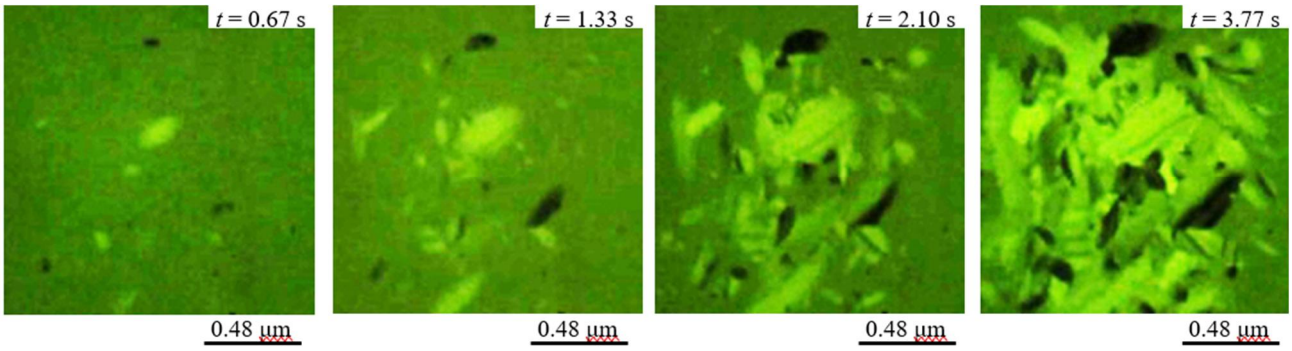

Fig. 1. Video frames of crystal growth in amorphous films of Sb_2Se_3 at electron beam irradiation. Time moments t, that have passed from the beginning of the recording of the crystallization process, are shown in the upper right corner of each frame.

[1] A. Bagmut, Funct. Mater., 26, 6 (2019). https://doi.org/10.15407/fm26.01.6.
[2] A. Kolmogorov, Bull. of the Acad. of Sciences of the USSR, Mathematics Series, 1, 355 (1937). https://www.scirp.org/(S(i43dyn45teexjx455qlt3d2q))/reference/ReferencesPapers.aspx?ReferenceID=880675.
[3] A. Bagmut, Problems of Atomic Science and Technology, 137(1), 64 (2022). https://doi.org/10.46813/2022-137-064.

Optical properties of Tl_3TaSe_4 chalcogenide crystals

O. V. Bokotey, O. O. Bokotey, P. P. Guranich, A. G. Slivka

Faculty of Physics, Uzhhorod National University, 3 Narodna Sqr., Uzhhorod, 88000, Ukraine
e-mail: obokotei@gmail.com

This paper introduces theoretical calculations of refractive parameters of Tl_3TaSe_4 crystals, and their potential applications in the creation of medical devices and also suggests medical areas for further research and development. One of the main tasks of modern nanophysics is to develop new low-cost semiconductor materials for functional elements of medical devices with much-improved detection properties. This fact is very important for the qualitative formation of medical imaging. Tl_3TaSe_4 crystals have shown considerable promise for these applications.

Tl_3TaSe_4 crystals are the ternary thallium chalcogenides materials and belong to the $T_d^3 - I\bar{4}3m$ space symmetry group. The compound is characterized by isolated [XY] tetrahedra in parallel orientation with the X atoms forming a body-centered cubic lattice, Tl occupying the middles of the edges and faces of the unit cell. The specific feature of the mentioned structures is the presence of $[XY_4]$ and $[TlY_8]$ structural complexes. The main feature of ternary thallium chalcogenides is the formation of numerous polymorphic modifications and the existence of isomorphic substitutions in sublattices. Scientific and practical interest in Tl_3TaSe_4 is caused by the ability to form continuous rows of solid solutions that allow use for different variations of physical and chemical properties.

Theoretical calculations of refractive index, optical dielectric constant, and reflection coefficient for Tl_3TaSe_4 crystal within the Harrison bonding orbitals model were carried out [1-3]. The calculations were performed for the spectral region far from the absorption edge, where the dispersion of the refractive index is absent. The refractive index evaluation is of considerable importance for applications in integrated optic devices, where materials refractive index is the key parameter for device design.

A full set of analytical expressions are obtained for studies on the optical and dielectric properties of the crystal under investigation. The tight-binding point of view offers directly a way to describe localized charges since each of the orbitals in which the electronic states are expanded is associated with a particular atom. It should be noted that, in our current analysis, we are assuming that all matrix elements between the bonding and anti-bonding states are neglected. It was shown that Harrison's model allows analyzing the optical parameters of Tl_3XY_4 type compounds. Crystals under investigation are expected to contribute to the development of nanophysics and personalized medicine for health monitoring and prevention. The theoretical technique developed in this paper to use for the theoretical description of the optical properties of materials.

[1] W.A. Harrison, Tight-binding theory of the dielectric susceptibilities and transverse charges of insulators. Phys. Rew. B, 2006, 74, 205101.
[2] K. Hoang, S. Mohanti. Journ. of Science: Advanced Materials and Devices 1, (2016).
[3] O.V. Bokotey, Theoretical calculations of refractive properties for $Hg_3Te_2Cl_2$ crystals. Nanoscale Res. Lett. 2016, 11:251.

Study of Structural and Mechanical Properties of the Half Heusler Alloy C_2CaNa

M. E. Ishaje[1], K. A. Minakova[2], V. A. Sirenko[3], I. S. Bondar[3]

[1] Department of Physics, Cross River University of Technology, P.M.B 1123, Calabar. Cross River State. Nigeria
[2] Department of Physics, National Technical University Kharkiv Polytechnic Institute Kharkiv, 2 Kyrpychova str., Kharkiv, 61002, Ukraine
[3] B. Verkin Institute for Low Temperature Physics and Engineering of NAS of Ukraine, 47 Nauky Ave., Kharkiv, 61103, Ukraine
e-mail: ibondar@ilt.kharkov.ua

Half Heusler alloys have attracted considerable interest owing to their exceptional thermoelectric, magnetic, and structural characteristics. These materials are versatile and hold promise for transforming numerous applications, such as thermoelectric generators, spintronic devices, and structural components. Comprehending the mechanical behavior of these alloys is crucial for effectively integrating them into real-world applications. In this investigation the structural and mechanical properties of C_2CaNa Half-Heusler Alloys using the first principle technique based on Density Functional Theory (DFT) was carried out.

Utilizing the Quantum Espresso simulation software suite, density functional theory calculations were carried out. Young's modulus (E) was calculated using the relation $E = 9BG / (3B + G)$, and the Poisson's ratio (ν) was calculated using the relation $\nu = -(C_{11} - 2C_{12}) / (2C_{12})$ to etermined other mechanical properties, such as the brittleness; hardness, resilience, and plasticity, using appropriate equations and QE model was used Perdew-Burke-Ernzerhof (PBE) functional in the form of a general gradient approximation (GGA) was used in this study to characterize the exchange and correlation [1-3].

Calculated values of G/B ratio is 0.505**;** this shows that C_2CaNa has low resistance opposed to shear deformation. The B/G ratio evaluated for C_2CaNa is 1.72. This implies that C_2CaNa is "brittle" in nature at ambient condition. Our calculated elastic constants (C_{11}, C_{12} and C_{44}) for C_2CaNa satisfied the following mechanical stability conditions for cubic structure: ($C_{11} - C_{12} > 0$, $C_{44} > 0$ and $C_{11} + 2C_{12} > 0$. The value of C_{12} is an indication that C_2CaNa is mechanically stable.

These findings provide valuable guidance for tailoring the mechanical properties of C_2CaNa alloys for specific applications, such as thermoelectric devices and spintronics. Overall, this study contributes to the understanding of the mechanical behavior of half-Heusler alloys and provides a foundation for further investigations and applications of C_2CaNa alloys in advanced materials.

[1] P. Giannozzi, S. Baroni N. Bonini, M. Calandra, R. Car, C. Cavazzoni, Ceresol, D., Chiarotti, G., Cococcioni, M., Dabo, I., Corso, A., de Goroncoli, S., Fabris, S., Gebauer, R., Gerstmann, U., Gougoussis, C., Kokolj, A., Lazzeri, M., Martin-samos, L., Marzari, N., Mauri, F., Mazzarello, R., Paolini, S., Pasquarello, A., Paulatto, L., Sbraccia, C., Scandolo, S., Sclauzero, G., Seitsonen, A.P., Smogunov, A., Umari, P., Wentzcovitch, R.M. QUANTUM ESPRESSO: a modular and open-source software project from quantum simulations of materials. J Phys. Condens. (2009) Matter 21 (39), 395502 (2009). http://doi.org/10.1088/0953-8984/21/39/395502
[2] S.B. Feodosyev, V.A. Sirenko, E.S. Syrkin, E.V. Manzhelii, I.S. Bondar, K.A. Minakova, Low Temp. Phys. 49, 34 (2023). https://doi.org/10.1063/10.0016473
[3] E. B. Ettah, K. Minakova, M. E. Ishaje, V. Sirenko, Low Temp. Phys. 49, 1389 (2023). https://doi.org/10.1063/10.0021371

Relationship between microhardness and yield strength of nanostructured CoCrFeNiMn high-entropy alloy at T = 77-290 K

L. S. Fomenko[1], H. V. Rusakova[1], S. N. Smirnov[1], E. D. Tabachnikova[1], M. A. Tikhonovsky[2], Y. Huang[3], T. Langdon[4]

[1] B. Verkin Institute for Low Temperature Physics and Engineering of NAS of Ukraine, 47 Nauky Ave., Kharkiv, 61103, Ukraine
[2] National Science Center "Kharkiv Institute of Physics and Technology" of NAS of Ukraine, 1 Akademichna Str., Kharkiv, 61108, Ukraine
[3] Department of Design and Engineering, Faculty of Science and Technology, Bournemouth University, Poole, Dorset BH12 5BB, UK
[4] Materials Research Group, Department of Mechanical Engineering, University of Southampton, Southampton SO17 IBJ, UK
e-mail: fomenko@ilt.kharkov.ua

Uniaxial deformation at a constant rate and microindentation are traditional methods for studying the mechanical properties of materials. It is natural to expect that there is a certain relation between the characteristics measured by these methods, namely between the yield strength and the microhardness. Numerous studies have been devoted to elucidating the nature of this relation and establishing quantitative relationships between the yield strength and the microhardness, but this issue has not yet received a final solution, and interest in this problem continues to this day. In this work, a comparative analysis of the temperature dependences of the Vickers microhardness $H_V(T)$ and the conditional yield strength $\sigma_{0.2}(T)$ [1], obtained in the temperature range T = 77-290 K, was carried out for coarse-grained (CG) and nanostructured (NS) samples of the high-entropy alloy CoCrFeNiMn. NS samples were obtained by severe plastic deformation via torsion under a quasi-hydrostatic pressure of 6 GPa at temperatures of 300 K (RT-HPT) and 77 K (cryo-HPT). The grain sizes of the NS and CG samples were on the order of 40-100 nm and 4 μm, respectively.

For CG and NS samples of the CoCrFeNiMn alloy, the values of the Tabor parameter $C_T = H_M/\sigma_Y$, where H_M is the Meyer microhardness (H_M = 1.08 H_V), were calculated; in this case, as yield strength σ_Y we used the conditional yield strength $\sigma_{0.2}$ determined in experiments on compression. It is shown that for all types of samples, temperature has little effect on the value of the Tabor parameter. In the temperature range T = 77-290 K, the average C_T values are: C_T » 2.85 for RT-HPT samples and C_T » 3.06 for cryo-HPT samples, that are close to the theoretical C_T value for a rigid-perfectly plastic solid (C_T = 3) [2]. This result indicates the applicability of this model to describe the deformation of NS samples of the high-entropy CoCrFeNiMn alloy in the studied temperature range. For CG samples, the average C_T value in the temperature range T = 77-290 K is C_T » 5.03, which is significantly higher than the C_T values for NS samples. This is probably due to the fact that CG cast samples of the CoCrFeNiMn alloy are prone to significant hardening during deformation and are described by the model of a rigid-strain hardening plastic solid. In this case, when calculating the Tabor parameter, the stress σ_r, corresponding to a representative strain ε_r of about 8%, should be used as the value σ_Y [2]. The high value of the C_T parameter for CG samples indicates that the stress σ_r can be approximately 1.6 times higher than the value of the conditional yield strength $\sigma_{0.2}$.

[1] H. V. Rusakova, L. S. Fomenko, S. N. Smirnov, A. V. Podolskiy, Y. O. Shapovalov, E. D. Tabachnikova, M. A. Tikhonovsky, A. V. Levenets, M.J. Zehetbauer, and E. Schafler, Mater. Sci. Eng. A828, 142116 (2021). https://doi.org/10.1016/j.msea.2021.142116.
[2] D. Tabor, Rev. Phys. Tech. 1, 145 (1970). https://doi.org/10.1088/0034-6683/1/3/101.

Annealing of PMA polyimide film. X-ray data

V. Geidarov, I. Braude, Yu. Pohribna

B. Verkin Institute for Low Temperature Physics and Engineering of NAS of Ukraine,
47 Nauky Ave., Kharkiv, 61103, Ukraine
e-mail: geydarov@ilt.kharkov.ua

The purpose of these studies was to obtain information about the effect of low temperatures on the nature of structural rearrangements in samples deformed far from the glass transition temperature of the film, upon removal of the external load and their subsequent warming to room temperature. This information makes it possible, at least qualitatively, to judge the real state of deformed samples and compare it with the state resulting from model concepts. For example, according to existing concepts [1,2], the molecular structure in glassy polymers is “frozen” and can remain unchanged when the samples are heated up to the glass transition temperature Tc. However, at higher heating temperatures, radical structural rearrangements can occur in these samples, up to complete (depending on the heating temperature and time) restoration of the original structural state.

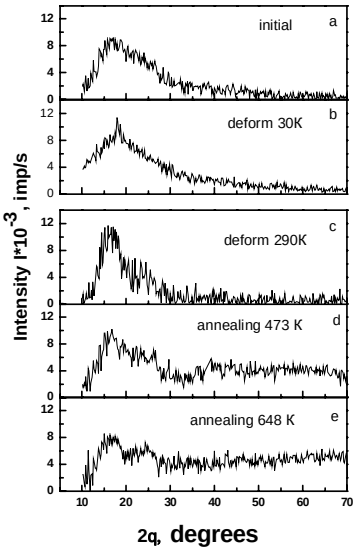

Figure 1 shows the distribution of X-ray scattering intensity from an undeformed sample of PMA polyimide film (Fig. 1a) and after external influences (deformations and annealing). It can be seen that as the annealing temperature increases, the structure of the sample gradually returns to the initial one, and the height of the background at large angles increases. It is shown that successive annealing leads to recovery of the length of the sample at temperatures of 600K and 700K (Fig. 1e). This may indicate a radical restructuring of the structure associated with the breaking of the C–C bonds and the transition of the system to a more balanced position. Similar effects were observed in work [3] on fullerene, which was due to chemical sorption processes, during which dissociation of molecules occurs.

Mechanical tests followed by unloading and annealing showed that near 150 K at a certain limiting temperature T*, the investigated temperature region is divided into two intervals, in which stretching of the same type of samples leads to the formation of structures that require different thermal stimulation to restore the initial state. It is possible that these structures arise due to the nucleation in the molecular system of the film of structural defects of various scales, which participate in the further evolution of this system under the influence of increasing load. However, this assumption needs further experimental confirmation.

1.В.А. Каргин, Г.Л. Слонимский, Краткие очерки по физико-химии полимеров, Химия (1967).
2.В.Е. Гуль, В.Н. Кузнецов, Структура и механические свойства полимеров, Высшая школа (1972).
I.V. Legchenkova, K.A. Yagotintsev, N.N. Galtsov, V.V. Meleshko, Yu.E. Stetsenko, A.I. Prokhvatilov, Low Temp. Phys. **40**, 685 (2014).

The influence of internal strains induced by hydrogen on the electrical resistivity of the nanocrystalline vanadium film

A. Grib, A. Kononenko, S. Petrushenko, S. Dukarov

V. N. Karazin National University, Svobody sq. 4, Kharkiv, 61022, Ukraine
e-mail: alexander.grib@karazin.ua

In the present report, the unusual changes of the electrical resistivity of a nanocrystalline vanadium film during diffusion of hydrogen in this film are considered. A part of the film was electrolytically saturated by hydrogen. Details of the saturation procedure are described elsewhere [1]. Changes in the electrical resistivity of another (non-saturated) part of the film due to diffusion of hydrogen were measured as functions of time. The electrical resistivity of the non-saturated part of the film should increase during time of diffusion due to the increase of the number of scatterers (protons) in this part because protons are impurities in the crystal lattice and consequently are scatterers of conduction electrons. However, we found that when the hydrogen concentration in the saturated part of the film is small (1-2% (at.)), the time-dependent resistivity of the non-saturated part can show quite different behavior. The resistivity decreases with time of diffusion at the beginning of the diffusion process to values smaller than the resistivity of the film before the saturation. After that, it increases after passing the minimum value at approximately 120-130 minutes after the saturation. The explanation of this effect is considered in the present work. The hypothesis about the influence of the internal strains caused by the migrating hydrogen on the electrical resistivity of this film is put forward and the model of the process is developed.

According to the developed model, the initial quasi-one-dimensional distribution of hydrogen along the film was stated at first, and distributions of hydrogen during the diffusion process were numerically calculated from solutions of the diffusion equation in the field of strains. Strains at a given point of the coordinate along the film are produced by a given concentration of hydrogen atoms. The dependence of the resistivity on strains is specified in the model. Changes of the resistivity along the non-saturated part of the film are summarized that gives the total change of the resistivity of this part.

We applied the described model to the approximation of the resistivity of the film which was successively twice saturated by hydrogen up to about 1% (at.) each time. The interval between saturations was four days. The resistivity of the non-saturated part showed the pronounced negative changes during the hydrogen diffusion. The approximation of the time-dependent resistivity by means of the developed model at the reasonable values of model parameters is quite adequate.

The decrease in the resistivity of the non-saturated part of the film has quite a simple explanation within a framework of the developed model. If the change of the resistivity caused by strains prevails over the one produced by the scattering of electrons by protons, the measured changes of the resistivity are produced solely by strains. Changes of the resistivity are negative if the film is compressed. Parts of the film with the higher hydrogen concentration compress parts with the smaller ones, resulting in a negative sign of changes of the resistivity of the non-saturated part at the beginning of the diffusion process.

[1] A. Grib, M. Vitort, S. Petrushenko, S. Dukarov, Low Temp. Phys. 49, 415 (2023). https://doi.org/10.1063/10.0017580.

Strength and plasticity of SPD magnesium alloy at low temperatures

T. Hryhorova[1], P. Zabrodin[1,2], S. Shumilin[1]

[1] B. Verkin Institute for Low Temperature Physics and Engineering of NAS of Ukraine, 47 Nauky Ave., Kharkiv, 61103, Ukraine
[2] Czech Academy of Sciences, Institute of Theoretical and Applied Mechanics, Prosecka 809/76, 190 00 Prague, Czech Republic
e-mail: grigorova@ilt.kharkov.ua

Nanostructured and ultrafine-grained materials have been the subject of intense research over the last few decades, and significant progress has been made in their processing and understanding of their fundamental properties. The main advantage of nanocrystalline materials is their high strength, which determines their attractiveness for practical use in various branches of mechanical engineering. In recent years, microgranular magnesium alloys have become promising for aviation, aerospace and instrumentation applications due to the combination of low density and high specific strength but with limited plasticity and significant mechanical anisotropy. The aim of this study was to determine the mechanisms controlling the plastic deformation of the processed by Severe Plastic Deformation (SPD) Mg-Al-RE alloy over a wide temperature range. Plastic deformation was carried out by tension at a constant strain rate in the temperature range of 0.5–400 K using special cryogenic high-performance equipment. The SPD method by Equal Channel Angular Pressing (ECAP, 8 passes) method was used to form the ultrafine-grain microstructure of the alloy.

It has previously been shown that the modification of the alloy microstructure during 8 passes of ECAP occurred due to a decrease in the average grain size, the increase in dislocation density, precipitation of intermetallic phases and change in crystallographic texture [1].

It has been shown that the main parameters of the "true stress σ – true strain ε" tensile curves depend on the test temperature. Low plasticity was observed at temperatures between 0.5–210 K, and it increases above 210 K. At 400 K, plastic deformation occurred without necking and with constant stress σ up to deformation $\varepsilon \approx 0.2$. The yield strength $\sigma_{0.2}$ changed insignificantly from 180 to 150 MPa in the range of 0.5-290 K but decreased sharply to 60 MPa at 400 K. In the range of 0.5–4.2 K, the so-called Low-Temperature Jump-like Deformation (LTJD) was observed. The average stress amplitude $\Delta\sigma$ and intensity of LTJD depend on the deformation temperature and stress. It may indicate the mechanism of dislocation avalanches dynamics under low temperatures and high stresses conditions as the cause of the LTJD process.

From the thermal activation analysis of the temperature dependences of the yield strength, it was found that in the temperature range of 0.5–400 K, the dominant mechanisms controlling the plastic deformation of the ECAP Mg-Al–RE alloy are the thermally activated overcoming obstacles by moving dislocations. Above 210 K, with increasing temperature, the recovery processes, stimulated by a high dislocation density and non-equilibrium grain boundaries, intensify, which, in turn, affects the parameters of thermally activated plasticity.

[1] P. Minarik, R. Kral, J. Cízek, F. Chmelík, Acta Mater. 107, 83 (2016). https://doi.org/10.1016/j.actamat.2015.12.050

Thermal conductivity analysis of composites with superlattice structure

Yu. V. Horbatenko[1], O. O. Romantsova[1,2], A. I. Krivchikov[1], O. A. Koroluyk[1]

[1] B.Verkin Institute for Low Temperature Physics and Engineering of NAS of Ukraine, 47 Nauky Ave., Kharkiv, 61103, Ukraine
[2] Institute for Low Temperatures and Structure Research, Polish Academy of Sciences, P.O. Box 1410, 50-950 Wroclaw, Poland
e-mail: horbatenko@ilt.kharkov.ua

The thermal properties studying of solids, in particular thermal conductivity, is an important direction of modern materials science, and it stimulates the creation of functional materials with specified properties. We were analyzed the temperature dependences of the thermal conductivity for thin films with different thicknesses, and they have a superlattice structures, in particular, LMOn/SMOn [1], AlN–GaN [2], $(AlN)_{4nm}$–$(GaN)_y$ [2], with different thicknesses of the GaN layer, etc. A superlattice is a structure made up of alternating layers of different materials. These layers are typically measured in nanometers, and the typical superlattice is extremely small. These structures are used in creation of new forms of semiconductors that exhibit different properties than their included materials [3]. It was shown that all temperature dependences of thermal conductivity demonstrate an exponential growth $\kappa(T)$ with temperature increasing as $\kappa_C = \kappa_0 \exp(-E/T)$, where κ_0 is a pre-exponential factor which characterizes the intensity of the heat transfer process, and E is the energy of the dominant excitations.

It is also shown that such representation of $\kappa(T)$ data can be used to describe the "coherent" contribution of thermal conductivity, or the wave mechanism of heat transfer, which is consistent with the unified theory of thermal conductivity [4].

[1] D. Meyer, D. Metternich, P. Henning, et. al., arXiv preprint arXiv:2108.05860 (2021), https://doi.org/10.48550/arXiv.2108.05860
[2] Y.K. Koh, Y. Cao, D.G. Cahill, & D. Jena, Adv. Funct. Materials, 19**,** 4, 610-615 (2009), https://doi.org/10.1002/adfm.200800984
[3] C. Chiritescu, D.G. Cahill, N. Nguyen, … & P. Zschack, Science, 315**,** 5810, 351-353 (2007), https://doi.org/10.1126/science.1136494
[4] M. Simoncelli, N. Marzari, & F. Mauri, Nature Physics 15**,** 8, 809-813 (2019), https://doi.org/10.1038/s41567-019-0520-x

Study of the process cryocapture of carbon dioxide molecules by solid water films

E. Korshikov, A. Aldiyarov, A. Nurmukan, O. Vorobyova, D. Sokolov

Al Farabi Kazakh National University, Almaty, 05000, Kazakhstan
e-mail: e.s.korshikov@physics.kz

To date, more than 140 different molecules have been identified in the interstellar medium. Dust particles were also discovered and some of these molecules were frozen at temperatures (10–20K) with the formation of molecular ice. Understanding the adsorption and desorption processes of these formed ices is critical to understanding the processes that lead to the formation of stars and planets. Highly sensitive surface sensing techniques, including temperature-programmed desorption and reflectance adsorption infrared spectroscopy, are increasingly used to study interactions between condensed objects. This kind of experimental data provides an understanding of the processes occurring in ice of astrophysical significant molecules from several surfaces of model cosmic surfaces.

The purpose of the research was to obtain experimental data on the processes of adsorption and thermal variation in thin films of cryocondensate of astrophysical significant molecules of substances. Research is aimed at understanding the mechanisms of adsorption and desorption on amorphous porous samples under conditions like those in outer space. Using the method of vacuum condensation of substances on cryogenic surfaces, experimental results of the structural transformation of films, their optical characteristics were obtained, and methodological recommendations for identification were developed. [1]

The fundamental knowledge obtained during the experiments has practical significance in the technologies and processes occurring on the low-temperature surfaces of cryogenic equipment of spacecraft. Thus, this article is devoted to the experimental study of the processes of adsorption and desorption of astrophysical significant molecules of substances formed on low-temperature surfaces of cryogenic vacuum equipment. Study of relaxation processes and thermally stimulated structural-phase transformations in samples condensed at low temperatures. The objects of research are cryocondensate of gases such as nitrogen, carbon monoxide, alcohol, water, and other substances whose condensation forms amorphous structures at low temperatures. The research results are aimed at establishing the relationship between condensation conditions (substrate temperature and gas phase pressure) and the properties of the resulting cryofilms, such as growth rate, optical characteristics and thermal adsorption.

[1] Golikov, O., Yerezhep, D., Akylbayeva, A. et al. Cryovacuum setup for optical studies of astrophysical ice. - 2023- Sci Rep 13, 21155 https://doi.org/10.1038/s41598-023-48541-3

Influence of phase disequilibrium on changes in elastic properties of superplastic eutectic alloys caused by prior plastic deformation and aging

V. F. Korshak[1], Y. O. Shapovalov[2], P. P. Pal-Val[2], L. N. Pal-Val[2]

[1] V. N. Karazin Kharkiv National University, 4 Svobody Sq., Kharkiv, 61022, Ukraine
[2] B. Verkin Institute for Low Temperature Physics and Engineering of NAS of Ukraine, 47 Nauky Ave., Kharkiv, 61103, Ukraine
e-mail: vera.korshak@gmail.com

The report presents the results of the first systematic study conducted by the authors on changes in Young's modulus E of superplastic eutectic alloys Sn-38wt.%Pb and Bi-43wt.%Sn under conditions of pre-plastic deformation, prolonged natural aging, and creep at room temperature at external stress σ, which is optimal for the manifestation of the superplasticity effect. The interest in studying these issues is largely determined by the lack of understanding of the role played by the non-equilibrium phase state of alloys in the emergence of this effect. This is naturally expected, considering the well-known fact that only rapidly quenched samples exhibit superplasticity.

The studied cast alloys were obtained under conditions of rapid crystallization under supercooling, which reached 34 °C for the Sn-38wt.%Pb alloy and 17 °C for the Bi-43 wt.%Sn alloy. Preliminary deformation was performed by compression on a hydraulic press by ≈ 70-75 %. Mechanical tests were carried out at a constant stress of σ = 4.5 MPa and σ = 9.0 MPa for Sn-38wt.%Pb and Bi-43wt.%Sn alloys, respectively. Young's modulus was determined from acoustic measurements using the composite piezoelectric vibrator method. The longitudinal vibration frequency was ≈ 102 kHz and ≈ 113 kHz, and the amplitude of ultrasonic deformation was $\varepsilon_0 \sim 10^{-7}$.

It was found that compression increases the Young's modulus of both alloys. The modulus also increases during aging in both cast and compressed samples. Grinding the surface layers of the original ingots leaves Young's modulus of the cast Sn-38wt.%Pb alloy almost unchanged with aging, while it decreases in the compressed samples to the values for the cast samples. The superplastic deformation of the alloys is accompanied by a noticeable decrease in Young's modulus as the relative elongation accumulates from 0 to ≈ 150%: by ≈ 15 % in the Sn-38wt.%Pb alloy and by ≈ 8 % in the Bi 43wt.%Sn alloy. Upon further elongation, the modulus experiences a periodic increase followed by a decrease [1].

Taking into account the obtained experimental data on changes in the phase composition of alloys the following conclusions were made. The increase in Young's modulus during aging is associated with the transition of alloys from the metastable to the equilibrium phase state at room temperature. The decrease in E under superplastic flow conditions results from the combined effects of the deformation and decomposition of supersaturated solid solutions formed in alloys under the selected crystallization conditions. The increase in E due to compression is caused by the emergence of internal stresses in the material. Preliminary mechanical treatment significantly affects the phase state of the studied alloys. The periodic increase in Young's modulus amidst its predominant decrease indicates the periodicity of phase formation processes in the studied metastable eutectic alloys under superplastic deformation conditions.

[1] V. F. Korshak et al., J. Mater. Sci., 53, 8590 (2018). https://doi.org/10.1007/s10853-018-2163-1

Electronic Structure of Sr-doped $CsPbCl_3$ Crystal: First Principles Investigation

M. Kovalenko, O. Bovgyra, Ya. Chornodolskyy, O. Pidhornyi

Ivan Franko National University of Lviv,
8, Kyrylo and Mefodiy, 79005 Lviv, Ukraine
e-mail: mariya.kovalenko@lnu.edu.ua

Organic-inorganic perovskites, particularly $CsPbCl_3$, are of significant interest in designing electronic devices like light-emitting diodes and solar cells due to their low cost and application feasibility. The efficiency of solar cell materials changes with their band gap, while the band gap depends on different physical parameters separately, such as a phase transition. $CsPbCl_3$, as is well known, is a direct band gap semiconductor that absorbs visible and ultraviolet light. Hence, this compound is used in photovoltaic and optoelectronic devices such as solar cells, photonic crystals, and light-emitting diodes.

A promising strategy to expand properties is the impurity doping of perovskite materials. For some metal ions (e.g., Zn^{2+}, Cr^{3+}, Nd^{3+}, Er^{3+}, Ce^{3+}), doping has been checked to be a hopeful way to improve the optical and electrical performance of perovskite materials, including the decrease of trap density and the boosts of stability, carrier mobility, and photoluminescence quantum yield. For example, Sr^{2+} dopants in $CsPbI_3$ perovskite nanocrystals enhance their stability and optical properties by increasing defect formation energy [1]. However, a mechanism of how doping influences the optical properties in perovskite nanocrystals is unobvious, and with it, no generalizable understanding is available that captures all observed effects. There are also no first-principles studies of the electronic structure of doped perovskites, which would make it possible to interpret the existence of experimental data. In this study, we report first-principles investigations of pure and Sr-doped $CsPbCl_3$ electronic properties.

All theoretical calculations are completed using the density functional theory (DFT). We apply the Perdew-Burke-Ernzerhof (PBE) parametrization for generalized gradient approximation (GGA) to describe the exchange-correlation functional. The cut-off energy was set as 450 eV; the convergence tolerance for energy was set as 5×10^{-6} eV/atom, and the tolerance for maximum force was 0.01 eV/Å. A 2×2×2 supercell was used to simulate the substitutional doping $CsPbCl_3$ system. First, we provide the geometry optimization of undoped $CsPbCl_3$ crystal using effectively Broyden-Fletcher-Goldfarb-Shanno algorithm. Next, we substituted the Pb atom for the Sr atom, and the optimization procedure was repeated. For a more accurate description of electronic spectra, Hubbard correction was applied to GGA, the so-called GGA+U method.

To understand the changes in electronic properties of Sr-doped $CsPbCl_3$ crystal, we initially performed calculations of structural and electronic properties for undoped ones. After structure optimization using GGA+U approximation, the lattice parameters are 5.706 Å, and the band gap of pure $CsPbCl_3$ crystal was 3.07 eV, which agrees with experimental data. Adding a Sr atom slightly changes the lattice parameters of $CsPbCl_3$ crystal to 5.722 Å, mainly due to a lengthening of Pb–Cl and Sr–Cl bond length. The calculated formation energy of Sr-doped $CsPbCl_3$ shows the value of −1.74 eV, indicating the thermodynamically favorable position of the dopant. The presence of the Sr atom changes the doped crystal's electronic structure and leads to the band gap widening to 3.39 eV. The main contribution to the expansion of the bandgap doped system is the appearance of d-states of Sr at the bottom of the conduction band. Our investigation provides a helpful reference for the deep understanding and further development of Sr-doped $CsPbCl_3$ perovskites.

This project has received funding through the EURIZON project, which is funded by the European Union under grant agreement No.871072.

[1] C. Chen, T. Xuan, W. Bai, T. Zhou, F. Huang, A. Xie, L. Wang, R. Xie, J. Nano Energy, 85, 106033 (2021). https://doi.org/10.1016/j.nanoen.2021.106033.

Temperature-induced phase transformation in $(As_{1-x}Bi_x)_2S_3$ glasses

S. Hasynets[1], V. Kryshenik[1], A. V. Gomonnai[1,2], V. Lopushansky[1], V. Loya[1], I. Chychura[1], V. Rubish[3]

[1] Institute of Electron Physics of NAS of Ukraine, 21 Universytetska Str., Uzhhorod, 88017, Ukraine
[2] Uzhhorod National University, 3 Narodna Sq., Uzhhorod, 88000, Ukraine
[3] Uzhhorod Laboratory of Institute for Information Recording of NAS of Ukraine, 4 Zamkovi Skhody str., Uzhhorod, 88000, Ukraine
e-mail: kryshenik@gmail.com

Introduction of metal dopants in the structure of chalcogenide glasses as well as a choice of the preparation technology essentially affect their physical properties, in particular, the value and type of electrical conductivity, optical and thermoelectric characteristics, photosensitivity, etc. Stability of their operating characteristics depends on their capability of structural relaxation, including crystallization, with increasing temperature.

$(As_{1-x}Bi_x)_2S_3$ glasses with $0 \le x \le 0.20$ were prepared from pre-synthesized As_2S_3 glass and needle-shaped Bi_2S_3 crystals loaded in desired amounts into evacuated quartz ampoules heated to 1023 K at a rate of 50 K/h with subsequent aging for 3 h and cooling at 30 K/h down to 873 K followed by air quenching. These glasses were shown to possess clearly amorphous structure in the whole compositional range [1]. This was essentially different from an earlier study [2], where introduction of more than 6 at. % Bi into As_2S_3 glass resulted in noticeable phase separation in the amorphous medium by formation of elemental bismuth and crystalline Bi_2S_3 inclusions.

In this study, we focus on the kinetic analysis of crystallization processes in Bi-doped $(As_{1-x}Bi_x)_2S_3$ glasses with $0.08 \le x \le 0.20$, using the possibilities of differential thermal analysis technique. The glass heating rate b was varied from 3 to 12 K/min. Our measurement showed the presence of a single (one-step) mechanism of the crystallisation process for all the glasses under investigation. As follows from X-ray diffraction measurements, the thermal annealing results in the formation of Bi_2S_3 crystallites in the amorphous glass matrix.

The activation energy E_c of the amorphous-to-crystalline transformation under study was determined by the linear isoconversional method of Kissinger, Akahira, and Sunose [3]. Note that the experimentally determined E_c values in our case were noticeably below those reported in the earlier study [2] for thermal crystallization effects in Bi-doped As_2S_3 glass with doping level closest to the $(As_{0.92}Bi_{0.08})_2S_3$ composition. The reason, in our opinion, is related to the fact that in our case the initial samples were clearly amorphous while those obtained by the authors [2] even at Bi content of 0.015–0.03 already initially contained crystalline inclusions what definitely follows from their own Raman spectra [4].

We found that while increasing the content of Bi in the $(As_{1-x}Bi_x)_2S_3$ glasses from $x = 0.08$ to $x = 0.20$, the temperature of the relaxation peak of thermal crystallization T_p at b=6 K/min gradually varied from 596 to 540 K. The experimentally determined crystallization parameters E_c and T_p as well as the glass transition temperature T_g and the melting temperature T_m enabled us to analyze how the increasing Bi content in the As_2S_3-based glass affects its thermal stability. The glass thermal stability characterized by a so-called Hrubý parameter is shown to decrease with the bismuth content.

[1] Y. Azhniuk, V. Lopushansky, S. Hasynets, V. Kryshenik, A. V. Gomonnai, and D. R. T. Zahn, J. Raman Spectroscopy. (2024). https://doi.org/10.1002/jrs.6658.
[2] M. V. Šiljegović, S. R. Lukić-Petrović, G. R. Štrbac, and D. M. Petrović, J. Therm. Anal. Calorim. 110, 379 (2012). https://doi.org/10.1007/s10973-012-2353-z
[3] H. E. Kissinger, J. Res. Nat. Bur. Stan. 57, 217 (1956). https://doi.org/10.6028/jres.057.026
[4] M. V. Šiljegović, S. R. Lukić-Petrović, G. R. Štrbac, N. Ćelić, and I. R. Videnović, Acta Phys. Polon. A 134, 498 (2018).

Features of thermal transport processes in van der Waals chalcogenides

V. Liubachko, Yu. Vysochanskii

Institute for Solid State Physics and Chemistry, Uzhhorod National University, Uzhhorod, Ukraine
e-mail: vitalii.liubachko@uzhnu.edu.ua

Previous research [1] has explained the thermal properties of metal phosphorus chalcogenides through phonon processes and strong anharmonicity. This anharmonicity is caused by factors such as disorder, hybridization of electronic levels, ion coordination, or size, which play a role in the second order Jahn-Teller (SOJT) effect. In [2], we studied the complex influence of the indium and copper cationic sublattices on the origin of ferrielectricity. The study has shown that indium is crucial in the polar ordering of $CuInP_2S_6$ crystals. This finding may also suggest the possibility of additional mechanisms affecting heat transfer properties, such as high-temperature diffusive heat transfer. Therefore, we attempted to estimate the contribution of the diffusive component to thermal conductivity in the $CuInP_2S_6$ crystal. Above the Debye temperature, the thermal conductivity deviates from the Eucken law as $\kappa(T) = 380/T + 0.29$, where the first term represents the three-phonon mechanism, and the second term represents the additional contribution to diffusive heat transfer. According to [3], a diffusive component has been estimated to increase just above $T_{Debye} \approx 90$ K (fig. 1a). This occurs in the temperature region where the contribution of the indium sublattice to the anharmonic dynamics begins to appear [2]. In the ferrielectric phase, below the first order phase transition $T_C = 315$ K, the copper disordering associated with the SOJT effect strongly inhibits thermal conductivity.

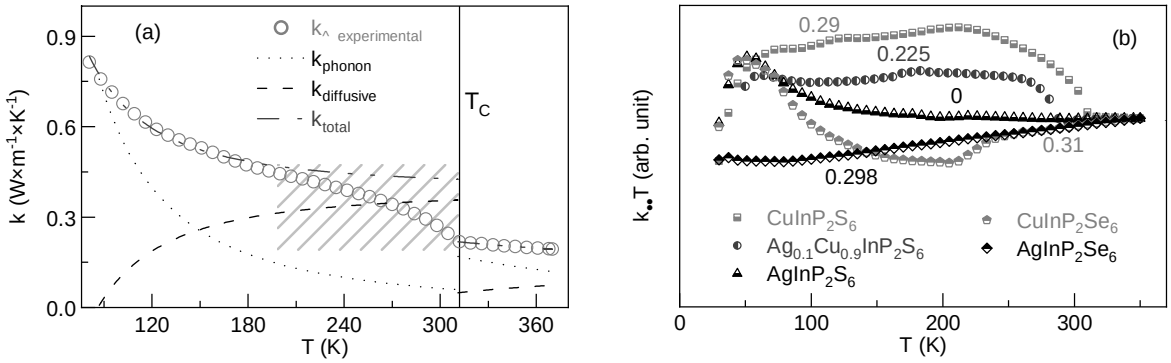

Figure 1. (a) thermal conductivity of $CuInP_2S_6$ crystal, measured perpendicular to the structural layers. The phonon and diffusive components are shown as dotted and dashed lines, respectively. The region with the stark decrease of κ, related to the disordering of Cu cations is shaded with light grey lines; (b) comparable thermal conductivity of van der Waals chalcogenides, measured parallel to the structural layers, presented in κT(T) coordinates.

At partial Cu by Ag substitution, the diffusive contribution is reduced (fig. 1b). This can be explained by the suppression of indium contribution due to the more covalent Ag bonding and a suppression of the SOJT effect. In $AgInP_2S_6$, only the three-phonon contribution has been observed in the high-temperature region. At S by Se substitution, the diffusive component was observed in the paraelectric phase of the $CuInP_2Se_6$ crystal. However, it was not found in the ferrielectric phase, which can be explained by the shallower double-well potential for Cu cations in the selenide compound what leading to a reduction in the phase transition temperature. In the case of the $AgInP_2Se_6$ crystal, a diffusive contribution is present over a wide temperature range.

[1] V. Liubachko, A. Oleaga, A. Salazar, A. Kohutych, K. Glukhov, A. Pogodin, Yu. Vysochanskii. Phys. Rev. Mater. 3, 104415(1-9) (2019). https://doi.org/10.1103/PhysRevMaterials.3.104415.
[2] Yu. Vysochanskii, V. Liubachko, R. Yevych, K. Glukhov, A. Kohutych, V. Hryts, A. Dziaugys, J. Banys. In:IEEE-ISAF (2023). https://doi.org/10.1109/ISAF53668.2023.10265377.
[3] V.A. Konstantinov. Low Temp. Phys. 29, 422 (2003). https://doi.org/10.1063/1.1542506.

The specificity of the interaction of palladium with hydrogen

O. M. Liubymenko

Donetsk National Technical University "Donetsk National Technical University",
str. Potebni, 56, Lutsk, 43000, Ukraine
e-mail: e.n.lyubimenko@gmail.com

At the current stage of Ukraine's development, in order to ensure its energy independence, there are still some questions that require the study and improvement of materials to ensure the safety of energy installations in which hydrogen is used and stored. The interaction of materials with hydrogen leads to the occurrence of internal stresses, such as hydrogen phase and concentration stresses. This can lead to breakdowns of power equipment. However, the influence of hydrogen can also have a positive effect on the structure and properties of materials, and this contributes to the development of new materials with various physical properties.

The research work is aimed at conducting experiments and studying the behavior of materials in different conditions, which will help in solving problems with storage and obtaining hydrogen.

As part of the experimental part of the study, the effect of changing the hydrogen content during degassing of the α-PdH_n alloy (where n is the hydrogen concentration in palladium) was analyzed. A cantilever was installed in the hydrogen-vacuum installation [1], and one end was fixed in a holder so that the side of the cantilever was on top, which is covered with a copper film that does not allow hydrogen to pass through and does not affect the shape of the cantilever change. Next, the hydrogen pressure in the chamber was raised to the specified value and the hydrogen saturation was carried out on one side of the cantilever made of pure palladium (99.99%), as a result, an α-PdH_n alloy was obtained. After that, this alloy was kept in a hydrogen environment to equalize the hydrogen concentration along the cross section of the cantilever and to reduce the hydrogen-concentration stresses. As a result of such experiments, alloys with different hydrogen content from n = 0.0184 H/Pd to 0.0062 H/Pd were obtained.

Next, the cantilever made of the α-PdH_n alloy was degassed in the chamber of the hydrogen-vacuum installation to a pressure of 1.33 Pa and observed through the window of the working chamber of the hydrogen-vacuum installation and the cathetometer behind the bends of the cantilever. The degassing process was recorded on video. This allowed us to obtain time-dependent changes in the shape of the cantilever during the formation of temporary palladium-hydrogen gradient alloys. As a result of such studies, it was established that the bending of the α-PdH_n alloy cantilever is completely reversible and occurs in two stages: the first stage is the achievement of the maximum bending and the formation of a plateau within 3-5 seconds, this stage is very short. The second, longer stage is the return of the cantilever to its initial state. It should be noted that the value of the maximum bend for the cantilever for such an alloy exceeds the bend that pure palladium can withstand, and this indicates the production of an alloy with increased plastic characteristics [2-3].

Thus, the formation process of the maximum bending of the cantilever for gradient alloys of α-PdH_n with an H-content from n = 0.0184 H/Pd to 0.0062 H/Pd is due to the diffusion transport of hydrogen, the redistribution of internal stresses in the cantilever during its bending (straightening) and the corresponding restructuring of the hydrogen concentration field, which changes the internal conditions of diffusion transport of hydrogen into the layers of the α-PdH_n alloy, which have different physical properties (lattice period, Young's modulus) than pure palladium.

[1] O. M. Lyubimenko, Metallofizika i Noveishie Tekhnologii, 45(2), 2023,
[2] E. P. Feldman, O. M. Lyubimenko, Journal Acta Mechanica. (2023).
O.M Lyubimenko, K. V. Gumennyk, E. P. Feldman. J. of Applied Physics, 127, № 24: 245104 (2020).

X-ray determination of the influence of cryodeformation on the microstructure of ultrafine-grained/nanocrystalline titanium

Yu. M. Pohribna, V. A. Moskalenko

B. Verkin Institute for Low Temperature Physics and Engineering of NAS of Ukraine,
47 Nauky Ave., Kharkiv, 61103, Ukraine
e-mail: Plotnikova@ilt.kharkov.ua

Investigation of the deformation microstructure of nanocrystalline (NC) and ultrafine-grained (UFG) materials is of great interest for optimizing their unique physical and mechanical properties. In most cases, to obtain materials of this class large plastic deformation modes [1]. Given the coexistence of anisotropy of physico-mechanical properties and crystallographic texture of hcp titanium, it is important to study the directional microstructural inhomogeneity or morphological anisotropy of structural elements.

In order to ascertain the anisotropy of the microstructure, a comparative analysis of diffraction patterns, relative integral intensities *I*, dimensions of crystallites (coherent scattering regions) *L* and microdeformation values $<e^2>^{1/2}$ in the rolling plane and in the plane perpendicular to the rolling direction (RD) was performed by comparison. The microstructural elements of the emerging structural states and their parameters were determined by the activity of deformation modes - slip and twinning. Their activity depended on the degree of cryorolling [2].

As a result, cryodeformation leads to a significant change in intensity distribution. The complex nature of the observed change in the height and width of the diffraction reflection profiles reflects the evolution of microstructure which is associated with the generation of a nanocrystalline state and determined by the level of defectiveness and by a decrease in the CSR size. The difference in intensity distribution for the planes parallel and perpendicular to the rolling direction is determined by crystallographic randomization of microstructural elements. It is established that dependencies of crystallite sizes on a degree of cryocompression for two mutually perpendicular surfaces are similar and correlate with the stage character of the change in grain size. The effect of morphological anisotropy of crystallites/grains is most pronounced for the nanocrystalline state. The observed complex variation in the microdeformation with compression deformation is well correlated with relative slip and twinning activity, which affect the level of local internal stresses and the possibility of their relaxation. The observed anisotropy with respect to the magnitude of microdeformations may be attributed to the presence of oriented grain boundaries associated with the shape anisotropy of crystallites/grains.

[1] M.A. Meyers, A. Mishra, D.J. Benson, Progr. Mat. Sci. **51**, 427 (2006).
[2] V.A. Moskalenko, A.R. Smirnov, A.V. Moskalenko, Low Temp. Phys. **35**, 905 (2009).

The electric field induced light birefrigence in $HoAl_3(BO_3)_4$

V. A. Bedarev, D. M. Merenkov, S. M. Poperezhai

B. Verkin Institute for Low Temperature Physics and Engineering of NAS of Ukraine,
47 Nauky Ave., Kharkiv, 61103, Ukraine
e-mail: poperegay@ilt.kharkov.ua

The noncentrosymmetric rare-earth aluminum borates $REAl_3(BO_3)_4$ (RE - rare earth) belong to a trigonal system with the space group *R*32. These materials are potential candidates for a variety of practical applications based on the giant magnetoelectric effect, which is manifested in them. The magnitude of the magnetoelectric effect strongly depends on the type of rare earth ion in these compounds. Holmium aluminum borate demonstrates the greatest magnitude of this effect among such compounds. The maximum measured value of electric polarization *P* reached 3.600 μC⁄m^2 at a magnetic field of 70 kOe at liquid helium temperature [1].

Previously, the electro-optical Pockels effect was discovered in rare-earth borate $TmAl_3(BO_3)_4$ ($P_{max} \approx 300$ μC⁄m^2 [2]) at room temperature [3]. The Pockels effect is associated with a changing in the dispersion law for the dielectric constant of the crystal. The change is caused by a Stark shift in the energy levels of rare earth ions under the influence of an external electric field. It is obvious that the structure of the energy levels of rare earth ions in $HoAl_3(BO_3)_4$ and $TmAl_3(BO_3)_4$ crystals is different, and the magnitude of the electro-optical effect, like the magnetoelectric one, depends on the type of rare earth ion. Therefore, we investigated the Pockels effect in holmium aluminum borate.

The single crystal plate with dimensions 4x4 mm and thickness near 230 μm was studied. Investigations were carried out with the wavelength of He-Ne laser (0.633 μm). In the experiments the light beam was directed along the crystal axis C_3 (*c*-axis) and the electric field was directed along the axis C_2 (*a*-axis). The electric field dependences of light birefrigence were measured at room temperature. The sample dimensions and experimental conditions strictly corresponded to the measurement conditions of the $TmAl_3(BO_3)_4$ crystal. The measurements were carried out in a constant field not exceeding 1.6 kV.

Based on experimental measurements, it was found that the induced birefringence Δn linearly depends on the applied field E_x: $\Delta n = \alpha E_x$ with a coefficient $\alpha = 1.6 \cdot 10^{-11}$ m/V. To assess the main piezoelectric characteristic of holmium aluminum borate - the electro-optical coefficient $r_g = \alpha / n_a^3$ - the Brewster angle was determined by measuring the angular dependence of the intensity of light reflected from the crystal surface parallel to the C_3 axis. The value of this angle was = 54.3°, which gives the reflection coefficient n_a = 1.39. Thus, the value of the electro-optical coefficient of the $HoAl_3(BO_3)_4$ single crystal is $5.9 \cdot 10^{-12}$ m/V, which is less than that of $TmAl_3(BO_3)_4$ ($6.6 \cdot 10^{-12}$ m/V [3]).

It was shown that the electric field induces linear birefringence in $HoAl_3(BO_3)_4$ crystal. By measuring the angular dependences of the intensity of light reflected from the sample surface the Brewster angles was determined and the value of the main refractive index crystal was obtained. The general electro-optic coefficient of $HoAl_3(BO_3)_4$ was established.

[1] K.-C. Liang, R.P. Chaudhury, B. Lorenz, Y.Y. Sun, L.N. Bezmaternykh, V.L. Temerov, and C.W. Chu, Phys. Rev B. 83(R), 180417 (2011). http://dx.doi.org/10.1103/PhysRevB.83.180417.
[2] R.P. Chaudhury, B. Lorenz, Y.Y. Sun, L.N. Bezmaternikh, V.L. Temerov and C.W. Chu, Phys. Rev B. 81(R), 220402 (2010). http://dx.doi.org/10.1103/PhysRevB.81.220402.
[3] M.I. Pashchenko, V.A. Bedarev, D.N. Merenkov, S.L. Gnatchenko, L.N. Bezmaternykh, A.L. Sukhachev and V.L. Temerov, Appl. Opt. 55, B11 (2016). http://dx.doi.org/10.1364/AO.55.000B11.

Dilatometric properties of Rb_2SO_4 crystals in the region of low temperatures

I. A. Pryshko[1], V. Yo. Stadnyk[1], O. V. Shtuka[1], I. S. Novosad[1,2]

[1] Physics Faculty, Ivan Franko National University of Lviv,
19 Dragomanov Street, 79005 Lviv, Ukraine
[2] Department of General Physics, Lviv Politechnic National University,
12 Bandery Str., UA-79013 Lviv, Ukraine
e-mail: pryshko_ivan@ukr.net

In this work we investigated the thermal expansion $(\Delta l/l)_i$ of rubidium sulfate (RS) Rb_2SO_4 crystals in the region of low temperatures. These crystals have a phase transition from pseudohexagonal to orthorhombic phase ($P\bar{3}m1 \leftrightarrow Pnam$) at $T_C \approx 922$ K.

The studied crystals were obtained by the method of slow evaporation at room temperature of an aqueous solution of repeatedly recrystallized pure rubidium sulfate salts Rb_2SO_4. The solution was at room temperature, which was controlled by a thermostat with an accuracy of 0.5 K. The growing was carried out from spontaneously formed seeds with a pseudo-hexagonal morphology for 20 days. The obtained crystals were of good optical quality and had the shape of an elongated prism, the size of which was approximately 6 × 8 × 8 mm. Thermal expansion was studied using a quartz dilatometer.

It was established that the linear dimensions decrease as the temperature decreases. For the X- and Y-directions, these changes are not significant and are practically the same $\alpha_{X,Y} = \frac{1}{l_0}\left(\frac{\Delta l}{\Delta T}\right)$ ≈ $1.8 \cdot 10^{-7}$ K^{-1} and $2.2 \cdot 10^{-7}$ K^{-1}, respectively. In the Z-direction of occurrence of ferroelastic deformation, these changes are slightly larger $\alpha_Z \sim 3{,}6 \cdot 10^{-7}$ K^{-1}.

The relative changes in the volume of the sample were also calculated based on the obtained data and according to the formula:

$$\Delta V/V_0 = (\Delta l/l_0)_x + (\Delta l/l_0)_y + (\Delta l/l_0)_z$$

It is established that as the temperature decreases, the volume of the crystal decreases almost linearly so that the coefficient of temperature change of the volume $\beta = \frac{1}{V_0}\left(\frac{\Delta V}{\Delta T}\right)$ ≈ $7.2 \cdot 10^{-7}$ K^{-1}. It was found that the parameters $(\Delta l/l_0)_i$ are strongly anisotropic. It is known that the following relations are used to estimate the quantitative parameters A describing the anisotropy of a certain physical characteristic f (in our case – relative linear thermal expansion) [23, 24]:

$$A = \sum_{i \neq j}^{n} \frac{|f_i - f_j|}{|f_i| + |f_j|} = \frac{|f_x - f_y| + |f_x - f_z| + |f_y - f_z|}{|f_x + f_y + f_z|}$$

It was found that at room temperature, the anisotropy coefficient A = 0.053 and it changes slightly with temperature: the decrease in temperature is accompanied by a decrease in A, which is due to the approach of the crystal to the isotropic state. At temperature T = 85 K the value of A = 0.037. The dependences of the $A(T)$ parameters make it possible to analyze the main regularities of the temperature behavior of dilation anisotropy in crystals.

[1] P.E. Tomaszewski, Phase Transit. 38 (1992). https://doi.org/10.1080/01411599208222899.
[2] Andriyevsky B., Czapla Z., Kardash V., Dacko S., Dumka Yu. Dilatative and refractive properties of diglycine nitrate crystals in the range of phase transition, Material Science and Engineering B. 95 (2002). https://doi.org/10.1016/S0921-5107(02)00199-X

Low-temperature micromechanical properties of epoxy resin/graphene oxide nanocomposites

H. V. Rusakova, L. S. Fomenko, S. V. Lubenets, A. V. Dolbin, N. A. Vinnikov, R. M. Basnukaeva, S. V. Cherednichenko

B. Verkin Institute for Low Temperature Physics and Engineering of NAS of Ukraine, 47 Nauky Ave., Kharkiv, 61103, Ukraine
e-mail: rusakova@ilt.kharkov.ua

The response of neat epoxy resin (ER) and ER/reduced graphene oxide (rGO) nanocomposites to the action of a localized load at temperatures T = 77-300 K was studied. It has been established that during indentation in the range of 77 K < T < T_{he}, where the threshold temperature of high elasticity T_{he} ≈ 210-240 K, the indenter impressions on the surface of the studied samples are completely restored when the load is removed and the samples are heated to room temperature. At the same time, at higher indentation temperatures T_{he} < T < 300 K, the impressions are preserved and and their dimensions can be measured to determine the Vickers microhardness H_V. The phenomenon of low-temperature elasticity was previously observed by us during indentation of a number of polymers and nanocomposites; it was associated with the formation of fibrillar-porous nanostructures with low glass transition temperatures during low-temperature local deformation [1].

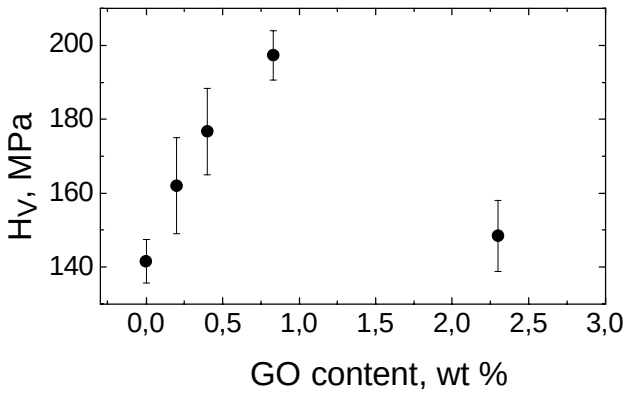

Fig. 1

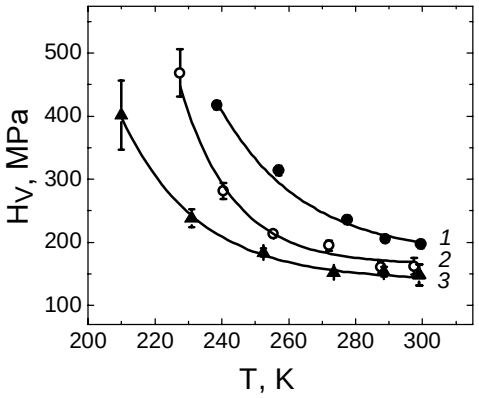

Fig. 2

At room temperature, the dependences of microhardness of nanocomposites on rGO content were obtained (Fig. 1). It can be seen from the figure that the introduction of graphene oxide into the epoxy matrix leads to a significant increase in microhardness. The maximum effect was observed for ER-0.83 wt% rGO nanocomposite, the microhardness of which exceeds H_V of neat ER by 40%. Reduction of microhardness for ER-2.3 wt% rGO nanocomposite is associated with the formation of rGO agglomerates.

The effect of temperature on the microhardness of neat ER and ER/rGO nanocomposites was studied in the temperature range from 300 K to T_{he} » 210-240 K. Fig. 2 shows the temperature dependences of microhardness for three nanocomposites: *1* – ER-0.83 wt% rGO, *2* – ER-0.2 wt% rGO, *3* – ER-2.3 wt% rGO. Lowering the temperature from 300 K to T_{he} » 210-240 K (depending on the rGO content) is accompanied by an approximately two-fold increase in microhardness, which indicates the thermally activated nature of the deformation process in the region of the indenter impression.

[1] A. V. Rusakova, L. S. Fomenko, S. V. Lubenets, A. V. Dolbin, N. A. Vinnikov, R. M. Basnukaeva, A. V. Blyznyuk, Low Temp. Phys. 46, 336 (2020). http://dx.doi.org/10.1063/10.0000699.

The reverse indentation size effect in heavily deformed materials

S. V. Lubenets, L. S. Fomenko, H. V. Rusakova

B. Verkin Institute for Low Temperature Physics and Engineering of NAS of Ukraine,
47 Nauky Ave., Kharkiv, 61103, Ukraine
e-mail: rusakova@ilt.kharkov.ua

Experiments performed on a large number of coarse-grained (CG) materials have shown that the value of the indentation load P (the depth of indenter penetration h), as a rule, can have a significant effect on the measured value of microhardness H_V. This effect is called the "indentation size effect" (ISE). It is usually observed in the region of low loads and consists in an increase in microhardness as the indentation load decreases. The effect has a different nature, but most often two reasons lead to it: the introduction of geometrically necessary dislocations (GNDs) during the indentation of crystalline materials that ensures the formation of an indent and the violation of the homogeneity of the surface layer caused by mechanical treatment of the sample surface before indentation. The aim of this work was to study the indentation load effect on the microhardness of materials subjected to severe plastic deformation (SPD). The dependences $H_V(P)$ obtained on the number of ultrafine-grained and nanocrystalline materials, namely, VT1-0 [1], Al [2], Cu [3] and Al-Li [4], subjected to cryorolling, equal channel angular pressing, direct hydroextrusion or combined direct and equal channel angular hydroextrusion were analyzed.

It is shown that in CG samples of all materials studied the usual ISE is observed: the microhardness value increases with decreasing the indenter load (indenter penetration depth); the dependences can be described within the framework of a simple GNDs model developed by Nix and Gao [5]. The model predicts that the microhardness of a rigid material should not strongly depend on the depth of indenter penetration. This is actually observed in measurements the microhardness of the samples preliminarily hardened by different SPD methods. An increase of microhardness with decrease of the load was very small or practically not registered during the indentation of VT1-0 [1], Al [2], Cu [3] and Al-Li [4].

Of some interest is the significant drop in the microhardness of SPD processed specimens in the region of low loads (reverse ISE). This effect may be due to the surface treatment of the sample prior to indentation. It is known that grinding usually hardens the surface layer of cast and annealed specimens. Pretreatment of the material by various SPD methods leads to the formation of a special structure in its volume that provides high microhardness. In this case, additional grinding of the surface destroys the microstructure created during SPD and thereby softens the surface layer. Experimentally this manifests itself in a decrease of the microhardness of samples at low loads, which was observed in SPD processed materials Al [2], Cu [3], Al-Li [4]. The dependence $H_V(h)$ allows to estimate the thickness Δh of the softened layer: $\Delta h \approx$ 5-6 μm for soft material, such as Al, and $\Delta h \approx$ 1-2 μm for stiff one, such as titanium.

[1] A. V. Rusakova. S.V. Lubenets, L. S. Fomenko, V. A. Moskalenko, and A. R. Smirnov, Low Temp. Phys. 41, 835 (2015). http://dx.doi.org/10.1063/1.4929593.
[2] Yu. Z. Estrin, L. S. Fomenko, S. V. Lubenets, S. E. Shumilin, and V.V. Pustovalov, Low Temp. Phys. 34, 771 (2008). http://dx.doi.org/10.1063/1.2973719.
[3] S. V. Lubenets, L. S. Fomenko, H. V. Rusakova, Low Temp. Phys. 48, 570 (2022). http://dx.doi.org/10.1063/10.0011606.
[4] A. V. Rusakova. S.V. Lubenets, L. S. Fomenko, and P. A. Zabrodin, Low Temp. Phys. 40, 330 (2014). http://dx.doi.org/10.1063/1.4869570.
[5] W. D. Nix, H. Gao, J. Mech. Phys. Solids 46, 411 (1998). http://dx.doi.org/10.1016/S0022-5096(97)00086-0.

Nonlinearity effect of highly elastic deformation of an amorphous polymer

V. D. Natsik, H. V. Rusakova

B. Verkin Institute for Low Temperature Physics and Engineering of NAS of Ukraine,
47 Nauky Ave., Kharkiv, 61103, Ukraine
e-mail: rusakova@ilt.kharkov.ua

The analysis of the kinetics of the tensile deformation of *amorphous polyimide* samples with a constant rate of $7\cdot10^{-5} < \dot{\varepsilon} < 6\cdot10^{-3}$ s^{-1} at constant values of the temperature T in the warm state (T = 293 K) and under the conditions of moderate (T = 77 K) and deep (T = 4.2 K) cooling begun in [1] was continued. The three-stage deformation diagrams $\sigma(\varepsilon;T,\dot{\varepsilon})$ were registered in [1], here $\varepsilon = \dot{\varepsilon} t$ is the relative deformation, σ is the deforming stress; one of the diagrams is shown in the figure. The initial stages of linear elasticity $\sigma_{\rm I}(\varepsilon;T,\dot{\varepsilon}) = M_e\varepsilon$ with Young's modulus $M_e = M_e(T)$ were recorded within $\varepsilon < 0.1$. The next relaxation stage $\sigma_{\rm II}(\varepsilon;T,\dot{\varepsilon})$ was interpreted in [1, 2] as a consequence of the thermomechanical activation of specific *elaston excitations* on molecular chains in an amorphous polymer, i.e., elementary acts of highly elastic deformation under the action of effective stress $\sigma^* = \sigma - \sigma_i(\varepsilon;T)$. Here, σ_i is the entropy component of internal stresses caused by changes in conformational entropy during the straightening of molecular chains. The stage of highly elastic deformation $\sigma_{\rm III}(\varepsilon;T,\dot{\varepsilon})$ is also determined by the kinetics of elaston excitations, it always has an extended linear component $\sigma_{\rm III} = \sigma_{fe} + M_{he}\varepsilon$ with the modulus of entropy elasticity $M_{he} = M_{he}(T)$ and the conditional limit of elasticity $\sigma_{fe} = \sigma_{fe}(T,\dot{\varepsilon})$. But when the part of the samples were deformed at T = 293 K, a significant deviation from the linear law was found within the strength limit of polymer $\varepsilon < \varepsilon_r$.

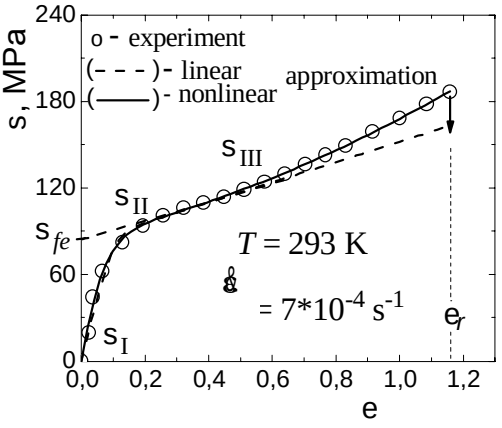

The nonlinearity of the stage $\sigma_{\rm III}(\varepsilon;T,\dot{\varepsilon})$ is interpreted as a consequence of the nonlinear dependence of $\sigma_i(\varepsilon; T)$ on deformation with the second-order elastic modulus $\mu_{he} = \mu_{he}(T)$:

$$\sigma_i(\varepsilon; T) = M_{he}\varepsilon + \mu_{he}\varepsilon^2. \qquad (1)$$

This assumption transforms the four-parameter nonlinear deformation equation [2] into a more complex five-parameter nonlinear equation, in which the kinetics of elaston activation is complicated by the consideration of nonlinearity (1):

$$\frac{d}{d\varepsilon}\sigma = M_e - (M_e - M_{he})\beta\,\mathrm{sh}\left[\frac{\sigma - M_{he}\varepsilon - \mu_{he}\varepsilon^2}{(M_e - M_{he})\varepsilon_T\sqrt{1+\beta^2}}\right] \qquad (2)$$

Parameters of this equation are isothermal coefficients of elasticity $M_e(T)$, $M_{he}(T)$, $\mu_{he}(T)$ and kinetic coefficients $\beta(T,\dot{\varepsilon})$, $\varepsilon_T(T,\dot{\varepsilon})$. Its solution with the initial condition $\sigma(0;T,\dot{\varepsilon}) = 0$ is described by the formula:

$$\sigma(\varepsilon;T,\dot{\varepsilon}) = (M_e - M_{he})\varepsilon_T\sqrt{1+\beta^2}\,\ln\frac{\sqrt{1+\beta^2}+\beta+1+\left(\sqrt{1+\beta^2}-\beta-1\right)\delta(\varepsilon)}{\sqrt{1+\beta^2}+\beta-1+\left(\sqrt{1+\beta^2}-\beta+1\right)\delta(\varepsilon)} + 2\mu_{he}\varepsilon_T^2[1-\delta(\varepsilon)] + (M_{he} - 2\mu_{he}\varepsilon_T)\varepsilon + \mu_{he}\varepsilon^2. \qquad (3)$$

The exponential function $\delta(\varepsilon) = \exp(-\varepsilon/\varepsilon_T)$ determines the shape of the deformation diagram within the relaxation stage $\sigma_{\rm II}(\varepsilon;T,\dot{\varepsilon})$. The solid line in the figure is the analytical approximation of experimental points by the graph of function (3) at the values of M_e = 1413 MPa, M_{he} = 52 MPa, μ_{he} = 34 MPa, $\varepsilon_T = 0.05$, $\beta = 0.6$.

[1] V. D. Natsik et al., Low Temp. Phys. 49, 521 (2023). http://dx.doi.org/10.1063/10.0017812.
[2] V. D. Natsik, H. V. Rusakova, Low Temp. Phys. 49, 228 (2023).

A study of composition and annealing temperature influence on the mechanical properties of Fe-Cr-Al alloys

V. O. Kharchenko[1,2], D. O. Kharchenko[1,2], O. M. Shchokotova[1], B. O. Lysenko[1], A. V. Dvornichenko[2]

[1] Institute of Applied Physics, National Academy of Sciences of Ukraine, 58 Petropavlivska Str., Sumy, 40000, Ukraine
[2] Sumy State University, 116 Kharkivska Str., Sumy, 40007, Ukraine
e-mail: shchokotova.o@gmail.com

Since 1960s the extensive experimental and theoretical studies of iron-based Fe-Cr-Al alloys has been carried out for use in nuclear applications for a wide range of compositions. By using different methods of multiscale modeling scheme, the significant progress in researching of such material properties was achieved. At the same time one of the open questions related to prediction the mechanical properties of these alloys remain actual. Indeed, an influence of alloying elements and annealing temperature onto the hardening and embrittlement in Fe-Cr-Al alloys is still under discussion. Moreover, a study of elastic fields evolution and defects dynamics under mechanical loads conditions is necessary to establish complete information about the physical mechanisms of hardening, that is important for further component selection, composition design and predicting of alloy durability and reliability.

In order to study the influence of alloy composition and annealing temperature on the changes in the mechanical properties of ternary Fe-Cr-Al alloys, it was performed the modeling of externally applied mechanical loading. For sample preparation we exploited a generalized model of the phase field with CALPHAD approach. Using the combination of the phase field method with the nonlinear elasticity theory, which was proposed in references [1-3], the simulation of plastic deformation of Fe-Cr-Al alloy samples was performed. Such approach makes it possible to describe the elastic fields redistribution, particularly elastic strain and stress, under mechanical loading. In this work we investigated processes of plastic deformation in the form of simple shear with constant strain rate $10^9 s^{-1}$.

The shear stress-strain curves were calculated for previously obtained Fe-Cr-Al alloy samples with different content of Cr and Al, which were annealed at different temperatures. The mechanical characteristics were determined from the deformation curves. The analysis of the obtained data showed that the yield strength and ultimate strength take lower values at higher values of the annealing temperature. It was found, that an increase of Cr content leads to the increasing of yield and ultimate strength, while the increase of Al content acts in an opposite manner. Thus, the decrease of the annealing temperature, decrease of the Al content and increase of Cr content result in growth of the material resistance to plastic deformation and strengthening of Fe-Cr-Al alloy. Obtained results are consistent with the general trends from both experimental investigations and simulations. Furthermore, the distributions of the elastic strain and stress were obtained. That allows to observe the formation and evolution of the slips composed of a pair of edge dislocations with opposite Burger vectors (dislocation dipoles). In considered model the slips are the fundamental flow units in plastic deformation. It was shown, that slips are mainly located around chromium-enriched precipitates in the softer (matrix) phase, whereas their edges are mostly trapped at interfaces.

[1] A. Onuki, Phase Transition Dynamics (Cambridge University Press, Cambridge 2002). https://doi.org/10.1017/CBO9780511534874.
[2] A. Onuki, Phys. Rev. E. 68, 061502 (2003). https://doi.org/10.1103/PhysRevE.68.061502.
[3] A. Minami and A. Onuki, Phys. Rev. B. 70, 184114 (2004). https://doi.org/10.1103/PhysRevB.70.184114.

On the degradation of structural polymers exposed to high-energy atomic oxygen ions

V. A. Shuvalov, N. B. Gorev, G. S. Kochubei, Yu. P. Kuchugurnyi, N. I. Pismennyi, N. A. Tokmak

Institute of Technical Mechanics (ITM), National Academy of Sciences of Ukraine,
15 Leshko-Popel' St., Dnipro 49005, Ukraine
e-mail: vashuvalov@ukr.net

This publication presents the results of experimental studies on the degradation of properties of polymer structural materials employed in space rocket hardware among which are Kapton-H polyimide and Teflon FEP-100A exposed to high-energy atomic oxygen (AO) ions. Polymers are used as coatings, blanket insulation, solar panel coverings, etc. It is found that at ion energies ~ 5…200 eV, polymer surface sputtering, mass loss, destruction, and erosion are governed by chemical etching.

The polymer erosion yield, erosion depth, mass loss, solar absorptance, and emittance are determined as a function of the AO ion energy and flux. The experimental values and relationships are approximated by a power function. The results obtained on the ITM plasma-electrodynamic setup are in agreement with those obtained in the Earth's ionosphere onboard the Mir orbital station, the International Space Station, the Space Shuttle, the Spot-1, 2, 4, etc.

With the help of a high-sensitivity microbalance, parameters of dynamic interaction in the AO ion – polymer system are determined: the drag force and the lift force acting on a flat plate. As a result, the normal and tangential momentum and energy transfer coefficients in the AO ion – polymer surface system are found as a function of the angle of attack of a flat plate: the angle between the plate surface normal and the ion velocity. We identified the effect of the surface roughness degree on the ion momentum and energy transfer coefficients as a function of the angle of attack of a flat plate.

Procedures are developed for accelerated endurance tests of polymers for resistance to long-term exposure (3…7 years) to hypersonic AO flows in very low-Earth orbits (150…3000 km).

Deformation behavior of hcp solid solutions Ti-Nb under tension in the temperature range 1.7 - 423 K

V. A. Moskalenko, R. V. Smolianets

B. Verkin Institute for Low Temperature Physics and Engineering of NAS of Ukraine,
47 Nauky Ave., Kharkiv, 61103, Ukraine
e-mail: smoljanets@ilt.kharkov.ua

The mechanical properties and physical mechanisms of plastic deformation in hcp metals (Ti, Zr, etc.) significantly depend on the concentration and type of impurities (alloying elements) dissolved in them. To date, the mechanisms of low-temperature plasticity in alloys based on alpha interstitial solid solutions, mainly the Ti–O system, have been studied in sufficient detail [1, 2]. At the same time, the systematic studies on the influence of substitution atoms on the deformation behavior of this metals group have not.

In this work, the patterns of alpha solid solutions plastic deformation in the Ti-Nb system (0.25, 1.05 and 2.1 at.% Nb) under tension are studied in the temperature range 1.7 - 423 K. High sensitivity to interstitial impurities makes it difficult when analyzing experimental results, separation of the two most probable plasticity mechanisms: dislocation overcomes of Peierls barriers and impurity barriers. Therefore, high-purity Ti and Nb electron beam melting was used to produce alloys.

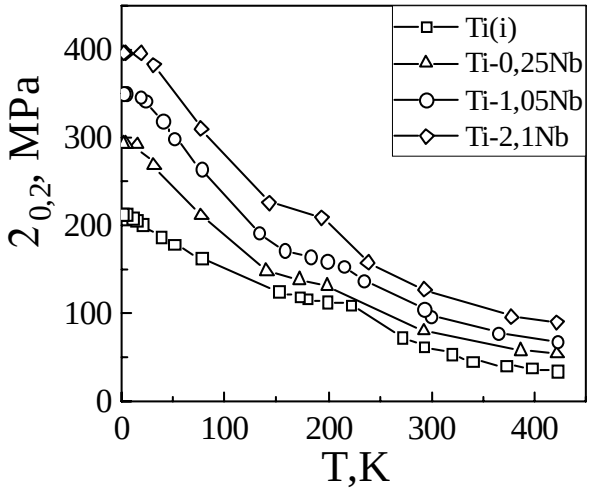

Fig. 1. Temperature dependence of yield strength $\sigma_{0.2}$ for Ti-Nb alpha-alloys.

On the temperature dependence curves of the yield strength $\sigma_{0.2}(T)$ in the studied alloys (Fig. 1), several sections can be distinguished that differ in the degree of sensitivity $\sigma_{0.2}$ to temperature changes. Two of them, which are separated by a diffuse kink in area T ≈ 200 K, correspond to the concept of dislocation thermally activated plasticity at temperatures above ~ 10 K. At lower temperatures, the dependence $\sigma_{0.2}(T)$ are decreasing and below ~ 2 K it becomes athermic because of the transition from thermally activated to dynamic (over-barrier) movement of dislocations. The analysis of experimental data was carried out within the framework of the of thermally activated dislocations model overcoming Peierls barriers according to the mechanism of nucleation, expansion, and annihilation of pair kinks.

The basis for this is the results of work [3], where it was shown that this mechanism for high-purity titanium (the basis of the alloys studied) is controlling. The dependence $\sigma_{0.2}(T)$ for it is shown in Fig. 1. The possibility of approximating experimental data by functions of the form $\sigma_{0.2}(T) = \sigma_{i0}(T) + a_1 - a_2 T^{4/5}$, obtained in this work, may indicate the conservation on the mechanism of overcoming Peierls barriers by dislocations in substitutional solid solutions of hcp metals.

[1] H. Conrad, Prog. Mater. Sci. 26, 123 (1981). https://doi.org/10.1016/0079-6425(81)900013
[2] V.N. Kovaleva, V.A. Moskalenko and V.D. Natsik, Phil. Mag. 70, 423 (1994). https://doi.org/10.1080/01418619408242549
[3] V. A. Moskalenko, V. D. Natsik, V. N. Kovaleva, Low Temp. Phys. 31, 907 (2005). http://dx.doi.org/10.1063/1.2126949

Dislocation mechanisms of low temperature acoustic relaxation and plastic deformation of a high-entropy alloy $Al_{0.5}CoCrCuFeNi$

Yu. O. Semerenko, V. D. Natsik, E. D. Tabachnikova

B. Verkin Institute for Low Temperature Physics and Engineering of NAS of Ukraine,
47 Nauky Ave., Kharkiv, 61103, Ukraine
e-mail: semerenko@ilt.kharkov.ua

High-entropy alloys (HEA) are solid-state metal systems of five or more components with a concentration close to equiatomic, developed at the beginning of the 21st century [1]. Such alloys are characterized by increased mixing entropy values compared to traditional multicomponent alloys, which explains their name. The significant contribution of the entropy of mixing during the formation of HEAs significantly increases the probability of realizing substitutional solid solutions with simple crystal lattices, while such lattices are significantly distorted, since they are formed by atoms of dissimilar elements with different electronic structures and sizes [2]. Thanks to these features of HEAs, their physical and mechanical properties differ significantly from the properties of traditional alloys; they have a favourable combination of strength and ductility, and high resistance to thermal and mechanical influences [2].

The main goal of this publication is to compare the mechanical properties of HEAs and traditional alloys, as well as to discuss the possibility of using the fundamental principles of modern dislocation theory, which were previously formed in the study of the plasticity and strength of traditional crystalline materials, to interpret these properties. The relationship between the acoustic and mechanical properties of $Al_{0.5}CoCrCuFeNi$ HEAs and the features of the dynamics and kinetics of elementary dislocation processes has been analyzed. Data from two different experimental methods were used with different intensities of influence on the dislocation structure in the alloy samples under study:

- method of resonant mechanical spectroscopy – excitation in samples of elastic-plastic deformations with an amplitude of $\sim 10^{-7}$, caused by short segments of dislocation strings (dislocation relaxers), which oscillate with amplitudes on the order of the lattice parameter;
- method of active deformation, which is used to achieve fairly large plastic deformations $\sim 3 \cdot 10^{-1}$, caused by the translational movement of extended dislocations over macroscopic distances.

Analysis of the results of a comprehensive study of the processes of plastic deformation [3] and acoustic relaxation [4] in HEA $Al_{0.5}CoCrCuFeNi$ made it possible to establish:

- the most important types of dislocation defects in the lattice structure of the alloy;
- types of barriers that prevent the movement of dislocation lines (strings);
- adequate mechanisms for thermally activated movement of various elements of dislocation strings through barriers under conditions of moderate and deep cooling;
- quantitative assessments of the most important characteristics of dislocations and their interaction with barriers.

[1] J.W. Yeh, S.K. Chen, S.J. Lin, J.Y. Gan, T.S. Chin, T.T. Shun, C.H. Tsau, S.Y. Chang // Adv. Eng. Mater. 6, 299 (2004). http://dx.doi.org/10.1002/adem.200300567.
[2] Y. Zhang, T.T. Zuo, Z. Tang, M.C. Gao, K.A. Dahmen, P.K. Liaw, Z.P. Lu // Progr. in Mat. Sci. 61, 1 (2014). http://dx.doi.org/10.1016/j.pmatsci.2013.10.001.
[3] E.D. Tabachnikova, M.A. Laktionova, Yu.A. Semerenko, S.E. Shumilin, A.V. Podolskiy, M.A. Tikhonovsky, J. Miskuf, K. Csach // Low Temp. Phys. 43, 1108 (2017). http://dx.doi.org/10.1063/1.5004457.
[4] Yu.A. Semerenko and V.D. Natsik // Low Temp. Phys. 46, 78 (2020). http://dx.doi.org/10.1063/10.0000367.

The influence of the Gorsky effect on the hydrogen diffusion and the formation of microcracks in vanadium films

A. Grib, A. Yaroshenko

V. N. Karazin National University, Svobody sq. 4, Kharkiv, 61022, Ukraine
e-mail: a.yaroshenko@student.karazin.ua

Studies of the diffusion coefficient of hydrogen in vanadium and vanadium films have become important nowadays because vanadium is a promising material for hydrogen storage. The goal is to obtain a sufficiently high rate of the hydrogen absorption and desorption from films. However, due to internal mechanical stresses which appear in a film during the saturation, the diffusion coefficient of hydrogen decreases [1]. This process was investigated numerically in the present work.

The hydrogen diffusion in a vanadium film in the presence of mechanical stresses produced by the initial inhomogeneous hydrogen distribution was investigated. Namely, the Gaussian distribution of hydrogen in the middle of the film was stated initially. Diffusion in an inhomogeneous field of mechanical stresses created by hydrogen in the saturated places of the film was calculated. The parameters of the model were the mobility of the hydrogen atoms, the diagonal component of the elastic moment tensor of the vanadium-hydrogen system, and the derivative of the dependence of the lattice parameter on the concentration in the vanadium-hydrogen system [2].

Spatial concentration distributions of hydrogen at any arbitrary moment of time were found. The concentration distributions were strongly deformed due to the influence of mechanical stresses. A strong dependence of the effective diffusion coefficient on the hydrogen concentration was revealed. There were critical concentrations of hydrogen (about 3.8% (at.) at 295 K, about 4.8 % (at.) at 350 K), at which the hydrogen accumulation appeared in the part of the film with the highest concentration. The explanation of this accumulation is as follows. Due to the inhomogeneous hydrogen distribution, parts of the film with the large hydrogen concentration were more stretched in comparison with the other ones, and therefore hydrogen flowed to the more stretched parts of the film (the Gorsky effect). We discussed the conditions for this effect to be realized, namely, the formation of areas with incoherent stresses in the film. We compared the temperature dependence of the critical concentration with the phase diagram of the vanadium-hydrogen system and discussed the temperature ranges of the effect. Since mechanical stresses tend to significantly accumulate in places with a critical concentration, it was assumed that microcracks were formed in places of the hydrogen accumulation. We discussed the formation of these microcracks and compared results with our experimental data of the hydrogen diffusion in the vanadium film.

[1] W. Huang et al., J. Phys. Condens. Matt. 29, 045402 (2017).
[2] G. Alefeld and J. Völkl (eds.), Hydrogen in metals, Springer Verlag, Berlin, Heidelberg, New York (1978), Vol. 1.

THEORY OF CONDENSED MATTER PHYSICS

Spectral characteristics and energy gaps of 2D and 3D quantum many-body systems in thermodynamic limit

I. V. Lukin[1,2], D. I. Bondar[3], A. G. Sotnikov[1,2]

[1] Karazin Kharkiv National University, 4 Svobody Square, Kharkiv, 61000, Ukraine
[2] Akhiezer Institute for Theoretical Physics, NSC KIPT, Kharkiv, 61108, Ukraine
[3] Department of Physics and Engineering Physics, Tulane University, New Orleans, LA 70118, USA
e-mail: a_sotnikov@kipt.kharkov.ua

We present an expression for the spectral gap, opening up new possibilities for performing and accelerating spectral calculations of quantum many-body systems. We develop and demonstrate one such possibility in the context of tensor network simulations. Our approach requires only minor modifications of the widely used Simple Update method and is computationally lightweight relative to other approaches. We validate it by computing spectral gaps of the 2D and 3D transverse-field Ising models and find strong agreement with previously reported perturbation theory results [1].

We further discuss an extension of the proposed methodology to analyze the dispersive relation $E(k)$ in the transverse-field Ising models. In terms of special operators creating excitations in the corresponding k-sectors, we show that it is not necessary to perform any advanced calculations, but only additional data processing. For finite-size systems, we compare our results from the imaginary time evolution to those from the exact diagonalization and observe a good quantitative agreement.

The authors acknowledge support by the National Research Foundation of Ukraine under the call “Excellent science in Ukraine” (2024-2026).

[1] I. V. Lukin, A. G. Sotnikov, J. M. Leamer, A. B. Magann, D. I. Bondar, Spectral Gaps of 2D and 3D Many-body Quantum Systems in the Thermodynamic Limit, preprint, arXiv:2401.14368 (2024), https://doi.org/10.48550/arXiv.2401.14368.

Quantum control and enhancement of superconducting pairing in one-dimensional Fermi-Hubbard chains

O. V. Povitchan[1], D. I. Bondar[2], A. G. Sotnikov[1,3]

[1] V.N. Karazin Kharkiv National University, Svobody Square 4, 61022 Kharkiv, Ukraine
[2] Department of Physics and Engineering Physics, Tulane University, 6823 St. Charles Ave., New Orleans, LA 70118, USA
[3] Akhiezer Institute for Theoretical Physics, NSC KIPT, Akademichna 1, 61108 Kharkiv, Ukraine
e-mail: povitrim@gmail.com

We theoretically study the system described by the spin-1/2 Fermi-Hubbard model in the presence of the driving near-resonant electromagnetic field. As it was previously shown [1-2], this system under external periodic driving can host non-trivial superconducting (η-paired) states. We employ the exact diagonalization to calculate the evolution of the system numerically. A two-photon absorption leads to the superconducting state excitation. For the fixed local interaction strength and pulse envelopes, we tune the amplitude and angular frequency and find that the level of the excitation highly depends on small parameter shifts. To enhance the superconducting pairing when the parameters of the laser pulse are not optimal, we apply Lyapunov control.

The system prepared in a particular many-body excited state can show a nonlinear response similar to the system prepared in another many-body state (here, by the same response we mean identical current characteristics). To show this, we apply tracking control [3-4] to analyze several specific cases: an initial many-body unperturbed state of the Fermi-Hubbard chain, as well as specific initial states with enhanced superconducting properties.

The authors acknowledge support by the National Research Foundation of Ukraine under the call “Excellence science in Ukraine” (2024-2026).

[1] T. Kaneko, T. Shirakawa, S. Sorella, and S. Yunoki, “Photoinduced η pairing in the Hubbard model,” Phys. Rev. Lett., vol. 122, p. 077002, Feb 2019. https://link.aps.org/doi/10.1103/PhysRevLett.122.077002.
[2] T. Kaneko, S. Yunoki, and A. J. Millis, “Charge stiffness and long-range correlation in the optically induced η-pairing state of the one-dimensional Hubbard model,” Phys. Rev. Res., vol. 2, p. 032027, Jul 2020. https://link.aps.org/doi/10.1103/PhysRevResearch.2.032027.
[3] G. McCaul, C. Orthodoxou, K. Jacobs, G. H. Booth, and D. I. Bondar, “Driven imposters: Controlling expectations in many-body systems,” Phys. Rev. Lett., vol. 124, p. 183201, May 2020. https://link.aps.org/doi/10.1103/PhysRevLett.124.183201.
[4] G. McCaul, C. Orthodoxou, K. Jacobs, G. H. Booth, and D. I. Bondar, “Controlling arbitrary observables in correlated many-body systems,” Phys. Rev. A, vol. 101, p. 053408, May 2020. https://link.aps.org/doi/10.1103/PhysRevA.101.053408.

Identification of Open Quantum Systems: A Novel Approach Based on Polynomial Optimization

Z. Popovych, D. Bondar

Department of Physics and Engineering Physics, Tulane University,
6823 St.Charles Avenue, New Orleans, LA 70118, USA
e-mail: zpopovych@tulane.edu

Open quantum systems are pivotal in enhancing quantum device performance. Conventional identification methods often fail to preserve quantum states' inherent properties, necessitating robust optimization strategies against complex, multimodal landscapes.

We propose a polynomial optimization problem (POP) approach to derive physically accurate master equations from experimental data, utilizing global optimization techniques for efficacy [1]. This study utilizes the polynomial system identification to determine the parameters of the Lindblad master equation [2]:

$$\frac{d\rho}{dt} = -\frac{i}{\hbar}[H,\rho(t)] + \mathcal{D}[\rho(t)] = -\frac{i}{\hbar}[H,\rho] + \sum_{\mathrm{l}=1}^{s-1}\left[J_{\mathrm{j}}\rho J_{\mathrm{j}}^{\dagger} - \frac{1}{2}\left\{J_{\mathrm{j}}^{\dagger}J_{\mathrm{j}},\rho\right\}\right] = \mathcal{L}[\rho]$$

using the associated unconstrained POP:

$$\underset{J_{\mathrm{j}},\ H}{\text{minimize}} \sum_{i=1}^{N}\left\|\rho_{(i)} - \rho_{(i-1)} - \mathcal{L}\left[\int_{t_{i-1}}^{t_i}\rho(t)dt\right]\right\|_F^2.$$

Our research validates this approach through a case study on the spin-boson system, indicating high fidelity between exact trajectories and model outputs, alongside the models' correlation with non-Markovian behaviors [3].

This novel method simplifies the identification process, reduces computational demands, and minimizes numerical errors. Our findings highlight the effectiveness of polynomial optimization in managing both Markovian and complex non-Markovian open quantum systems, promising advancements in quantum system control [4-6].

Keywords: Open quantum systems, system identification, polynomial optimization, Lindbladian master equations, Markovianity, spin-boson system.

[1] Denys I. Bondar et al. "Recovering models of open quantum systems from data via polynomial optimization: Towards globally convergent quantum system identification". arXiv, 2022, url: https://arxiv.org/abs/2203.17164
[2] G. Lindblad. "On the generators of quantum dynamical semigroups". en. In: Communications in Mathematical Physics 48.2 (June 1976), pp. 119–130.
[3] Heinz-Peter Breuer, Elsi-Mari Laine, and Jyrki Piilo. "Measure for the Degree of Non-Markovian Behavior of Quantum Processes in Open Systems". en. In: Physical Review Letters 103.21 (Nov. 2009), p. 210401
[4] Jie Wang, Victor Magron, and Jean-Bernard Lasserre. TSSOS: A Moment-SOS hierarchy that exploits term sparsity. arXiv:1912.08899 [math]. May 2020. url: http://arxiv.org/abs/1912.08899
[5] D. Henrion, Milan Korda, and Jean-Bernard Lasserre. The moment-SOS hierarchy: lectures in probability, statistics, computational geometry, control and nonlinear PDEs. Series on optimization and its applications vol. 4. New Jersey: World Scientific, 2021.
[6] Jiawang Nie. Moment and polynomial optimization. MOS-SIAM series on optimization. Philadelphia: Society for Industrial and Applied Mathematics, 2023. ISBN: 978-1-61197-760-8.

Effects of symmetry breaking in four component interacting Fermi gas in periodic potential

V. I. Unukovych[1], A. G. Sotnikov[2]

[1] V.N. Karazin Kharkiv National University, 4 Svobody Square, Kharkiv, 61000, Ukraine
[2] Akhiezer Institute for Theoretical Physics, NSC KIPT,
Akademichna Str. 1, 61108 Kharkiv, Ukraine
e-mail: unukovich.vladislav@gmail.com

The spin symmetry of the ultracold fermionic mixture plays a crucial role in defining its physical properties. In practice, both the SU(N)-symmetric system and N-component mixture with lower spin symmetry can be prepared for specific values of the number of fermionic components N in the experiments with ^{87}Sr, ^{173}Yb, or alkali metal atoms [1,2]. This raises a question of possible advantages of one particular spin symmetry realization over the other.

To answer the question, we study a four-component ultracold Fermi gas in the framework of the Hubbard model, considering two different amplitudes of the on-site interaction between different spin flavors, as well as the case of different hopping amplitudes. In the strong-coupling limit, we obtain explicit expressions for the nearest-neighbor magnetic couplings in the corresponding Heisenberg model and calculate the energy spectra of both models. Additionally, we analyze the effect of the symmetry breaking on the entropy distribution and the real-space separation of atoms in the harmonic trap.

The authors acknowledge support by the National Research Foundation of Ukraine under the call “Excellent science in Ukraine” (2024–2026). V.U. also acknowledges financial support of STCU via the IEEE program “Magnetism for Ukraine 2023”, Grant No. 9918.

[1] S. Taie, Y. Takasu, S. Sugawa, R. Yamazaki, T. Tsujimoto, R. Murakami, and Y. Takahashi, Phys. Rev. Lett. 105, 190401 (2010).
[2] J. S. Krauser, J. Heinze, N. Fläschner, S. Götze, O. Jürgensen, D.-S. Lühmann, C. Becker, and K. Sengstock, Nat. Phys. 8, 813 (2012).

Magnetic states in the XY Heisenberg model on the honeycomb lattice

I. V. Lukin[1,2], M. O. Luhanko[1], A. G. Sotnikov[1,2]

[1] Karazin Kharkiv National University, 4 Svobody Square, Kharkiv, 61000, Ukraine
[2] Akhiezer Institute for Theoretical Physics, NSC KIPT, Kharkiv, 61108, Ukraine
e-mail: luhanko2021tya11@student.karazin.ua

Understanding the intricate behaviors of many-body quantum systems poses a significant challenge in contemporary physics. Tensor networks have emerged as a promising framework in the realm of quantum many body simulations, offering a versatile approach to represent quantum states. In this study, we aim to provide insights into the many-body correlations in quantum spin models using the infinite projected entangled-pair states (iPEPS). Our investigation extends to the exploration of properties on 2D honeycomb lattices, presenting findings in the Heisenberg-type models with rotational and transitional symmetries, which allows to limit the number of tensors for representation of the environment [1]. Construction of iPEPS allows us to efficiently represent quantum system for computational schemes on classical computers. We emphasize on the derivation of complex numerical algorithms and the full utilization of abelian symmetries for treating interacting lattice models within the fermionic iPEPS framework.

Tensor network contraction is exponentially difficult task, thus it can be done approximately using corner transfer matrix (CTM) method. CTM method allows to represent large variety of states and calculates properties using corner matrices with respect to the symmetries of a system. It also allows to reduce infinitely large system to a subsystem, which we use for analysis and approximating results of infinitely large system. For gaining insights in the system properties, we employ the gradient descent algorithms, which are based on the auto-gradient approaches. As a result, in the XY Heisenberg model on the honeycomb lattice we calculate the magnetic correlation functions and observe a quantum phase transition between the XY-Néel and Ising-type phases with the continuous change of the next-nearest-neighbor coupling amplitude.

The authors acknowledge support by the National Research Foundation of Ukraine under the call "Excellent science in Ukraine" (2024-2026).

[1] I.V. Lukin and A.G. Sotnikov, Phys. Rev. B 107, 054424 (2023).

Residual symmetry and classification of degenerate states of equilibrium SU(4) magnets with spin s=3/2

M. Yu. Kovalevsky, A. A. Rozhkov

National Scientific Center "Kharkov Physics and Technology Institute"
Kharkiv, 61108, Ukraine
e-mail: mik@kipt.kharkov.ua

The equilibrium states of magnets with spin s=3/2 and symmetry SU(4) of exchange interaction have been studied. The approach we are developing essentially uses the symmetry properties of Hamiltonian, representation about residual symmetry of the equilibrium state, and the form of the order parameters. This representation turned out to be very effective in the analysis of degenerate equilibrium states for complex cases of broken symmetry of condensed matter. For example, for superfluid He-3 [1,2] and high-spin magnets [3]. On this basis, without use of any model assumptions, classification equations for magnetic order parameters were obtained. At analyzing and solving these equations, we used various representations of magnetic integrals of motion. These include the matrix representation (Weyl basis) and the Racah basis. Their choice is determined by a specific symmetry subgroup. Solutions of classification equations are given in cases of violation of SU(4) symmetry and its subgroups, which include SU(3), SO(3), SO(3)xSO(3), SO(4), SO(5) symmetry. The equilibrium structures of order parameters are presented in terms of the spontaneous anisotropy parameters of the residual symmetry generator.

[1] D. Volfart, P. Volfle, *The superfluid phases of He-3* World Scientific, Singapore (1990).
[2] М.Ю. Ковалевский, С.В. Пелетминский, Статистическая механика квантовых жидкостей и кристаллов, Физматлит, Москва (2006).
[3] А.В. Глущенко, М.Ю. Ковалевский, Физика низких температур, 2017, Т. 43, № 9, С. 1324-1333.
[4] M.Yu. Kovalevsky, Fizyka Nyzkykh Temperatur/Low Temperature Physics, 2024, v. 50, № 2, P. 147-155.

Dynamics of acoustic superradiance model in the ferromagnetism method

S. F. Lyagushyn, A. I. Sokolovsky

Oles Honchar Dnipro National University,
72 Gagarin Ave., Dnipro, 49010, Ukraine
e-mail: lyagush.new@gmail.com

The dynamics of the Wagner model describing acoustic superradiance [1] is considered. Its Hamiltonian in the mathematical sense is close to the Dicke Hamiltonian of the corresponding optical phenomenon theory

$$\hat{H} = \sum_k \hbar\omega_k a_k^+ a_k - D\sum_n \hat{s}_n^z + \sum_{n,k} \kappa_{nk}(a_k^+ + a_k)(\hat{s}_n^+ + \hat{s}_n^-), \quad (1)$$

where standard notations are used. We consider the model as a system of phonons and N identical particles with spin $s = 1/2$ (this approach is proposed by us for the first time). The nonequilibrium state of the system is described by the average values of operators $\hat{\eta}_a$: $\hat{\eta}_k = a_k^+ a_k$, $\hat{\eta}_1 = \sum_n \hat{s}_n^z$, $\hat{\eta}_2 = \sum_{n\neq\nu} \hat{s}_n^+ \hat{s}_\nu^-$ (reduced description parameters). In the main approximation by interaction with a small κ_{nk}, the statistical operator (SO) of the system has the form

$$\rho_0 = \exp(\Omega - \sum_{a=k,1,2} Z_a \hat{\eta}_a) \qquad (\mathrm{Sp}\,\rho_0 = 1, \quad \mathrm{Sp}\,\rho_0 \hat{\eta}_a = \eta_a). \quad (2)$$

Small corrections to ρ_0 are sought in the Peletminskii–Yatsenko method, which requires the calculation of the traces of the products of operators $\hat{\eta}_a$ with the SO ρ_0. The traces with products of phonon Bose operators a_k, a_k^+ are calculated using Wick's theorem. Traces with products of spin operators $\hat{s}_n^z, \hat{s}_n^\pm$ with the CO ρ_0 cannot be calculated since its exponent includes a quadratic form $\hat{\eta}_2 = \sum_{n\neq\nu} \hat{s}_n^+ \hat{s}_\nu^-$. Such traces can be calculated using the SO ρ_0^0

$$\rho_0^0 = \exp(\Omega^0 - \sum_{a=k,1} Z_a^0 \hat{\eta}_a) \qquad (\mathrm{Sp}\,\rho_0^0 = 1, \quad \mathrm{Sp}\,\rho_0^0 \hat{\eta}_a = \eta_a), \quad (3)$$

to calculate averages with which rules of the Wick's type were developed for the needs of the ferromagnetism theory [2] (we simplified their basic formula somewhat).

This makes it possible to study the dynamics of the Wagner model for a small deviation $\delta\eta_2$ of the parameter η_2 from its value in the state with the SO ρ_0^0, that is for $\eta_2 = \mathrm{Sp}\,\rho_0^0 \hat{\eta}_2 + \delta\eta_2$. Such program is implemented in our work. Since the parameter η_2 describes correlations in the system, our theory investigates the model in the approximation of small correlations. Such idea for researching small correlations in the Dicke model was put forward in our paper [3].

As a result, all objects of the theory are calculated in the perturbation theory by the interaction κ_{nk} of phonons and spins and additionally in the perturbation theory by the deviation $\delta\eta_2$. In particular, the dynamic equations are obtained for the reduced description parameters η_a defined as

$$\dot{\eta}_a = L_a(\eta_{ak}, \eta_1, \delta\eta_2). \quad (4)$$

It was established that the power expansion of their right-hand parts in $\delta\eta_2$ begins with contributions of the second order.

[1] Ao-Lin Guo, Le-Tian Zhu, Guang-Can Guo, Zhi-Rong Lin, Chuan-Feng Li, and Tao Tu, Phys. Rev. A 109, 033711 (2024). https://doi.org/10.1103/PhysRevA.109.033711
[2] V. G. Vaks, A. I. Larkin, and S. A. Pikin, Sov. Phys. JETP 26, 188 (1968).
[3] S. F. Lyagushyn and A. I. Sokolovsky, Journal of Physics and Electronics 31(1), 7 (2023).

Application of Langevin dynamics for machine learning and optimization tasks

O. Borysenko

National Science Center "Kharkiv Institute of Physics and Technology",
1 Akademichna Str., Kharkiv, 61108, Ukraine
e-mail: borisenko@kipt.kharkov.ua

A rapid growth of Machine Learning (ML) applications in different areas has been faced in recent years. Training of ML models is performed by finding such values of their parameters $x = (x_1, x_2, \mathrm{K}, x_N)$ that optimize (minimize) an objective (loss) function $U(x)$. Usually, the number of parameters is large and the training dataset is massive. To reduce computational costs, a gradient $dU(x)/dx$ of the objective function with respect to the model parameters is computed on relatively small subsets of the training data, called mini-batches. If these mini-batches are selected randomly from the training data, then the estimated values of the loss $\hat{U}(x)$ and its gradient $d\hat{U}(x)/dx$ are the stochastic approximations of their exact values.

The first order stochastic gradient descent (SGD) is the simplest optimization method and is the method of choice for many applications. Formally it may be written as

$$\Delta x_{n+1} = x_{n+1} - x_n = -lr \times d\hat{U}(x)/dx, \tag{1}$$

where *n* is an iteration number and the constant *lr* is known as a learning rate.

With the approporiate choice of the learning rate value, Eq. (1) converges to the single minimum of a convex objective function.

But many ML applications require optimization of nonconvex objective functions. These functions have multiple local minima, and finding the global (deepest) one with SGD approach (1) becomes a complicated problem.

The same problem is often found in physical simulations and may be resolved by the methods of Langevin dynamics with Simulated Annealing, which is a well-established approach for minimization of many-particle potentials. This analogy provides useful insights for non-convex stochastic optimization in ML. In our recent work we performed integration of the discrete Langevin equation to develop Coolmomentum – a method for stochastic optimization by Langevin dynamics with simulated annealing [1]. Here we show that integration of the discretized Langevin equation gives a coordinate updating rule equivalent to the famous Momentum optimization algorithm:

$$\Delta x_{n+1} = r_n \times \Delta x_n - \tfrac{1}{2}(1 + r_n) \times lr \times d\hat{U}(x)/dx, \tag{2}$$

where r_n is a momentum coefficient. To implement simulated annealing (or slow cooling, in physical terms), we apply a certain schedule for the gradual momentum coefficient decrease in the range

$$0 \le r_n \le r_0. \tag{3}$$

In this talk we demonstrate that application of Langevin dynamics (2) with simulated annealing (3) to multidimension optimization tasks gives promising results in artificial intelligence [1], quantum computing [2] and optical engineering [3].

The author acknowledges support by the National Research Foundation of Ukraine under the call “Excellence Science in Ukraine” (2024-2026).

[1] O. Borysenko, M. Byshkin, Sci Rep 11, 10705 (2021). doi: 10.1038/s41598-021-90144-3.
[2] Daisuke Tsukayama et al. Jpn. J. Appl. Phys. 62, 088003 (2023). doi:10.35848/1347-4065/acea0a.
[3] Z. Zhang et al. Photonics 10, 102 (2023). doi: 10.3390/photonics10020102.

Asymmetry-induced ratchet effect in polariton graphene

O. M. Bahrova[1,2], S. V. Koniakhin[2]

[1] B.Verkin Institute for Low Temperature Physics and Engineering of NAS of Ukraine, 47 Nauky Ave., Kharkiv, 61103, Ukraine
[2] Center for Theoretical Physics of Complex Systems, Institute for Basic Science (IBS), Daejeon 34126, Republic of Korea
e-mail: bahrova@ilt.kharkov.ua

Due to its unique electronic and optical properties graphene is widely used in the state-of-the-art technology as well as fundamental material science. Nanomechanical resonators based on carbon nanotubes (rolled-up sheets of graphene), are employed in the measurement of qubit states and are base tool for performing logic gate operations in quantum computing. Furthermore, optoelectronic devices based on graphene have broad applications. Additionally, graphene-based optoelectronic devices have wide-ranging applications, including notable implementations in photodetectors and advancements in high-resolution optical microscopy, see review Ref.[1]. However, the remarkable attributes stemming from graphene's unique configuration, such as its Dirac-cone band structure, make it suitable for applications in photonics via creating artificial honeycomb lattices.

At the same time, the spatial inversion symmetry breaking in electronic or mechanical systems can lead to the so-called ratchet effect. As a result, the nonlinear directed transport has its implementation in engineering and various fields of natural sciences. There are various origins for the occurrence of ratchet phenomena. In graphene under asymmetric periodic strain the classical ratchet effect has been considered in [2] see also Ref.[3] Further, the magnetic ratchet electron motion in a single graphene layer which is subject to the static magnetic and alternating electric fields, was observed in [4]. Nevertheless, the ratchet effect due to asymmetric scattering [5] on trigonal defects has been theoretically investigated in [6].

In the present work we consider the polariton analog of a single-layer graphene. Thus, we are interested in the ratchet effect in such a system where the spatial symmetry is broken via embedding of triangle-shaped defects. Our numerical simulations using the corresponding Gross-Pitaevskii equation show presence of the ratchet motion as a consequence of scattering on the defects. The classical and quantum limits when the characteristic size of a defect is of order of the de Broglie wavelength, are taken into account. In addition, we numerically simulate linear kinetic equation taking into account obtained scattering rates, using the Monte-Carlo method. This allows one to draw the correspondence and capture complex dynamics with simpler model within statistical approach. We also employ the obtained results in order to suggest a possible setup for an experimental observation of the ratchet with microcavity exciton-polaritons.

[1] F. Bonaccorso, Z. Sun, T. Hasan, A.C. Ferrari, Nature Photon. 4, 611 (2010).
[2] A.V. Nalitov, L.E. Golub, E.L Ivchenko, Phys. Rev.B 86, 115301 (2012).
[3] E. Monch *et al.*, Phys. Rev.B 105, 045104 (2022).
[4] C. Drexcler *et al.*, Nature Nanotech. 8, 104 (2013).
[5] V.I. Belinicher, B.I. Sturman, Sov. Phys. Usp. 23, 199 (1980).
[6] S.V. Koniakhin, Eur. Phys. J. B 87, 216 (2014).

Investigation of the opto-electronic properties of $RbGeI_3$ cubic perovskite solar material

T. Abera

Wachemo University, Hossana, Ethiopia
e-mail: tejur2785@gmail.com

The structural, electronic and optical response for inorganic lead-free germanium halide perovskite $RbGeI_3$ compound, to examine the possible utilization as future photovoltaic material by using density functional theory (DFT) approximations in conjunction with the plane wavepseudopotential method to investigate structural, electronic, and optical properties of Pb-free cubic perovskite $RbGeI_3$ material. With regard to the toxicity of Pb and the instability of organic elements, inorganic lead-free perovskites (ILPs) have been extensively studied to achieve comparable or greater photovoltaic performance. In order to develop ILPs as an alternative for solar cell applications, we performe $RbGeI_3$ perovskite. The energy cut-off, optimized value for the k-point grid, and Lattice parameter must be obtained for $RbGeI_3$ and this must be comparable with available empirical and other values. The band structure of the perovskite material $RbGeI_3$ may shows either direct or indirect band gap. Optical performance of the compound is accomplished through the investigation of real & imaginary dielectric tensor components, optical absorption, reflectivity and refractivity spectra. Promising electronic and optical properties obtained for the perovskite compound affirms the potential utilization in photo-voltaic and other opto-electronic applications.

Reset dynamics of a photon detector based on a flux-biased phase qubit

O. A. Ilinskaya[1,2], A. I. Ryzhov[1,3], S. N. Shevchenko[1]

[1] B.Verkin Institute for Low Temperature Physics and Engineering of NAS of Ukraine, 47 Nauky Ave., Kharkiv, 61103, Ukraine
[2] G. V. Kurdyumov Institute for Metal Physics, 36 Acad. Vernadsky Blvd., Kyiv 03142, Ukraine
[3] Theoretical Quantum Physics Laboratory, Cluster for Pioneering Research, RIKEN, Wakoshi, Saitama, 351-0198, Japan
e-mail: ilinskaya@ilt.kharkov.ua

The operation cycle of a photon detector can be divided into three stages (see, for example, Ref. [1]). At the capture stage, the signal to be detected enters the system. At the readout stage, the system responds to this signal, and this response is measured. The aim of the reset stage is to return the system to the initial state, that is, to prepare it for the detection of the next signal.

In this work, we theoretically study [2] the reset stage of a photon detector based on a flux-biased phase qubit. Following Ref. [3], the system is considered as a multilevel one (a qudit). An external signal, which is assumed to be in a coherent state, induces the Rabi oscillations between the two "working" energy levels, which are localized in different wells of the asymmetric two-well potential. A transition from the 1st "working" level localized in the shallow well to the 2nd "working" level localized in the deep well is followed by the relaxation to the lowest level in the deep well. The transition between the wells is accompanied by the change of the direction of the supercurrent in the loop of the superconducting qubit. Measuring this direction is the readout of the detector. Then, one needs to reset the system, i.e. to return the quasiparticle to the 1st "working" level. This is done by the linear change of the external magnetic flux applied to the qudit. During the reset, there are six subsequent Landau-Zener-Stückelberg-Majorana transitions of the quasiparticle (level 1 – level 2, level 2 – level 3, etc.).

Solving the Lindblad equation numerically, we obtained the occupations of the levels as a function of the external magnetic flux. This dependence is shown in the figure. The resulting occupation of the "working" level is sufficiently small (about 0.65) because the relaxation was chosen to be rather high for illustrative purposes. We also calculated the same dependence analytically using an approximate rate equation method and obtained sufficiently good agreement with the numerical calculations.

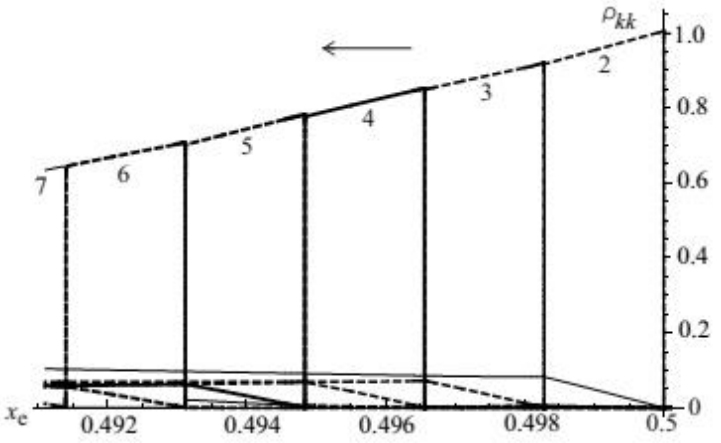

Fig. The dependence of the occupations of the qudit energy levels on the external magnetic flux (normalized to the flux quantum). Numbers of the energy levels are shown under the corresponding curves.

Acknowledgment: This research is sponsored by NATO Science for Peace and Security Multi-Year Project G5796 and Grant of the NAS of Ukraine for young scientists (No. 0123U103073).

[1] K. Koshino, K. Inomata, Z. Lin, Y. Nakamura, and T. Yamamoto, Phys. Rev. A 91, 043805 (2015), https://doi.org/10.1103/PhysRevA.91.043805.
[2] O.A. Ilinskaya, A.I. Ryzhov, S.N. Shevchenko, https://arxiv.org/abs/2402.07801.
[3] V. I. Shnyrkov, Wu Yangcao, A. A. Soroka, O. G. Turutanov, and V. Yu. Lyakhno, Low Temp. Phys. 44, 213 (2018), https://doi.org/10.1063/1.5024538.

Quantum Signal Processing with adiabatic impulse model

D. O. Shendryk[1,2,3], O. V. Ivakhnenko[2,4] and S. N. Shevchenko[2]

[1] Ruhr University Bochum 44780, Germany
[2] B. Verkin Institute for Low Temperature Physics and Engineering, Kharkiv 61103, Ukraine
[3] V. N. Karazin Kharkiv National University, Kharkiv 61022, Ukraine
[4] Theoretical Quantum Physics Laboratory, Cluster for Pioneering Research, RIKEN, Wakoshi, Saitama 351-0198, Japan
e-mail: diana.shendryk@ruhr-uni-bochum.de

Quantum Signal Processing (QSP) framework, is a method to transform the state of quantum subsystems under almost arbitrary polynomial functions with a limited number of unitary transformations, this framework was originally developed for early control of quantum two-level systems with nuclear magnetic resonance [1]. We find that QSP has a lot of similarities with the adiabatic impulse model (AIM) with alternating of the rotating around the z-axis (adiabatic evolution) and x-axis (diabatic evolution) on the Bloch sphere. We can easily map parameters for the QSP into AIM, which can give the parameters for the QSP algorithm, which can be used for experimental purposes, we developed a technique in which input data for QSP is mapped into well-understood parameters of the adiabatic-impulse model for experimentalists such as amplitude and frequency of the qubit driving signal [2]. By using this approach, we investigate a connection between the abstract parameters, such as phases and angles, required for QSP and the comprehensible parameters of a two-level system, such as Landau-Zener-Stückelberg-Majorana (LZSM) probability, Stückelberg phase, and ultimately, the amplitude, duration, and frequency of the signal. In Fig.1 we can see the realization of QSP with parameters given by the adiabatic impulse model for the "BB1" pulse sequence [3] and for the trivial case with no processing.

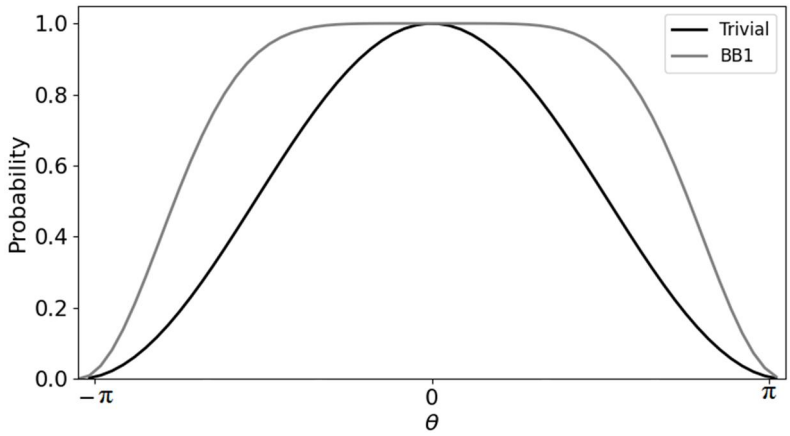

Fig. 1. The transition probabilities which map $|0\rangle \rightarrow |0\rangle$ for the LZSM system with LZSM parameters after applying zero-processing QSP (shown in blue) and QSP with BB1 sequence processing depending on x-rotation angle θ.

[1] J.M. Martyn, et al., «Grand Unification of Quantum Algorithms», PRX Quantum, vol. 2, no. 4, 040203, 2021.
[2] A. I. Ryzhov, O. V. Ivakhnenko, S. N. Shevchenko, M. F. Gonzalez-Zalba, and Franco Nori, «Alternative fast quantum logic gates using nonadiabatic Landau-Zener-Stückelberg-Majorana transitions» arXiv:2310.17932 [quant-ph], 2023.
[3] S. Wimperis, «Broadband, Narrowband, and Passband Composite Pulses for Use in Advanced NMR Experiments», Journal of Magnetic Resonance, Series A, vol. 109, 1994.

Many-body hamiltonian on the basis of spherical tensor operators for studying collective phenomena in quantum high-spin systems

M. Bulakhov[1], A. S. Peletminskii[1,2], and Yu. V. Slyusarenko[1,2]

[1] Akhiezer Institute for Theoretical Physics, National Science Center "Kharkiv Institute of Physics and Technology", NAS of Ukraine, 1 Akademichna Str., 61108 Kharkiv, Ukraine
[2] V.N. Karazin Kharkiv National University, 4 Svobody Sq., 61022 Kharkiv, Ukraine
e-mail: bulakh@kipt.kharkov.ua

We employ the representation properties of the rotation group through the apparatus of spherical tensor operators to construct a many-body Hamiltonian of pairwise interacting spin-F atoms [1,2]. This Hamiltonian, valid for finite-range potentials, includes the effects of multipolar exchange interaction as well as the coupling of any multipole moment (dipole, quadrupole, octupole, etc.) with an external field. It can be applied to study the collective phenomena in quantum Bose and Fermi gases of high-spin atoms, whose interaction is not specified by s-wave scattering length associated with delta-like contact pseudopotential. Following the reduced description method of quantum systems [3], we obtain the respective kinetic equation in the collisionless approximation. Next, we employ it to explore the high-frequency collective excitations such as zero sound [4] and spin-waves for the specific system representing a weakly interacting gas of spin-3/2 atoms.

The authors acknowledge support by the National Research Foundation of Ukraine under the call “Excellence Science in Ukraine” (2024-2026). One of the authors, M. Bulakhov, also acknowledges support by STCU project “Magnetism in Ukraine Initiative”, Grant No. 9918.

[1] E.P. Wigner, Group Theory and its Application to the Quantum Mechanics of Atomic Spectra (Academic Press, New York, 1959).
[2] U. Fano and G. Racah, Irreducible tensorial sets. Pure and Applied Physics, v.4 (Academic Press, New York, 1959).
[3] A.I. Akhiezer and S.V. Peletminskii, Methods of Statistical Physics (Oxford University Press, Oxford, 1981).
[4] M. Bulakhov, A.S. Peletminskii, and Yu.V. Slyusarenko, J. Phys. A: Theor. Math. **56**, 435001 (2023). DOI 10.1088/1751-8121/acfc0a

Calculation of optical modes for chalcogenide compounds $Sn_2P_2X_6$ (X=S, Se)

V. Yu. Klevets, N. D. Savchenko, A. G. Slivka, A. I. Susla, V. Yu. Bihanych

Uzhhorod National University, 88000, Uzhhorod, Voloshin Str., 54, Ukraine
e-mail: klevetsvyu@gmail.com

Modeling from the first principles of electronic structure and properties of complex materials are of a importance for the development of new generation sensors. In present work we have calculated of electronic structure and optical modes for the materials with ferroelectric properties of $Sn_2P_2X_6$ (X=S, Se) group.

The calculations were performed for the model basis constructed from P_2X_6 molecular units and Sn atoms. It was supposed that both covalent and ionic bonds are formed between Sn atoms and chalcogen atoms. Optical vibrational frequencies were computed in terms of linear combination of atomic orbitals method developed by W. A. Harrison [1] allowing analysis of vibrational spectra of partially covalent bonded solids. We have used the concept of bond polarity (α_p) different from the other two bond polarity definitions introduced by L. Pauling and by W. A. Phillips.

For $Sn_2P_2Se_6$ compounds the calculated longitudinal optical phonon frequency values (in cm^{-1}) and experimental data (given in parentheses) for the comparison are: Sn-Sn – 62 (56), Sn-Se – 125 (134), P-P –281 (290), P-Se – 436 (454) [2]. The dependences of longitudinal optical phonon frequency values and bond polarity on internuclear distance along with correlation between the reduced mass values and internuclear distance for different groups of atoms and P_2X_6 molecule have been analyzed.

[1] Harrison W. A., Elementary Electronic Structure. New Jersey, London, Singapore, Shanghai, Hong Kong, Taipei, Chennai: World Scientific Publishing Co. 2004.
[2] Kliche G. J. Sol. State Chem., 1984, 51, pp.118-126.
[3] Zamaraite I., Svirskas S., et al. Dielectric, pyroelectric and ferroelectric properties of lead-doped $Sn_2P_2S_6$ crystals. Phase Transitions, 2019, v. 92, p. 500 - 507.
[4] Glukhov K., Fedyo K., Banys J., Vysochanskii Y. Electronic Structure and Phase Transition in Ferroelectic $Sn_2P_2S_6$ Crystal. *Int. J. Mol. Sci.* 2012.
[5] Milutinović A., Popović Z.V., Tomić N., Dević S. Materials Science Forum, 2004, 453-454 pp. 299-304.
[6] Voroshilov Yu.V., et al. Sov. Phys. Crystallogr., 33, 761 1988.
[7] Eijt S., Maior M.M. J. Phys. and Chem. of Solids, 60, 631, 1999.
[8] R.Caracas et al. Phys. Rev. B 66, 104106, 2002

Nonequilibrium protection effect and spatial localization of noise-induced fluctuations under gas flow scattering on partially penetrable obstacle

S. P. Lukyanets, O. V. Kliushnichenko

Institute of Physics of NAS of Ukraine, 46 Nauky Ave., Kyiv, 03028, Ukraine
e-mail: lukyan@iop.kiev.ua

The scattering of gas flow on an obstacle results in the formation of nonequilibrium steady states (NESS), like stationary obstacle wake. Often such systems undergo nonequilibrium phase transition leading to the onset of nonlinear steady-state gas structures at certain critical parameters, in particular, the structure like stratum formed, due to the blockade effect in a gas, ahead of obstacle [1–4]. Formation of such structures can be considered as the growth of a nucleus of a dense gas phase near an obstacle which plays the role of a nucleation center. It is natural to suppose that the nucleus boundary (usually having the kink-like form) has to protect the state of its center (obstacle) against the fluctuations in a gas as well as the noise of the external driving field. To demonstrate the possibility of this effect we resort to the particular case of the driven lattice gas doped with static impurities in a narrow channel with ring topology [4]. We implement the obstacle as a transverse channel cell partially occupied by impurity particles with mean concentration U, supposing that a nonconservative driving field g is applied along the channel. In the limiting case, the narrow channel can be described as a quasi-one-dimensional lattice with a partially penetrable (impurity) site corresponding to the obstacle. To describe NESSs and gas fluctuations near them we use the combination of the local equilibrium approach and the mean-field approximation neglecting the fast processes and short-range correlations [5–7]. In this setting, the nonequilibrium transition manifests itself in the onset of a two-domain gas structure. The dense gas phase is confined by two domain walls, the first one is pinned by the impurity site, and the second wall is located far from the impurity and can be associated with a topological defect (nucleus boundary). The system undergoes the transition when the mean gas concentration $\bar{n}$, driving field g and impurity concentration U exceed certain critical values $\bar{n}_c$, g_c, and U_c. In the subcritical regime, the gas fluctuations are slightly accumulated near the impurity site. In the overcritical regime, the gas density fluctuations are strongly localized near the topological defect and are totally suppressed for the impurity site. The state of the impurity site behaves similarly to the local first integral (or adiabatic invariant), and is insensitive to the fluctuations, in particular, to the noise of the external driving field. The state of impurity site is the local order parameter for this nonequilibrium transition. Its invariant value corresponds to the half-filling of this site by gas particles $n_0 = (1 - U)/2$, and does not depend on the gas concentration $\bar{n} > \bar{n}_c$ and driving field $g > g_c$ which determine the sizes and densities of two gas domains in the overcritical regime. The described effect can be associated with the nonequilibrium protection effect of the obstacle state [8].

[1] V. N. Tsytovich and N. G. Gusein-zade, Plasma Phys. Rep. 39, 515 (2013).
[2] S. A. Janowski and J. L. Lebowitz, Phys. Rev. A 45, 618 (1992).
[3] K. Mallick, Physica A 418, 17 (2015). https://doi.org/10.1016/j.physa.2014.07.046
[4] S. P. Lukyanets and O. V. Kliushnichenko, arXiv:2311.11658v3 [cond-mat.stat-mech] (2024).
[5] A. Chumak and A. Tarasenko, Surf. Sci. 91, 694 (1980).
[6] A. A. Tarasenko, P. M. Tomchuk, and A. A. Chumak, *Fluctuations in the Bulk and on the Surface of Solids* (Naukova Dumka, Kyiv, 1992).
[7] D. N. Zubarev, *Nonequilibrium Statistical Thermodynamics* (Plenum Press, New York, 1974).
[8] S. Shankar, A. Souslov, M.J. Bowick, M.C. Marchetti, and V. Vitelli, Nat. Rev. Phys. 4, 380 (2022).

Electron-impact excitation and ionization of K atom

V. Roman

Institute of Electron Physics, National Academy of Sciences of Ukraine,
21 Universytetska Str., Uzhhorod 88017, Ukraine
viktoriyaroman11@gmail.com

The study of ionization of atoms is very relevant today, because electron impact ionization cross-sections are widely used in applications such as modeling of plasma syntheses in tokamaks, modeling of radiation effects for both materials and medical research and aeronomy, as well as in basic research in astrophysics, atomic, molecular and plasma physics. This is confirmed by a large number of experimental and theoretical studies of the ionization process of atoms, in particular alkali metal atoms [1–5]. Previously, we studied the ionization cross sections for the rubidium atom [6]. Here we consider the capabilities of the most widely used theoretical approaches, relativistic distorted-wave (DW) and binary-encounter-dipole (BED), for the single electron impact ionization of the K atom in the impact energy range from the 4s threshold up to 700 eV using the standard software package Flexible Atomic Code (FAC) [7].

In addition to direct ionization, the complete cross-section of ionization also includes the excitation of subvalent shells - the process of autoionization. The autoionization cross section was obtained by us as the sum of the excitation cross sections of 96 autoionization states of configurations $3p^5$ ($4s^2$, 3d4s, 4s4p, 4s5s, 3d5s, 4d4s) and 38 states of configurations 3s ($4s^2$, 4s4p, 4s4d, 4s5s, 4s3d, 5s5p, 4s6s). Figure 1 shows a comparison of the theoretical complete cross sections of the single ionization of an atom with experimental data [1-2].

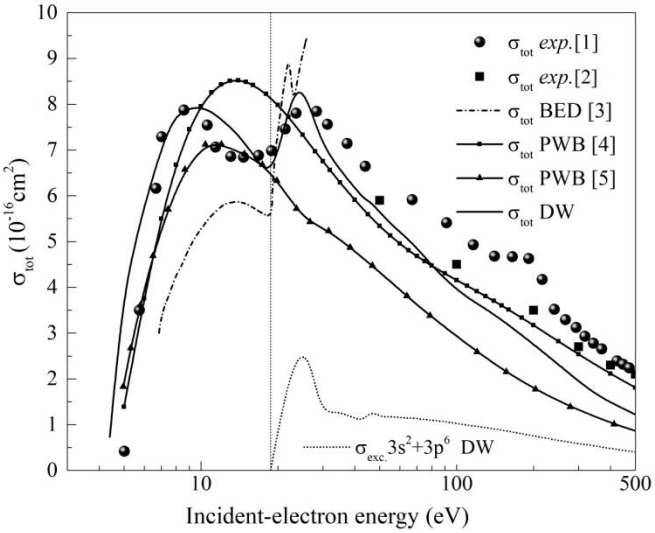

Figure 1. The total ionization cross-sections of the K atom

As the analysis shows, the total ionization and autoionization cross sections calculated by us, obtained in the DW approximation, best correspond to the experimental ionization cross section. Therefore, this relativistic approximation is optimal for such a heavy atom as potassium.

[1] J. Tate, P. Smith, Phys. Rev. 46, 773 (1934).
[2] R. Mcfarland, et al, Phys. Rev. 137, 1058 (1965).
[3] B. Roy, D. Rai, Phys. Rev. A. 8, 849 (1973).
[4] P. Bartlett, et al, At. Dat. and Nucl. Dat. Tabl. 86, 235 (2004).
[5] E. McGuire, Phys. Rev. A. 16, 62 (1977). https://doi.org/10.1103/PhysRevA.16.62
[6] V. Roman, et al, J. Phys. B. 48, 205204 (2015). https://doi:10.1088/0953-4075/48/20/205204
[7] M. Gu, Can. J. Phys. 86, 675 (2008). https://doi.org/10.1139/p07-197

TECHNOLOGIES AND INSTRUMENTATION FOR PHYSICAL EXPERIMENTS

Control of the effective value of b_L parameter in an RF SQUID by the high-frequency electromagnetic field

V. I. Shnyrkov[1,2], V. Yu. Lyakhno[1,3], O. G. Turutanov[4,3], O. O. Leha[3]

[1] G.V. Kurdyumov Institute for Metal Physics, N.A.S. of Ukraine, 36 Academician Vernadsky Boulevard, 03142 Kyiv, Ukraine
[2] Kiev Academic University, 36 Academician Vernadsky Boulevard, Kiev 03142, Ukraine
[3] B.Verkin Institute for Low Temperature Physics and Engineering of NAS of Ukraine, 47 Nauky Ave., Kharkiv, 61103, Ukraine
[4] Department of Experimental Physics, Comenius University, 842 48 Bratislava, Slovakia
e-mail: lyakhno@ilt.kharkov.ua

The Radio Frequency Superconducting Quantum Interference Device (RF SQUID) is a highly sensitive instrument utilized in various scientific and technological domains. It contains a superconducting ring that is closed by a Josephson junction, a crucial component in superconducting electronics. The SQUID magnetic behaviour is determined by dimensionless parameter b_L, which is proportional to the Josephson junction critical current and the loop inductance, and distinguishes between hysteretic ($b_L > 1$) and non-hysteretic ($b_L < 1$) operation modes.

Analytical models effectively describe RF SQUID behavior at low parameter b_L ($b_L << 1$), but are qualitatively valid for higher b_L, up to 1. They predict a virtual change in b_L, or critical current, under a high-frequency (HF) electromagnetic field.

The influence of microwave fields on the amplitude-frequency and signal characteristics of an RF SQUIDs, along with experimental validation, is studied in this work.

In the experimental setup, the interferometer loop is inductively coupled to a resonant tank circuit driven by an RF current with frequency close to the tank's resonance frequency. By applying a microwave field with amplitude and frequency considerably higher than the tank's resonance frequency, the parameter b_L can be effectively reduced. This causes a change for a non-hysteretic-like operation mode that is evidenced by corresponding amplitude-frequency characteristics. Additionally, this adjustment leads to a notable enhancement in the conversion factor and sensitivity of the RF SQUID at certain HF field amplitudes, as discussed herein.

This study shows how variations in the HF field amplitude affect the performance of the RF SQUID, suggesting a potential connection to stochastic resonance phenomena [1]. Also, our results obtained on a single RF SQUID could potentially be extended to metamaterials which are arrays of RF SQUIDs, enabling the manipulation by coherence behavior in metaatoms through resonance frequency tuning [2].

This work was carried out within the framework of the project G5796 funded by the NATO SPS Program and supported by the IEEE program "Magnetism for Ukraine 2023", project number 9918. O.T. acknowledges support of the EU NextGenerationEU funded through the Recovery and Resilience Plan for Slovakia under the project No. 09I03-03-V01-00031

[1] O. G. Turutanov, V. Yu. Lyakhno, M. E. Pivovar, V. I. Shnyrkov, Low Temp. Phys.45, 60 (2019). https://doi.org/10.1063/1.5082311
[2] A. P. Zhuravel, Seokjin Bae, A. V. Lukashenko, A. S. Averkin, A. V. Ustinov, S. M. Anlage, Appl. Phys. Lett. 114, 082601 (2019). https://doi.org/10.1063/1.5064658

System spectral analysis of infrasonic waves in the atmosphere caused by a powerful explosion of a unique volcano

L. F. Chernogor[1], O. I. Liashchuk[2], M. B. Shevelev[1], N. M. Tilichenko[1]

[1] V.N. Karazin Kharkiv National University Ministry Education and Science of Ukraine
Svobody Square, 4, Kharkiv, 61022, Ukraine
[2] Main Center of Special Monitoring
Kosmichna, 1, urban village Gorodok, Zhitomir region, 12265, Ukraine
e-mail: mykyta.b.shevelev@karazin.ua

On January 15, 2022, nature staged a unique experiment. In the time interval 04:00–05:00 UT, five explosions of the Tonga super volcano occurred with an air wave energy of up to 18 Mt TNT [1]. They were accompanied by an earthquake with a magnitude of 5.8, the generation of a tsunami up to 90 m high above the volcano, the release of explosion products with a mass of 2.9 Gt, a volume of 1.9 km^3 and thermal energy of 3.9×10^{18} J to a record height of 58 km, the generation of a shock wave in the atmosphere, Lamb waves, infrasound, atmospheric gravitational wave. Significant disturbances took place in the tectonosphere, the World Ocean, atmosphere, ionosphere and magnetosphere. A “hole” has formed in the ionosphere with a total electron content deficit of 13- 18 TECU and a size of up to 10 Mm. The magnitude of the magnetic effect reached several tens of nT. The Lamb wave circled the globe five times and was recorded for seven days. The sound from the explosion due to nonlinear transformations was heard at a distance of $r \approx 9$ Mm. The amplitude of infrasound near the antipode was about 100 Pa, i.e. about 0.1% of atmospheric pressure [2].

Infrasound was recorded by a network of Ukrainian infrasonic stations, including at the V.I. Vernadsky Antarctic station ($r \approx 8868$ km).

The purpose of the report is to present the results of a system spectral analysis of temporal variations in atmospheric pressure recorded at the V. I. Vernadsky Ukrainian Antarctic Station.

System spectral analysis was proposed by L. F. Chernogor [3]. It consists of three mutually complementary short-time and adaptive Fourier transforms, as well as a wavelet transform. The first of them has a better resolution in time, the second has better resolution of periods. The wavelet transform, which is a mathematical microscope, «equalize» the chances of components with different periods and amplitudes.

The main results of the analysis of observational data are as follows. The blast wave in the atmosphere, having an initial speed of more than 1000 m/s, caused the generation of an undamped non-dispersive Lamb wave and infrasound. The first had a period of about 450 s, a speed of about ~315 m/s, an amplitude of ~220 Pa and a duration of ~30- 40 minutes. The infrasound had a period of ~10- 100 s, a speed of 280-300 m/s, an amplitude of ~50 Pa and a duration of 150 minutes. The infrasound generated by the tsunami had the lowest speed (about 200 m/s) and amplitude (~10 Pa).

Let us add that the Lamb wave also generated a tsunami of atmospheric origin with a propagation speed of about 300 m/s.

It was confirmed that the amplitude and speed of waves of various physical natures in the atmosphere depended significantly on the orientation of the path and weather conditions.

These studies were carried out with the support of the MESU project (state registration number 0124U000461).

[1] L. F. Chernogor, J. Atmos. Solar-Terr. Phys. 253, 106157 (2023). https://doi.org/10.1016/j.jastp.2023.106157
[2] L. F. Chernogor, M. B. Shevelev, Space Sci. Tech., 30(1), 66- 79 (2024). http://doi.org/10.15407/knit2024.01.066.
[3] L. F. Chernogor, Geomag. Aeron., 48(5), 652 – 673. https://doi.org/10.1134/S0016793208050101.

Microcomputers’ applications at robotic medical systems prototypes

V. V. Anufriiev, O. O. Kravchuk, E. P. Fedorenko

Kharkiv National University of Radio Electronics, 14 Nauky Ave., Kharkiv, 61166, Ukraine
e-mail: valentyn.anufriiev@nure.ua

A microcomputer is a small, relatively inexpensive computer that consists of a central processing unit, memory elements, and input/output circuitry mounted on a printed circuit board.

In robotic medical assistants, microcomputers are used as computing elements that analyse data, control movements and provide real-time feedback, ultimately enabling these robots to perform complex tasks with accuracy, efficiency and adaptability within a compact and cost-effective design. The purpose of this paper is to review the existing microcomputers used in robotic medical systems, their advantages and application features.

Microcomputers can be used to implement a wide range of robotic systems for use in healthcare facilities. These include logistics robots for delivering medicines and collecting information about patients' health status, various surgical manipulators, etc. [1-3].

Currently, the most common microcomputers on the market are [4]:

– Raspberry Pi is a computer that was developed in the UK to stimulate the teaching of computer science in schools. It has become more popular than expected and is even used in robotics. This computer runs on Linux, which allows you to implement robotic systems based on the Robot Operating System (ROS) [5];

– Arduino is an open source platform. The main advantage of this platform is its easy-to-use hardware and software. The programming language is a simplified version of C++ and the IDE is based on Processing, which makes programming much easier and clearer.

– Tinker Board is a single-board computer produced by ASUS, which is designed for a variety of electronic projects and mobile robots. This computer also runs on Linux and has the same functionality as the Raspberry Pi, but due to the more powerful central processing unit, all calculations will be faster than its competitor.

In summary, microcomputers are playing an important role in robotic medical systems due to their compact size, low cost and ample computing power. They enable the integration of complex algorithms for tasks such as image processing, machine learning and sensor data fusion, expanding the capabilities of robotic medical assistants while keeping costs manageable. Their versatility allows for the development of customised solutions tailored to specific medical needs, driving innovation and development in medical robotics.

[1] В. В. Ануфрієв, О. В. Глухов, О. О. Кравчук, Є. В. Левченко. Grail of Science 31, 197–201 (2023) https://doi.org/10.36074/grail-of-science.15.09.2023.33
[2] V. A. Chekubasheva, O. O. Kravchuk, H. Hlukhova, O. V. Glukhov. Biosensors and Bioelectronics: X, (11) (2022) https://doi.org/10.1016/j.biosx.2022.100215
[3] О. О. Кравчук, В. А. Чекубашева, О. В. Глухов, Є. В. Левченко та Є. В. Роговець. Матеріали XXI Всеукраїнської науково-технічної конференції молодих вчених, аспірантів та студентів, 188–190, (2021) https://openarchive.nure.ua/handle/document/15816
[4] Almer C. and Sempere V. Autonomous medical robot. Hogskolan I Skovde, Institutionen For Ingenjorsvetenskap (2020) http://urn.kb.se/resolve?urn=urn:nbn:se:his:diva-18602
[5] В. В. Ануфрієв, І. М. Бондаренко. XXVIII Міжнародний молодіжний форум «Радіоелектроніка і молодь у XXI столітті» (2024).

Development of low-temperature cell for IR Fourier-spectroscopy of hydrocarbon materials

A. Kenbay[1], D. Yerezhep[2], A. Aldiyarov[1], E. Korshikov[1]

[1] Al-Farabi KazNU, 71 Al-Farabi Ave., 050040, Almaty, Kazakhstan
[2] Satbayev University, 22a Satpaev str., 050013, Almaty, Kazakhstan
e-mail: mr.kenbay@gmail.com

Initial motivation of this work arose from the desire to develop a specialized low-temperature measuring cell with cryogenic capillary system for IR spectral analysis of hydrocarbon materials at atmospheric pressure. Since most IR spectroscopy analysis of hydrocarbons is performed in high vacuum, we are confident that our setup will be effective in generating new low-temperature spectroscopy analysis results if experiments are performed at atmospheric pressure. This work aimed to show the proof of measurement technique efficiency and functionality of the developed low-temperature measuring cell with cryogenic capillary system [1]. In order to confirm them we carried out two experiments with studying ethanol at low temperature and provided their comparison. The first one was conducted using our specially designed low-temperature measuring cell integrated into diffuse reflection attachment of the FSM 2203 Fourier spectrometer and with cryogenic capillary system to achieve low temperature conditions under normal atmospheric pressure. Results of this experiment was compared with the second experiment involving PVD in a vacuum chamber. Methodology involves performing two types of experiments and comparing the IR spectra of ethanol at low temperatures under different pressures – ambient and vacuum [2].

Results: Infrared spectra of low molecular weight amorphous and crystalline ethanol were obtained under low temperature conditions, both in normal and vacuum environments, and compared at 150K. The experimental data confirms the functionality of the developed setup. Recommendations: The created low-temperature cell shows potential for further research into the low-temperature properties of hydrocarbon substances, addressing the urgent need for alternative fuel energy. Additionally, the data obtained is valuable for astrochemists studying extraterrestrial ices. Researchers in the field of low-temperature spectroscopy at normal pressure can utilize these results for future investigations.

[1] Golikov O.Yu., Kenbay A.A., Aldiyarov A.U., Yerezhep D.E. Investigation of the ir spectra of ethanol for fuel energy using a developed specialized low-temperature cell. The Journal of The Open Systems Evolution Problems, 2022, vol. 1-2, pp. 98-105.
doi: 10.26577/JPEOS.2022.v24.i1.i6
[2] Kenbay A.A., Golikov O.Yu., Aldiyarov A.U., Yerezhep D.E. Low-temperature cell for IR Fourier spectrometric investigation of hydrocarbon substances. Scientific and Technical Journal of Information Technologies, Mechanics and Optics, 2023, vol. 23, no. 4, pp. 696–702. doi: 10.17586/2226-1494-2023-23-4-696-702

In vitro pilot study of temperature field dynamics with cryoimpact

G. Kovalov[1], M. Chyzh[1], V. Globa[1], G. Shustakova[2], Yu. Fomenko[2], E. Gordienko[2], D. Nikolenko[3]

[1] Institute for Problems of Cryobiology and Cryomedicine of NAS of Ukraine, 23, Pereyaslavska str., Kharkiv, Ukraine 61015
[2] B. Verkin Institute for Low Temperature Physics and Engineering of NAS of Ukraine, 47 Nauky Ave., Kharkiv, 61103, Ukraine
[3] V. N. Karazin Kharkiv National University, 4 Svobody Sq., Kharkiv, 61022, Ukraine
e-mail: kovalyovhome@ukr.net

Cryosurgery sets the goal of guaranteed destruction of pathological tissue with maximum preservation of adjacent healthy tissues. The clinical use of generally accepted methods of visualization of the freeze-thawing does not fully answer the question of whether the cryodestruction zone was sufficiently formed. Therefore, when planning a surgery, especially in oncodermatology, it is extremely important to predict the movement of the freezing front as well as dynamics of the temperature field inside and outside the frozen zone for various modes of cryoimpact and features of the impact objects.

In order to predict the freezing zone during cryodestruction of biological tissues *in vivo*, a pilot study of the thermal field dynamics during local contact cryoimpact in a model system *in vitro* has been performed. For research, a laboratory measuring assembly was developed. It included: a transparent container for a model liquid, microthermometers with an analog-digital converter and a device for fixing them in the area of interest; video cameras for remote monitoring and analysis of the instantaneous shape and size of the ice zone in various angles; a special original infrared camera with an extended temperature range of up to minus 150 °C for monitoring and analyzing the thermal field dynamics on the model system surface. Control of monitoring systems, data recording and real-time observation of freeze-thawing processes was carried out via a PC.

The temperature dynamics in the zone of low-temperature impact was studied in a model system with a gel of 5% gelatin solution. The results of a thermal imaging study of the dynamics of ice spot surface growth in the freezing zone and temperature distribution in it coincided with the ones of direct thermometry (according to the data of thermometers at the corresponding points) and the corresponding sizes of the ice zone (according to the analysis of video recordings from cameras). Immediately after touching the applicator to the gel surface, the formation of an ice zone was observed, the diameter of which on the gel surface was nearly one and a half times greater than the depth of freezing. At this initial stage, the highest rate of cooling and ice growth was also observed. During further growth (about 1.5 min of cooling later), the ice lump reached a hemispherical shape, which remained so during the cryoexposure (15 min), while the rate of growth and cooling of the ice gradually slowed down.

Further research involves the use of various cryoinstruments and freeze-thawing modes, varying the composition and temperature of the model system, simulating the presence of blood vessels in the zone of cryoimpact, etc.

This work was funded by the National Research Foundation of Ukraine with the grant titled as "Thermal imaging study of soft tissues with thermal injury and mathematical modeling of the processes accompanying it" (Grant No. 2022.01/0094, Grant State Registration No. 0123U103506).

The advanced device for the fine purification of synthetic organic conductors for the quantum point-contact sensors development

M. Romanov[1], D. Harbuz[1], V. Gudimenko[1], O. Pospelov[2], D. Chudak[3], G. Kamarchuk[1]

[1] B. Verkin Institute for Low Temperature Physics and Engineering of NAS of Ukraine, 47 Nauky Ave., Kharkiv, 61103, Ukraine
[2] National Technical University "Kharkiv Polytechnic Institute", 2 Kyrpychov Str., Kharkiv, 61002, Ukraine
[3] V. Karazin Kharkiv National University, 4 Svobody Sq., Kharkiv, 61077, Ukraine
e-mail: m.d.romanov.1997@gmail.com

Breath sensors are one of the areas of knowledge that attracts a lot of attention in modern physics and chemistry. The reason is that breath contains countless amounts of information about the state of the human body: from hidden diseases to the emotional states of a person. Despite the variety of techniques that can be used in breath analysis, the principle of conductivity change remains one of the most universal and practical for the daily usage of sensors. Recently, quantum point-contact sensors provided a breakthrough in the comprehensive analysis of complex gas media including breath by the discovery of the quantum mechanisms of selective detection of such objects [1].

TCNQ-based salts are promising materials to be used as a sensitive layer for the conductive gas sensors. They are semiconductive, which enhances the performance of the sensor devices, and their crystals tend to grow as complex structures, such as nanoneedles or nanotubes [2]. Despite the advantages, the use of TCNQ-based materials for quantum sensor development and the realization of the quantum mechanisms of selective detection is restricted by the purity of the original substances. One of the reasons for that is that the commercially available compounds do not meet the purity requirements for use in gas sensing [3]. This work is aimed at the development and modernization of the device for the fine purification of synthetic conductors, that is used for the synthesis of quantum point-contact sensors for breath analysis. As a tested compound, the commercial TCNQ substances with a purity of 98% were used for the purification. The ability of TCNQ to sublimate in vacuum conditions was used as a main mechanism for the purification process.

The method of vacuum zone sublimation was implemented in the developed device. The substance for sublimation was located inside the quartz tube, and the heater was moved slowly in one direction along the tube axis. The vacuum pump evacuated air from a tube, creating a vacuum condition. The fusion zone was limited by the Teflon piston. Displacement of the heater along the tube axis was carried out by the stepper motor, connected to the microchip, and the motion speed was programmed on the personal computer connected to the purification device. The temperature of the heater was also controlled by the microchip connected, and the temperature values were registered by the thermocouple integrated into the heater design. It allowed us to finely control temperature during the sublimation process by the computer interface.

The composition of the purified TCNQ compound was determined by spectrophotometry. A high degree of purification was confirmed. The purified salt was used for the synthesis of the functional point-contact sensors. The experiments showed that the point-contact sensitive elements obtained from the purified substance correspond to the criteria of the Yanson point-contacts and provide realization of the quantum detection mechanisms for breath analysis [1].

[1] G. Kamarchuk, A. Pospelov, L. Kamarchuk et al. Sci Rep. 13, 21432 (2023).
[2] D.A. Harbuz, A.P. Pospelov et al., Molecular Crystals and Liquid Crystals, 718(1), 25 (2021)
[3] O. Pyshkin, G.Kamarchuk et al., J. Breath Res., 5(1), 016005 (2011).

AUTHOR INDEX

L

M

N

O

P

R

S

T

U

V

W

Y

Z